

A Thesis Submitted for the Degree of PhD at the University of Warwick

Permanent WRAP URL:

<http://wrap.warwick.ac.uk/97342>

Copyright and reuse:

This thesis is made available online and is protected by original copyright.

Please scroll down to view the document itself.

Please refer to the repository record for this item for information to help you to cite it.

Our policy information is available from the repository home page.

For more information, please contact the WRAP Team at: wrap@warwick.ac.uk

COCHLEAR MODELS

by

J.K. CANNELL B.E. (Adel.) M.Sc. (Birm.)

A thesis submitted at the University of Warwick

for examination for the degree of

Doctor of Philosophy

School of Engineering Science

September 1969

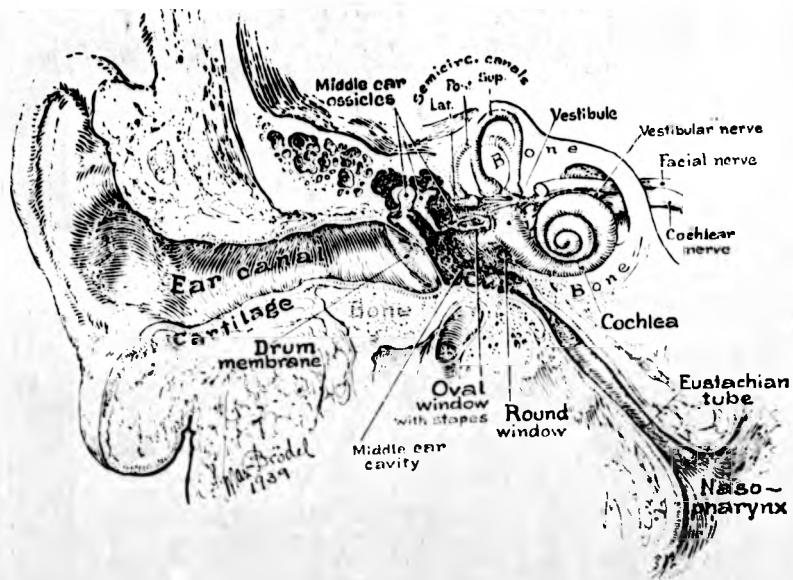


Figure 1-1. A composite drawing of the ear
 (from Max Brodel, 1946)

COCHLEAR MODELS

by

J.K. CANNELL B.E. (Adel.) M.Sc. (Birm.)

A thesis submitted at the University of Warwick

for examination for the degree of

Doctor of Philosophy

School of Engineering Science

September 1969

ACKNOWLEDGEMENTS

This research activity was initiated and supported by The University of Warwick from October 1965 for a period of $3\frac{1}{2}$ years. In January 1969 I received an award from The James Clayton Fund of The Institution of Mechanical Engineers, without which I could not have continued with this research, and since April 1969 I have been grateful for support as a Senior Research Fellow provided by a Science Research Council Grant.

I acknowledge the support given to me for the execution and completion of this programme of research by The University of Warwick and by the School of Engineering Science and the Head of the School, Professor J.A. Shercliff, in particular. I am grateful for the confidence in my ability to organize and perform this work shown by my supervisor, Dr.V.Marples, to whom I am also grateful for encouragement and support and for comments on and corrections to thesis manuscripts.

I am indebted to the University Workshops and to senior technicians Mr.Howard Fowkes, for his steadfast efforts and ingenuity during the period of manufacture of cochlear models, and Mr.John Darmon, for his enthusiastic and able assistance with experiments in his metrology room, and for help offered and interest shown by these and many other technicians of the School on many occasions. I thank Mr.A.Whitehead for his willing and competent photographic services and Miss C.Phillips for her care in preparing many of the enclosed drawings. I also wish to record a particular debt of gratitude to Dr.Michael Bevir for the interest he showed in these researches and for opportunities to discuss my work with him.

Senior E.N.T. Consultant Surgeons Mr.P.Roland and Mr.G.Rice both gave up many hours answering queries concerning anatomy and surgery of the ear. Thanks are also due to the staff of The University of Warwick Computer Unit for their efficient handling of more than 400 jobs, which occupied the Elliot 4130 computer for a total of some 37 hours, and for their generous assistance with certain programming difficulties.

Finally, I thank my wife for her cheerful patience, and for her competent typing of most of the thesis.

J.K.C.

ABSTRACT OF THESIS

The intention of the research activity described in this thesis is to contribute to the dynamical theory of the cochlea of the human inner ear.

The Science of Hearing, being disseminated in a wide range of frequently independent or unco-ordinated disciplines, is advancing far in the fields of subjective human acoustics, middle ear restorative surgery, medical diagnostic electro-encephalography and cochlear-nucleus-to-thalamus neural communications research. At the same time, exploitation, in auditory research, of the techniques and resources of modern engineering science, which may be particularly appropriately applied to analyses of the peripheral hearing system, has not been manifest to any great degree. It was therefore hoped that a first-principles engineering approach to the subject of cochlear action would demonstrate the need for a mathematical and quantitative type of analysis of the response of this key organ of hearing and also indicate the extent to which cochlear science is at present to be found in a state of disarray.

The writer's principal thesis is that a considerably greater potential for discrimination of the frequencies and intensities of pure and complex tones is attributable to the mechanical action of the cochlea than is generally supposed. That thesis will be more fully proven (it is expected) when current research is considerably extended and improved to permit the computation of spatial arrays of cochlear hair cell cilia shearing force patterns and electrical responses. The studies reported herein are relevant and fundamental to this aim and are limited to considerations of the dynamical response of the cochlear partition as a whole.

This research has included approximately equal parts of review, physical cochlear model experimentation and mathematical analysis. The first two chapters and sections of most of the other chapters concentrate on defining the system and reviewing the literature. Chapters 3 and 4 estimate the order and ranges of the physical properties of mass and

stiffness of the scala media (or cochlear partition), these properties being essential to the subsequent design of both physical and mathematical models of the cochlea in Chapters 5 and 6 respectively. The final chapter adds to the comments in other chapters on the credibility of the physical constants previously deduced in the thesis and tested in the models, the performance of the models, the particular problems clearly requiring further research effort and the relevance of the work to a more complete comprehension of human auditory theory.

NOTES ON THE FORMAT OF THESIS

As some chapters of this thesis have been prepared for publication, and the writer's programme of research has involved a number of different reviews, experimental techniques and separate theoretical analyses, each chapter is generally independent of the others, and cross-referencing between chapters is rare.

Each chapter contains its own table of contents, page, figure, table and reference numbering systems, introduction, bibliography, and usually, conclusions, and where required an appendix. Considering the extent of the thesis, and the necessity for frequent excursions into the fields of biology and physiology as well as various engineering sciences, it is hoped that by preserving clarity, the one-theme-at-a-time approach will assist the reader as much as it has the writer.

Included in the rear cover pocket are print outs of two I.C.S. Elliott 4130 Fortran computer programmes.

The first programme is typical of some of the computation involved in Chapter 3 on scala media effective masses, and the second is representative of a great many similar programmes involved in the response of the mathematical model of Chapter 6.

stiffness of the scala media (or cochlear partition), these properties being essential to the subsequent design of both physical and mathematical models of the cochlea in Chapters 5 and 6 respectively. The final chapter adds to the comments in other chapters on the credibility of the physical constants previously deduced in the thesis and tested in the models, the performance of the models, the particular problems clearly requiring further research effort and the relevance of the work to a more complete comprehension of human auditory theory.

NOTES ON THE FORMAT OF THESIS

As some chapters of this thesis have been prepared for publication, and the writer's programme of research has involved a number of different reviews, experimental techniques and separate theoretical analyses, each chapter is generally independent of the others, and cross-referencing between chapters is rare.

Each chapter contains its own table of contents, page, figure, table and reference numbering systems, introduction, bibliography, and usually, conclusions, and where required an appendix. Considering the extent of the thesis, and the necessity for frequent excursions into the fields of biology and physiology as well as various engineering sciences, it is hoped that by preserving clarity, the one-theme-at-a-time approach will assist the reader as much as it has the writer.

Included in the rear cover pocket are print outs of two I.C.S. Elliott 4130 Fortran computer programmes.

The first programme is typical of some of the computation involved in Chapter 3 on scala media effective masses, and the second is representative of a great many similar programmes involved in the response of the mathematical model of Chapter 6.

24-6 Physical and Mathematical Cochlear Models

J. K. Cannell
School of Engineering Science
University of Warwick
Coventry, England

V. Marples
School of Engineering Science
University of Warwick
Coventry, England

Quantitative effects of varying certain physical, mechanical and geometric properties of the human cochlea have been investigated.

It is considered that this work is required in an effort to establish the critical properties and conditions of the cochlea which have to be most carefully reproduced in the design of a mathematical model to yield accurate and realistic "mean human" cochlear microphonics. A contribution towards the understanding of the processes by which the property of sharp frequency discrimination is achieved by subsequent neuron codings, themselves elicited by uniquely spatially distributed and time/phase dependent hair cell responses is the final intention of this and associated research. It is, of course, realized that suggested and anticipated mathematical co-relations between cochlear signals and neuron action may be seriously masked by incomplete data in the arrangement of cochlear electrical activity. Hence every attempt is made to include the usable, relevant physiological information available in the design of the theoretical (digital computer) cochlea model.

Such an intention is by no means new. However, by-products of these studies have included the means to check on whether skull-vibration in some modes can give rise to this type of bone-conducted hearing, and also the means, not yet fully exploited, to make comparative quantitative checks of the effects of changing certain middle ear bone, muscle, and stiffness properties, and oval window motions, on theoretical microphonics generated in the cochlea.

PHYSICAL MODEL STUDIES. The refinement of the theoretical model has been supported by a programme of examination of eleven physical models of the cochlea scalae, each of twelve times full size and as nearly dynamically similar to the human cochlea as possible.

These models have been manufactured in perspex, contain glycerol solutions modelled on perilymph, and permit undistorted viewing of their inter-scalae elastic partitions, for which were used several impermeable latex membranes. Each model has been used to introduce a single boundary variable but with two or three changes of membrane stiffness and/or taper width, one change per test.

Model 1. An "unwound", straight model, it contains no scala media, the vestibular and tympanic scalae separated by a latex membrane of scaled width, taper and stiffness. This is seated (as in all models) across a joint with a very small, parallel sided inset either side of the membrane for undistorted external viewing through the polished perspex sides of the cavity. The ducts are geometrically similar in cross section to the distorted elliptical shape of "mean human" scalae, and were cut using model templates.

Longitudinally the ducts also display characteristic scalae necking and tapers.

Model 2. was of simplified design, consisting of two equally sized, circular section, uniformly tapering channels, separated again by a single elastic membrane of variable (scaled) width and stiffness.

Models 3 and 4. were similar to model 2, but with duct section diameters proportionately increased and decreased respectively.

Models 5 and 6. were similar to model 2, but with basal end diameter increased for model 5, and apical end diameter decreased for model 6, both with the same taper as model 2.

Model 7. contains two equally sized, circular, ducts of constant diameter.

Model 8. is similar to model 2 but with a non-uniform changing taper which more closely approximates model 1 scalae.

Model 9 includes the scala media, and, using the ducts of model 1, contains a model basilar membrane and a Reissner's membrane. The scala media contains gelatinous glycerol.

Model 10 was cast from moulds made of model 1 and, as nearly as was possible, simulates the spiral form of the human cochlea.

Model 11, the final physical cochlea model, is a spiral form of model 9.

Each model contains a helicotrema, membranous round window, and an electromechanical vibrator set variably in an oval window. A waveform generator and amplifier drive the vibrator, models are isolated, and oscilloscopes and meters check vibrator head amplitudes and motions via an (integrated) accelerometer signal. Stroboscopic illumination of membranes and insertion of metallic powders have assisted photographic methods of recording membrane responses, and micrometer screws permitted some measurement of membrane amplitudes.

MATHEMATICAL MODEL. The computer programme calculation is based on the laws of fluid (wave) motion and on force equations linking wave pressures above and below the partition to local inertia and distributed elastic membrane forces. Scala sectional areas and their variations have been introduced in detail, but sectional shapes have not. The programme has been used with some success to check basilar membrane displacements concurrently with physical model testing of corresponding boundary variations. This has resulted in some quite important improvements to the programme. In particular, the mathematical model has temporarily overtaken physical model work in seeking to demonstrate the ability of the mechanical part of the inner ear to considerably sharpen frequency discrimination in the cochlea, by calculating effects relative to sliding between cilia and the tectorial membrane. The assumed direction of maximum sensitivity of hair cell shearing for release of electric stimuli is towards kinocilia.

COCHLEAR MODELSContents

Acknowledgments	
Abstract of thesis	
Notes on the Format of thesis	
Conference Paper :- Physical and Mathematical	

Cochlear Models

Table of Contents

Chapter 1 The Ear and Hearing

I. The Anatomy of the Ear	Page 1- 1
II. The Inner Ear	Page 1- 5
III. Motions within the Cochlea	Page 1-10
IV. Auditory Nervous System	Page 1-15
V. Hearing	Page 1-18
VI. References	Page 1-22

Chapter 2 Theories of Hearing andCochlear Experimental Data

I. Historical Development	Page 2- 1
II. Recent Development	Page 2- 4
III. Cochlear Experimental Response Data	Page 2- 9
IV. Current Cochlear Theories	Page 2-19
V. References	Page 2-28

Chapter 3 Effective Mass of the Cochlear Partition

I. Formulation of the Model	Page 3- 4
II. Effective Mass Calculation	Page 3-13
III. Discussion of Theoretical Effective Mass Ratio.	Page 3-24
IV. Discussion of Typical Cochlear Effective Mass.	Page 3-27
V. Conclusions	Page 3-30
VI. References	Page 3-31
App.I. Theory of Incompressible Potential Flow	Page 3-32
App.II. Solution of the Field for Specified Membrane Displacements	Page 3-34

acts also display character-
ing and tapers.
fied design, consisting of
ircular section, uniformly
eparated again by a single
variable (scaled) width and

imilar to model 2, but with
rs proportionately increas-
pectively.
imilar to model 2, but with
ncreased for model 5, and
decreased for model 6, both
as model 2.

qually sized, circular,
ameter
model 2 but with a non-
er which more closely ap-
calae.

ala media, and, using the
ntains a model basilar
ner's membrane. The scala
inuous glycerol.
oulds made of model 1 and,
isible, simulates the spiral
chlea.

ical cochlea model, is a
9.

a helicotrema, membranous
lectromechanical vibrator
window. A waveform gene-
rative the vibrator, models
lloscopes and meters check
s and motions via an (inte-
signal. Stroboscopic illu-
and insertion of metallic
photographic methods of
ponses, and micrometer screen
ment of membrane amplitudes.

The computer programme
n the laws of fluid(wave)
uations linking wave pres-
the partition to local in-
astic membrane forces.
and their variations have
ill, but sectional shapes
me has been used with some
ar membrane displacements
ical model testing of cor-
rrections. This has resulted
t improvements to the prog-
the mathematical model has
physical model work in seek-
ability of the mechanical
to considerably sharpen
on in the cochlea, by calcu-
e to sliding between cilia
rns. The assumed direction
of hair cell shearing for
small is towards kinocilia.

THE EAR AND HEARING

Chapter 1

Contents

1.	The Anatomy of the Ear	Page 1
1a.	General	Page 1
1b.	The Outer Ear	Page 2
1c.	The Middle Ear	Page 2
2.	The Inner Ear	Page 5
2a.	Bony Labyrinth	Page 5
2b.	Membranous Labyrinth	Page 6
2c.	The organ of Corti	Page 8
3.	Motions within the Cochlea	Page 10
3a.	General	Page 10
3b.	The Hair Cells	Page 11
4.	Auditory Nervous System	Page 15
4a.	Neuro anatomy	Page 15
4b.	Relevance of Neurophysiology to Cochlear Theories	Page 17
5.	Hearing	Page 18
5a.	The Analysis of Sound	Page 18
5b.	Principal Phenomena of Hearing	Page 19
1.	Pitch	Page 19
2.	Loudness	Page 19
3.	Interaction of Tones	Page 20
6.	References	Page 22

1. THE ANATOMY OF THE EAR

1a. General

All the higher vertebrates, and many more primitive animals, possess a specialized organ for the reception of sound waves. The ear of vertebrates is by definition the organ in which are centred the sensors of hearing and equilibrium. In its simpler forms the organ of hearing has a particular biological value in mating, as it enables the sexes to find one another, but its most general adaptive function lies in its service in warning of impending danger. In man, considering the remarkable precision by which he can discriminate frequency and intensity differences, his binaural sense of hearing sometimes overtakes his other senses in locating distant objects and in orienting himself with respect to such objects. In birds and mammals, hearing is particularly developed for communication, and in man it attains its highest utility in articulate speech and the art of music.

The ear is considered in three parts; the outer, middle and inner ear. (See Figs. 1 and 2) The outer or external ear intercepts and receives airborne sound pressure waves; the middle ear conducts them inwards; and the internal ear, through its curious fluid/membrane anatomy and its intricate arrangements of receptor cells, translates the effects of these pressure waves from a mechanical domain into patterns of electrical nerve impulses that are sent through the auditory nerve, from the inner ear, to the brain centres, where they finally give rise to auditory perceptions.

In this chapter the characteristics of the hearing organs are considered, sometimes originally, from an engineering system viewpoint as well as from the classical, anatomical point of view.

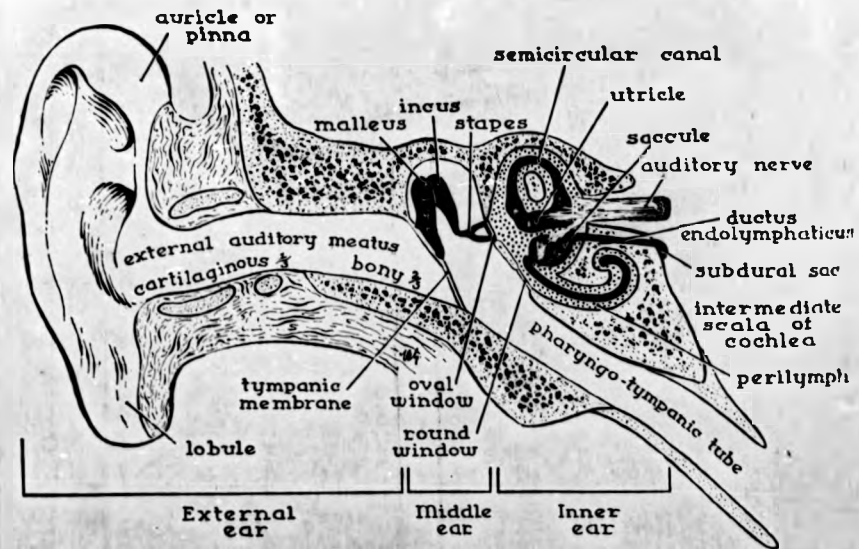


Figure 1-2. Diagram of an ear, showing the relations of the external, the middle and the inner ear

1b. The Outer Ear

This consists of the fleshy, cartilagenous outer flap (auricle or pinna) and the opening and its inwardly directed tube (external auditory meatus). The auricle is formed by a yellow fibrocartilage covered by skin. Round the margin in its upper three-quarters is a rim called the helix, concentric with which is a secondary rise the antihelix. Surrounded by the antihelix is a deep depression known as the concha, from whose anterior part the meatus passes inward into the skull. A protective flap called the tragus overlaps the meatus in front. The lower part of the auricle, the lobule, contains no cartilage.

The auricle can be moved slightly by the anterior, superior and posterior auricular muscles, but even with this limited facility, it is too small in man to serve any important acoustical purpose, although it does assist in directionally localizing high frequency sounds.

The external auditory meatus is about 2½cm long, 0.7cm mean diameter, its outer third being cartilaginous and its inner two-thirds bony. It is lined in its whole length with skin, the secretory glands of which are modified to produce a waxlike substance, cerumen, and it is closed by the generally impermeable tympanic membrane or eardrum.

The meatus undoubtedly imparts its own characteristic frequency response to that of the ear, responding most naturally to sounds of 3 to 4 kHz.

1c. The Middle Ear

Beyond the eardrum is the middle ear, or tympanum, a small, irregularly shaped, air-filled cavity in the temporal bone. From it the Eustachian tube runs forward, inward and downward to open into the nasopharynx, above the mouth. From the upper part of the posterior

nal

le
tory nerveductus
ndolymphaticus

subdural sac

intermediate
scala of
cochlea

perilymph

to tube

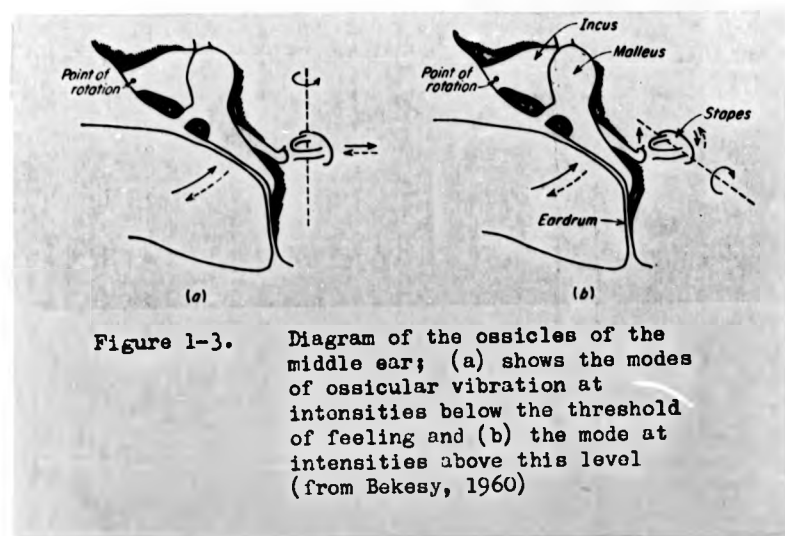


Figure 1-3. Diagram of the ossicles of the middle ear; (a) shows the modes of ossicular vibration at intensities below the threshold of feeling and (b) the mode at intensities above this level (from Bekesy, 1960)

wall of the middle ear an opening leads backward into the air cells of the mastoid process. Lower down is a little pyramid containing the stapedius muscle, and at the base of this is a small opening allowing passage of the chorda tympani branch of the facial nerve.

The roof (attic) of the tympanum is formed by a very thin plate of bone which separates the cavity from the middle depression (fossa) of the skull. The inner wall of the cavity shows a promontory caused by the spiral shaped cochlea. Above and behind the inner wall is the oval window (area 3 to 4 mm²); below and behind lies the round window (area 2 to 3 mm²), closed by a membrane. Curving round above and behind the windows and the cochlea promontory is a ridge caused by the Fallopian canal, in which is carried the facial nerve.

The outer wall is largely occupied by the tympanic membrane, which is circular (about 9 mm. dia.) and so placed that it slopes downward and inward from above. It is broadly conical in form with its apex, or umbo, of height about 2 mm., directed inward. Externally the eardrum is lined by skin, internally by mucous membrane and between these two layers is a firm, fibrous tissue.

The whole tympanum is about one and a half cms long from front to back and its volume is about 2 cm³. It is spanned from side to side by three small bones (ossicles), of which the malleus (or hammer) is external. (See Figs.2, 3) The malleus is attached by its long process (or handle) (about 6mm in length) to the eardrum, and lies radially on the upper portion of the eardrum from the apex almost to its outer fold. The head of the malleus lies in the attic and articulates posteriorly with the bulbous upper part of the next ossicle, the incus or anvil. The long projection of the incus (some 7mm) runs downward and terminates in a lens-shaped nodule which is jointed to the third ossicle, the stapes or stirrup bone (which is about 3½mm in length) whose name efficiently

describes its shape. The two branches of the stirrup are anterior and posterior, and its elliptically shaped footplate (3mm major axis by 1.5mm minor) fits into the oval window to which it is bound by an annular ligament. The stapes lies nearly at right angles to the long process of the incus, and for all but the most severe movements, tends to rock about the footplate-ligament attachment at the anterior end, the ligament being less restricting and slightly folded at the opposite, lower end. The ossicles are suspended in the tympanum by a number of ligaments. When the handle of the malleus is pushed inward by the tympanic membrane, its head moves outward; the head of the incus, attached to it, also moves out; and the end of the long process of the incus moves in, pressing the posterior side of the stapes footplate into the oval window.

Two minute muscles act upon the ossicular chain; one, the tensor tympani, when it contracts, tends to pull the head of the malleus outward, and the other, the tensor stapedius, acts so as to rotate the stapes outward in the opposite direction to that stimulated by tensor tympani response. As a response for one tensor cannot normally be elicited without the other also contracting, one effect of contractions is to tighten the ossicular linkage, thereby probably inhibiting the low frequency response of the stapes. The most commonly reported function of the two muscles is to protect the ear against excessive impulses, for example, explosions. However they are not ideally suited to this role since their latency (response) time is so relatively large that an unexpected explosion has occurred before they have had time to contract fully. Their response is involuntary, they are innervated by the facial nerve rather than the auditory nerve, and they help to change and limit the overall locus of motion of the ossicles during continuous exposure to very loud sounds.



Figure 1-4a. Photograph by the writer showing an exposed portion of the basal turn of the bony labyrinth of the cochlea - taken during sectioning of a human temporal bone.

The function of the middle ear is the efficient transmission of sound energy to the inner ear by matching the high impedance of the cochlea with the very low impedance of the eardrum. The tympanic membrane presents a large surface on which air pressure waves impinge, whose force is applied through the ossicular chain to the small surface covered by the stapes footplate, and the result may be a magnification in pressure of about 10 to 25 times. This pressure magnification is a function of both amplitude and frequency.

The efficiency of middle ear sound transmission varies from about 15% at extreme frequencies to 30% at frequencies approaching 1 kHz, which may be compared with an efficiency of perhaps 0.1% obtaining with no middle ear mechanism.

Being a system of elastic elements, each with a characteristic mass distribution, linked by joints with real stiffness and damping components, the middle ear constitutes a non-linear mechanism whose frequency response is not fully chartered either theoretically or experimentally.

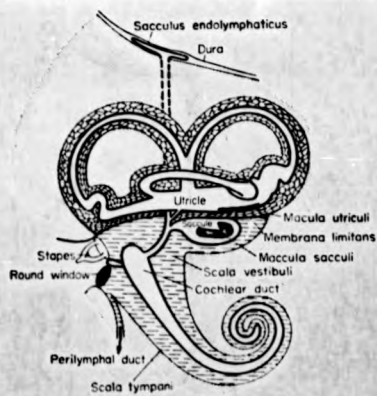
2. THE INNER EAR (Refs. 1 to 7)

2a. Bony Labyrinth

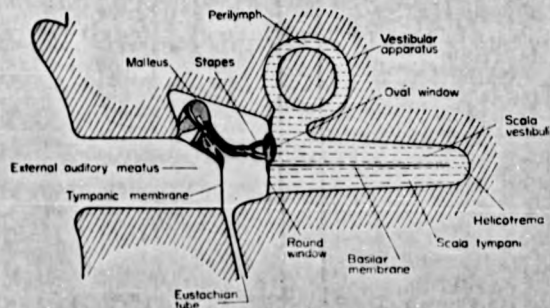
This is composed of the vestibule, semicircular canals, both of which sections are concerned with sense of balance, and the cochlea (Fig.4). The vestibule lies just internal to the rear part of the tympanum, and there would be communication between the two were it not for the stapes footplate. At the rear the three semi-circular canals open into the vestibule. Anteriorly the vestibule leads into the cochlea which is twisted about $2\frac{1}{2}$ times round a central pillar called the modiolus - the whole cochlea forming a rounded cone similar to the shell of a snail,



Figure 1-4b. Close-up photograph by the writer of a sectional preparation showing the osseous spiral lamina of the middle turn of the bony labyrinth of a cochlea.



(a)



(b)

Figure 1-5 Schematic drawings of (a) the cochlea membranous labyrinth and (b) the elements of the ear system (after Bekeasy, 1942) (Published by Littler 1965 Ref. 3)

though only about 5mm from base to apex. Projecting from the modiolus is a horizontal bony plate, the shelf-like, osseus spiral lamina, which runs helically round the modiolus from base to apex. This bony shelf stretches about halfway across the canal of the cochlea and carries branches of the auditory nerve. If it could be unwound and straightened out, the adult human cochlea would be about $3\frac{1}{2}$ cms. long.

2b. Membranous Labyrinth (See Fig.5)

The membranous labyrinth lies in the bony labyrinth but does not fill it; between the two is the fluid perilymph, which is watery and saline, whereas inside the membranous labyrinth is the liquid endolymph, of different chemical composition and having slightly greater viscosity than perilymph. (1A)

In the bony vestibule lie two membranous vesicles, one of which, the saccule, is in front, and the other, the utricle, behind; each has a patch of sensory epithelium called macula to which fine branches of the auditory nerve are supplied, terminating around specialized sensory hair cells.

The bony semicircular canals are considerably larger in section than their membranous enclosures, and each membranous semicircular canal contains a ridge made up of modified epithelium containing sensory hair cells resembling those in the maculae. All the canals open into the utricle.

From the lower part of the saccule runs a small canal called the endolymphatic duct. Anteriorly the saccule communicates with the membranous cochlea, or scala media, by a short connecting duct.

A section through any part of each turn of the cochlea (See Fig.6) shows the bony spiral lamina which is continued right across the canal by the basilar membrane, thereby dividing the canal into an upper and

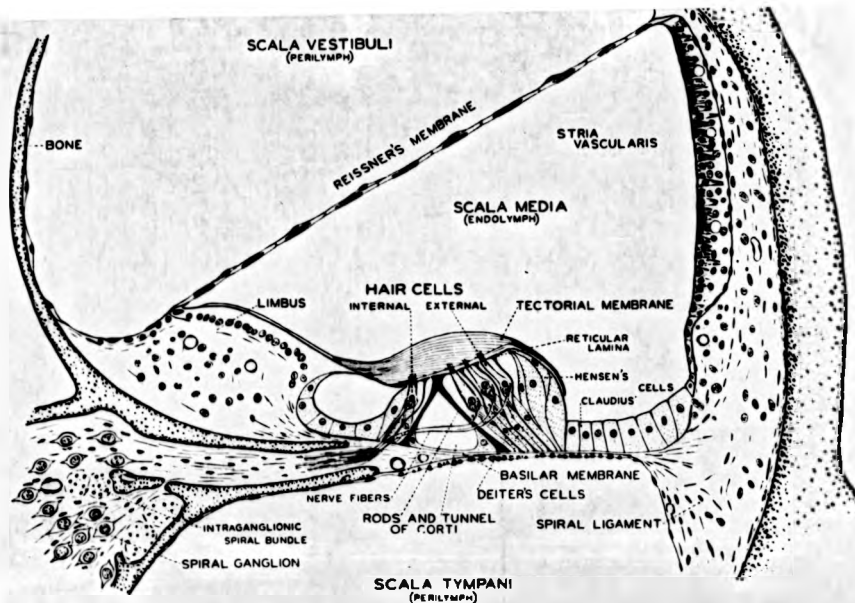


Figure 1-6 Sectional diagram of the second turn of a cochlea showing the organ of Corti (after Davis, 1953).

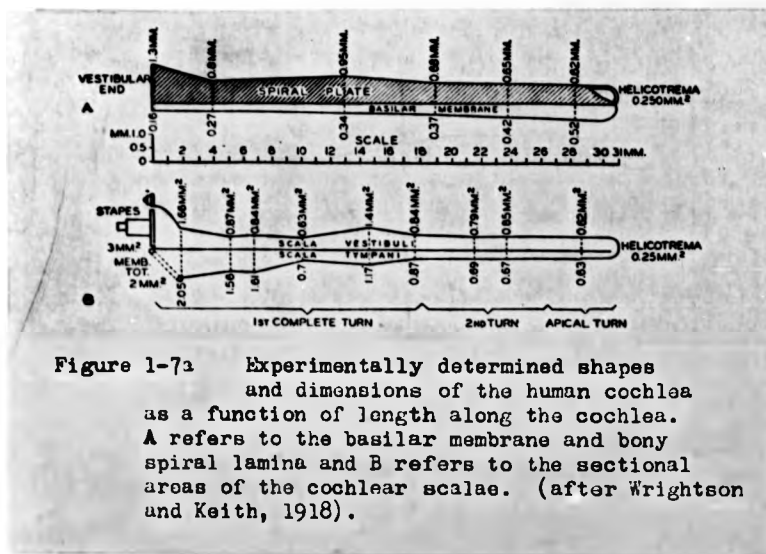


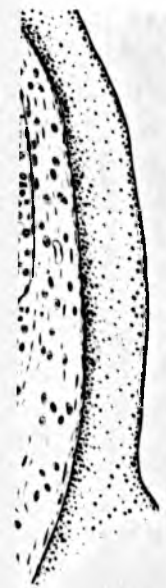
Figure 1-7a Experimentally determined shapes and dimensions of the human cochlea as a function of length along the cochlea. A refers to the basilar membrane and bony spiral lamina and B refers to the sectional areas of the cochlear scalae. (after Wrightson and Keith, 1918).

a lower half, and connected with the outer wall by a strong spiral ligament. Near the free end of the bony shelf the membrane of Reissner is attached and runs outward and upward to the outer wall, taking a triangular slice out of the upper half of the canal.

Three canals may thus be seen in section : the upper is the scala vestibuli; the middle, scala media, is the cochlea duct or true membranous cochlea; and the lower is the scala tympani. At the base of the cochlea, the perilymph in the scala vestibuli is continuous with that in the vestibule, whereas the perilymph in the scala tympani bathes the round window membrane on its inner surface, the outer surface of which is in communication with the air of the tympanum. Perilymph in the scala tympani also communicates through a capillary system called the cochlear aqueduct with the space between brain covering layers, in the posterior cranial fossa.

The scala tympani and the scala vestibuli also communicate at the apex of the cochlea, in which region, known as the helicotrema, the basilar membrane is absent and the scala media is closed, so that here perilymph can pass from one canal to the other. At the opposite, basal end, the scala media, containing endolymph, communicates with the saccule through the fine connecting canal of Hensen.

The cross sectional area of the two perilymphatic channels, the scalae vestibuli and tympani, reduces at sections closer to the apical or helicotrema end, and their overall variation is frequently described as approximating a linear diametral taper. In fact the scala vestibuli displays a less regular section than the tympani duct, presenting an effective cross section of at least 3mm^2 immediately inward from the stapes, reducing to about 1mm^2 halfway along the first turn, then widening again to $1\frac{1}{2}\text{mm}^2$ a few millimetres further along, to continue in a more uniformly decreasing taper until at the apex ($3\frac{1}{2}\text{cms.}$ along the ducts) its area is about $\frac{3}{4}\text{mm}^2$. (compare with Fig.7)



turn
of

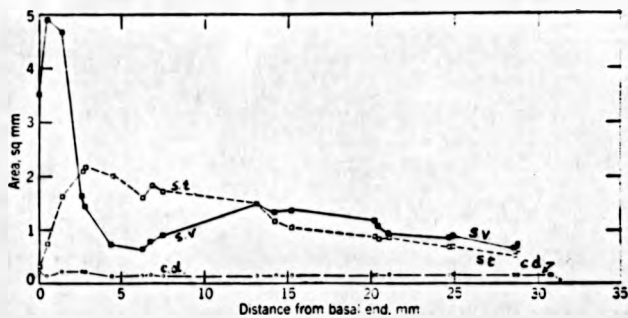


Figure 1-7b. Cross-sectional areas of the human cochlear passages. s.v. refers to scala vestibuli, s.t. to scala tympani and c.d. to cochlear duct or scala media, (from Wever, 1949)

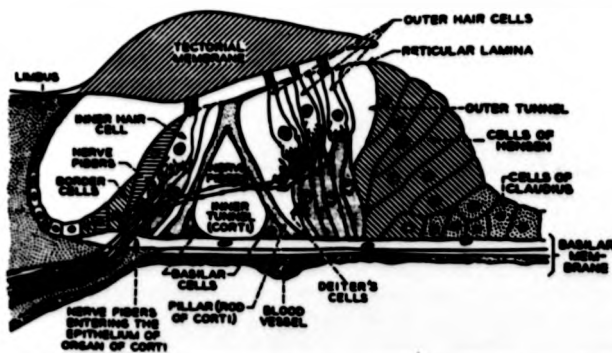


Figure 1-8 Cross section of the organ of Corti (after Davis, 1951).

The most striking variation in the membranous labyrinth, however, is the space between the limit of the bony shelf and the opposite wall of the duct, which is occupied by the basilar membrane, on which is mounted the organ of Corti. The span of the basilar membrane increases remarkably uniformly from about 0.10 to 0.18 mm very near to the stapes to 0.49 to 0.65 mm just before the helicotrema, a normal variation of 4 to $4\frac{1}{2}$ times. This variation gives rise to a large variation in stiffness, or resistance to fluid pressures of the cochlear partition, decreasing some several hundred fold from the basal end towards the apex. Similarly, because of the integral nature of the scala media and the basilar membrane, the scala media becomes more massive as the helicotrema is approached.

2c. The organ of Corti

The scala media contains the essential organ of hearing, the organ of Corti, which lies upon the vestibular side of the basilar membrane; it consists of a tunnel bounded on each side by the inner and outer rods of Corti. Some researchists believe that unlike the remainder of the scala media, the tunnel of Corti contains perilymph. On either side of this arch of Corti are the inner and outer hair cells numbering about 20,000, and the outer hair cells are supported within their rows by Deiter's cells, and externally by the larger Hensen's cells. (See Fig. 8)

A delicate membrane called the reticular lamina covers the top of all of these cells, and is pierced by the cilia of the hair cells. Above this lies the tectorial membrane which is loose enough to follow, with some inherent damping, any up and down movements of the active cochlear partition, but which is rather stiff in either transverse direction. The tips of the longest cilia in each bundle of 90 to 120 cilia sustained by any one outer hair cell are believed to be lightly embedded in the lower side of the tectorial membrane. (Refs. 10,11,13,16, 18,26)

The tectorium is attached to the osseus spiral lamina near to its outer tip, and within the attachment of Reissner's membrane.

Thus the scala media, or cochlear partition, is bounded by the three principal sides. The roof of this triangular, endolymph-filled enclosure, in contrast with the floor, is very thin, for Reissner's membrane is composed of only two layers of epithelial cells, and is electrically insulating. The outer wall of the duct is made up of the spiral ligament, already mentioned, contained on the inner side of which is the stria vascularis. This is rich in blood vessels, and is thought by some investigators (Refs. 14,21,24,27,28) to provide a source for the endolymphatic electrical potentials known as cochlear microphonics, which by means of two fine electrodes, one applied to the endolymph of the scala media and the other adjacently to either of the perilymph canals, can be easily measured at any section along the cochlea where the cochlear partition is responding to sound excitations.

Bekegy demonstrated a resting d.c. potential of more than +80 m.v. in the endolymph of guinea pigs. The third boundary of the scala media, the basilar membrane, with its organ of Corti, tunnel, Deiter's, Hensen's and hair cells complex is also electrically non-conducting as a partition. The basilar membrane itself is the only one of these membranous and cellular elements which appears to contain any mechanically-definable elasticity or stiffness. Its histology is uniquely characterised by definite layers of apparently elastic transverse fibres, which are believed to impart its elastic nature, embedded in a dense mat of collagenic fibres and homogeneous material. As is discussed in Chapter 4, ultra-microscopic studies during the last few years (Refs. 15,16,17) have confirmed the belief held by anatomists since the last century concerning the existence of two dis-similar membranous zones associated

with the basilar membrane at every section. It is now clear that the inner or arcuate zone, of the basilar membrane, projecting outwards from its medial attachment at the limbus, and supporting the pillars of Corti, is a relatively thick complex of densely packed, irregular fibrous bundles. Near the base of the outer pillar, a discontinuity exists, outwards from which the pectinate zone reaches to the spiral ligament. In this outer zone two regular fibrous stratum are to be found, the membrane being thinner and more elastic, and, in addition, displaying an increase in the transverse fibrous area in sections taken from the apical end towards the basal (stapes) end. Fibrillary arrangement as regular and parallel as that found in the lower fibrous layer of the pectinate zone is considered to indicate that this part of the membrane must be influenced by direct tension forces. This observation is developed in the appropriate chapter.

3. MOTIONS WITHIN THE COCHLEA

3a. General

When under the influence of, for example, an airborne sound of constant amplitude and of low frequency, the footplate of the stapes is momentarily (cyclically) pressed inward, the pressure exerted on the perilymph of the inner ear is relieved mainly by a corresponding outward bulging of the round window membrane. As the footplate moves outwards, the round window membrane is similarly sucked inward, and as the frequency of the exciting tone increases, a small phase difference appears between these motions due mainly to the fluid of the scalae not being wholly incompressible. Varying pressures thereby induced in the liquid of the two adjacent scalae result in cyclic pressure differences across the cochlear partition, and the magnitude and phase of these pressure differences will vary from section to section along the cochlea.

Also varying along the cochlea, mainly because of the four-fold variation in width of the basilar membrane, are the mass and stiffness properties of the scala media partition, and so it is to be expected, as has been observed experimentally, (Refs. 8,9) that the scala media, and in particular the basilar membrane, vibrates in response to the main scalae cyclic pressure differentials, and that for sounds in the normal human audio frequency range, from 20,000 Hz to about 50 Hz, only a limited part of the scala media, being best tuned to the input sound, undergoes any appreciable vibration.

3b. The Hair Cells

The mechanics of the processes by which the sensory cells are excited, generate partially encoded electrical voltages, give rise to endolymphatic microphonic potentials and enervate their various interconnected nerve fibres, is not well understood, and has become a major research activity for many neuro-anatomists, neuro-physiologists and sensory cell morphologists, and is mainly outside the scope of this thesis. × However, so much has very recently been discovered (Refs. 10 to 25 inc.); the ciliated protrusions, like groups of microscopic hairs, supplied by each outer hair cell, are all oriented in very much the same relative direction in relation to the axis of the cochlea. An outer hair cell bundle crosscut close to and above the cell surface (cuticular plate) and the reticular lamina is usually the shape of a W, formed by three rows of sensory hairs (called stereocilia), with a total number of up to 120 of these fine hairs (0.15 micron mean diameter and of height from 1 to 8 microns, erect, stiff and brittle) on each cell. Symmetric with the base of the W and just outside it lies a small basal body or centriole, which has been compared with the single kinocilium (unusually large, viscous and flexible cilia) existing

in vestibular end organ sensory cells and in several other sensory receptor mechanisms. Whether or not the basal body is an evolutionary atrophication of a kinocilium is debatable, but this basal body does provide a measure of the orientation of cilia bundles, and all outer hair cell bundles are oriented with their basal bodies pointing towards the Hensen's cells, across the cochlea. The longest stereocilia are invariably found in the central, lower region of the W and cilia behind these uniformly reduce in height until at the extremities of the W they are quite short. In side view, a bundle or tuft of cilia having roots deeply embedded in the cuticle and tips stiffly mutually supporting, and with the tips of the longest hairs, near to the basal body, embedded in the lower lamina of the tectorium, rather resembles an abutment, or triangular bracket, which is well suited for the transmission of shearing forces with minimum deflection: for example, shearing forces induced by relative parallel motions of the tectorial membrane with respect to the reticular lamina and basilar membrane. This particular point appears to have escaped mention or attention in the discussions of the research workers involved.



In one of his many famous series of experiments, von Békésy⁽⁸⁾ (and others⁽²⁸⁾) studied the cochlea microphonic effect obtained by inducing slight shearing motions between the tectorial and reticular membranes using vibrating needle probes applied to "in vivo" guinea pig cochleas. He showed that, at a given spot on the tectorial membrane which had been carefully exposed, movements of the needle in only one certain direction gave a maximum microphonic output.

The sensitivity was greatest in the radial direction (that is, for an "unwound" cochlea, in a transverse direction) and minimal in the longitudinal direction when the needle was placed on the outer edge of

the tectorial membrane. When the vibrating tip was placed on the inner edge of the membrane, the direction of maximum sensitivity was changed and was more nearly in the direction where the minimum was previously.

This experimentally observed direction of sensitivity corresponds very closely with the direction of orientation of the outer hair cell tufts for maximum shear force transmission. It has also been stressed by the group of Swedish physiologists (Refs. 12,13,16,18,20,22,25) whose recent outstanding researches have thrown much light on this subject, that in both human vestibular mechanism organs, and in fish and mammals, the orientation of sensory hair bundles in relation to the kinocilium in the bundle is certainly indicative of the direction of maximal sensitivity of these organs.

The difference in arrangement of the hairs on the inner and outer hair cells is one of the many striking differences between these two sets of auditory sensory elements. Cilia supplied by the single row of inner hair cells, which number less than half as many per inner hair cell as do the cilia of outer hair cells, are arranged roughly in two lines parallel to the row of cells. Inner hair cell cilia are also considerably coarser (0.35 micron mean diameter) shorter, and, presumably, stiffer, than outer cilia, and their straight alignment, lengthwise parallel to the basilar membrane, suggests they only respond to shearing movements in the radial direction.

It has also been demonstrated^(21,23) via further micro-electrode studies that inner hair cells are less sensitive to normal acoustic sound levels than are outer hair cells, and also that, in the event of disorientation and destruction of cochlea structures caused by violent sound levels, lesions develop among the sensitive outer cells before inner hair cells are damaged.

Concluding the discussion on physiology and morphology of hair cells, it is considered^(Ref.13) that while inner hair cells have a very limited direction-of-shearing (and amplitude-of-shearing) sensitivity, the W shaped bundle of outer hair cell cilia indicates an adaptation which, while providing one direction of maximum sensitivity, also increases their outer hair cell sensitivity to movements in several directions, oblique as well as radial and longitudinal.

It is only fairly recently that theories of hair cell excitation by shearing forces have been advanced, and, usually, accepted, to the exclusion of former widely held theories of hair cell and cilia bending, in which the cilia themselves were suspected of an initiating transducer action. Another theory whose abandonment has taken a long time in some professional circles in this country assumed a simple cyclic tugging and bumping of hair cells as the basilar membrane vibrated towards and away from the tectorial membrane.

The most acceptable modern-day theory is that cilia bundles passively transmit the energy of the relative shearing movements of the tectorium to the utricular plate and, thus, to the basal body and its associated organelles, and it is the basal body which may be regarded as the component essential to the excitation and polarization of the hair cell.

It is feasible to calculate the amount of sliding occurring in both transverse and longitudinal directions between the tectorial membrane and the reticular lamina when the instantaneous deflected shapes of the basilar membrane are known, provided, of course, that the geometry of the organ of Corti, the spatial relationships between its components, and their natural loci of movement are also known.

The work of Rhode and Geisler^(ref.26) outlines a simple approach which it is intended to develop in the future.

4. AUDITORY NERVOUS SYSTEM

4a. Neuro Anatomy

Before continuing with the relevance of this theory of hair cell excitation by shearing forces to a dynamical analysis of cochlear partition response to sound excitation by the stapes, which is the subject of this thesis, a brief summary of the auditory nervous system, as it innervates the cochlea sensory hair cells, is offered. (Refs. 3,4,5,7,27 to 30)

The various spiral and radial nerve fibres from the hair cells connect to ^{cell} ~~cell~~ bodies in what is known as the spiral ganglion of Corti, which is situated within the modioliis. The basic units of the nervous system are nerve cells or neurons, and they are made up of a central structure, the cell body, with one or more processes (two in the auditory system). One and only one of these processes, the axon, acts as a transmitter, conveying information in the form of nerve impulses, called action potentials, as high as 30mV, at a speed of about 9,000 cm/sec. away from the cell body. The other processes are receptors, and are called dendrites, conveying other nerve impulses into the cell body. Both dendrites and axons may have several terminal branches. There are two general classifications of nerves:- efferent, conveying instructions from the brain, and afferent, conveying, for example, sensory information to the brain. In the course of a neural pathway, the fine terminal branches of an axon may each communicate with one of the dendrites of the cell body of another neuron across an apparent discontinuity known as a synapse, or synaptic junction. This synapse imparts a variable time delay, of the order of 0.5 m.sec., which, after repeated stimulation, decreases,

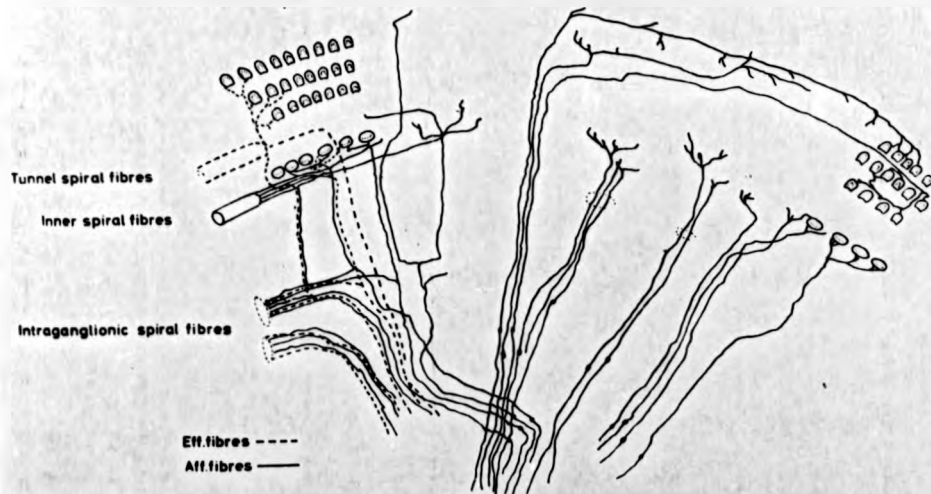


Figure 1-9

Schematic diagram of part of a basal turn in the organ of Corti showing the distribution of afferent and efferent nerve fibres (from Wersall, 1965).

and also has a most important characteristic in that transmission across a synapse can only occur in one direction (for ^a different fibres this is towards the cortex). An "all-or-nothing" principle describes nerve conduction: providing a stimulus delivered to a dendrite at a synapse is of sufficient magnitude, the size of the inevitable response and its speed of propagation are independent of the size of the stimulus. Also, following the discharge of an impulse, a nerve remains for a very short period in a state of exhaustion. This refractory period is usually about 1 m.sec., but may increase when the nerve is repeatedly or continuously stimulated. Thus auditory nerves do not normally respond continuously beyond 300 or so times per second, although the refractory time may then be somewhat reduced by greater stimuli. Thus, other than for a sensory mechanism which invokes more neurons when intensities being sensed increase, the only gradation which can be taken to represent intensity of stimulus of a single nerve is the number of impulses per second.

There are about 30,000 nerve cells in the cochlea, forming what is known as the spiral ganglion, more densely distributed in the basal than in the apical region. The innervation of the two types of hair cell is seen in Fig. 9 to be different. Each inner hair cell is innervated by one of two radial fibres and each radial fibre is connected to one or two hair cells, whereas the outer hair cells have numerous innervations. In some regions the multiple connections of a single outer fibre extend to many hundred outer hair cells, over about half a turn of the cochlea. This multiple innervation of the outer hair cells should be noted in association with morphological differences in the two types of cells already discussed. Also, in the cochlea, it is common for an axon to branch



basal
ing
d
ball,

off into several fibrils, permitting one neuron to make interconnections with many others, and vice versa. Two common effects of multiple connection at synapses may be mentioned; summation, when a series of stimuli, each of which would be incapable of singly exciting a nerve, can do so jointly, and inhibition, which is known to occur in the auditory nucleus, when spontaneous, natural nervous activity can be checked by additional stimuli occurring at synaptic junctions due to an added sound.

4b. Relevance of Neurophysiology to Cochlear Theories

From the brief physiological summary above, it is apparent that the performance of the auditory nervous system, at least as regards all the separate afferent nerves, which number the great majority of cochlear nervous fibres, is a time domain process but depends entirely upon the frequency, place, phase and intensity performance of the 20,000 separate sensory cells of the cochlea. Consequently the ability to perceive and to accurately discriminate frequency and amplitude and time components of the sounds in which man lives depends upon the ability of his cochlear sensory mechanism to present to the adjacent neural complex all the information defining and describing the sounds intercepted. Therefore, in any theoretical attempt to seek a better understanding of cochlear dynamics, whether as a preparation for work for the relief of peripheral hearing defects, or in order to provide the neurophysiologist with much-needed information concerning cochlear sensory cell response, it is imperative that the aim should be to deduce the nature and patterns of hair cell - tectorial membrane - basilar membrane mechanical shearing action. Co-relations between hair cell action and neuron actions are slowly being developed, but are as yet admitted to be fragmentary and confused. However it is clear that every part of the hair cell dynamic response pattern may be equally relevant.

5. HEARING

Many clues to the characteristics of the three parts of the ear, and of the auditory nervous system can be gleaned from what is called subjective experimentation;- an immense subject which, at the neural end of its spectrum, becomes less subjective, and tends towards experimental psychology. A few commonly accepted principles and laws, derived from subjective hearing test data, are categorized below, these being undoubtedly relevant to an appreciation of the properties required of theoretical ear models.

5a. The Analysis of Sound

A general definition, not necessarily acceptable beyond the world of science, is that basically periodic sounds are heard as tones and aperiodic ones as noises. Periodic sounds may vary in frequency, intensity, phase and wave-form. In simple tones, the phase is not perceived except when a difference in phase of lower frequency tones is detected between the two ears and the directional localization of the source thereby discovered. For a single ear, when two or more pure tones interact their phase relations are perceived and sustained by the hearing system.

The resolution of a compound tone into a fundamental and a series of overtones, with indications of the relative magnitudes and phase relations of the components, may be accomplished both mathematically and in the laboratory using oscilloscopes and harmonic analysis apparatus, and this type of analysis can also be achieved by the ear. On this remarkable analytic capacity depends much of the peculiar value of the sense of hearing. The ear follows Ohm's law in a general way, but by no means exactly. Acoustic impedances of the various sections of the ear, or of the assembly at various sections display prominent reactive components

as well as resistive, depending upon the frequency of the sound, and to a lesser degree upon its intensity.

The changes in the sound patterns produced within the ear take two forms, frequency distortion and non linear amplitude distortion.

The former is a reflection of the fact that the sensitivity of the ear, and its separate sections, varies greatly over the audio frequency range, and that the hearing system does not respond to sounds below and above certain limits. Hence, certain components of a complex sound will be favoured more than others.

Non linear distortion represents a failure of the ear's response to correspond in a simple way to the energy of the stimulating sound. For example, a pure tone, if it stimulates the ear at greater than a relatively moderate intensity, will produce a compound effect and be heard as a fundamental with a series of overtones, and it has been indicated by innumerable animal dissection and subjective tests that these overtones mostly have their origin within the inner ear.

5b. Principal Phenomena of Hearing

1. Pitch

The normal range of audibility for man covers 9 or 10 octaves, from 15 to 40 Hz up to perhaps 23,000 Hz for children, or 10,000 Hz for normal hearing persons over 60 years of age.

2. Loudness

The subjective loudness of a sound is a function of both its frequency and its energy (that is, power or intensity, or, as is used most commonly, its pressure). Sensitivity to loudness is greatest for sounds in the middle high frequency range, from 1 kHz to about 4 kHz, and it appears that man has developed, for this frequency region, maximum practical sensitivity of hearing

(if ears were any keener they would respond to natural molecular motions of air particles). The power range from this level of threshold of hearing to the loudness level at which pain intrudes and where damage may result is about 10^{12} times.

The perceived loudness, however, is less extensive, according to the interpretations made of subjective data. The ear may be said to follow the other senses in compressing the intensity dimension. The ear generally adheres to a principle of sensation known as Weber's law, which states that an energy change, in order to be perceptible, must be a constant fraction of the former energy level rather than a simple increment of it. Thus the perceived magnitude of a sound varies as the logarithm of its energy.

3. Interaction of Tones

Two pure tones of similar intensity, differing only slightly in frequency, induce a subjective periodic loudness variation known as beating. This effect is discernable up to a frequency differential of about 20 Hz.

Two tones with dominant fundamentals and fairly great intensity, different in frequency by 50 to about 1,500 Hz, generate subjective combination tones, which may be difference tones or summing tones. For example, it is not difficult to hear a tone of 500 Hz when two strong tones of 2,000 and 2,500 Hz are presented to the ear, and with great care, a tone of 4,500 Hz may be recognized if it is not wholly masked by the original sounds. A loud tone of 1,000 Hz will seriously mask another quieter tone of close frequency, for example, of 900 Hz, but will have practically no effect on an 100 Hz tone. Overtones resulting from the original will also mask other sounds of similar frequency to the overtones.

All of these effects are said to originate principally in the inner ear, although careful engineering analyses of middle ear action, which have not yet been reported, may show the middle ear to be less linear than hitherto assumed. Other subjects, equally vast, and sometimes alluded to in the script include types of deafness, the localization of sounds, modern psychologic, medical and surgical practice, and hearing and sensory system research techniques, both subjective and anatomical, as well as neurological, but these subjects must remain outside the scope of the present study.

6. REFERENCES

1. The Surgical Anatomy of the Temporal Bone and Ear.
B. J. Anson and J. A. Donaldson
W. B. Saunders. Co., Philadelphia 1967
- 1A. The Vestibular and Cochlear Aqueducts
B. J. Anson et al
3rd Symposium on the role of the vestibular
organs in space exploration N.A.S.A. SP-152, 1967.
2. Foundations of Experimental Psychology - Hearing
H. Hartridge and H. Banister
Carl Murchison 1929
3. The Physics of the Ear
T. S. Littler
Oxford, Pergamon Press Ltd., 1965, 1st Edition.
4. Physiological Acoustics
E. G. Wever and M. Lawrence
Princeton N.J., Princeton University Press, 1954.
5. The Physiology of Hearing
I. C. Whitfield
Progress in Biophysics; Vol 8, 1957, pp 2-47
Also: The Auditory Pathway
Physiol. Soc. Monograph No. 17, Arnold, 1967, Autumn
6. Histology - Ch. 31 - The Ear
A. W. Ham
Pitman Medical Pub. Co. Ltd., London. Edition 5, 1965.
7. The Encyclopaedia Britannica 1968 Republication
"Ear" and "Hearing"
8. Experiments in Hearing
G. von Békésy
McGraw Hill. New York 1960

9. Measurement of basilar membrane vibration with the Mossbauer technique

A.J.F. Boyle and B.M. Johnstone.

Proc. of Physiol. Soc. November 1967.

Jnl. Physiol. 194, No. 86 P.

As the text was withheld by request of authors, a privately obtained abstract from the relevant meeting (courtesy of Dr. E.F. Evans, Dept. Communications, Univ. of Keele) is available.

Also: Science; Vol 158, 20th Oct 1967, pp 389-390.

10. Hairs of the Cochlear Sensory Cells and their Attachment to the Tectorial Membrane.

R.S. Kimura.

Acta Otolaryngologica Vol. 61. Fasc. 1-2. January 1966

pp. 55-72.

11. Fine Morphology of the Sensory Cells in the Organ of Corti in Man.

R.S. Kimura, H.F. Schuknecht, I. Sands.

Acto Oto-laryngologica. Vol.58. Fasc. 5. November 1964.

pp.390-408

12. Morphological Basis of Directional Sensitivity of the Outer Hair Cells in the Organ of Corti.

A. Flock et al

Jnl. Acoust. Socy. Am. Vol.34. No.9. Sept. 1962 - Part 2.

pp. 1351-1355.

13. Structure and Functions of the Sensory Hairs of the Inner Ear.

H. Engstrom, H.W. Ades, J.E. Hawkins

Jnl. Acoust. Socy. Am. Vol.34. No.9 September 1962 -

Part 2. pp. 1356 - 1367.

21. **A Model for Transducer Action in the Cochlea**
H. Davis.
Symposia on Quantitative Biology, Cold Spring Harbour,
Vol. XXX, 1965, pp. 181 - 190.
22. **Morphological Polarization and Orientation of Hair Cells in
the Labyrinth and Lateral Line Organ.**
A. Flock, J. Wersall.
Jnl. Cellular Biology. Vol. 15. 1962.
23. **Effect of High Intensity Noise on Inner Ear Sensory Epithelia**
H. Engstrom and H.W. Ades.
Acta Oto-Laryngologica. Suppl. 158. 1960. p.219.
24. **Exploration of Cochlear Potentials in Guinea Pig with a
Microelectrode.**
I. Tasaki, H. Davis, D.H. Eldredge
Jnl. Acoust. Socy. Am. Vol. 26. 1954. pp. 765 - 773.
25. **Les Mecanismes Fondamentaux..... de L'Epithelium Neuro-
Sensoriel des Recepteurs Vestibulaires - Symposium August 1960.**
Acta Oto-Rhino-Laryngologicum Suppl.163.
26. **Model of the Displacement between Opposing Points on the
Tectorial Membrane and Reticular Lamina**
W.S. Rhode and G.D. Geisler.
Jnl. Acoust. Socy. Am. Vol. 42. July 1967.
27. **Cochlear Response to Acoustic Transients.**
D.C. Teas, D.H. Eldredge, H. Davis.
Jnl. Acoust. Socy. Am. Vol. 34, No.9, Sept. 1962.
part 2. pp. 1438 - 1459.

28. Mechanism of Excitation of Auditory Nerve Impulses.
H. Davis,
included in, and including
Neural Mechanisms of the Auditory and Vestibular Systems
G.L. Rasmussen and W.F. Windle.
Thomas: Springfield, Illinois, U.S.A. 1960.
29. Auditory-Evoked Potentials from Cochlea to Cortex.
J.E. Desmedt.
Jnl. Acoust. Socy. Am. Vol.39. No.9. September 1962.
Part 2. pp.1478 - 1496
30. Auditory Intensity - Perception and Neural Coding.
R.A. Campbell
Jnl. Acoust. Socy. Am. Vol. 39, No.6, 1966, pp.1030-1033.

THEORIES OF HEARING
AND
COCHLEAR EXPERIMENTAL DATA

Chapter 2

Contents

I	Historical Development	Page 1
II	Recent Development	Page 4
IIa.	Place Theory	Page 4
IIb.	Frequency, Volley and Place-Volley Theories	Page 6
III	Cochlear Experimental Response Data	Page 9
IIIa.	Georg Von Bekesy	Page 9
	1) Cochlear Window Response	Page 9
	2) Cochlear Partition Response	Page 11
	(i) Place of Maximum Vibration	Page 12
	(ii) Distribution of Amplitude vs Place	Page 12
	(iii) Distribution of Amplitude vs Frequency	Page 13
	(iv) Phase Changes	Page 14
	(v) Non Linearities	Page 15
IIIb.	Boyle and Johnstone	Page 18
IV	Current Cochlear Theories	Page 19
IVa.	Ranke	Page 21
IVb.	Zwislocki	Page 25
IVc.	Peterson and Bogert	Page 26
V	References	Page 28

THEORIES OF HEARINGI Historical Development

With the beginnings of experimental research and human cadaver dissection in the Renaissance, the first anatomy-based theories of hearing were formulated, and it was as early as the 17th century that the inner ear was considered as the section of the ear appropriate to frequency discrimination. In the succeeding period the osseus spiral lamina, being still recognizable after the dissection techniques of the day, was attributed with the powers of a frequency selective mechanism, being hard, slender and brittle, and being a broad shelf at the basal end of the cochlea and narrower at the apical end. The locus of frequency response this implied, of low frequency tones causing a response at the basal end of the cochlea, is opposite in sense to modern theory, but as a theory of the peripheral analysis of sounds by resonance in the inner ear it is remarkable in that it was formulated two centuries before the revolutionary theory of cochlear resonance advanced in 1857 by Helmholtz.

For a comprehensive survey of theories of hearing up to Helmholtz' time, and beyond, Wever's book (Ref. 1) is recommended.

Helmholtz was particularly affected by the observation made by Ohm in 1843 that the ear was able to analyse complex sounds into a series of pure tones similar to the mathematical postulate by Fourier (1822). Having only meagre anatomical information on which to base his theory (which was the principle reason for the rejection

THEORIES OF HEARINGI Historical Development

With the beginnings of experimental research and human cadaver dissection in the Renaissance, the first anatomy-based theories of hearing were formulated, and it was as early as the 17th century that the inner ear was considered as the section of the ear appropriate to frequency discrimination. In the succeeding period the osseus spiral lamina, being still recognizable after the dissection techniques of the day, was attributed with the powers of a frequency selective mechanism, being hard, slender and brittle, and being a broad shelf at the basal end of the cochlea and narrower at the apical end. The locus of frequency response this implied, of low frequency tones causing a response at the basal end of the cochlea, is opposite in sense to modern theory, but as a theory of the peripheral analysis of sounds by resonance in the inner ear it is remarkable in that it was formulated two centuries before the revolutionary theory of cochlear resonance advanced in 1857 by Helmholtz.

For a comprehensive survey of theories of hearing up to Helmholtz' time, and beyond, Wever's book (Ref. 1) is recommended.

Helmholtz was particularly affected by the observation made by Ohm in 1843 that the ear was able to analyse complex sounds into a series of pure tones similar to the mathematical postulate by Fourier (1822). Having only meagre anatomical information on which to base his theory (which was the principle^{al} reason for the rejection

THEORIES OF HEARINGI Historical Development

With the beginnings of experimental research and human cadaver dissection in the Renaissance, the first anatomy-based theories of hearing were formulated, and it was as early as the 17th century that the inner ear was considered as the section of the ear appropriate to frequency discrimination. In the succeeding period the osseus spiral lamina, being still recognizable after the dissection techniques of the day, was attributed with the powers of a frequency selective mechanism, being hard, slender and brittle, and being a broad shelf at the basal end of the cochlea and narrower at the apical end. The locus of frequency response this implied, of low frequency tones causing a response at the basal end of the cochlea, is opposite in sense to modern theory, but as a theory of the peripheral analysis of sounds by resonance in the inner ear it is remarkable in that it was formulated two centuries before the revolutionary theory of cochlear resonance advanced in 1857 by Helmholtz.

For a comprehensive survey of theories of hearing up to Helmholtz' time, and beyond, Wever's book (Ref. 1) is recommended.

Helmholtz was particularly affected by the observation made by Ohm in 1843 that the ear was able to analyse complex sounds into a series of pure tones similar to the mathematical postulate by Fourier (1822). Having only meagre anatomical information on which to base his theory (which was the principle^{al} reason for the rejection

of the theory by many other theorists during the next 60 years) he believed that the changes in the dimensions of the cochlea from base to apex demonstrated the natural use of the principle of resonance. A series of independent, tuned elements, like piano strings of varying mass and tension, must, he said, be excited within the cochlea, and the rods of the tunnel of Corti were selected as being the most likely elements. Within 10 years the basilar membrane was sufficiently well charted as to replace the rods of Corti as being the seat of the principal resonating receptors, which remained as transversely tuned elements, lying between the bony shelf and the opposite wall of the channel. Helmholtz' mathematical analysis almost anticipated the findings of later workers, including Hensen in 1867, for he showed that if the basilar membrane was homogeneous, rather than a series of separate elements, then its resonance frequency response could not be sharp or precise. Wilkinson and Gray (Ref. 2) in 1924, on observing the variations in bulk of the spiral ligament, suggested that the variation in differential pull it would need to exert on the basilar membrane to attain a typical audio-frequency range response could certainly be accommodated by other human materials. Nevertheless, many other theorists preferred non-resonance theories, which did not rely on frequency discrimination by *place* along the cochlea. Even in the time of Wilkinson and Gray, which is the beginning of the modern cochlear theory era, the state of theories of hearing in this country was such that they discussed cochlear partition stiffness and mass under a heading *Theories which assume that sound is analysed in the cochlea.*

The most plausible original alternative to the resonance theory was offered by Rutherford (Ref. 3) in 1886. In the general

subdivision of all cochlea theories into two types, place theories and frequency theories, which subdivision persists sometimes to-day, Rutherford's was the classic telephone theory. He supposed that all hair cells could be stimulated by every sound and that individual frequencies were carried to the brain, but by using large numbers of cells there was a high sensitivity to change of wave form. Thus the character of a sound was assessed as the basis of a vibratory pattern. Although Rutherford himself yielded that there was some spatial frequency selectivity for high frequencies at the basal end of the cochlea (because of the severe demands his theory made on the transmitting properties of individual nerve fibres), several modified telephone theories followed. These included Ayers in 1892, Bonnier in 1895, Hardesty in 1908, for whom the tectorium was the responding mechanism, and Wrightson and Keith (Ref. 4) in 1918 in whose theory stapes pressures were communicated instantaneously to all parts of the cochlea and the whole basilar membrane moved simultaneously (Ref. 4). In these theories frequency analysis was therefore performed centrally rather than peripherally.

In 1898 Ewald stipulated a Membrane Resonance theory, better known as a Sound-Pattern theory, in which standing waves with characteristic shapes like Lissajous figures were set up in the cochlear partition and interpreted via hair cell action. This theory did not account for the analysis of complex sounds.

For a few years after 1900, the theories of Hurst, Meyer, ter Kuile and Watt were considered. These were non-resonant *travelling bulge* theories. Waves or bulges being induced in the basilar membrane travelled up the cochlea and were either reflected back from the apical end, or were damped before arriving at the

apical end. Sensory elements detected wave lengths of bulges or bulge extinction positions (see Hartridge and Banister, Ref. 5).

II Recent Development

IIa. Place Theory

During the past 40 years it has been agreed that any theory of hearing must include both the theory of cochlear dynamics and the train of neural events stimulated by cochlear mechanical response.

The place theory and the frequency theory are not yet wholly integrated; they are sometimes treated as competitive theories in the low frequency range, where it should be clear that either theory, as such, presents an excessive simplification of the means available to discriminate amplitude, frequency and phase.

In its simplest form, the place theory stipulates that receptors in a given part of the cochlea are stimulated by a given narrow band of sound frequencies, and those receptors set off impulses in the particular nerve fibres supplying them. The ability to discriminate frequency depends upon which receptors and nerve units are excited. Experiments conducted by von Békésy⁽⁶⁾ showed that the stiffness of the basilar membrane generally determines the stiffness of the whole cochlear partition, and that the membrane at rest is not in any significant state of tension. It does, however, decrease in elasticity from base to apex by some hundreds fold, and can not be considered similar to the Helmholtz model which consisted of large numbers of independent, transverse tuned resonators.

However, variations in mass and particularly elasticity displayed by the cochlear partition, considered as a homogeneous membrane, are clearly sufficient to provide frequency analysis in the cochlea, and the experimental techniques by which this has been confirmed include

- a) observation under the microscope of motions of intra-cochlear structures when the ear is stimulated by pure and compound tones (von Bekesy)
- b) examination of basilar membrane motions by the Mossbauer technique (Boyle and Johnstone⁽⁷⁾),)
- c) testing of hearing before and after experimental damage to parts of the organ of Corti
- d) recording of electrical activity (cochlear microphonics) from electrodes implanted at different points within the cochlea
- e) micro-electrode neuron action-potential studies in the spiral ganglion cells.

For example, the highest perceptible frequencies at weak intensities set into motion a small length of the basilar membrane and cochlear partition near to the basal (stapes) end of the cochlea. As sound intensity is increased at that frequency, there is some spread of activity along the basilar membrane and consequently more receptor cells and their nerve fibres are excited. Low frequency response (i.e. below 500 Hz) is considerably more widely spread (at the apical end of the cochlea) for sounds of low intensity near thresholds of perception, and for intense sounds there is some evidence to show that receptors over most of the cochlea respond.

There has always been a tendency to confuse place theory and resonance theory terminology. A place theory does not necessarily

require a condition of membrane partial resonance in order to fulfill the defined requirement that sensory cells in one area only are stimulated by any one pure tone.

It is probable that relations of phase or rate of change of phase with distance along the cochlea of the vibrating cochlear partition are, in some frequency ranges, more relevant to frequency discrimination by sensory cell and neural action than are maximal vibratory amplitude conditions. It has also been stressed by Zwislocki^(8, 9, 10) that the hydrodynamics of the cochlea complicate what often tends to be treated as the simple response of a lightly damped, single degree of freedom partition. Very complex phase-change relationships along the cochlea, giving rise to equally complex three dimensional shearing movements between the basilar membrane and the tectorium, are introduced to the excitation of a strongly damped membrane by travelling pressure waves, and the concept of resonance, particularly when a non linear dynamic system is involved, is inadequate for the description of sensory cell excitation zones.

I Ib. Frequency, Volley and Place-Volley Theories

Experiments have provided evidence not only in support of a place theory but also suggesting that frequency theory may be partly correct. When electrophysiological methods were used to record activity in the auditory nerve it was found that bursts of impulses in the whole nerve, which is made up of many thousands of fibres, were, as regards timing, synchronous in frequency with a pure tone applied to the ear; that is, for each cycle of the sound wave there

require a condition of membrane partial resonance in order to fulfill the defined requirement that sensory cells in one area only are stimulated by any one pure tone.

It is probable that relations of phase or rate of change of phase with distance along the cochlea of the vibrating cochlear partition are, in some frequency ranges, more relevant to frequency discrimination by sensory cell and neural action than are maximal vibratory amplitude conditions. It has also been stressed by Zwislocki^(8, 9, 10) that the hydrodynamics of the cochlea complicate what often tends to be treated as the simple response of a lightly damped, single degree of freedom partition. Very complex phase-change relationships along the cochlea, giving rise to equally complex three dimensional shearing movements between the basilar membrane and the tectorium, are introduced to the excitation of a strongly damped membrane by travelling pressure waves, and the concept of resonance, particularly when a non linear dynamic system is involved, is inadequate for the description of sensory cell excitation zones.

11b. Frequency, Volley and Place-Volley Theories

Experiments have provided evidence not only in support of a place theory but also suggesting that frequency theory may be partly correct. When electrophysiological methods were used to record activity in the auditory nerve it was found that bursts of impulses in the whole nerve, which is made up of many thousands of fibres, were, as regards timing, synchronous in frequency with a pure tone applied to the ear; that is, for each cycle of the sound wave there

was a burst of nerve impulses. This synchronism occurred for lower range frequencies only, up to 4000 Hz. For higher frequencies, synchronism between nerve response and stimulus could not be recognized.

Since the individual nerve fibres in the auditory nerve of the mammals used in these studies do not fire at rates beyond about 300 per second, the volley principle of Wever^(1, 1A, 11) was advanced to explain the firing of the total nerve in regularly spaced bursts at frequencies of 4000 or more per second. This principle assumes that impulses in some separate nerve fibres are elicited by the first wave of a stimulating tone, others by the second, and so on, the result being that, by the alternate firing of different groups of nerve fibres, the end result of synchronism between total nerve discharge and sound stimulus frequency is achieved.

This is an attractive theory at all frequency levels, particularly when the different groups of nerve fibres are attributed with their discrete anatomical spatial orientations, and may be married fairly naturally with the place theory. Two further points may be made in favour of such a place-volley theory

a) it provides a theory to explain one purpose for the somewhat puzzling complex of efferent fibres leading back to the hair all bodies. Several of to-day's neurophysiological investigators⁽¹²⁾ contend that some of the multiple synaptic junction inhibition of neural signals that goes to refine frequency discrimination is achieved at the hair cells rather than, as usually supposed, all in the spiral ganglion or cochlear nucleus. For example, nerve endings with a maximum nerve firing rate of 300 times per second terminating at hair cells being mechanically stimulated at 3000 Hz may be safely

inhibited by adjacent neural activity for all but (roughly) every tenth or twentieth cycle, then to be sufficiently stimulated by summing potentials to ensure a discharge on that cycle.

b) The instantaneously observed, longitudinally varying shape of the basilar membrane in an excited zone, and its so-called *travelling-wave* characteristics are imparted by the continual variation in phase of the responding membrane with distance along the cochlea.

This phase lag vs. distance characteristic is different for each frequency. Hence the instantaneous travelling wave deflected membrane shape occurring at one region differs from the wave shape occurring at another region due to a frequency shift. Consequently, a different *pattern* of hair cell stimulus results at each frequency shift, and even in the lower frequency range, when the spread of sensory cell activity is broad and the area of response loses definition, changes in sensory element stimulus patterns may still be recognized, and volley theory detection techniques remain partly in the domain of place theory for all but lowest frequencies.

It is clear that both place and frequency principles must be considered in explaining discrimination of sound frequency differences. In addition, auditory theory must account for discriminations involving intensity, phase and complex relationships between tones. It is currently understood that increases of pure tone intensity result in a spread of activity within the cochlea. More receptor cells are stimulated along the basilar membrane and nerve impulses are set off in more of the nerve fibres leading into the central nervous system. Also, experiments have shown an increase in the rate of firing of nerve fibres that are already active⁽¹²⁾. This relationship between stimulus intensity and rate of flow of

nerve impulses appears to be true for higher centres of the auditory nervous system as well as at the periphery.

III Cochlear Partition and Window Experimental Response Data

IIIa. G. von Bekesy⁽⁶⁾

In his most famous series of experiments conducted between 1924 and 1948 von Bekesy made observations and optical measurements of the patterns of vibration of the cochlear partition and cochlear membranes, in fresh preparations of the human ear, during stimulation by pure tones. To observe these patterns he drilled openings in the accessible portions of the bony walls of cochleas and cemented glass windows into these openings. These highly skilled and painstakingly developed techniques required that each cochlea-temporal bone preparation be mounted, prepared and examined immersed in a water tank and stroboscopes and microscopes were mounted directly above the exposed portions of cochleas in the tank. A brief outline of some of the experiments he performed and their results is given. (The dates in brackets give the year when the relevant work was first published.)

1) Cochlear Window Response (1942)

He excited by air-borne sound (pure tones) introduced into the meatus some eighty separate fresh, intact temporal bone specimens possessing normal eardrum, ossicles and cochlea, intending to measure the amplitude and phase response of cochlear fluids at the round

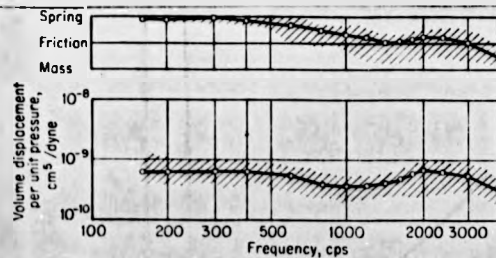
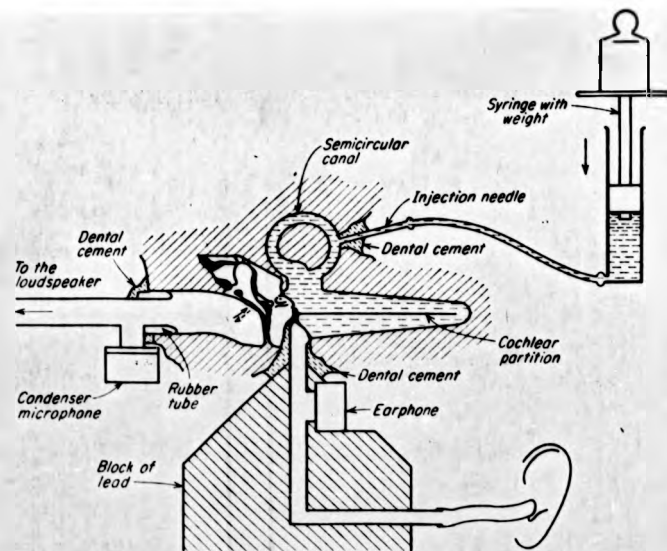
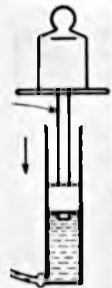


Figure 2-1 Diagrams illustrating von Békésy's experiments on the response of the round window membrane to sound. In the graphical diagrams, the upper curve shows the phase angle and the lower curve the volume displacement per unit of pressure (from Békésy, 1960)

window. A plan of the technique and a plot of results obtained are given in Fig. 1.

These unique results by Bekesy contain certain implicit deficiencies. Firstly, his oval window was excited by sound pressures and neither the oval nor the round window displacement responses were ever ascertained as such: phases of sound pressures generated outside the cochlea round window were discovered by a sound interference technique employing an additional earphone sound generator. Hence round window-excited air pressure waves would have been in advance of round window displacements by a phase angle, ϕ_1 , of very nearly 90° , and the round window displacements would, at low frequencies, have lagged behind oval window displacements by about 180° , this angle, ϕ_2 , depending on compressibility effects. Also at low frequencies the angle ϕ_3 by which malleus and eardrum displacements lagged behind driving pressures at the eardrum would be in the order of 90° . Another phase lag, ϕ_4 , almost certainly occurs in the middle ear, particularly at higher frequencies, when the middle ear mechanism is known to present a somewhat complex transfer function. The phase lag, ϕ_5 , between driving pressures at the oval window and the displacement response of the stapes footplate, which angle describes the input impedance of the whole inner ear system, is not known.

It could be argued that this angle ϕ_5 may approach π radians when high frequency inertia effects predominate, and $\frac{\pi}{2}$ when fluid viscosity effects become most significant for large amplitude inner ear excitation. At low frequencies, if oval and round windows were sufficiently stiff, the angle could approach zero. At the same time, when the oscillating oval window is considered as primarily inducing



esy's
f the
the
hows
he
ure

transverse wave motion in the cochlear partition, and is compared with a surface wave-making piston at the end of a long channel, the angle ϕ_5 could approach $-\frac{\pi}{2}$.

Therefore, if ϕ_R is the phase of round window motions with respect to original sound pressure variations in the meatus, then

$$\phi_R = \phi_2 + \phi_5 + \phi_4 + \phi_3$$

whereas the *overall* phase lag, ϕ_B , recorded by Bekesy, is evidently

$$\phi_B = \phi_R + \phi_1 = \phi_1 + \phi_2 + \phi_3 + \phi_4 + \phi_5$$

As is shown in a later chapter, a good estimate of phase angles ϕ_2 and ϕ_5 in particular is required in order to check solutions to cochlear mathematical models. It is clear that such data cannot reasonably be extracted from these tests by Rekesy.

2) Cochlear Partition Response

By grinding away part of the apical bone surround, Bekesy was able to expose, section by section, nearly half of the cochlea, and with an underwater microscope and adjacent stroboscope illumination, he viewed motions of the basilar membrane, looking through Reissner's membrane. For these experiments an electro-mechanical vibrator drove an artificially built up oval window membrane, the middle ear having been removed from each specimen. The series of experiments was repeated, much improved, twice, some years later and data are included herein.

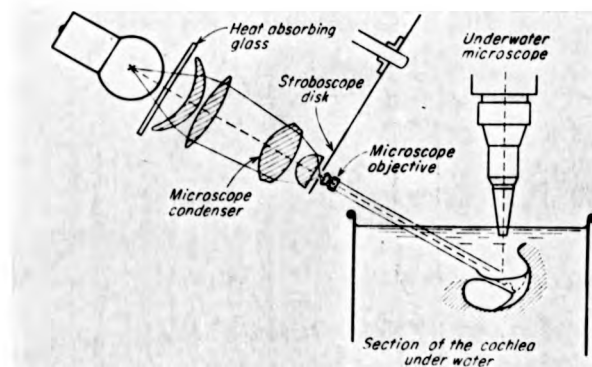


Figure 2-2a Diagram illustrating von Bekesy's method of stroboscopically illuminating and inspecting cochleas (from Bekesy, 1960).

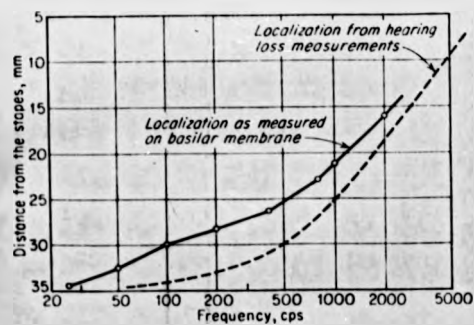


Figure 2-2 Graphical results of a comparison by von Bekesy of the place of localization of tonal action of the basilar membrane as observed directly and as derived from measurements of hearing loss. (from Bekesy, 1960).

(i) Place of Maximum Vibration in the Cochlea (1942)

Using a microscope condenser lens, light was so concentrated that, in the plane of a rotating stroboscopic disc a beam of 0.1 mm diameter was achieved, and light rays progressing into the examination tank were made parallel by a microscope objective lens (Fig 2A). Starting examination from the apical end, very close to the helicotrema, sound excitation frequencies were adjusted until the fine area of basilar membrane being microscopically viewed responded maximally, and the spot location and the appropriate frequency were noted. Bekesy's published result is given as Figure 2. Using this technique of exposing the cochlea, it was not possible to investigate basilar membrane response in the basal half of the cochlea.

(ii) Distribution of Amplitude along the Cochlear Partition
as a Function of Frequency and Place (1943)

Again, despite the experimental expertise, only the apical turn, representing a distance of from 27 to 35 mm from the stapes, could be exposed to microscopic examination. In order to expose more basal areas, the apical end of the cochlea under test had to be completely ground away.

Over a fairly wide range of vibration input amplitudes, Bekesy noted that the amplitude of vibration of the cochlear partition, as observed at any particular point, increased in proportion to the amplitude of vibration of the vibrator system.

At frequencies below about 30 Hz, the whole partition near the

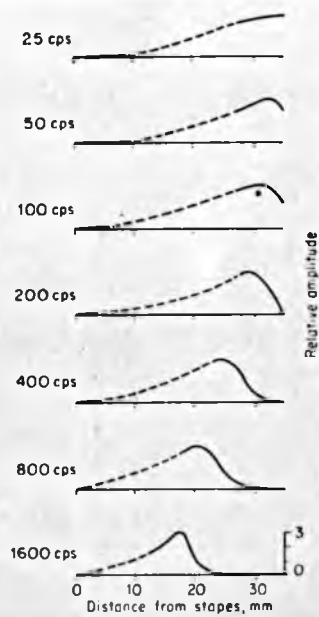


Figure 2-3 Patterns of vibration of the cochlear partition as measured by von Békésy on cadaver specimens for various frequencies, showing relative amplitude envelopes as a function of place along the cochlea. (from Békésy, 1960).

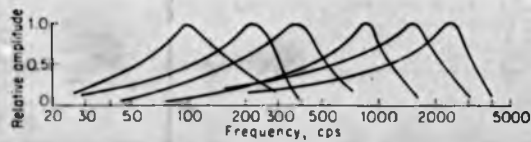


Figure 2-4 Forms of resonance curves for six positions along the cochlear partition as measured on cadaver specimens (from Békésy, 1960).

helicotrema vibrated with almost uniform amplitude and phase. As the frequency was raised partition motions receded from the area of the helicotrema until, at frequencies above 800 Hz, no further vibrations could be induced in the exposed spiral.

The measured amplitudes of vibration were expressed in volume displacements per millimetre of length of the partition. Bekesy's published results are shown in Figure 3, but his ordinate scale, expressing the above units, is apparently arbitrary. Amplitudes were measured from millimeter to millimeter along the partition. The figures display broken lines on the basal side of each maximum. Here the investigator had to take excessive measures in shortening each specimen from the apical end in order to make access to the basal regions. Subsequent model tests showed that readings thereby made when a normally active part of the cochlea, which was still displaying fluid motions, was apically truncated were only slightly in error.

(iii) Resonance Curves - Amplitude as a function
of frequency (1943)

Tests were repeated using a considerably more difficult technique to expose parts of the cochlear partition for frequency response examination. Only six points, in the apical half, were examined, but for each the response to a large number of different frequencies up to 4 KHz were obtained, vibration input intensity being kept constant. Again absolute values of amplitude are not recorded. Bekesy notes that the many different specimens tested all gave strikingly similar response curves. These are shown in Figure 4.

(iv) Phase Changes along the Basilar Membrane

Probably the most highly valued of all of Bekesy's experimental data is contained in a paper published in 1947 in which the shape of the travelling waves excited on the basilar membrane is described by means of phase delay diagrams.

The hypothetical test which theorists of his time required Bekesy to perform, the terms of which are frequently mis-understood to-day, was to investigate whether elements of the cochlear partition, which were and are frequently considered to behave like separate resonant elements, displayed a phase lag relative to the driving force of up to π radians as driving frequency was changed continuously.

Thus this phase test was supposed to ascertain whether or not any element of the cochlear partition

- a) could be considered as a single degree of freedom system
- b) displayed resonance, or, in the event that damping was greater than critical, at least displayed a phase change of about π .

In fact, the angle of phase at which elements of the partition vibrated changed, for most elements, by 3π or 4π radians. This fact has frequently confused the situation, and as a result of this apparently excessive phase variation, the concept of partition element resonance has been queried. The main point that should be made at this stage is simply that this data does not invalidate the single degree of freedom element-of-partition concept. As the chapter describing a theoretical model illustrates, the phase of the partition-exciting pressure difference between the two scalae itself

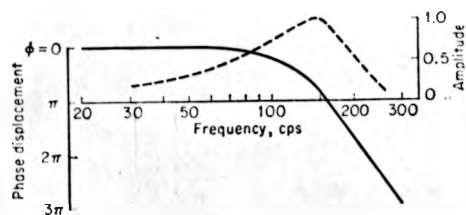


Figure 2-5 Phase displacement relative to stapedial motion (solid line) and resonance curve (dashed line) for a point on the cochlear partition 30 mm. from the stapes. (from Bekesy, 1960).

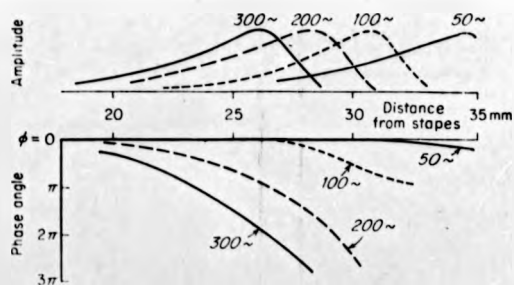


Figure 2-6 Phase lag and relative amplitude envelopes for four low frequency tones (from Bekesy, 1960).

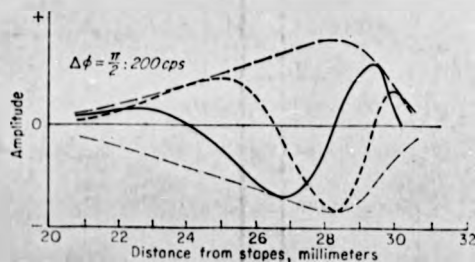


Figure 2-7 Detail of the form of vibration of the cochlear partition showing two instantaneous shapes of the travelling wave occurring at 200 Hz. The two instants are 1/4 cycle or 1/800 sec. apart (from Bekesy, 1960).

constantly changes with distance along the cochlea.

Bekesy's cochlear partition phase change data are both unique and authoritative, and are presented in Figures 5, 6 and 7. For several reasons involving his complicated and difficult experimental technique, Bekesy favours the result for 200 Hz as being less subject to experimental error than results at higher frequencies. Note that the instantaneous travelling wave shape shown in Figure 7 is obtained directly from the data for 200 Hz in Figure 6.

Based on figure 6, the following figures give the approximate phase angle of partition vibration, relative to the motion of the stapes, at the point of maximum amplitude. Loci of maximum amplitude compare approximately with those shown in Figure 2.

<u>Frequency Hz</u>	<u>Distance from Stapes, mm</u>	<u>Phase Angle degrees</u> <u>relative to stapes motions</u>
50	34.4	36
100	30.8	120
200	28.2	284
300	26.3	340

(v) Non Linearities in the Vibration of the

Cochlear Partition (1947)

Bekesy attempted to determine whether one physiological non-linear effect, that pure tones below 800 Hz become lower in apparent pitch when loudness is increased, could be ascribed to the cochlea.

A point 30 mm from the stapes was observed in the same series

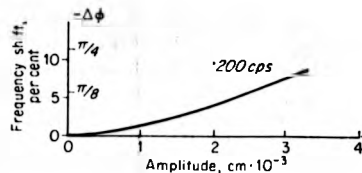


Figure 2-8 The effect of sound intensity on the position of the maximum amplitude response along the cochlear partition. The ordinate shows the percentage of change in frequency necessary to keep the response pattern in one place as sound intensity was changed. The frequency shift is also expressed as a phase change. (from Békésy 1960)

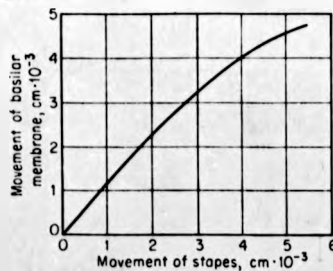


Figure 2-9 Amplitude of Vibration of the basilar membrane as a function of stapedia amplitude measured at a point 30 mm from the stapes with an intense tone of 200 Hz. (from Békésy, 1960).

of experiments as described in section (iv) above, and the phase angle of partition response at this point relative to the stapes was measured for several different amplitudes. He showed that with increasing amplitude (and it must be noted that he was already dealing with large amplitudes of the order of 10^{-3} cm, corresponding to extremely intense sounds of the order of 120 to 140 db.) the observed phase angle lag, relative to stapes motions, decreased; that is, wavelengths local to the 30 mm point became larger. Bekesy particularly noted that the pattern of partition vibration was displaced towards the helicotrema, corresponding in terms of sensory cell and neural element excitation to a lowering of perceived pitch. This result is reproduced as Figure 8.

In terms of the response of single degree of freedom systems, this clearly indicates a *hardening spring* effect, which is a theme taken up in another chapter.

Bekesy expected that, in the event of the cochlear partition possessing a non linear hard spring stiffness characteristic, the ratio of basilar membrane maximum amplitude to stapes amplitude at any fixed frequency (200 Hz) would decrease as stapes amplitudes increased. This he showed to be the case (Figure 9).

No similar data exists for sounds at other frequencies, and in view of the limiting of this perceived pitch-loudness effect to sounds below 800 Hz, it was believed that this non linear effect is confined to the apical half of the cochlea. However, modern evidence from the most recent neurophysiological research and from cochlear electrophysiological experiments suggests that the cochlea may display similar intensity non-linearities over all of its frequency

4
 intensity on the
 amplitude
 position. The
 change in
 response
 intensity was
 also
 from Bekesy 1960)

the basilar
 stapedial
 mm from the
) Hz.

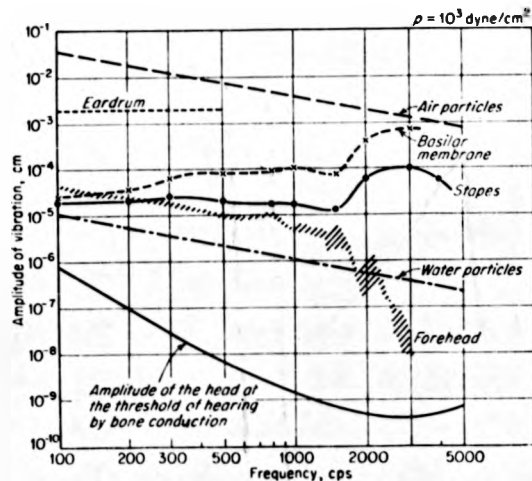


Figure 2-10 Upper six curves show von Békésy's estimations of amplitudes of vibration of the human head, eardrum, stapes, basilar membrane and air and water particles for a sound pressure of 10^3 dynes/cm² (134db.) Lower curve shows the amplitude of vibration of the skull at the threshold of hearing by bone conduction. (from Békésy, 1960).

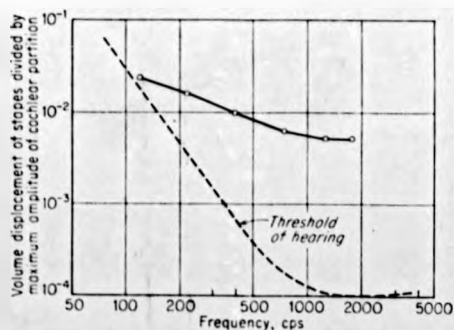


Figure 2-11 Curve showing von Békésy's estimate of the ratio between the volume displacements of the stapes and the maximum amplitude of the cochlear partition as a function of frequency (solid line). The broken line is merely an attempt by von Békésy to represent, on the same quantitative graph, the subjectively-determined threshold of hearing, in order to indicate that a stronger dependence of auditory threshold on frequency must obtain in the cochlea than the solid line would indicate. (from Békésy, 1960).

range. This view was recently expressed by Dr. Hallowell Davis at the IX International Congress of Audiology, London, 15th-19th September 1968. It has also been implied in several papers published in the Journal of the Acoustic Society of America during the last 18 months.

Finally Figure 9 touches on the subject of the frequency response of the basilar membrane in terms of the magnitude of its vibration as a function of stapes amplitude and frequency. It would be expected from Figure 9 that at 200 Hz, and at low amplitudes, there is a ratio of about unity between partition and stapes amplitude. This is roughly borne out by a diagram published by Bekesy in 1948, reproduced as Figure 10, and applicable only to intense sounds (134 db.). Figure 10 also shows that, at 134 db, the same ratio approaches 10 for frequencies above 1 KHz.

Figure 11 data, based on Bekesy's 1943 experiments, may be extrapolated for a stapes footplate area of about 3 mm^2 to give a ratio of partition to stapes amplitude of about 1 at 100 Hz, 6.5 at 1 KHz and 10 at 10 KHz. In a much more recent review paper, published in 1952, Bekesy admitted that, at the time the experiments reported were performed, there was little concern with the amplitude of movements, and that most of the appropriate experimental data he published referred to the case when the cochlea was under intense stimulation, at about 130 db.

It follows, therefore, that in the likely event of there being non linear effects always present in cochlear dynamic responses, the Bekesy results discussed above, especially data giving basilar membrane to stapes amplitude ratios, may be misleading at moderate

sound intensity levels.

As is evident from succeeding sections and chapters, no cochlear mechanics investigator since Bekesy has admitted either to this possibility, or to the probable non-linear nature of the response of the cochlear partition. Every theoretical model proposed for the cochlea has assumed a wholly linear cochlear partition stiffness. For low sound intensity levels and small partition displacements, this assumption is probably very reasonable, provided that realistic linear stiffness terms are employed. However, neither Bekesy's cochlear dynamic response data, with which the response of mathematical models has always been compared, nor Bekesy's cochlear partition static stiffness data, from which linear and non linear stiffness terms must be derived, is appropriate to small partition displacements.

IIIb. Boyle and Johnstone⁽⁷⁾

Boyle and Johnstone have made a successful application of the Mossbauer technique to experimental determination of the pattern of vibrations of cochlear partitions. Unlike Bekesy, they gave attention to the measurement of absolute values of membrane amplitudes of vibration. Their experiments were all conducted on guinea pigs.

Their only reported measurements were carried out at a point very near to the basal end of the cochlea, at a distance of 1.5 mm from the stapes. This, for the guinea pig as well as for the human, is a high audio frequency response area, as compared with all of Bekesy's results in the second and third turns of the cochlea. They

were also able to conduct reasonable tests at other than intense amplitudes: their technique permitted measurement of velocities of the order of 0.1 mm/sec, corresponding to peak amplitudes of only 7 \AA for a 20 kHz pure tone.

Basilar membrane tuning curves plotted for the 1.5 mm point showed a maximum amplitude occurred at that point at between 18 and 21 kHz. Boyle and Johnstone also estimated that basilar membrane peak amplitudes were about 50 times greater than the corresponding stapes amplitudes. This is significantly greater than the ratio of about 10 for partition to stapes amplitude for human cochleas extrapolated by Bekesy from his own low frequency data.

Tuning curves obtained resemble those by Bekesy (Figure 4) but are considerably more sharply peaked. Some response of the partition at the point at which the experiments were conducted was obtained for frequencies as low as 350 Hz. No details of the phase of vibration of the partition with respect to the motions of the stapes are presented by Boyle and Johnstone.

IV Current Cochlear Theories

During the past thirty years there have been about a dozen serious attempts to formulate mathematical theories yielding reasonable solutions to cochlear dynamic frequency response. These are engineers' theories, concerning themselves with both hydromechanics and system dynamics, and many of them are important stages or landmarks in the formerly uncharted plain of cochlear applied mathematics. Most of the semi-mathematical models whose originators are set out

below are referred to or discussed in this chapter and in following chapters and from the fact that these theories are listed in chronological order it should not be inferred that the most recent theories are always the most advanced or the most accurate:

Kucharski	1930
Ranke	1931, 1934, 1935
Reboul	1938
Ranke	1942
de Rosa	1947
Zwislocki	1948 ⁽⁸⁾
Ranke	1950 ⁽¹³⁾
Zwislocki	1950 ⁽⁹⁾
Peterson and Bogert	1950 ⁽¹⁵⁾
Fletcher	1951 ⁽¹⁴⁾
Zwislocki	1953 ⁽¹⁰⁾
Hause	1963 ⁽¹⁶⁾
Klatt	1964 ⁽¹⁷⁾
Klatt and Peterson	1966 ⁽¹⁸⁾
Huxley	1969 ⁽¹⁹⁾

The most outstanding of these contributions are probably those of Ranke, Zwislocki and Peterson and Bogert. These works are briefly discussed in this chapter. Note that the excellent contributions made by several other well known cochlear response investigators, particularly Flanagan and also Siebert and Greenwood, are not discussed in this review. Their studies did at no time involve analysis of equations of motion or first-principles synthesis of mathematical models of the cochlea, but were rather restricted to extrapolative, empirical logic, based on the classical von Békésy experimental results, for approximate

prediction of basilar membrane response patterns under conditions not investigated by Bekey. Doubtless the type of computer simulations of basilar membrane displacement developed by Flanagan (1958-1964) involving impulse response functions rigorously derived from the experimental data, will prove an invaluable means of refining cochlear response theory when the data which they extrapolate have been verified, improved, and extended. However, up to the present time this type of approach has apparently stimulated no further development and has aroused little interest compared with the engineering theories of cochlear mechanics.

a. Ranke

Ranke was the originator of modern hydrodynamical cochlear theory, although in his writings he criticises the suggested application of fluid wave equations by Frank (1926) to solve cochlear behaviour. Ranke's first preoccupation in all of his publications concerns the pressure force - inertia *momentum* equation of fluid motion, applied to the longitudinal direction of perilymph displacement along the two main channels or *scalae* of the cochlea. In 1931 he first drew attention to the fact that the neglect of transverse fluid motion in a *scala*, particularly in an area of the *scala* adjacent to large transverse amplitudes of cochlear partition vibration, in favour of longitudinal fluid motions was not necessarily valid, despite its mathematical convenience. He introduced the concept, later taken up by Zwislocki, of water waves propagating under deep and shallow conditions. A wave length which is long compared to the depth of water in which it propagates he called a shallow-water wave, as assumed to invariably apply in the cochlea

by Frank and Kucharski and all other authors since, and typical deep water waves (Ranke waves) he defined as those of relatively high frequency and of short wavelength compared with depth. In the extreme case of very small depth, h , the velocity of propagation c (of shallow water waves) is

$$c = \sqrt{gh}$$

which is independent of frequency and wave length, while for deep water waves

$$c = \frac{g}{2\pi f} = \sqrt{\frac{g\lambda}{2\pi}}$$

where c depends on frequency f or wave length λ . As the point of transition between these two types of waves occurs when

$$\frac{\lambda}{2\pi} = \frac{c}{2\pi f} = h$$

then, if the mean depth of a cochlear scala from its partition interface (representing a free wavy surface) is about 0.1 cm, the wave type transition occurs when frequency $f = \frac{10c}{2\pi}$ Hz where c is the wave propagation velocity in cm/sec. According to Bekesy's data, c is about 100 cm/sec at the area of maximum partition amplitude for a 200 Hz tone, and decreases on the helicotrema side of the maximum response area.

At the time he began his studies on the cochlea, Ranke was alone among scientists in attempting to contradict the theory of cochlear frequency discrimination by resonance. In 1935 he devised a mathematical solution for *deep-water* fluid wave motion, taking into account fluid wave motion in two simultaneous directions, which he made integral with an approximate solution to cochlear mechanics published in 1942. Here he used lumped elastic constants to describe the cochlear partition. He solved the Navier equations of fluid

motion for a two-dimensional case, neglecting fluid friction, and with equations thus simplified applied a velocity potential field approach. He treated the cochlea spiral as an unwound pair of channels, and took into account the mass, elasticity and damping of the cochlear partition. He assumed that the natural (resonant) frequency of narrow, unloaded, sections of the partition, (without the surrounding liquid) decreases exponentially from base to apex, and that the membranes were uniformly damped at all sections. He realized that there must be equilibrium at every instant and at every section between the force of the liquid and the forces of and within the membrane.

The final 1950 Ranke results⁽¹³⁾ for partition dynamical response compared remarkable well with the Bekesy data as regards the shape of the relative amplitude envelope, although details of how he selected such vital physical variables as partition stiffness in order to achieve this degree of matching are somewhat obscure by virtue of the difficulty of making total translations of his papers from the German. The fact remains that his physical constants are not based on Bekesy's or any other direct static measurements. The locations of his calculated response areas along the cochlea as a function of frequency are roughly in agreement with Bekesy's data, but a serious deficiency lies in his phase characteristic as a function of distance. Ranke's short wave theory necessarily resulted in a decrease of partition travelling wave velocity as the point of maximum partition amplitude of vibration was approached and passed, followed first by an area of minimum wave velocity at a short distance beyond the maximum amplitude point and then by a rapidly recovering wave velocity.

motion for a two-dimensional case, neglecting fluid friction, and with equations thus simplified applied a velocity potential field approach. He treated the cochlea spiral as an unwound pair of channels, and took into account the mass, elasticity and damping of the cochlear partition. He assumed that the natural (resonant) frequency of narrow, unloaded, sections of the partition, (without the surrounding liquid) decreases exponentially from base to apex, and that the membranes were uniformly damped at all sections. He realized that there must be equilibrium at every instant and at every section between the force of the liquid and the forces of and within the membrane.

The final 1950 Ranke results⁽¹³⁾ for partition dynamical response compared remarkably well with the Bekesy data as regards the shape of the relative amplitude envelope, although details of how he selected such vital physical variables as partition stiffness in order to achieve this degree of matching are somewhat obscure by virtue of the difficulty of making total translations of his papers from the German. The fact remains that his physical constants are not based on Bekesy's or any other direct static measurements. The locations of his calculated response areas along the cochlea as a function of frequency are roughly in agreement with Bekesy's data, but a serious deficiency lies in his phase characteristic as a function of distance. Ranke's short wave theory necessarily resulted in a decrease of partition travelling wave velocity as the point of maximum partition amplitude of vibration was approached and passed, followed first by an area of minimum wave velocity at a short distance beyond the maximum amplitude point and then by a rapidly recovering wave velocity.

In this his final contribution to cochlear hydromechanics, Ranke made one innovation, namely, that there are no pressure wave reflections within the scalae during normal inner ear excitation. He had previously hypothesized on there being a strong wave reflection near to the point of maximum amplitude of vibration of the partition, occurring at the place where waves had ceased to be long in comparison with the dimensions of the cochlea. In his 1950 paper, however, he considered that long wave equations were inadequate in this region, and he used more complex equations appropriate to short waves. Thus the strength of his approach lies in the fact that, purely from a hydrodynamic point of view, short waves propagate along the cochlear canal and reach a maximum amplitude at a point dependent upon frequency.

The essential weakness in his theory is assessed from his partition travelling wave propagation velocity results. Both model test data and experimental *in vitro* cochlear test results by Bekesy confirm that wave velocities display no minima for any but (possibly) very low frequency tones, and on the helicotrema side of the maximum amplitude region, partition wave velocities and wave lengths continue to decrease, giving rise to a continually increasing phase lag for partition vibrations.

Physical model tests performed for and reported in this thesis also strongly reinforce Bekesy's results in this regard.

b. Zwislocki

Zwislocki's 1953 paper⁽¹⁰⁾ is invaluable as a review of his own work and that of Ranke⁽¹³⁾, Kucharski, Reboul, Peterson and Bogert⁽¹⁵⁾ and Fletcher⁽¹⁴⁾.

His own analyses of cochlear dynamics are contained in his 1948⁽⁸⁾ and 1950⁽⁹⁾ papers.

While Ranke's main contribution was to draw attention to the hydrodynamic response of the cochlea and the possibility of short, *deep-water* wave motion, Zwislocki concentrated on proving that the so-called cochlear resonators were in fact highly damped; viscous damping effects were shown to have a most significant effect on partition travelling wave response. He therefore classified his theories (and those of Ranke, who attempted to include damping in partition dynamics equations) as non-resonance theories, being superior to all other (resonance) theories.

A resume of his solution is given in Appendix I of this chapter. His results are very similar in nature to Bekesy's in all respects. However he did not attempt to reduce the limited data on cochlea physical properties to more than order of magnitude accuracy, nor did he estimate any detailed transverse shapes of the deflected basilar membrane upon which shapes hair cell shearing actions must be based. In his later equations he also ignored perilymph viscosity and compressibility. He ignored mass and damping variations for the cochlear partition, assumed linear elasticities, and did not consider longitudinal stiffness or the restraints applied to elements of the partition by neighbouring elements. He did not allow for cochlear

duct sectional area variations in his numerical solutions. It is difficult to re-apply his expressions, especially the more complex ones, and it is also difficult to extract information other than partition response, for example, round window response and oval window impedance, from his relationships. Nevertheless, his theories and reviews have, up to the present time, contributed far more complete an understanding of the nature and reasons for non-resonance, damped, cochlear partition travelling waves, which display a discrete amplitude maximum, than have any other theoretical solutions.

It is unfortunate that no investigator has expanded or improved upon Zwislocki's work. This may be partly due to some difficulty in reading his (and Ranke's) publications and partly to occasional lack of clarity in his mathematical logic.

c. Peterson and Bogert

The single paper published by Peterson and Bogert⁽¹⁵⁾ is particularly easy to read, and of the treatises mentioned in this review, presents the most obviously plausible approximate solution to linear cochlear dynamical theory. The authors developed a formulation similar to those of Ranke and Zwislocki, but with fewer geometrical and physical simplifying assumptions. They conceived of two compressional pressure waves travelling at high speed up the cochlea, one in the scala vestibuli and the other in the scala tympani. The resulting cyclic pressure difference between these waves at sections along the cochlea caused a partition displacement wave which propagated at relatively low speed.

Despite the clarity of their mathematical model, they were restricted in the complexity of the situations for which numerical solutions were required by not having, at that time, access to an electronic computer. In particular, they were obliged to omit damping terms from cochlear partition dynamic equations. A summary of and further comments on Peterson and Bogert's theory is given in Appendix II of this chapter.

REFERENCES

- 1 Theory of Hearing
E. G. Wever
Wiley, New York, 1949
- 1A Physiological Acoustics
E. G. Wever and M. Lawrence
Princeton N. J., Princeton University Press, 1954
- 2 Mechanism of the Cochlea
G. Wilkinson and A. A. Gray
Macmillan 1924 London
- 3 A New Theory of Hearing
W. Rutherford
Journal Anat. Physiol 21, 1886, pp 166-168
- 4 The Analytical Mechanism of the Internal Ear
Sir Thomas Wrighton, M.I.C.E., Bart, and
Arthur Keith, M.D., F.R.S.
Macmillan 1918 London
- 5 Hearing.— H. Hartridge and H. Banister
Chapter 7 of Foundations of Experimental Psychology
Carl Murchison 1929 London
- 6 Experiments in Hearing
Georg von Békésy
McGraw-Hill New York 1960

- 7 Basilar Membrane Vibration Measured with the Mossbauer Technique
A. J. F. Boyle and B. M. Johnstone
Proceedings of the Physiological Society 10-11 November 1967
Jnl. Physiology; 1968; 194; 86 P (full paper not published)
Also: Science Vol 158, October 1967, pp 389-390
- 8 Theorie Der Schneckenmechanik
J. Zwislocki-Moscicki
Acta Oto-Laryngologica Suppl. 72 1948
- 9 Theory of the Acoustical Action of the Cochlea
J. Zwislocki
Jnl. Acoust. Socy. Am. Nov 1950, Vol 22, No. 6, pp 778-784
- 10 Review of Recent Mathematical Theories of Cochlear Dynamics
J. Zwislocki
Jnl. Acoust. Socy. Am. July 1953, Vol 25, No. 4, pp 743-751
- 11 The Physics of the Ear
T. S. Littler
Pergamon Press Ltd. 1965 Oxford
- 12 The Physiology of Hearing
I. C. Whitfield
Progress in Biophysics Vol 8 1957 pp 2-47
Also: The Auditory Pathway
Physiolog. Socy. Monograph No. 17
Arnold 1967
- 13 Theory of Operation of the Cochlea : Contribution to the
Hydromechanics of the Cochlea
O. F. Ranke
Jnl. Acoust. Socy. Am. Vol 22, 1950, pp 772-777

- 14 On the Dynamics of the Cochlea
H. Fletcher
Jnl. Acoust. Socy. Am. Vol 23, 1951, No. 6, pp 637-645
- 15 A Dynamical Theory of the Cochlea
L. C. Peterson and B. P. Bogert
Jnl. Acoust. Socy. Am. Vol 22, May 1950, No. 3, pp 369-381
- 16 Digital Simulation of the Cochlea
A. D. Hause
Bell Telephone Labs. Inc. N.J. Report MH-1276-ADH, 1963
Summary in Jnl. Acoust. Socy. Am. Vol 35, Nov 1967, No. 11 P 1896
- 17 Theories of Aural Physiology
D. Klatt
Univ. Mich. Commun. Sci. Lab. Rept. No. 13, Nov 1964
- 18 Re-examination of a Model of the Cochlea
D. H. Klatt and G. E. Peterson
Jnl. Acoust. Socy. Am. No. 40 Jan 1966 No. 1 pp 54-61
- 19 Is Resonance Possible in the Cochlea After All?
A. F. Huxley
Nature Vol 221 March 8th, 1969, pp 935-940

APPENDIX 2-I

SUMMARY OF ZWISLOCKI'S COCHLEAR THEORY^(8,9)

From the basic equations of fluid mechanics, assuming partition waves are long with respect to the depth of the cochlear ducts, Zwislöcki deduced a dynamic differential wave equation containing, he claimed, all of the factors which influence the process of vibration:-

$$\frac{\partial^2 p}{\partial x^2} = 2 \frac{\rho}{F_0 J} \frac{\partial p}{\partial t} + 2 \frac{R_1}{F_0 J} p$$

where x is the distance from stapes, t is a co-ordinate of time, p is the instantaneous pressure difference between the two scalae at distance x , ρ is the fluid density, R_1 is the coefficient of fluid friction of perilymph per unit length of a scala, F_0 is the mean cross sectional area of the scalae and J is the impedance of the cochlear duct per unit length.

For the compliance C , of the cochlear partition (inverse of elasticity), at any section x , he derived the following expression from Bekeasy's static pressure test data:-

$$C(x) = C_0 \exp(\beta x)$$

where C_0 is the compliance at the stapes end and the dimensions of length units are cm, with $\beta = 1.5$ per cm. The general impedance of the partition, J , becomes

$$J = R_2 + j \left[w \zeta - \frac{1}{w C_0} \exp(-\beta x) \right]$$

where R_2 is a friction or damping coefficient, ζ is the effective mass of the partition, both functions of x , and w is the angular frequency.

The general wave equation then becomes

$$\frac{\partial^2 p}{\partial x^2} = \frac{2}{F_0} \frac{(R_1 + j w \rho) p}{(R_2 + j(w \zeta - \frac{1}{w C_0}))}$$

When friction coefficients and mass are eliminated, the solutions to the resulting equation:-

$$\frac{\partial^2 p}{\partial x^2} + p w^2 \frac{2 \rho C_0}{F_0} \exp(\beta x) = 0$$

represent Bessel functions, which, together with the ends-of-scalae boundary conditions, generate standing waves in the cochlear partition, whose wave lengths, velocities of propagation and pressure amplitudes decrease towards the helicotrema, and whose displacement amplitudes go on increasing.

If friction only is eliminated, the relations become:-

$$\frac{\partial^2 p}{\partial x^2} = \frac{2 w^2 \rho}{F_0 \epsilon (w^2 - \frac{1}{\epsilon c})} p$$

$$\lambda = \frac{1}{2 \pi \sqrt{\epsilon c}}$$

$$x = \frac{1}{\beta} (\log_e \frac{1}{4 \pi^2 \epsilon c_0} - 2 \log_e \lambda)$$

when resonance may occur if the denominator of the first equation equals zero, that is, if

$$w^2 = \frac{1}{\epsilon c}$$

and then λ gives the corresponding resonance frequency and the lower equation gives the location of the resonance.

However, argued Zwislocki, for either linear or non-linear dynamic systems, the maximum amplitude of vibration cannot occur at the location of resonance as derived above, but when damping is present will occur towards the region of higher elastic impedance. The greater the damping the greater the shift of the maximum oscillation from the site of resonance. Therefore, with sufficient damping a state of resonance is not essential for the production of an area of maximum oscillation.

Having illustrated the influence of the various cochlear component mechanical properties on the type of response obtainable, whether standing waves or a resonant condition, Zwislocki observed that the elasticity (or stiffness) of the partition decreases rapidly with increase of distance from the stapes, while (he considered) mass, friction and damping remain approximately constant. Because the damping is,

presumably, large, maxima of vibration will occur distantly from the locus of resonance in a section of the cochlear duct in which its inertia force plays no essential part with regard to other forces of motion.

On these grounds he offered an approximate solution, in which mass was eliminated, to his original wave equation:-

$$p = B H_0^{(2)} \left\{ \left[1 - j(\omega R_2 C_0 \exp(\beta x) + \frac{R_1}{\omega \rho}) \right] \frac{\omega}{\beta} \sqrt{\frac{2 C_0 \rho}{F_0}} \exp\left(\frac{\beta x}{2}\right) \right\}$$

where B is an arbitrary constant and $H_0^{(2)}$ represents a Hankel function of the second kind, order zero.

This equation prevents waves for frequencies greater than 100 Hz from ever reaching the helicotrema, thereby avoiding wave reflections.

Zwislocki used this expression to derive two approximate expressions, one giving displacement amplitudes, and the second giving locations of maxima and phase relations for the travelling wave.

APPENDIX 2 - IISUMMARY OF COCHLEAR THEORY OF PETERSON AND BOGERT⁽¹⁵⁾

The origin of the co-ordinate system was fixed in a plane containing the oval and round windows. The positive x direction is towards the helicotrema, which is located at x = l. Their notation is as follows:-

- A(x) = area of either scala, the two being assumed of equal area, at x, and $A(x) = (0.029 - 0.005 x^2) \text{ cm}^2$
- b(x) = width of (uniform) basilar membrane and $b(x) = (0.019 + 0.0093 x) \text{ cm}$.
- k(x) = stiffness of basilar membrane as a pressure per unit deflection, and $k(x) = 1.72 \times 10^9 x e^{-2x} \text{ dyne/cm}^3$.
- m(x) = mass of scala media and partition membranes per unit area and $m(x) = 0.143 \text{ gm/cm}^2$.
- ρ = average density of perilymph = 1.0 gm/cm^3 .
- c = velocity of sound in perilymph = $1.43 \times 10^5 \text{ cm/sec}$.
- p = gauge pressure at any point x in a scala, dynes/cm^2 .
- u = particle velocity at any point x in the positive x direction in a scala in cm/sec .

subscript v refers to quantities in the scala vestibuli

subscript t refers to quantities in the scala tympani

$v(x,t)$ = vertical (downwards) membrane velocity cm/sec . at point x and time t.

$r(x)$ = velocity resistance (viscous damping) of membrane per unit area.

Hence the fluid equations of motion for the channels are

$$\frac{\partial u_v}{\partial t} = - \left(\frac{1}{\rho} \right) \frac{\partial p_v}{\partial x}$$

and

$$\frac{\partial u_t}{\partial t} = - \left(\frac{1}{\rho} \right) \frac{\partial p_t}{\partial x}$$

when fluid viscosity effects are neglected.

Also assuming small membrane displacements, Peterson and Bogert's continuity equations become:-

$$\frac{\partial(u_v \Lambda)}{\partial x} = -\frac{\Lambda}{\rho c^2} \frac{\partial p_v}{\partial t} - v b$$

$$\frac{\partial(u_t \Lambda)}{\partial x} = -\frac{\Lambda}{\rho c^2} \frac{\partial p_t}{\partial t} + v b$$

where u , Λ , p , v , and b are all functions of x , and u , p and v are also functions of t . Note that compressibility effects have been included.

Their equation for membrane motion was

$$p_v - p_t = m \dot{v} + r v + k \int^t v dt$$

The following variables are then introduced, corresponding to different normal modes of propagation, (longitudinal and transversal).

$$p_+ = \frac{1}{2} (p_v + p_t), \quad p_- = \frac{1}{2} (p_v - p_t)$$

$$u_+ = \frac{1}{2} (u_v + u_t), \quad u_- = \frac{1}{2} (u_v - u_t)$$

The two fluid motion equations and the two continuity equations may thus be combined to give the following two equations:-

$$\left. \begin{aligned} \frac{1}{\Lambda} \frac{\partial}{\partial x} \left(\Lambda \frac{\partial p_+}{\partial x} \right) &= \frac{1}{c^2} \frac{\partial^2 p_+}{\partial t^2} \\ \text{and } \frac{1}{\Lambda} \frac{\partial}{\partial x} \left(\Lambda \frac{\partial p_-}{\partial x} \right) - \frac{b \rho}{\Lambda} \frac{\partial v}{\partial t} &= \frac{1}{c^2} \frac{\partial^2 p_-}{\partial t^2} \end{aligned} \right\} \quad (1)$$

in which the variables in u are eliminated.

$$\text{and } p_- = \frac{1}{2} (m \dot{v} + r v + k \int^t v dt) \quad (2)$$

Hence

$$\left. \begin{aligned} \frac{\partial p_+}{\partial x} &= -\rho \frac{\partial u_+}{\partial t} \\ \text{and } \frac{\partial p_-}{\partial x} &= -\rho \frac{\partial u_-}{\partial t} \end{aligned} \right\} \quad (3)$$

If all variables oscillate sinusoidally with respect to time at frequency ω rad/sec., then writing

$$p_+ = P_+ e^{j\omega t}, \quad p_- = P_- e^{j\omega t}$$

$$v = V e^{j\omega t}$$

$$u_+ = U_+ e^{j\omega t}, \quad u_- = U_- e^{j\omega t}$$

and substituting these relationships in equations 1, 2 and 3, the authors obtained equations 4 to 8, in which the prime denotes differentiation with respect to x :-

$$\frac{1}{A} (A P_+)' + \frac{w^2}{c^2} P_+ = 0 \quad (4)$$

$$\frac{1}{A} (A P_-)' + \frac{w^2}{c^2} P_- - \frac{jwb\rho}{A} V = 0 \quad (5)$$

$$P_- = \frac{1}{2} (j w m + r - j \left(\frac{k}{w} \right)) V \quad (6)$$

$$P_+' = -j w \rho U_+ \quad (7)$$

$$P_-' = -j w \rho U_- \quad (8)$$

Defining a partition impedance as $Z(x, w)$

$$\text{where } Z(x, w) = k(x) - m(x) w^2 + j w r(x) \quad (9)$$

then from equation (6)

$$V = \left(\frac{2jw}{Z} \right) P_-$$

which, substituted in equation (5) gives

$$\frac{1}{A} (A P_-)' + \frac{w^2}{c^2} \left(1 + \frac{2b\rho c^2}{AZ} \right) P_- = 0 \quad (10)$$

$$\text{or } \frac{1}{A} (A P_-)' + \left(\frac{w^2}{c^2} \right) \gamma^2 P_- = 0 \quad (11)$$

$$\text{where } \gamma^2 = 1 + \frac{2b\rho c^2}{AZ}$$

Thus if A' is approximately constant it is clear from the P_+ wave equation (4) that the P_+ wave travels along the scale with the velocity of sound in perilymph, c , while equation (11) shows that the P_- wave, which disturbs the basilar membrane, travels at a velocity $\frac{c}{\gamma}$.

Peterson and Bogert made approximate calculations of the variation of γ with frequency, and in doing so the viscous damping term $r(x)$ was neglected, and at low frequencies below 100 Hz, they also neglected the mass component of impedance. Wave velocities at low frequency compared roughly with velocities derived from Bekesy data. They demonstrated that for resonant frequencies when Z approaches zero, γ becomes infinite and the travelling wave is attenuated. They thereby showed that the distance x at which this occurs approaches zero for a frequency of 18 k Hz., which is approximately the upper limit of hearing.

Thus they contributed a clear understanding of the travelling wave, and up to this point their theory is no more a resonance theory than is Zwislocki's. They did not, however, consider any numerical trends or solutions for the general case of a complex partition impedance in which damping was allowed which must generate a complex value for γ , and by admitting real and imaginary components to displaced values of P^- and P^+ in equation (11), result in out-of-phase components in all variables.

Their approximate numerical solutions are also outlined:-

Boundary conditions were stipulated, and the authors decided that at the helicotrema,

$$P^- (1) = 0$$

$$\text{and } U^+ (1) = 0$$

and at the round window,

$$P^+ (0) = P^- (0)$$

and at the oval window,

$$P^+ (0, w) = 1.00 \text{ for convenience.}$$

Introducing the numerical equation for $A(x)$ into equation (4) they obtained

$$\frac{1}{5.8 - x} \frac{d}{dx} \left[(5.8 - x) \frac{dP^+}{dx} \right] + \frac{w^2}{c^2} P^+ = 0$$

whose solution is

$$P^+ = K_1 J_0 \left[\frac{w}{c} (5.8 - x) \right] + K_2 N_0 \left[\frac{w}{c} (5.8 - x) \right]$$

where J_0 and N_0 are zero order Bessel functions of the first and second kind respectively, and K_1 and K_2 are constants determined from the boundary conditions that $U^+ (3.5) = P^+ (3.5) = 0$ and $P^+ (0, w) = 1.0$, and are found to be linked by first order Bessel functions of both kinds.

Hence an exact expression for P^+ , in terms of J_0 , J_1 , N_0 and N_1 Bessel functions of x was obtained, and the only relatively major or gross simplification involved in this exact solution is that perilymph viscous effects were ignored.

No analytical procedure to solve equations (11) for the P- wave could be found and so the equation was rather laboriously solved by numerical methods, without the benefit of an electronic digital computer. For three frequencies for which a singularity did not exist in equations (11), namely 31.6, 100 and 316 Hz, numerical integration was commenced at the helicotrema end, $x = 3.5$, where $P-(3.5) = 0$ and a small positive value ϵ was given to $P'-(3.5)$, and a step by step calculation carried backwards to the origin, and, the problem being linear, solutions obtained for pressures along the cochlea and at the oval window normalised to make $P-(0) = 1.0$.

For higher frequencies, between 10 and 1 kHz, a singularity in equations (11) could not be avoided, and a series solution for P- around the singularity was successfully employed. This necessarily introduced complex values for P- during the excursion of the solution around each singularity, which complicated the calculations considerably.

As no damping was included in the numerical solutions for equations (11), the final amplitude curves are undoubtedly steep resonance curves which consequently bear little similarity to the Bekegy experimental data, either as regards frequency loci or phase variations.

Comments on Peterson and Bogert's Theory

Despite the disappointing results published by Peterson and Bogert, their ingenuity in getting numerical solutions may be noted.

A few features of their theoretical formulation are open to criticism, while others are very useful. The following notes summarise these features:-

1. the form in which the wave equations (4) and (11) are presented has relieved much of the previous confusion surrounding scalae pressure variations.

2. the coefficients of these pressure wave equations being seen to yield good approximations to fluid pressure wave velocities, the simplicity of these equations could be sacrificed in order to include scala fluid viscosity effects; also in order to allow for differences between scala vestibuli and scala tympani sectional areas, and equally, to permit other than simple linear variations in the physical properties, such as A , m etc. of the system.
3. partition impedances are limited to the case of linear stiffness components.
4. the singularities encountered by the authors could have been avoided had real damping coefficients for the cochlear partition been included in impedance data. The author's intention to reduce the difficulties of numerical solution by neglect of damping coefficients was in any case thwarted by their being obliged to introduce complex notation in order to continue solutions around the resultant discontinuities.
5. the two authors point out that future cochlear theories should include both damping effects and a solution for continuous flexible membrane response, rather than the treatment, applied by themselves and all other cochlear theorists, of the partition as an assemblage of independent pistons.

Note that a distributed-parameter, membrane-system treatment, assuming many degrees of freedom and the possibility of longitudinal tensions restraining adjacent portions of membrane, will not have exactly the same effect as increased viscous damping of separate elements, despite Zwislocki's implications that adequate damping can make the mathematical model wholly realistic.

EFFECTIVE MASS OF THE COCHLEAR PARTITION

CHAPTER 3

Contents

	Introduction and Review	Page 1
I	Formulation of the Model	Page 4
IA.	Application of Potential Theory with Point Sources	Page 7
IB.	Application of Potential Theory with Distributed Sources	Page 10
II	Effective Mass Calculation	Page 13
IIA.	Right-Angled Triangular Representation	Page 13
IIB.	Non Right-Angled Triangular Representation	Page 16
III	Discussion of Theoretical Effective Mass Ratios	Page 24
IV	Discussion of Typical Cochlear Effective Masses	Page 27
V	Conclusions	Page 30
VI	References	Page 31

Appendices

I	Theory of Incompressible Potential Flow	Page 32
II	Solution of the Field for Specified Membrane Displacements	Page 34
IIA.	Symmetrical Displacement $v(x)_1$	Page 35
IIB.	Assymetrical Displacement $v(x)_2$	Page 38
IIC.	Assymetrical Displacement $v(x)_3$	Page 42
IID.	Solution of Integrals	Page 44

Introduction and Review.

The problem of estimating the mass of the membranes and fluids of the inner ear which contribute to the inertia forces of a vibrating scala media and cochlear partition has confronted many investigators designing theoretical models of the human inner ear.

In most analyses of cochlear dynamics, a set of equations may be written representing the fluid mechanics of the two major scalae of the cochlea and another set of equations may then describe the motion of the partition scala which separates the two main scalae. By careful representation of the physical parameters involved and with considerable subsidiary mathematical calculation, these latter equations can be shown to be second-order, possibly non-linear, partial differential equations, with variable coefficients, in D_z , the membrane displacement. The problem may be conveniently handled with reasonable justification by recourse to "wedge" theory, in which, via digital computer techniques, the membrane response to pure-tone stimulation is calculated repeatedly at different sections along the cochlea for small incremental lengths, the membrane properties being considered uniform within each application but discontinuous between applications. Most theoretical cochlear mechanics investigators have either simplified the system to a two dimensional single-degree-of-freedom linear differential equation or have reduced the variables to convenient functions of X only, making in particular the stiffness term linear. The evaluation of the solutions to either the partial or the reduced differential equations is dependent, inter alia, upon ascribing functional variations and values to the effective mass of the cochlear partition. No agreement exists concerning either of these.

Some authors including Budde⁽¹⁾ and Wilkinson and Gray⁽²⁾ in 1924 have argued that masses of columns of fluid between round and oval windows together with the excited portion of the cochlear partition were directly relevant to the subject. Among authors who have discussed these so-called resonance column hypotheses are von Békésy⁽³⁾, Neve⁽⁴⁾ and Littler⁽⁶⁾. Littler's review

includes an outline of the relevance of the factor of mass to several of these theories. In a sense of course, fluid column masses are relevant to all theories but perilymph motion, as well as other main scalae properties, can be precisely and conveniently described only in more complete analyses, as by separate equations already mentioned.

Ranke (1931⁽⁷⁾, 1942⁽⁸⁾, 1950⁽⁹⁾), in his treatises on fluid motion in the cochlea and partition response, apparently considered the actual mass of the cochlear partition in his theoretical calculations, although details of and justification for actual values tested are hard to establish.

Wever (1949⁽⁴⁾ and 1954⁽⁵⁾) drew attention to the variation in mass per unit length of the basilar membrane and its associated cellular structures, which he showed to vary about $4\frac{1}{2}$ fold, increasing from stapes towards helicotrema, as compared with Hartridge and Bannister's⁽¹⁰⁾ estimate of 12 times. He gave details of mean cross sectional areas of this basilar membrane/cellular complex which lie between about 0.005 mm^2 at basal end and about 0.022 mm^2 at apical end. In another context he described typical cross sectional areas of scalae media, between 0.1 and 0.3 mm^2 area.

Peterson and Bogert⁽¹¹⁾, in their mathematical treatment of the problem, stated clearly that the effective mass of the basilar and cochlear duct was assumed to be due to the mass of fluid in the duct, which, having roughly 25% of the cross-sectional area of the main scalae, yielded a uniform mass per unit area for the partition of 0.143 gm/cm^2 . This gives approximately 0.002 gm/cm at the stapes end and 0.0075 gm/cm at the helicotrema.

Fletcher⁽¹²⁾ introduced a radiant mass concept to a section of plate vibrating in fluid, and estimated that, for a uniform square basilar membrane section of side $b \text{ cm}$, its effective mass when oscillating was $1.75 b^3 \text{ gm}$. Including the mass of local cellular and membranous structures. Considering each of these square elements to extend over the normal width of the basilar membrane he showed that this implied that as a function of distance (X) along the cochlea, $m = 10^{(-5.31 + X/2)} \text{ gm}$. This yields an effective mass variation between stapes and helicotrema of from 0.0004 gm/cm to 0.005 gm/cm .

In his discussions on scala media mass, Zwislocki (1950⁽¹³⁾, 1953⁽¹⁴⁾) defines an effective mass of the cochlear partition which he says should be based on the mean cross sectional area of the cochlear duct. In as far as this term is relevant to his arguments and theory, it was assumed to be approximately constant.

Hause⁽¹⁵⁾ used a constant value of 0.05 gm/cm^2 , which, although chosen mainly for purposes of demonstration of his techniques, lies within the Fletcher results.

Klatt⁽¹⁶⁾ justified a factor of $\frac{2}{3}$ of the effective partition mass which was later applied by Klatt and Peterson⁽¹⁷⁾, who quoted two ranges of values for mass as being experimental data. The first of these ranges, quoted as being from Fletcher, although the values do not agree with Fletcher's, is 0.000033 gm/cm at the stapes end to 0.0018 gm/cm at the apical end. The second range is said to include the mass of the entire scala media and is constant at 0.0067 gm/cm . However, in their mathematical model they used a different, very wide range of 0.0000167 gm/cm at the basal end to 0.0067 gm/cm at the apex.

Table 1 summarizes these figures.

In the present state of the subject it seems that any mathematical theory of cochlear action is compared with and judged by the classical Bekesy experimental data. (This comparison is as much by phase change along the length of the cochlear as by amplitude response of the basilar membrane.) It is neither adequate nor acceptable simply to devise a mathematical formulation and solution which fits, more or less, the results. If a serious attempt is to be made to introduce physical parameters which will describe the real situation it is imperative that better-than-order-of-magnitude accuracy is achieved.

This study is an attempt to achieve such accuracy via an experimentally supported hydrodynamic analysis and computer evaluation. It is only when the available experimental data has been analysed with accuracy that an extrapolation into the region of the cochlea for which little experimental data exists has any validity.

Table 1. Review of cochlear partition effective mass ranges as employed by various cochlear theory investigators.

<u>Reference</u>	<u>Mass/unit distance along cochlea in gm/cm</u>		<u>Mass/unit area of basilar membrane in gm/cm²</u>	
	<u>Stapes end</u>	<u>apical end</u>	<u>Stapes end</u>	<u>apical end</u>
Before 1930	Resonance and fluid column hypotheses.			
Rankes(7),(8),(9).	A varying effective mass, based on the section of scala media.			
Peterson and				
Bogert (11)	0.002	0.0075	0.143	0.143
Fletcher (12)	0.0004	0.0055	0.03	0.11
Mause (15)	0.0007	0.0026	0.05	0.05
Klatt and Peterson(17)	0.000017	0.007	0.001	0.13

I. FORMULATION OF THE MODEL

The length of the human adult scala media is 30 to 35mm, its width, in the plane of the basilar membrane and the osseous spiral lamina, varies between 0.75 and 1.5mm, and its height, that is the dimension normal to the latter plane and between it and the top of Reissner's membrane, adjacent to the scala vestibuli, varies between 0.3 and 0.9mm. The mean cross sectional area of the scala media is 0.10 to 0.35mm². The scala media itself is surrounded by perilymph, which has a density very close to that of the endolymph which fills the scala media. Pressure waves in the perilymph, that is in the two main scalae of the cochlea, disturb the cochlear partition, (the scala media and enclosing membranes) and set it vibrating in certain regions along its length. Associated with a pressure wave in a fluid there is always an accompanying particle motion, and in the vicinity of a section of the cochlear partition which has been set into vibration there is necessarily a matching transverse vibration of the surrounding fluid in the two main scalae. So it is to be expected, considering the viscosity of endolymph, that an induced movement of the basilar membrane will be accompanied by motion of adjacent liquid in the scala media, with corresponding motion of other fluid in the scala and of the relatively light, flaccid Reissner's membrane, and that this integral motion of the whole partition will tend to occur in a direction perpendicular to the basilar membrane and not be diffused longitudinally along the cochlear.

It has been deduced from the experimental stiffness test data contributed by von Békésy that it is mainly the basilar membrane itself, but also the additional stiffening effects of its supported structures, cells and membranes and the resistance to deflection which is the result of tectorial membrane/reticular lamina/cilia shearing action, which governs the elasticity of the cochlear partition.

Consequently, any local unbalance of fluid pressure in the two main scalae at some section along the cochlea would be expected to deflect the scala media local to that section in a manner dependent upon the elastic characteristics

of the basilar membrane and its cellular complex. Now it is clear that if the scala media is wholly filled with a near incompressible liquid, any motion of any part of its fluid or enclosing membranes must result in a natural and repeatable motion of some other part of it according to the equation of continuity $\text{div}(\rho v) = 0$. Applying this equation and assuming that the fluid field contains potential flow, (i.e. fluid particles are irrotational and inviscid within the scala media) it follows that the deflecting shape of the basilar membrane will determine the vector representing motion of each and every moveable particle comprising the scala media at that section. This also applies to Reissner's membrane when this is considered as having negligible stiffness compared with the basilar membrane. In fact in the fluid mechanic sense, one can model the Reissner boundary as one which, being very flaccid and of much the same density as the liquid on either side of it, the liquid does not notice. That is, its motions are dictated by the surrounding fluid motions which are themselves approximately continuous across this boundary.

Thus one major property of the theoretical model of the scala media, by which its effective mass in the oscillating state is to be calculated, is that of a potential flow field, within which inertia forces on each fluid particle will predominate over Reissner's membrane elastic forces, endolymph compressibility forces and endolymph viscous forces, in which case the whole scala media at any section must vibrate completely in phase. Allowance for endolymph viscosity must be made in order to justify the assumption that scala media movement is confined to the transverse direction and is not diffused longitudinally. Other effects of endolymph viscosity are confined to the viscous damping coefficients in the equations for scala media motion. (not the scope of this paper).

As regards compressibility, if the speed of sound in endolymph is of the order of 1500 m/sec, then at a section responding to 15 kHz, the wave length being 1cm, the phase lag across a mean height of scala media of 0.5mm will not

be greater than 0.10π which even at the basal end of the scala media is sufficiently small to have an unimportant effect on the ensuing calculations. There is no experimental evidence of a phase difference greater than this occurring in the scala media.

Some evidence for the assumptions regarding localization of the response, phase insensitivity and the part played by Reissner's membrane can be found in von Bekesy's experimental observations:

- 1) The cochlear duct acts in such a way as to prevent any lateral flow in response to rapidly changing transverse movements.
- 2) The displacement of the cochlear partition for frequencies below 2-3 kHz showed no phase difference between movements of scala media membranes.
- 3) There were no phase differences observed among movements of the basilar membrane, the organ of Corti and the tectorial membrane.
- 4) If Reissner's membrane was removed along the cochlear partition, it was easily seen with the phase stroboscope that the tectorial membrane, the organ of Corti, and the visible part of basilar membrane vibrated completely in phase, so that it is proper to consider the entire cochlear partition as a single structure.
- 5) The measurements show that it is, as Hensen and Helmholtz have argued, the basilar membrane that determines the movement of the cochlear partition.
- 6) The deflection of the partition closely resembles that of a bar fixed at one end (limbus) and whose free end becomes a membrane completing the partition.
- 7) (For guinea pig.) When the point of maximal transverse vibration along the basilar membrane was observed and the frequency was increased three times, no subdivision of the basilar membrane in the transverse direction could be found, but there remained a small phase difference between the centre and the edge of the membrane. From this observation comes the theoretically important conclusion that the mechanical load concentrated at one point of the basilar membrane by the pillars of Corti is relatively small compared with the load of the surrounding fluid.

- 8) If the cochlea is exposed to very intense sound, then in general the first event is that the cells of Hensen separate from the basilar membrane and the reticular membrane. They float in the endolymph freely.

IA Application of potential theory with point sources

Consider the scala media as a right angled triangle with no flow across its orthogonal boundaries and the centre of the basilar membrane represented by a single simple source. Applying mirror-image sources at $(c,0)$ and $(-c,0)$ (Fig.1) there will be no streamlines across the $x = 0$ or the $y = 0$ boundaries, but there will be a streamline co-incident with these boundaries. This infinite field is of ever decreasing velocity (as $\bar{w} = m/r$), becomes less significant with distance from the sources, and is well represented in the physical situation by the transverse motion of the perilymph in the scala vestibuli, and further out still, by longitudinal perilymph wave motions, by which all transverse motion is initiated. For the two point sources shown, (see Appendix I)

$$W = m \log_e (z - c) + m \log_e (z + c)$$

where W is a function of $(x + iy)$.

But ϕ is the potential function,

ψ is the stream function.

$$\therefore \frac{\phi}{m} = \log_e \sqrt{(x-c)^2 + y^2} + \log_e \sqrt{(x+c)^2 + y^2}$$

$$\therefore \frac{\phi}{m} = \log_e R_1 R_2$$

And

$$\psi = m \tan^{-1} \frac{y-0}{x-c} + m \tan^{-1} \frac{y-0}{x+c}$$

$$\therefore \frac{\psi}{m} = \tan^{-1} \frac{y}{x-c} + \tan^{-1} \frac{y}{x+c}$$

$$\therefore \frac{\psi}{m} = \tan^{-1} \left(\frac{\frac{y}{x-c} + \frac{y}{x+c}}{1 - \frac{y^2}{x^2 - c^2}} \right)$$

$$\therefore \frac{\psi}{m} = \tan^{-1} \left(\frac{2xy}{x^2 - y^2 - c^2} \right)$$

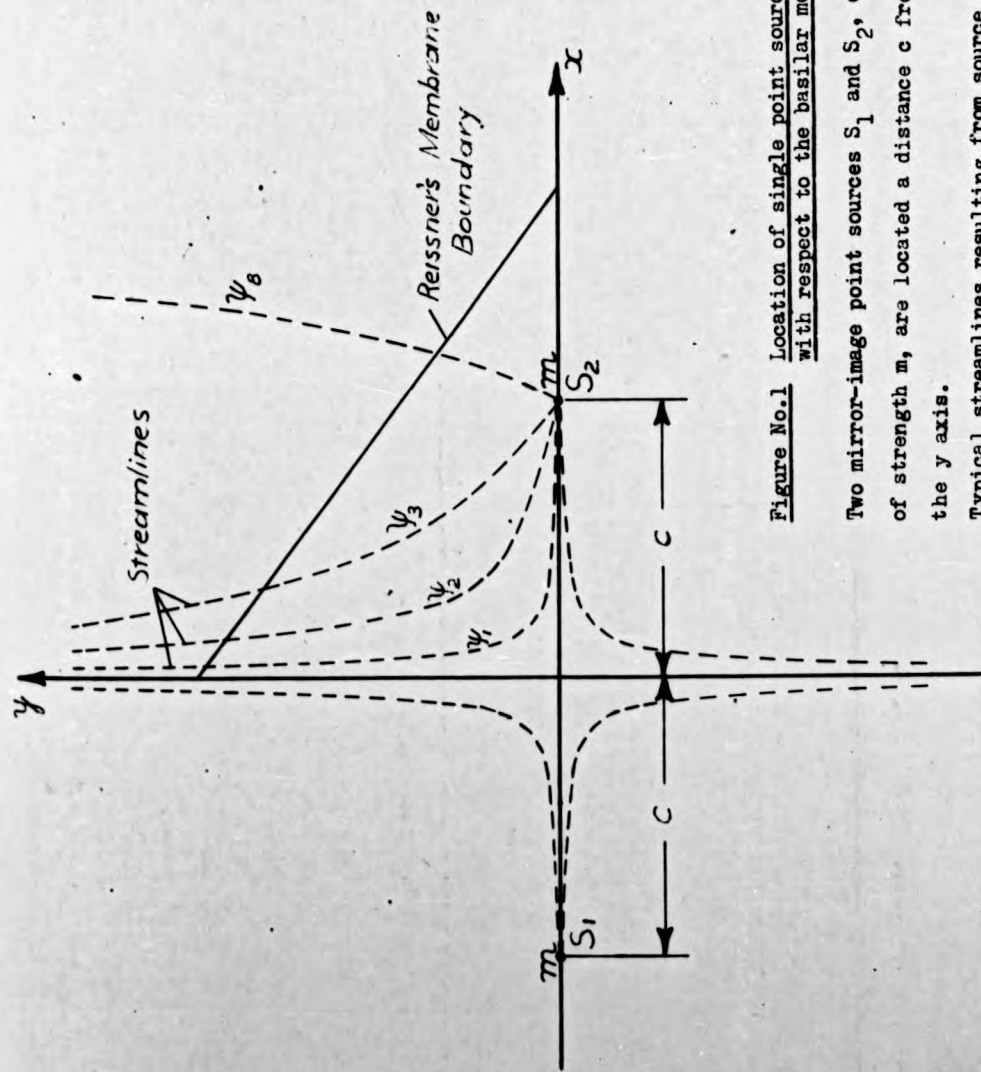


Figure No.1 Location of single point sources with respect to the basilar membrane

Two mirror-image point sources S_1 and S_2 , each of strength m , are located a distance c from the y axis.

Typical streamlines resulting from source S_2 .
FIGURE No.1

$$\text{Also } \left| \frac{dW}{dz} \right| = \left| \bar{w} \right| = r \quad \text{and} \quad \frac{dW}{dz} = u - iv$$

From equation for ϕ above

$$\left. \begin{aligned} u &= \frac{\partial \phi}{\partial x} = \frac{m(x-c)}{(x-c)^2 + y^2} + \frac{m(x+c)}{(x+c)^2 + y^2} \\ v &= \frac{\partial \phi}{\partial y} = \frac{my}{(x-c)^2 + y^2} + \frac{my}{(x+c)^2 + y^2} \end{aligned} \right\} \text{(1)}$$

Consider components of u and v at the boundary along Reissner's membrane, when this has slope $M_R (= a/b = \tan K)$ (Fig.2).

Let V_M be the velocity at any point at right angles to the Reissner boundary,

$$y = a - M_R x$$

$$\text{Then } V_M = \frac{\partial \phi}{\partial M_R}$$

Resolving $\frac{\partial \phi}{\partial y}$ and $\frac{\partial \phi}{\partial x}$ into components parallel and perpendicular to this line it follows that

$$\frac{\partial \phi}{\partial M_R} = \frac{1}{\sqrt{M_R^2 + 1}} \frac{\partial \phi}{\partial y} + \frac{M_R}{\sqrt{M_R^2 + 1}} \frac{\partial \phi}{\partial x}$$

Substituting for $\frac{\partial \phi}{\partial x}$ and $\frac{\partial \phi}{\partial y}$ from eq.(1) into this equation, then V_M , which is the velocity across the imaginary Reissner boundary, which is considered equal to the velocity of Reissner's membrane,

$$V_M = \frac{m}{\sqrt{M_R^2 + 1} \left((x-c)^2 + y^2 \right) \left((x+c)^2 + y^2 \right)} \left(y \left((x+c)^2 + y^2 \right) + y \left((x-c)^2 + y^2 \right) + M_R (x-c) \left((x+c)^2 + y^2 \right) + M_R (x+c) \left((x-c)^2 + y^2 \right) \right)$$

Substituting for $y (= a - M_R x)$

$$V_M = \frac{m(-4M_R c^2 x + 2ax^2 + 2ac^2 + 2a^3 + 2aM_R^2 x^2 - 4a^2 M_R x)}{\sqrt{M_R^2 + 1} \left((x^2 - c^2)^2 + (a - M_R x)^4 + 2(a - M_R x)^2 (x^2 + c^2) \right)}$$

and for unit strength ($m=1$)

$$V_M = \frac{2ax^2 (1 + M_R^2) - 4M_R x (c^2 + a^2) + 2a(c^2 + a^2)}{\sqrt{M_R^2 + 1} \left((x^2 - c^2)^2 + (a - M_R x)^4 + 2(a - M_R x)^2 (x^2 + c^2) \right)}$$

This velocity pattern has been computed (via a GEC 90/2 digital computer) for a series of triangular shapes, with $a = 1$, and variations in both the slope of the Reissner boundary (M_R) and the location of the single point source (c), and the results are given in table 2.

Generally Reissner's boundary velocity pattern as calculated from this type

Figure No.2 Positive velocity components in the model scala media section

The positive velocity normal to the line representing Reissner's membrane is labelled $\frac{\partial \phi}{\partial M_r}$.
 Note that $K = \tan^{-1}\left(\frac{a}{b}\right) = \tan^{-1}(M_r)$.

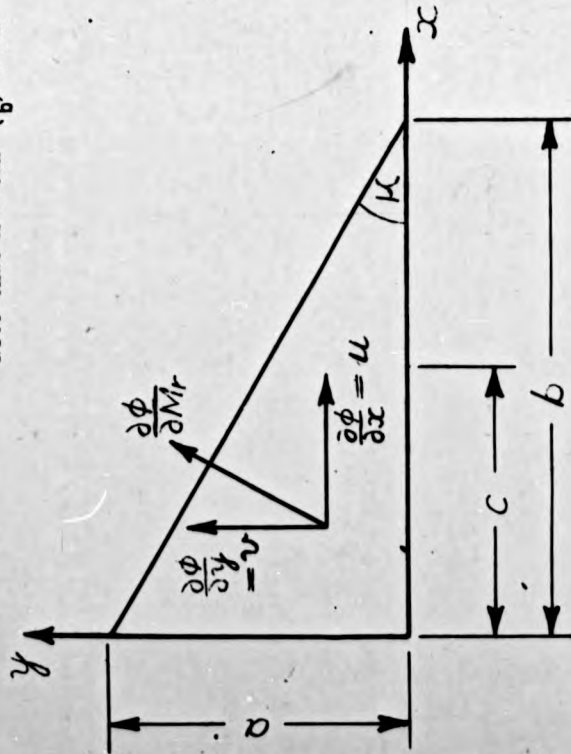


Table 2. Variation of velocity of Reissner's Membrane with abscissa x , when x is expressed as a fraction of the duct width b , for point source excitation (see fig.1). Various configurations representing the slope of Reissner's Membrane, M_r , and the position, c , of the point source (again in terms of width b) are included, and the units of velocity are arbitrary.

Slope M_r	Position of Source, c .	Velocity at abscissa $x =$				
		<u>0.1b</u>	<u>0.3b</u>	<u>0.5b</u>	<u>0.7b</u>	<u>0.9b</u>
0.5	0.2b	1.76	2.07	1.66	0.98	0.58
0.5	0.6b	0.71	0.80	1.51	2.96	1.13
1.0	0.2b	1.63	2.28	2.81	2.61	1.33
1.0	0.6b	1.14	1.36	1.86	3.46	3.33
1.5	0.2b	1.33	2.00	2.95	3.69	3.16
1.5	0.6b	1.10	1.46	2.00	3.40	5.32
2.0	0.2b	1.09	1.70	2.75	4.18	4.42
2.0	0.6b	0.97	1.38	2.00	3.33	6.75

of analysis should, except for the regions very near to the x and y axes where even a flimsy membrane must impede fluid movements, approximate that of Reissner's membrane during fundamental harmonic vibration of the cochlear partition. These values show that the largest velocities and hence the largest amplitudes of vibration occur towards the lower end of Reissner's membrane. This becomes more marked as the slope increases, the location of the maximum becoming less dependent upon the actual location of the source. Even at low membrane slopes, the maximum amplitude occurs on that side of the point source towards the lower end of the membrane. This accords well with the fact that the lower attachment of Reissner's membrane to the limbus is mechanically rather weak and even folded, and with Bekesy's repeated observations that the lower portions of Reissner's membrane moved with maximum amplitude during static tests, and apparently also during dynamic tests.

Hence it is suggested that while assumptions inherent in a potential field model of the scala media are quite unacceptable in the general dynamic situation, the approach is sound enough for the estimation of cochlear partition effective mass.

The question then arises as to the influence of the actual shape of the amplitude (and velocity) function of the vibrating basilar membrane. In the above elementary analysis a point source has been assumed. As a source, however, the basilar membrane may occupy as much as half of the width, b , of the scala media, and its region of maximum vibration amplitude may not be assumed to lie centrally.

One method of approximating the true basilar disturbance function is to apply a number of spatially distributed point sources and their images, all of varying strengths relative to one another. This approach would introduce a number of mathematical singularities and would cause difficulties in later calculations which rely on mathematical transformation of the scala shape. Furthermore the number of such point sources required to model the disturbance function sufficiently accurately would result in voluminous and clumsy

mathematics which would not be amenable either to generalization or further refinement.

I.B. Application of potential theory with distributed sources.

Let the potential flow field bounded in the first quadrant by $x = 0$ and $y = 0$ be excited by a simple harmonic function modelling the basilar membrane displacement and velocity pattern, beginning at the point $(x_1, 0)$ and extending to $(x_1 + f, 0)$. The effects of the following assumed functions have been assessed. See Fig.3.

$$1). \quad v(x)_1 = M \left((x - x_1)^2 - f(x - x_1) \right)$$

This is a symmetric function about $(x_1 + f/2)$ and is parabolic. It represents closely the pressure-deflected shape of a pure membrane.

$$2). \quad v(x)_2 = N \left((x - x_1)^3 - f(x - x_1)^2 \right)$$

This is an asymmetric function with zero slope at $x = x_1$ and having maximum amplitude at $x = x_1 + 2f/3$. It represents the mirror image of the shape of the basilar membrane under pressure loading.

$$3). \quad v(x)_3 = P \left((-x + x_1 + f)^3 - f(-x + x_1 + f)^2 \right)$$

This is also an asymmetric function, with zero slope at $x = x_1 + f$ and having maximum amplitude at $x = x_1 + f/3$. It represents, as closely as any simple expression can, the displacement pattern observed for the basilar membrane by von Bekesy.

Using potential function ϕ ;

$$\text{Let } \phi(x, y) = X(x) Y(y)$$

$$\therefore Y \frac{d^2 X}{dx^2} + X \frac{d^2 Y}{dy^2} = 0$$

$$\therefore \frac{1}{X} \frac{d^2 X}{dx^2} = -\frac{1}{Y} \frac{d^2 Y}{dy^2} = -\alpha^2, \text{ say, giving}$$

$$\frac{d^2 X}{dx^2} + \alpha^2 X = 0 \quad \text{and} \quad \frac{d^2 Y}{dy^2} - \alpha^2 Y = 0$$

The linearly independent solutions of these equations are:

$$X = A^1 \sin \alpha x + B^1 \cos \alpha x \quad \text{and} \quad Y = C^1 e^{\alpha y} + D^1 e^{-\alpha y}$$

$$\begin{aligned} \therefore \phi &= A e^{\alpha y} \sin \alpha x + B e^{\alpha y} \cos \alpha x + C e^{-\alpha y} \sin \alpha x + D e^{-\alpha y} \cos \alpha x \\ \therefore \frac{\partial \phi}{\partial x} &= \alpha (A e^{\alpha y} \cos \alpha x - B e^{\alpha y} \sin \alpha x + C e^{-\alpha y} \cos \alpha x - D e^{-\alpha y} \sin \alpha x) \\ \text{and } \frac{\partial \phi}{\partial y} &= \alpha (A e^{\alpha y} \sin \alpha x + B e^{\alpha y} \cos \alpha x - C e^{-\alpha y} \sin \alpha x - D e^{-\alpha y} \cos \alpha x) \end{aligned}$$

Now boundary conditions are

$$\left(\frac{\partial \phi}{\partial x} \right)_{x=0} = 0 \quad \text{_____ (2)}$$

$$\left(\frac{\partial \phi}{\partial y} \right)_{y=0} = 0 \quad \text{_____ (3)}$$

$$\left(\frac{\partial \phi}{\partial y} \right)_{y=\infty} = 0 \quad \text{_____ (4)}$$

$$\left(\frac{\partial \phi}{\partial y} \right)_{(x,y)} = \left(\frac{\partial \phi}{\partial y} \right)_{(-x,y)} \quad \text{_____ (5)}$$

From conditions (2), (4) and (5) it is clear that the acceptable condition is that

$$\phi = D e^{-\alpha y} \cos \alpha x$$

If now, appropriate to the second boundary condition eq.(3), a function $g(\alpha)$ in series form is introduced which is obtainable by inverse Fourier transforms, and which satisfies the ϕ potential function, then this function $g(\alpha)$ can be used to define the x axis boundary conditions.

$$\begin{aligned} \text{That is } \phi &= \int_0^{\infty} e^{-\alpha y} \cos \alpha x g(\alpha) d\alpha \\ \text{Then } \frac{\partial \phi}{\partial x} &= \int_0^{\infty} -\alpha g(\alpha) e^{-\alpha y} \sin \alpha x d\alpha \\ \text{And } \frac{\partial \phi}{\partial y} &= \int_0^{\infty} -\alpha g(\alpha) e^{-\alpha y} \cos \alpha x d\alpha \\ \text{and } \left(\frac{\partial \phi}{\partial y} \right)_{y=0} &= \int_0^{\infty} -\alpha g(\alpha) \cos \alpha x d\alpha \end{aligned} \quad \left. \vphantom{\begin{aligned} \phi \\ \frac{\partial \phi}{\partial x} \\ \frac{\partial \phi}{\partial y} \\ \left(\frac{\partial \phi}{\partial y} \right)_{y=0} \end{aligned}} \right\} \text{_____ (6)}$$

But $\left(\frac{\partial \phi}{\partial y} \right)_{y=0}$ is defined as $v(x)$ which, on the line $y=0$ is zero for $-x_1 \leq x \leq x_1$ and for $|x| \geq |x_1 + f|$ but is non-zero for $|x_1| < |x| < |x_1 + f|$

$$\text{Then } \int_0^{\infty} -\alpha g(\alpha) \cos \alpha x d\alpha = v(x)$$

and by an inverse Fourier Transform, applying to a half plane solution

$$-\alpha g(\alpha) = \frac{2}{\pi} \int_{x_1}^{x_1+f} v(x) \cos \alpha x dx \quad \text{_____ (7)}$$

It is shown in Appendix II that, for the symmetrical velocity pattern $v(x)_1$, determination of $g(\alpha)$ and integration according to equations (6) leads to

$$\begin{aligned} \frac{\pi}{2M} \left(\frac{\partial \phi}{\partial y} \right) &= yf - \frac{y}{4} (2A-f) \log_e \left(\frac{y^2 + A^2}{y^2 + C^2} \right) - \frac{y}{4} (2B-f) \\ &\log_e \left(\frac{y^2 + B^2}{y^2 + C^2} \right) - \frac{1}{2} (y^2 - AC) \tan^{-1} \left(\frac{fy}{y^2 + AC} \right) - \frac{1}{2} (y^2 + BD) \tan^{-1} \left(\frac{fy}{y^2 - BD} \right) \end{aligned} \quad \text{_____ (8)}$$

(A2-10)

and

$$\frac{\pi}{2M} \left(\frac{\partial \phi}{\partial x} \right) = -x_1 - \frac{1}{4}(y^2 - AC) \log_e \left(\frac{y^2 + A^2}{y^2 + C^2} \right) + \frac{1}{4}(y^2 + BD).$$

$$\log_e \left(\frac{y^2 + B^2}{y^2 + D^2} \right) + \frac{y}{2}(2A - f) \tan^{-1} \left(\frac{fy}{y^2 + AC} \right) - \frac{y}{2}(2B - f) \tan^{-1} \left(\frac{fy}{y^2 - BD} \right) \quad (9)$$

(A2-11)

where $A = x_1 + f + x$, and $B = x_1 + f - x$ and $C = x_1 + x$, and $D = x - x_1$

} (10)

The above expressions, eqns (8) and (9), satisfy the boundary conditions of eqns (2), (3), (4) and (5).

For the asymmetrical velocity pattern $v(x)_2$, it is shown in Appendix IIB that

$$\begin{aligned} \frac{\pi}{2N} \left(\frac{\partial \phi}{\partial y} \right) = & -\frac{yf}{2}(4x_1 + f) - \frac{y}{4}(y^2 - A(3A - 4f) - f^2) \log_e \left(\frac{y^2 + A^2}{y^2 + C^2} \right) - \\ & \frac{y}{4}(y^2 - B(3B - 4f) - f^2) \log_e \left(\frac{y^2 + B^2}{y^2 + D^2} \right) + \frac{1}{2}(y^2(3A - 2f) - AC^2) \tan^{-1} \left(\frac{fy}{y^2 + AC} \right) \\ & + \frac{1}{2}(y^2(3B - 2f) - BD^2) \tan^{-1} \left(\frac{fy}{y^2 - BD} \right) \quad (11) \end{aligned}$$

(A2-16)

and

$$\begin{aligned} \frac{\pi}{2N} \left(\frac{\partial \phi}{\partial x} \right) = & \frac{xf}{2}(4x_1 + f) + \frac{1}{4}(y^2(3A - 2f) - AC^2) \log_e \left(\frac{y^2 + A^2}{y^2 + C^2} \right) - \frac{1}{4}(y^2(3B - 2f) - BD^2) \\ & \log_e \left(\frac{y^2 + B^2}{y^2 + D^2} \right) + \frac{y}{2}(y^2 - A(3A - 4f) - f^2) \tan^{-1} \left(\frac{fy}{y^2 + AC} \right) - \frac{y}{2}(y^2 - B(3B - 4f) - f^2) \tan^{-1} \left(\frac{fy}{y^2 - BD} \right) \quad (12) \end{aligned}$$

(A2-17)

For the oppositely asymmetrical velocity pattern $v(x)_3$, (see Appendix IIC)

$$\begin{aligned} \frac{\pi}{2P} \left(\frac{\partial \phi}{\partial y} \right) = & \frac{yf}{2}(4x_1 + 3f) + \frac{y}{4}(y^2 - A(3A - 2f)) \log_e \left(\frac{y^2 + A^2}{y^2 + C^2} \right) + \frac{y}{4}(y^2 - B(3B - 2f)) \\ & \log_e \left(\frac{y^2 + B^2}{y^2 + D^2} \right) - \frac{1}{2}(y^2(3A - f) - A^2C) \tan^{-1} \left(\frac{fy}{y^2 + AC} \right) - \frac{1}{2}(y^2(3B - f) + B^2D) \\ & \tan^{-1} \left(\frac{fy}{y^2 - BD} \right) \quad (13) \end{aligned}$$

(A2-19)

and for the velocity in the direction parallel to the x axis,

$$\begin{aligned} \frac{\pi}{2P} \left(\frac{\partial \phi}{\partial x} \right) = & -\frac{xf}{2}(4x_1 + 3f) - \frac{1}{4}(y^2(3A - f) - A^2C) \log_e \left(\frac{y^2 + A^2}{y^2 + C^2} \right) + \\ & \frac{1}{4}(y^2(3B - f) + B^2D) \log_e \left(\frac{y^2 + B^2}{y^2 + D^2} \right) - \frac{y}{2}(y^2 - A(3A - 2f)) \tan^{-1} \left(\frac{fy}{y^2 + AC} \right) \\ & + \frac{y}{2}(y^2 - B(3B - 2f)) \tan^{-1} \left(\frac{fy}{y^2 - BD} \right) \quad (14) \end{aligned}$$

(A2-20)

From section IA, the line $y = a - M_T x$ represents Reissner's membrane, and the velocity normal to this line is given by

$$\frac{\partial \phi}{\partial M_T} = \frac{1}{\sqrt{M_T^2 + 1}} \frac{\partial \phi}{\partial y} + \frac{M_T}{\sqrt{M_T^2 + 1}} \frac{\partial \phi}{\partial x}$$

Hence the normal velocity pattern of the membrane may be computed for each of the $v(x)_1$, $v(x)_2$ and $v(x)_3$ distributed sources, and will, according to the assumptions made, be very closely representative of the actual velocity function of this membrane except at and very close to the x and y axes. A detailed knowledge of the velocity pattern is an essential prerequisite for any effective mass calculation.

II. Effective Mass Calculation

II.A. Right-angled triangular representation.

To calculate the effective mass of fluid enclosed in a right-angled triangular scala media, the following assumptions and concepts are employed:

- a). frictionless, potential flow fields exist for the in-phase mass components (only) as has been applied in the analysis so far.
- b). the total energy within the oscillating scala media at any instant is its kinetic energy at that instant. That is, the total energy is the sum of the kinetic energies of all particles within the cochlear partition (i.e. no body forces or potential energy).
- c). the total energy for fluid and cell particles comprising the cochlear partition is equal to the total kinetic energy for particles in an idealized, potential column of matter having basilar membrane width f , and height H , the mass of which column is then defined as the effective mass of the cochlear partition.

Consider a column of fluid of height H , density ρ , of unit thickness and of width f , seated coincident with the basilar membrane, and having motion identical with it, so that, as a bounded potential field, the velocity of any element (x, y) within the column is equal to the velocity $\vec{w} = \vec{i} \circ + \vec{j} \left(v(x) = \frac{\partial \phi}{\partial t}(x, 0) \right)$ of the basilar membrane at that same value of x , and is independent of y . For a

thin vertical section of this column of width dx , (Fig.4),

$$\text{kinetic energy} = \frac{1}{2} \rho H v^2(x) dx.$$

Hence for basilar membrane velocity function $v(x)_1$, the total energy of the

$$\text{column, } E_1, = \int_{x_1}^{(x_1 + f)} \frac{1}{2} \rho H v^2(x)_1 dx = \frac{\rho H M^2}{2} \int_0^f (x^4 + f^2 x^2 - 2fx^3) dx$$

$$\therefore E_1 = \frac{\rho H M^2 f^5}{60}$$

and for basilar membrane velocity function $v(x)_2$, total energy in column, E_2 , is

$$E_2 = \int_{x_1}^{(x_1 + f)} \frac{1}{2} \rho H v^2(x)_2 dx$$

$$\therefore E_2 = \frac{\rho H M^2 f^7}{210}$$

Now consider the right angled triangle representing the scala media (Fig.4).

Dividing each of its two perpendicular sides into K small equal strips will

yield approx. $\frac{K^2}{2}$ small rectangles of intersection within the triangle. Consider

any one of these small elements having unit depth, and sides $\frac{a}{M_r}$, $\frac{a}{K}$.

Considering the fluid enclosed in the scala media to have the same mean density,

ρ , as that of the idealized equivalent column, the energy of the small rectangle

$$\text{of fluid at } (x, y) = \frac{1}{2} \rho \frac{a}{M_r} \frac{a}{K} \left(\left(\frac{\partial \phi}{\partial x} \right)^2_{(x,y)} + \left(\frac{\partial \phi}{\partial y} \right)^2_{(x,y)} \right)$$

The total energy of matter within the triangle can be obtained by summing

all of the elements, giving,

$$E = \frac{1}{2} \rho \frac{a^2}{K^2 M_r} \sum_x \sum_y \left(\left(\frac{\partial \phi}{\partial x} \right)^2_{(x,y)} + \left(\frac{\partial \phi}{\partial y} \right)^2_{(x,y)} \right)$$

Hence in case of $v(x)_1$

$$H = \frac{120 a^2}{M_r K^2 f^5 \pi^2} \sum_x \sum_y \left(\left(\frac{\pi}{2M} \frac{\partial \phi}{\partial x} \right)^2 + \left(\frac{\pi}{2M} \frac{\partial \phi}{\partial y} \right)^2 \right)$$

and for $v(x)_2$

$$H = \frac{420 a^2}{M_r K^2 f^7 \pi^2} \sum_x \sum_y \left(\left(\frac{\pi}{2M} \frac{\partial \phi}{\partial x} \right)^2 + \left(\frac{\pi}{2M} \frac{\partial \phi}{\partial y} \right)^2 \right)$$

The mass of the idealized, equivalent column of unit thickness,

$$A_e = H f \rho$$

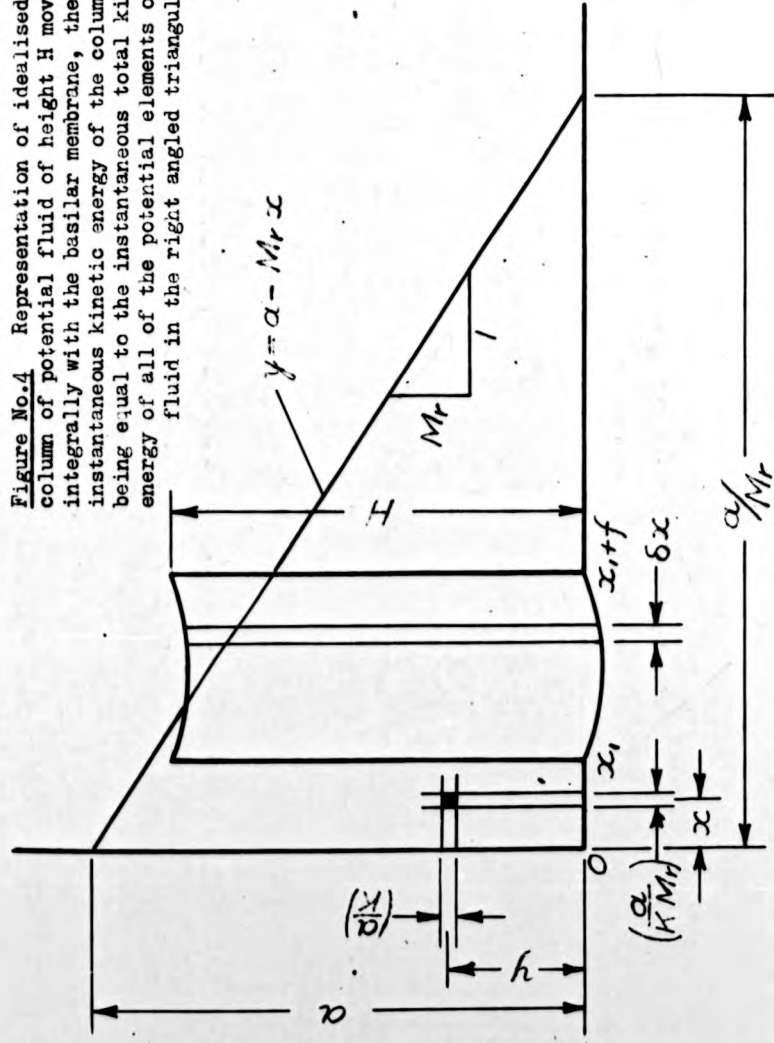
while actual mass of the scala media, for unit thickness,

$$A_a = \frac{1}{2} \frac{a}{M_r} \rho$$

\therefore Ratio of effective mass/actual mass of scala media

$$r = \frac{A_e}{A_a} = \frac{2H M_r f}{a^2}$$

Figure No.4 Representation of idealised column of potential fluid of height H moving integrally with the basilar membrane, the instantaneous kinetic energy of the column being equal to the instantaneous total kinetic energy of all of the potential elements of fluid in the right angled triangular space.



which in the case of $v(x)_1$ yields

$$r_{v(x)_1} = \frac{240 a^2}{K^2 f^4 \pi^2} \sum_x \sum_y ()$$

and for $v(x)_2$,

$$r_{v(x)_2} = \frac{840 a^2}{K^2 f^6 \pi^2} \sum_x \sum_y ()$$

The summation over the elements was carried out using an Elliott 4130 digital computer. Programmes evaluated the Reissner boundary amplitude and velocity profiles and, in particular, the effective scala masses for any value of M_r , x_1 and f .

Comparison of results was facilitated by normalizing the scala media sizes of the several shapes for which solutions have been sought by expressing all dimensions as a percentage of the height of the partition, i.e. the partition height has been reduced to unity throughout. It is the shape of this scala, including the geometry of its basilar membrane location relative to the wall of the spiral ligament which is the main factor of significance to the effective mass. As it is suspected that the density of the relatively small bulk of the cellular structures adjacent to the basilar membrane is very close to that of the endolymph, namely about 1.05 to 1.10 as compared with 1.05, a single density value (1.05) was assigned to the whole scala at this stage, although it is relatively simple to assign different densities to different areas of the scala in the computer programmes.

It has been established that for a range of K^2 of 100, 400, 1600 to 6400 and with the most critical values of M_r , x_1 and f , that K^2 of 1600 yielded results of adequate accuracy (worst error 1 part in 10^4).

Hence, as finally programmed, the following expressions were employed.

$$r_{v(x)_1} = \frac{60}{1600 \pi^2 f^4} \sum_x \sum_y \left(\left(\frac{\pi}{N} \frac{\partial \phi}{\partial x} \right)^2 (x,y)_1 + \left(\frac{\pi}{N} \frac{\partial \phi}{\partial y} \right)^2 (x,y)_1 \right)$$

$$r_{v(x)_2} = \frac{210}{1600 \pi^2 f^6} \sum_x \sum_y \left(\left(\frac{\pi}{N} \frac{\partial \phi}{\partial x} \right)^2 (x,y)_2 + \left(\frac{\pi}{N} \frac{\partial \phi}{\partial y} \right)^2 (x,y)_2 \right)$$

Typical values of r computed for various geometric variations are presented in Table 3. (for angle $\alpha = 90^\circ$)

A general mathematical technique is thus developed, based on the Laplacian or potential field model, to compute the effective mass, based on

energy considerations, of any right angle triangle-sectioned uniform fluid duct which is disturbed by a partial boundary membrane, moving, or vibrating with simple harmonic motion, in a known mode.

II.A. Non-right angled triangular representation.

It is unfortunate that the best triangular approximations to the shape of the scala media include both acute and obtuse angled triangles at different sections along the length of the cochlea.

By applying the technique of conformal transformation, it is possible to calculate the velocity vector field in a general (deformed) triangular space by referring each point considered to a more conveniently analysed right angled triangular space, both spaces still retaining the qualities of a potential field. Consider the $t(u, v)$ plane and the $z(x, y)$ plane (Fig.5). By application of the transformation

$$z = \frac{c}{n} t^n$$

the space bounded by the typical λ and u lines in the t plane (whose included angle is $\frac{\pi}{2n}$), may be conformally transformed into the space bounded by the right angled axes y and x respectively in the z plane.

$$\text{From } z = \frac{c}{n} t^n$$

$$\text{i.e., } x + iy = \frac{c}{n} (u + iv)^n$$

$$\text{Thus } x = r \cos \theta = \frac{c}{n} R^n \cos(n\phi)$$

$$\text{and } y = r \sin \theta = \frac{c}{n} R^n \sin(n\phi)$$

which must be true for all values of r and θ

$$\text{Hence } r = \frac{c}{n} R^n$$

$$\theta = n \phi$$

Thus the point $z(x_1, 0)$ transforms to $t(u_1, 0)$, both on the x or u axes, in which case, as both θ and $\phi = 0$, $\therefore u_1 = \left(\frac{n}{c} x_1\right)^{\frac{1}{n}}$

The point $z(0, y_1)$ transforms to $t(u_2, v_2)$ and all points on the z plane y axis transform to points all on the t plane λ line. Conversely the point $t(u, v)$ transforms to $z(x, y)$ as detailed above.

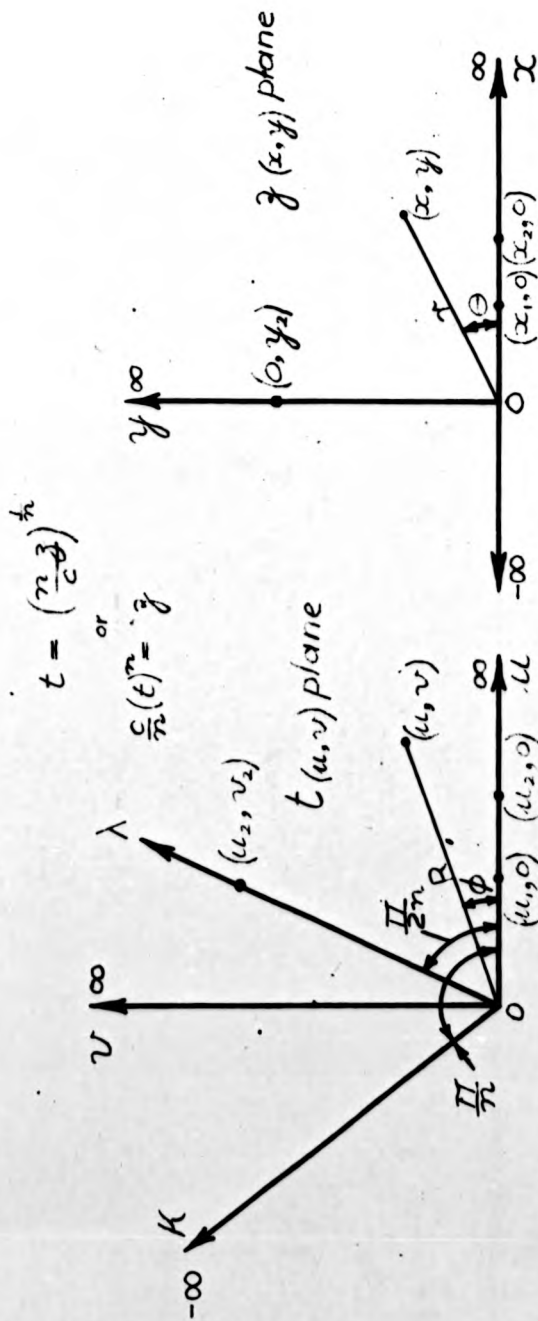
Similarly as

$$t = \left(\frac{n}{c} z\right)^{\frac{1}{n}}$$

$$\text{i.e. } u + iv = \left(\frac{n}{c}\right)^{\frac{1}{n}} (x + iy)^{\frac{1}{n}}$$

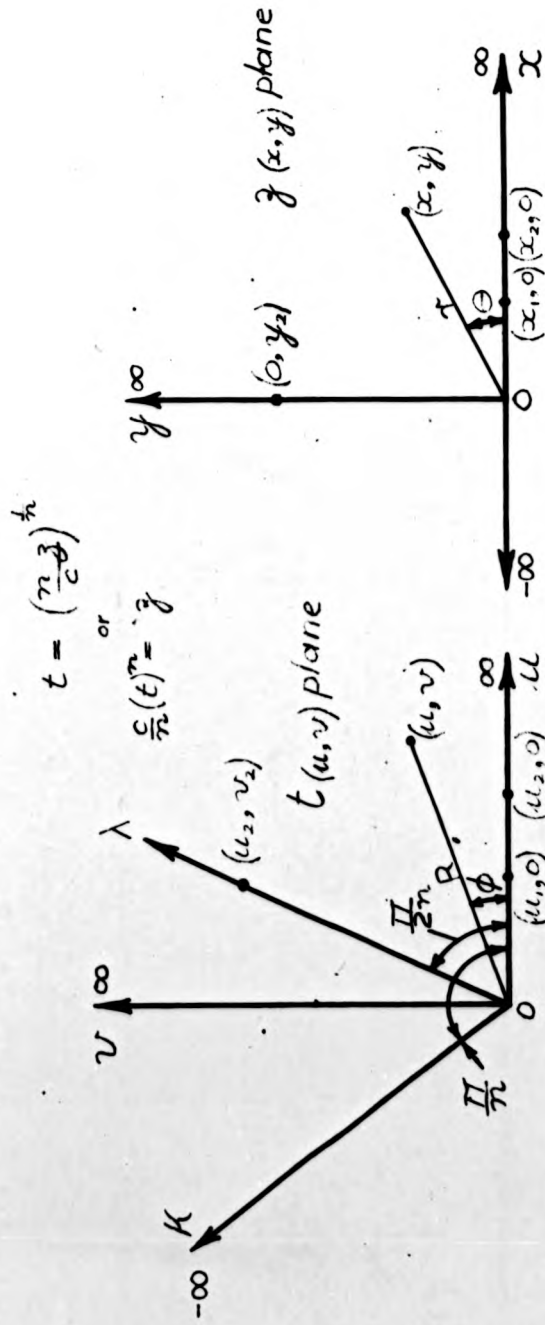
$$\therefore R(\cos \phi + i \sin \phi) = \left(\frac{R}{c}\right)^{\frac{1}{n}} r^{\frac{1}{n}} (\cos \theta/n + i \sin \theta/n)$$

Figure No.5 Co-ordinate system for original and transformed shapes



Points $(u_1, 0)$, $(u_2, 0)$, (u_2, v_2) and (u, v) in the t plane are conformally transformed to points $(x_1, 0)$, $(x_2, 0)$, $(0, y_2)$ and (x, y) respectively in the z plane via the transformation formulae.

Figure No.5 Co-ordinate system for original and transformed shapes



Points $(u_1, 0)$, $(u_2, 0)$, (u_2, v_2) and (u, v) in the t plane are conformally transformed to points $(x_1, 0)$, $(x_2, 0)$, $(0, y_2)$ and (x, y) respectively in the z plane via the transformation formulae.

$$\therefore R (\cos \phi + i \sin \phi) = \left(\frac{n}{c}\right)^{\frac{1}{n}} r^{\frac{1}{n}} (\cos \theta/n + i \sin \theta/n)$$

$$\text{giving } u = R \cos \phi = \left(\frac{n}{c}\right)^{\frac{1}{n}} r^{\frac{1}{n}} \cos \theta/n,$$

$$v = R \sin \phi = \left(\frac{n}{c}\right)^{\frac{1}{n}} r^{\frac{1}{n}} \sin \theta/n$$

$$\text{and } R = \left(\frac{n r}{c}\right)^{\frac{1}{n}}$$

Consider two possible shapes of scala media described in fig.6 as triangles in the t plane and let the apex of each triangle be the point $(u_3, v_3 = a)$ where, in each case, a is the height of this point above the u axis.

Let each of these t plane triangles be conformally transformable via the formula $z = \frac{c}{n}(t)^n$ into a right angled figure in the z plane of height also a , i.e. apex of z plane triangle is the point $(0, a)$.

$$\text{Then } v_3 = a = R_3 \sin \frac{\pi}{2n} \quad \text{in } t \text{ plane}$$

$$\text{and } a = r_3 \sin \frac{\pi}{2} = r_3 = \frac{c}{n} R_3^n$$

$$\therefore R_3 = a (\sin \frac{\pi}{2n})^{-1}$$

$$\text{and } R_3 \sin \frac{\pi}{2n} = \frac{c}{n} R_3^n$$

$$\therefore (R_3)^{1-n} \sin \frac{\pi}{2n} = \frac{c}{n}$$

$$\text{Hence } \frac{c}{n} = (a)^{1-n} (\sin \frac{\pi}{2n})^n$$

As before, a was maintained as 1 in all computations, and in the computer programmes, the insertion of

$$\frac{c}{n} = (\sin \frac{\pi}{2n})^n$$

ensured that both t plane and z plane triangles were of unit height. Using this identity, any point within a t plane triangle may be transformed to the z plane.

The straight line representing the Reissner boundary in the t plane transforms into a curve in the z plane, and a point $(u_1, 0)$ in the t plane transforms to the point $(\frac{c}{n} (u_1)^n, 0)$,

$$\text{that is, } ((u_1 \sin \frac{\pi}{2n})^n, 0)$$

on the x axis of the z plane.

In order to determine actual velocities, a velocity transformation from z -plane to t -plane must be executed.

$$\text{From } z = \frac{c}{n} (t)^n$$

$$\begin{aligned} x+iy &= \frac{c}{n} (u+iv)^n \\ \therefore \frac{\partial x}{\partial u} + i \frac{\partial y}{\partial u} &= c (u+iv)^{n-1} \\ &= c R^{n-1} (\cos(n-1)\phi + i \sin(n-1)\phi) \\ \frac{\partial x}{\partial v} + i \frac{\partial y}{\partial v} &= c i (u+iv)^{n-1} \\ &= c i R^{n-1} (\cos(n-1)\phi + i \sin(n-1)\phi) \\ &= c R^{n-1} (-\sin(n-1)\phi + i \cos(n-1)\phi) \end{aligned}$$

$$\text{Hence } \frac{\partial x}{\partial u} = \frac{\partial y}{\partial v} = c R^{n-1} \cos(n-1)\phi$$

$$\frac{\partial y}{\partial u} = -\frac{\partial x}{\partial v} = c R^{n-1} \sin(n-1)\phi$$

$$\text{But } \frac{\partial \phi}{\partial u} = \frac{\partial \phi}{\partial x} \frac{\partial x}{\partial u} + \frac{\partial \phi}{\partial y} \frac{\partial y}{\partial u}$$

$$\therefore \frac{\partial \phi}{\partial u} = \frac{\partial \phi}{\partial x} c R^{n-1} \cos(n-1)\phi + \frac{\partial \phi}{\partial y} c R^{n-1} \sin(n-1)\phi$$

$$\text{And } \frac{\partial \phi}{\partial v} = -\frac{\partial \phi}{\partial x} c R^{n-1} \sin(n-1)\phi + \frac{\partial \phi}{\partial y} c R^{n-1} \cos(n-1)\phi$$

$$\therefore \text{if } z = \frac{c}{n} t^n = \left(\sin \frac{\pi}{2n}\right)^n t^n$$

$$\therefore \frac{\partial z}{\partial u} = z'_u = n \left(\sin \frac{\pi}{2n}\right)^n t^{n-1}$$

if $\mathcal{R}(z'_u) =$ real part of z'_u

and $\mathcal{F}(z'_u) =$ imaginary part of z'_u

$$\text{Then } \left(\frac{\partial \phi}{\partial u}\right)_{t \text{ plane}} = \left(\frac{\partial \phi}{\partial x}\right)_z \mathcal{R}(z'_u) + \left(\frac{\partial \phi}{\partial y}\right)_z \mathcal{F}(z'_u)$$

$$\text{and } \left(\frac{\partial \phi}{\partial v}\right)_{t \text{ plane}} = -\left(\frac{\partial \phi}{\partial x}\right)_z \mathcal{F}(z'_u) + \left(\frac{\partial \phi}{\partial y}\right)_z \mathcal{R}(z'_u)$$

It is this format which has been used successfully in the computations.

Any point in the t plane for which vertical $\frac{\partial \phi}{\partial v}$ or horizontal $\frac{\partial \phi}{\partial u}$ components of velocity are required, and such points include the Reissner boundary as well as the general net of grid points considered in the effective mass energy summation, is first transformed into the z plane. At this z plane location, with its orthogonal boundaries, $\frac{\partial \phi}{\partial x}$ and $\frac{\partial \phi}{\partial y}$ are evaluated.

The complex function z'_u is then evaluated for the point on the t plane

being considered using the expression $z'_u = n \left(\sin \frac{\pi}{2n} \right)^n (t)^{n-1}$.

The real and imaginary parts of z'_u are then used in the appropriate equations with $\frac{\partial \phi}{\partial x}$ and $\frac{\partial \phi}{\partial y}$ for the transformed point to yield $\frac{\partial \phi}{\partial u}$ and $\frac{\partial \phi}{\partial v}$ at the t plane point considered. As regards the boundary velocity functions $v(x)_1$ and $v(x)_2$, etc., it is clear that they will be changed in a conformal transformation from one plane to the other, the transformed function becoming more distorted relative to the original function as n departs further from unity.

Now the functions $v(x)_1$, $v(x)_2$ and $v(x)_3$ are, for the sake of mathematical convenience, necessarily only applicable to the z plane. It therefore remains to express these as t plane functions, and to assess their distortion when in the t plane.

Consider the point $(u_2, 0)$ on the u axis of the t plane transformed from the point $(x_2, 0)$ in the z plane, (Refer to Figs. 5 and 6).

$$u_2 = (x_2)^{\frac{1}{n}} / \sin \frac{\pi}{2n} = S(x_2)^{\frac{1}{n}}$$

$$\text{where } S = 1 / \sin \frac{\pi}{2n}$$

∴ for x_2 in terms of u_2 ,

$$x_2 = \left(\frac{u_2}{S} \right)^n$$

$$\text{Considering } v(x)_1 = M \left((x - x_1)^2 - f(x - x_1) \right)$$

$$\text{Let } u_1 = G, f_1 = x_2 - x_1, u_2 = G + F$$

where G is the distance, in the non-right angled triangular representation, from the origin of co-ordinates to one side of the region of excitation and $(G+F)$ is the distance to the other side of the region, the width of the region therefore being F . These distances correspond to x_1 , $(x_1 + f)$ and f respectively in the right angled triangular representation and also in the z -plane transformation.

$$\text{Hence } v(u)_1 = M \left[\left(\left(\frac{u}{S} \right)^n - \left(\frac{G}{S} \right)^n \right)^2 - \left(\frac{G+F}{S} \right)^n - \left(\frac{G}{S} \right)^n \left(\left(\frac{u}{S} \right)^n - \left(\frac{G}{S} \right)^n \right) \right]$$

$$\therefore v(u)_1 = \frac{M}{S^{2n}} \left(u^{2n} - u^n \left((G+F)^n + G^n \right) + G^n (G+F)^n \right)$$

This is zero when $u = G$ and when $u = G + F$ and displays a shape very similar to the z -plane shape of $v(x)_2$ as n rises from 1 towards 2

$$\text{As } \frac{dv(u)_1}{du} = M \left(2n u^{2n-1} - n \left((G+F)^n + G^n \right) u^{n-1} \right) / S^{2n}$$

This displays a maximum negative value of $v(u)_1$ when $(u)^n = \frac{(G+F)^n + (G)^n}{2}$

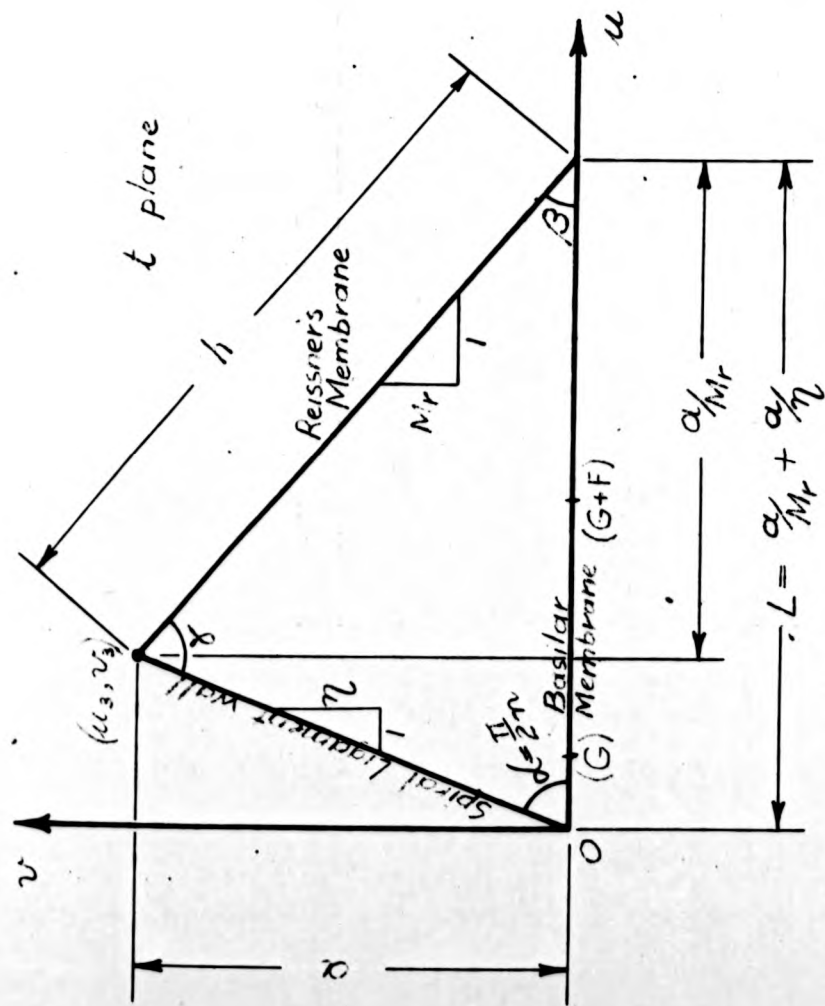


Figure No.6a t plane representation of non-right angled triangular scala media shape

Fig.6a is for the acute case when $n > 1$

If, for the purposes of illustrating the location of these maxima for variations in n , the severest case is assumed when θ (and hence x_1) is almost zero, and F (and hence f) is large in comparison,

$$\text{then consider } u = \frac{\frac{F}{1}}{(2)^n} .$$

Clearly, when $n = 1$ and there is no transformation, i.e. the t plane axes are orthogonal, and the maximum occurs at $u = F/2$ i.e. the function $v(x)_1$ is symmetric.

When $n = 2$, $u = 0.7F$ gives the location of the maximum, which implies a less symmetrical function than $v(x)_2$ in which the maximum occurs at $0.67 f$.

When $n = 1.2$, representing a 75° included angle in the t plane, which is the smallest angle expected to be encountered in cochlear variations, the maximum is located at $u = 0.55 F$.

When $n = 0.75$, representing a 120° included angle in the t plane, which is the largest angle expected to be encountered, the maximum is located at $u = 0.4 F$.

Hence between 120° and 75° included angle variations, the use of the basilar boundary velocity function $v(x)_1$ will present an approximately symmetric function to the real (t plane) model, but one which varies more towards the likely correct basilar membrane actual velocity pattern, (as described by $v(x)_3$) in the regions for which $n < 1$.

Similarly, the function $v(x)_2$ which is assymmetrically loaded towards the limbus and bony spiral lamina in the z plane will more or less retain this characteristic in the t plane. But for areas where $n < 1$, where the included angle becomes obtuse, the shape of the function will tend to approach the symmetry of $v(x)_1$. It should be clear therefore that the choice of velocity functions $v(x)_1$, $v(x)_2$, $v(x)_3$ etc. is influenced not only by their z plane shapes but also by the variations in included angle of the t plane axes, representing variations in organ of Corti geometry. As there is a limit to the number of such functions for which the potential analyses can be made, it remains a matter of interpolation as to which function to apply to any one section of the cochlea. In any case, as the results will indicate, the different functions have only a limited effect on

the effective mass of the scala media.

Considering
$$v(x)_2 = N \left[(x-x_1)^3 - (x_2-x_1)(x-x_1)^2 \right]$$

As before, if $u_1 = G$, $u_2 = G + F$, and $(u, 0)$ represents the t plane transformation of z plane point $(x, 0)$

then
$$v(u)_2 = N \left[\left(\left(\frac{u}{S} \right)^n - \left(\frac{G}{S} \right)^n \right)^3 - \left(\left(\frac{G+F}{S} \right)^n - \left(\frac{G}{S} \right)^n \right) \left(\left(\frac{u}{S} \right)^n - \left(\frac{G}{S} \right)^n \right)^2 \right]$$

$$\therefore v(u)_2 = \frac{N}{S^{3n}} \left[u^{3n} - u^{2n} (2G^n + (G+F)^n) + u^n (G^{2n} + 2G^n(G+F)^n) - G^{2n}(G+F)^n \right]$$

Again this checks as being 0 when $u = G$ and $u = G + F$.

It is now possible to perform a recalculation of energy of idealised fluid columns. The concept of a bounded, ideal column of potential (in the irrotational sense) matter, mounted upon the basilar membrane, maximum kinetic energy of which column is equal to the maximum kinetic energy of the matter comprising the scala media, has been outlined in section IIA.

In order to use this concept for the inclined axes situation, it is now necessary to calculate the equivalent of the term $\int_{x_1}^{x_1+F} v^2(x) dx$.

Thus for $v(u)_1$ velocity distribution in the t plane,

$$(v(u)_1)^2 = \frac{M^2}{S^{4n}} \left[u^{4n} - 2u^{3n} ((G+F)^n + G^n) + u^{2n} (2G^n(G+F)^n + ((G+F)^n + G^n)^2) - 2u^n G^n(G+F)^n ((G+F)^n + G^n) + G^{2n}(G+F)^{2n} \right]$$

$$\therefore \int_G^{(G+F)} (v(u)_1)^2 du = \frac{M^2}{S^{4n}} \left[\frac{u^{4n+1}}{4n+1} - 2 \frac{u^{3n+1}}{3n+1} ((G+F)^n + G^n) + \frac{u^{2n+1}}{2n+1} (2G^n(G+F)^n + ((G+F)^n + G^n)^2) - 2 \frac{u^{n+1}}{n+1} G^n(G+F)^n ((G+F)^n + G^n) + u G^{2n}(G+F)^{2n} \right]_{(G)}$$

And this expression has been programmed and computed in this form.

Similarly for $v(u)_2$

$$\int_G^{(G+F)} (v(u)_2)^2 du = \frac{N^2}{S^{6n}} \left[\frac{u^{6n+1}}{6n+1} - 2 \frac{u^{5n+1}}{5n+1} (E4) + \frac{u^{4n+1}}{4n+1} (E4^2 + 2.E2) - 2 \frac{u^{3n+1}}{3n+1} (E6 + E4.E2) + \frac{u^{2n+1}}{2n+1} (E2^2 + 2.E4.E6) - 2 \frac{u^{n+1}}{n+1} (E2.E6) + u(E6)^2 \right]_{(G)}$$

Where $E2 = G^{2n} + 2G^n (G + F)^n$

$E4 = 2G^n + (G + F)^n$

$E6 = G^{2n} (G + F)^n$

As for $v(u)_1$, the above integral of the square of $v(u)_2$ is required for calculating the kinetic energy of the idealized fluid column, and this expression has been programmed in terms of E2, E4 and E6 as shown and computed in this form.

Four cases are here considered :- for $v(u)_1$ and $v(u)_2$ in acute angled and obtuse angled triangles.

1. Acute case with $v(u)_1$ (see Fig.6a)

In the computation, a and L were each divided into $K = 40$ strips for the particle energy summation. Let $\eta = \tan^{-1} (\pi/2n)$. Hence η is positive.

∴ Max. Kinetic energy of each small rectangle

$$= \frac{1}{2} \rho \frac{a^2}{K^2} \frac{(M_r + \eta)}{M_r \eta} \left(\left(\frac{\partial \phi}{\partial u} \right)^2 + \left(\frac{\partial \phi}{\partial v} \right)^2 \right)$$

Total max. energy of whole scale

$$= \frac{1}{2} \rho \frac{a^2}{K^2} \frac{(M_r + \eta)}{M_r \eta} \frac{M^2}{\pi^2} \sum^u \sum^v \left(\left(\frac{\pi}{M} \frac{\partial \phi}{\partial u} \right)^2 + \left(\frac{\pi}{M} \frac{\partial \phi}{\partial v} \right)^2 \right)$$

Total max. kinetic energy of equivalent ideal column, height H,

$$= \frac{1}{2} \rho \frac{H M^2}{S^{4n}} \left(\text{integrand of } (v(u)_1)^2 \right)_{(a)}^{(a+F)}$$

$$\text{Hence H} = \frac{a^2 (M_r + \eta) S^{4n} \sum^u \sum^v \left(\left(\frac{\pi}{M} \frac{\partial \phi}{\partial u} \right)^2 + \left(\frac{\pi}{M} \frac{\partial \phi}{\partial v} \right)^2 \right)}{K^2 M_r \eta \pi^2 \left(\text{integrand of } (v(u)_1)^2 \right)}$$

But effective mass = mass of ideal column of same energy

$$= \rho H F$$

And actual mass per unit thickness of the triangular scale

$$= \frac{1}{2} \rho a^2 (M_r + \eta) / (M_r \eta)$$

∴ Ratio r = $\frac{\text{effective mass}}{\text{actual mass}}$

$$= \frac{2 H F M_r \eta}{a^2 (M_r + \eta)}$$

$$\text{Hence } r_1 \text{ acute} = \frac{2 F \sum^u \sum^v \left(\left(\frac{\pi}{M} \frac{\partial \phi}{\partial u} \right)^2 + \left(\frac{\pi}{M} \frac{\partial \phi}{\partial v} \right)^2 \right)}{\left(\sin \frac{\pi}{2n} \right)^{4n} \pi^2 K^2 \left(\text{integrand of } (v(u)_1)^2 \right)_{(a)}^{(a+F)}}$$

2. Acute case with $v(u)_2$

Similarly

$$r_2 \text{ acute} = \frac{2F \sum^u \sum^v \left(\left(\frac{\pi}{M} \frac{\partial \phi}{\partial u} \right)^2 + \left(\frac{\pi}{M} \frac{\partial \phi}{\partial v} \right)^2 \right)}{(\sin \pi/2n)^{6n} \pi^2 K^2 \left(\text{integrand of } (v(u)_2)^2 \right)^{(6+F)}$$

3. Obtuse case with $v(u)_1$. See Fig. 6b

In these computations involving an obtuse angled triangle, a and a/M_r were each divided into $K = 40$ strips for the particle energy summation.

∴ Maximum kinetic energy of each small rectangular element of matter

$$= \frac{1}{2} \rho \frac{a^2}{K^2 M_r} \left(\left(\frac{\partial \phi}{\partial u} \right)^2 + \left(\frac{\partial \phi}{\partial v} \right)^2 \right)$$

Total max. energy of whole scala media

$$= \frac{1}{2} \rho \frac{a^2 M^2}{K^2 M_r \pi^2} \sum^u \sum^v \left(\left(\frac{\pi}{M} \frac{\partial \phi}{\partial u} \right)^2 + \left(\frac{\pi}{M} \frac{\partial \phi}{\partial v} \right)^2 \right)$$

Total max. kinetic energy of equivalent ideal column of matter, height H , mounted on the basilar membrane

$$= \frac{1}{2} \rho H \frac{M^2}{S^{4n}} \left(\text{integrand of } (v(u)_1)^2 \right)$$

$$\text{Hence } H = \frac{a^2 S^{4n} \sum^u \sum^v \left(\left(\frac{\pi}{M} \frac{\partial \phi}{\partial u} \right)^2 + \left(\frac{\pi}{M} \frac{\partial \phi}{\partial v} \right)^2 \right)}{K^2 M_r \pi^2 \left(\text{integrand of } (v(u)_1)^2 \right)}$$

But effective mass = mass of ideal column of same energy

$$= \rho H F$$

And actual mass per unit thickness of the triangular scala

$$= \frac{1}{2} \rho \frac{a^2 (M_r + \eta)}{M_r \eta} \quad \text{where } \eta \text{ is now negative}$$

and $|\eta| > |M_r|$

∴ Ratio $r = \frac{\text{effective mass}}{\text{actual mass}}$

$$= \frac{2 \cdot H \cdot F \cdot M_r \cdot \eta}{a^2 \cdot (M_r + \eta)}$$

$$\text{Hence } r_1 \text{ obtuse} = \frac{2 \cdot F \cdot \tan^{-1} \left(\frac{\pi}{2n} \right) \cdot \sum^u \sum^v \left(\left(\frac{\pi}{M} \frac{\partial \phi}{\partial u} \right)^2 + \left(\frac{\pi}{M} \frac{\partial \phi}{\partial v} \right)^2 \right)}{(\sin \pi/2n)^{4n} \cdot \pi^2 \cdot K^2 \cdot (M_r + \tan^{-1} \pi/2n) \cdot \left(\text{integrand of } (v(u)_1)^2 \right)^{(6+F)}$$

2. Acute case with $v(u)_2$

Similarly

$$r_2 \text{ acute} = \frac{2F \sum^u \sum^v \left(\left(\frac{\pi}{N} \frac{\partial \phi}{\partial u} \right)^2 + \left(\frac{\pi}{N} \frac{\partial \phi}{\partial v} \right)^2 \right)}{(\sin \pi/2n)^{6n} \pi^2 K^2 \left(\text{integrand of } (v(u)_2)^2 \right)_{(6)}}$$

3. Obtuse case with $v(u)_1$. See Fig. 6b

In these computations involving an obtuse angled triangle, a and a/M_r were each divided into $K = 40$ strips for the particle energy summation.

∴ Maximum kinetic energy of each small rectangular element of matter

$$= \frac{1}{2} \rho \frac{a^2}{K^2 M_r} \left(\left(\frac{\partial \phi}{\partial u} \right)^2 + \left(\frac{\partial \phi}{\partial v} \right)^2 \right)$$

Total max. energy of whole scala media

$$= \frac{1}{2} \rho \frac{a^2 M^2}{K^2 M_r \pi^2} \sum^u \sum^v \left(\left(\frac{\pi}{M} \frac{\partial \phi}{\partial u} \right)^2 + \left(\frac{\pi}{M} \frac{\partial \phi}{\partial v} \right)^2 \right)$$

Total max. kinetic energy of equivalent ideal column of matter, height H , mounted on the basilar membrane

$$= \frac{1}{2} \rho \frac{H M^2}{S^{4n}} \left(\text{integrand of } (v(u)_1)^2 \right)$$

$$\text{Hence } H = \frac{a^2 S^{4n} \sum^u \sum^v \left(\left(\frac{\pi}{M} \frac{\partial \phi}{\partial u} \right)^2 + \left(\frac{\pi}{M} \frac{\partial \phi}{\partial v} \right)^2 \right)}{K^2 M_r \pi^2 \left(\text{integrand of } (v(u)_1)^2 \right)}$$

But effective mass = mass of ideal column of same energy

$$= \rho H F$$

And actual mass per unit thickness of the triangular scala

$$= \frac{1}{2} \rho \frac{a^2 (M_r + \eta)}{M_r \eta} \quad \text{where } \eta \text{ is now negative}$$

and $|\eta| > |M_r|$

∴ Ratio $r = \frac{\text{effective mass}}{\text{actual mass}}$

$$= \frac{2.H.F.M_r \cdot \eta}{a^2.(M_r + \eta)}$$

$$\text{Hence } r_1 \text{ obtuse} = \frac{2.F. \tan^{-1} \left(\frac{\pi}{2n} \right) \cdot \sum^u \sum^v \left(\left(\frac{\pi}{M} \frac{\partial \phi}{\partial u} \right)^2 + \left(\frac{\pi}{M} \frac{\partial \phi}{\partial v} \right)^2 \right)}{(\sin \pi/2n)^{4n} \cdot \pi^2 \cdot K^2 \cdot (M_r + \tan^{-1} \pi/2n) \left(\text{integrand of } (v(u)_1)^2 \right)_{(6)}}$$

4. Obtuse case with $v(u)_2$

Similarly

$$\tau_2 \text{ obtuse} = \frac{2 F \left(\tan^{-1} \frac{\pi}{2n}\right) \sum_u \sum_v \left(\left(\frac{\pi}{N} \frac{\partial \phi}{\partial u}\right)^2 + \left(\frac{\pi}{N} \frac{\partial \phi}{\partial v}\right)^2 \right)}{\left(\sin \frac{\pi}{2n}\right)^{6n} \pi^2 K^2 \left(M_T + \tan^{-1} \frac{\pi}{2n}\right) \left(\text{integrand of } (v(u)_2)^2\right)_{(G)}^{(G+F)}}$$

where 1) F is the t plane actual width ascribed to the basilar membrane.

2) n is the factor in $\pi/2n$ which gives the included angle between the basilar membrane and the spiral ligament straight wall of the t plane model of the scala media.

III. Discussion of theoretical effective mass ratios

Results of calculations performed on the Elliott 4130 computer are summarized in Table 3.

The variables involved in scala media effective mass calculations up to this point are M_T , G, F, n and $v(u)$ (or $v(x)$) and for ranges of each of these variables the effective mass ratio r is tabulated, where r is the ratio of the mass of an imaginary basilar membrane having the same total instantaneous energy as that of the whole scala media to the actual mass of the whole scala media.

With each value of r, as given in Table 3, there has been added a lower case letter, a, b, c, d, e or f which is intended to categorize the shape of the amplitude envelope of Reissner's membrane. The letter a indicates that the membrane has highest velocity and, assuming sinusoidal motion, largest displacement amplitude very near to its higher attachment. The letter c or f indicates the displacement pattern noted by von Békésy for static displacements, with maximal displacement very near to its lower end, adjacent to the attachment of the tectorial membrane. These categories are indicated graphically in Fig. 7.

From Table 3 the following observations can be made.

1). Reducing the obtuseness and increasing the acuteness of the triangular representation of the scala media (increasing n), while maintaining other

Figure No.7 Shape index giving diagrammatic representation of six velocity and displacement patterns for Reissner's membrane (not to scale).

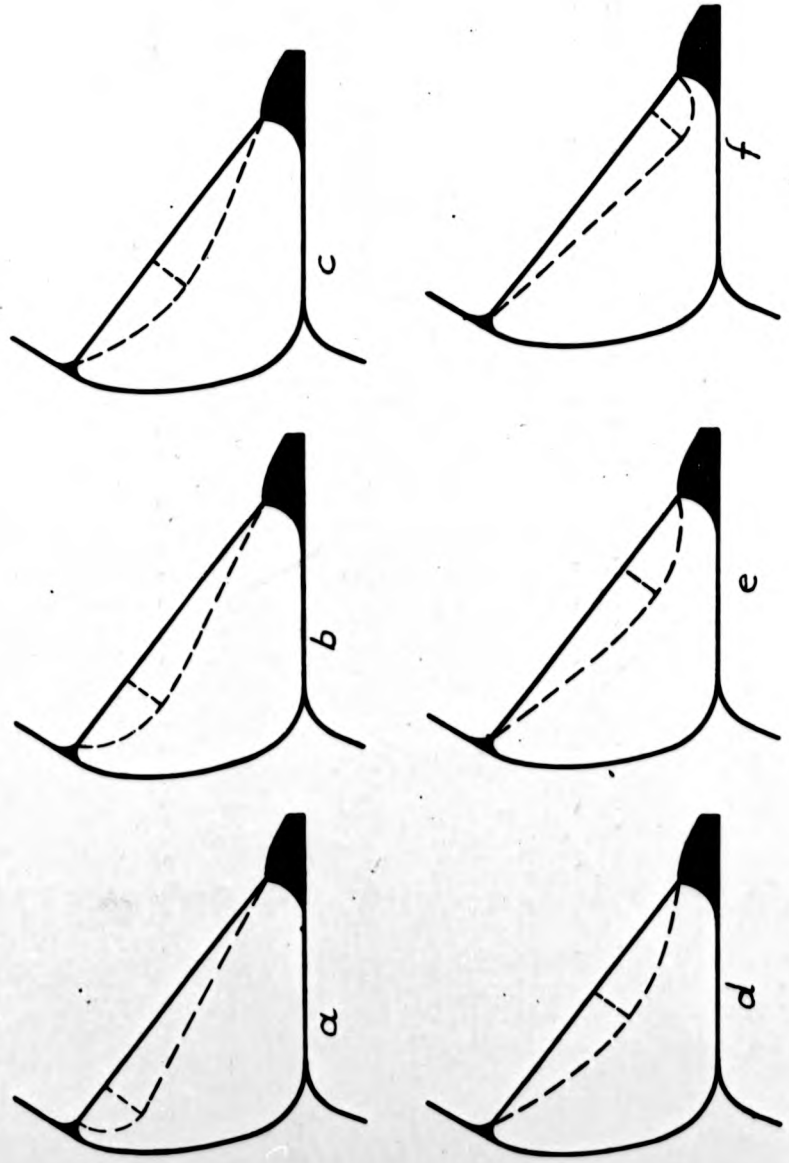


Table No.3

Effective Mass Ratios, r .

n	α	M_r	β	G	F	For $v(x)_1$		For $v(x)_2$	
						r	index	r	index
acute angled triangles	72°	2.00	63½°	0.01	0.10	0.014	d	0.013	e
				0.01	0.30	0.129	d	0.117	e
				0.01	0.50	0.319	e	0.286	e
				0.01	0.30	0.129	d	0.117	e
				0.11	0.30	0.140	e	0.126	e
				0.01	0.30	0.129	d	0.117	e
	45°	1.00	45°	0.01	0.10	0.010	c	0.009	c
				0.01	0.30	0.092	c	0.083	c
				0.01	0.50	0.241	c	0.218	c
				0.01	0.30	0.092	c	0.083	c
				0.11	0.30	0.102	c	0.092	c
				0.21	0.30	0.107	c	0.097	d
	26½°	0.50	26½°	0.01	0.10	0.006	b	0.005	b
				0.01	0.30	0.059	b	0.054	b
				0.01	0.50	0.160	b	0.146	b
				0.01	0.30	0.059	b	0.054	b
				0.11	0.30	0.067	b	0.060	b
				0.21	0.30	0.071	b	0.064	c
right angled triangles	90°	2.00	63½°	0.01	0.10	0.052	e	0.045	e
				0.01	0.30	0.269	e	0.228	e
				0.11	0.50	0.211	f	0.182	f
	45°	1.00	45°	0.01	0.10	0.030	c	0.026	d
				0.01	0.30	0.174	d	0.149	d
				0.01	0.50	0.352	d	0.299	d
				0.01	0.30	0.174	d	0.149	d
				0.11	0.30	0.149	d	0.131	d
				0.21	0.30	0.133	d	0.118	e

n	α	M_T	β	G	F	For $v(x)_1$		For $v(x)_2$							
						Reissner's shape <u>r</u> index	Reissner's shape <u>r</u> index	Reissner's shape <u>r</u> index	Reissner's shape <u>r</u> index						
1.00	90°	0.50	$26\frac{1}{2}^\circ$	0.01	0.10	0.017	b	0.014	b						
					0.30	0.102	b	0.087	b						
					0.50	0.218	b	0.187	c						
				0.01	0.30	0.102	b	0.087	b						
						0.11	0.30	0.090	b	0.079	b				
						0.21	0.30	0.082	b	0.073	c				
						0.75	120°	1.0	45°	0.01	0.10	0.093	e	0.076	e
										0.01	0.30	0.301	e	0.233	f
				obtuse angled triangles			$26\frac{1}{2}^\circ$	0.11	0.30	0.160	f	0.128	f		
										0.50	0.10	0.036	c	0.029	c
0.01	0.30	0.139	c									0.111	c		
0.01	0.50	0.236	d					0.186	d						
0.01	0.30	0.139	c					0.111	c						
		0.11	0.30					0.089	c	0.076	c				
		0.21	0.30					0.070	d	0.061	d				

Refer to Fig.No.6 for diagrams defining the t plane variables; G (distance from the inner extremity of the basilar membrane to the foot of the straight line of slope = $\tan \alpha$, where $\alpha = \pi/2n$, representing the spiral ligament/stria vascularis inner wall of the scula media), F (width of the basilar membrane), M_T (slope of Reissner's Membrane = $\tan \beta$). The height, a, of the triangle representing the scula media is unity in each case.

Refer to Fig. No.7. for the index to the deflected shape functions of Reissner's membrane and to Fig.No.3 for the shape of the two velocity functions $v(x)_1$ and $v(x)_2$ defining the z plane deflected shape of the basilar membrane.

parameters constant (M_p , G , F , $v(x)$) results, in general, in decreasing values of r . This trend may be arrested by several means; for example by moving the basilar membrane towards the limbus, that is, by increasing D , in which case r for the obtuse angled case diminishes.

- 2). The effect of reducing the slope of Reissner's membrane (M_p), all other parameters remaining constant, is to give a consistent reduction in the values of r and to raise the area of maximum displacement of Reissner's membrane away from the limbus.
- 3). The effect of varying G , which fixes the location of the basilar membrane, or the ratio, τ , of effective to actual mass, seems to depend on the relationship of the basilar membrane to the apex of the triangular representation of the scala media in that the value of r falls as this source of excitation is moved away from an area directly below the apex, whether to right or left. For example, in acute angled triangles, increases in G are associated with increases in r for the range of values of G tested. In obtuse angled triangles, the opposite trend is apparent.
- 4). With increasing basilar membrane width, F , the value of r , not expectedly, increases sharply in all cases and the area of maximum excitation of Reissner's membrane moves down the membrane towards the limbus. This is the most significant functional relationship for controlling r and follows from the fact that a wider basilar membrane excites more field and imparts larger, more widespread fluid velocities.
- 5). With the symmetrical exciting function $v(x)_1$, the point of maximum excitation of Reissner's membrane tends to occur higher up the slope, a little further away from the limbus, than with the asymmetrical excitation given by $v(x)_2$, but it should be noted that with the non-right angled triangular sections the actual exciting function is somewhat distorted, depending on n .

The value of r derived from fluid velocities based on $v(x)_1$ is larger in every case than r for $v(x)_2$. (Note that the volumetric flow difference between these velocity patterns is not relevant to this observation, the theory for

which is wholly normalised). In many cases the difference between the two values of r calculated from the two basilar membrane velocity and displacement pattern assumptions is small (about 10%) and at the greatest it is 30%.

When $n = 0.75$, the actual velocity pattern $v(u)_1$, obtaining at the basilar membrane in the t plane when using $v(x)_1$ in the z plane, is very similar to $v(x)_3$, and close to the pattern as described by von Békésy and as predicted from static deflection shapes. Also the pattern obtaining using $v(x)_2$ for $n = 0.75$ is similar to the undistorted $v(x)_1$ envelope, obtaining when $n = 1.0$. This allows a partial comparison to be made between results for $n = 0.75$ and $n = 1.0$ for constant $v(u)$. Similarly, $v(u)_2$ [$= v(x)_2$] in $n = 1.0$ is very nearly equal to $v(u)_1$ in the cases where $n = 1.25$.

It is considered that in view of the closeness of the results for the two velocity functions for which results have been computed, extrapolation of results to allow for other functions is quite reasonable at this stage.

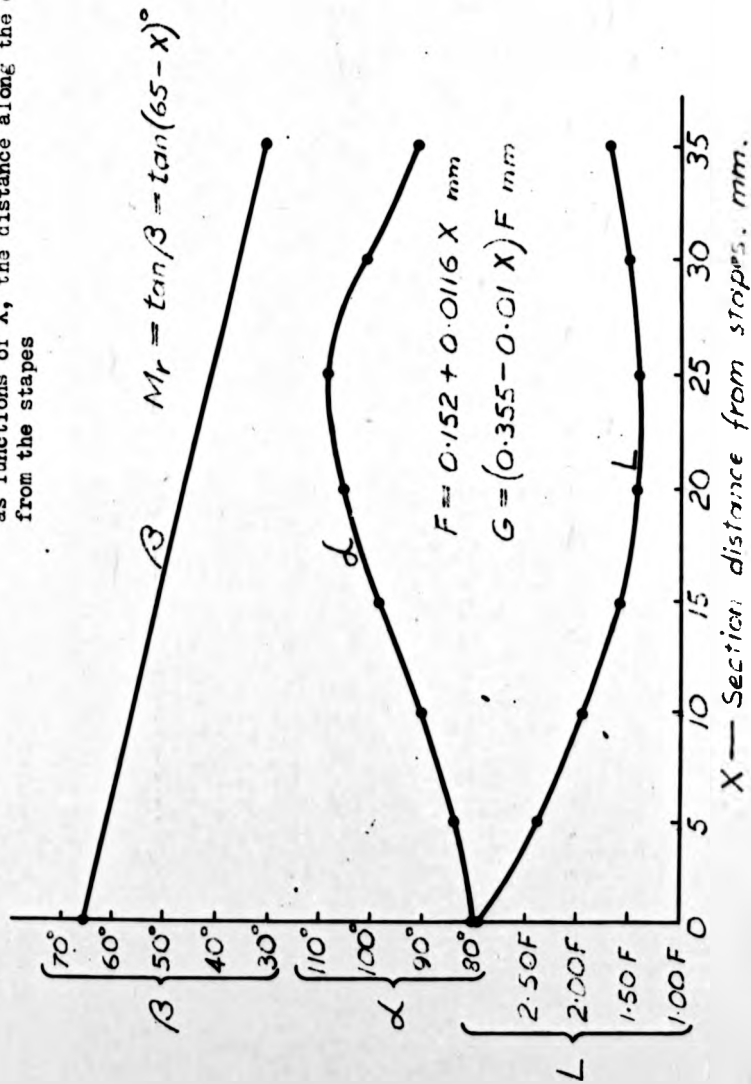
To conclude the discussion about the dependence of r on the various geometric functions, it is clear that the most important variable is the width of the basilar membrane, and that, for conversion of r into an actual mass per unit length, this width factor outweighs even the likely variations in scala media cross sectional area. It should be observed that since the greatest value of r displayed in the table is 0.35, it is inconceivable that more than a half of the actual mass of the scala media could be considered as a load integral with the basilar membrane and it is probable that a figure much smaller than this is appropriate. As regards the amplitude and velocity envelopes for Reissner's membrane, in no case did condition 2 apply. For the 86 results, the incidence of each of the 6 cases is given as:-

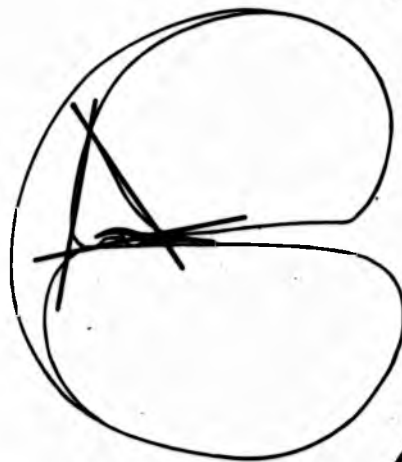
a - 0	d - 18
b - 21	e - 18
c - 23	f - 6

Predictably, when the basilar membrane was situated close to the lower end of Reissner's membrane, as, for example, when H_2 was larger, the lower end of the

Figure No. 8a Typical variations of scala media
and organ of Corti geometry

In Fig. 8a all the geometric variables are defined
as functions of X , the distance along the cochlea
from the stapes

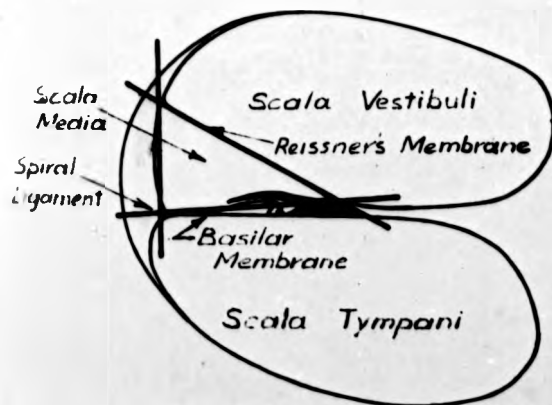




Section near stapes
at $X=0$ mm.



Section at
 $X=20$ mm



Section near apex $X=35$ mm.

Figure No. 8b.
Typical variations of
scala media and organ
of Corti geometry

Fig. 8b shows the manner
in which triangles may
approximate scala media
shapes.

FIGURE No 8 b

membrane did tend to move with maximum amplitude. Although it is not so included in the computer tests whose results are shown in the table, the same effect applies for low M_T when a relatively broad basilar membrane is inserted, especially if G is large enough to displace the latter membrane more to the right.

These results appear to be as much in accord with von Békésy's observations as one can judge from the paucity of his dynamic test data.

IV. DISCUSSION OF TYPICAL EFFECTIVE MASSES

The variation in effective width, F , of the basilar membrane is itself well documented. Also it is possible, from the reports and photographs of several investigators (2,3,4,5,6,18,19,20) to determine overall dimensions of the scala media, and dimensions and angles of inclination of Reissner and stria/vascularis/spiral ligament boundaries.

Consider the types of triangle used to approximate the shape of the scala media (Figs.6a and 6b). Also refer to Figs.8a and 8b.

In each case γ is defined as $\delta = \pi - (\gamma + \beta)$

$$\text{Therefore } a = \frac{L \sin \alpha \sin \beta}{\sin \gamma} \quad \text{and } h = \frac{L \sin \alpha}{\sin \gamma}$$

$$\therefore \text{ Area of triangle } A = \frac{L^2 \sin \alpha \sin \beta}{2 \sin \gamma}$$

The effect of variation in width of the basilar membrane is discussed elsewhere. Based mainly on the references (2), (3), and (4), the following linear expression is used, (see Chapter 5, table 1, page 5-16)

$$F = 0.152 + 0.0116 X. \text{ mms.}$$

where X mms is the sectional position from the stapes. As this dimension F is the only dimension of the cochlear partition on which agreement is reasonable, it has been used as the basis for defining the dimensions G and L (see table 4). As is seen from Fig.8b, the dimension G is not critical and is arranged to suit the mean slope and curvature of the spiral ligament wall. In setting the straight line at inclination angle α' to approximate this normally curved boundary, some care must, of course, be taken to ensure reasonable inclusion of the stronger potential field nearer to the basilar membrane, at the

expense, if need be, of areas further removed from the source (i.e., areas nearer the upper attachment of Reissner's membrane.)

Satisfactory agreement has resulted from checking the variations of L with distance along the cochlea, relating L to F in each case, against published information. Table 4 and Fig. 8 set out the variations in these variables. There is close agreement between the areas calculated from the selected variables and both the mean cross sectional area of the scala media of 0.19 mm^2 given by Littler⁽⁵⁾ and the value of 0.20 mm^2 , representing a variation from 0.15 to 0.25 mm^2 , given by Wever⁽⁴⁾.

It may also be noted that the dimension h was calculated so as to test the von Békésy implication that the sectional length of Reissner's membrane in cochleas on which he conducted scala media stiffness tests was approximately constant. Results in Table 4 show only 25% variation in h, which remains constant in the apical half of the cochlea. The constant width Békésy apparently observed is calculated as being 1.20 mm. The results in table 5 are calculated for the typical scala media sections as detailed in Table 4 and Figure 8. A mean fluid and cell density of 1.05 was assumed. Results were also obtained for the simple case of a uniform scala media model, having angle α constant at 90° and angle β constant at 45° , and a constant height of 0.633 mm., giving a uniform area of 0.20 mm^2 .

From table 5, it is immediately apparent that the mass for unit area on the basilar membrane of the scala media varies by less than 2.4 times from one end of the cochlea to the other, and that the range of results for the detailed case is only slightly wider than the range for the simple case. As has been concluded elsewhere, the varying width of the basilar membrane is therefore the most significant variable in any effective mass calculation.

The ratio of effective mass per unit length at the helicotrema ($X = 35$) to that at the stapes end ($X = 0$) is slightly greater for excitation $v(x)_1$ than for the excitation case $v(x)_2$. This ratio is about 6 for the simple uniform scala case and 8.5 for the detailed case.

It is now possible to recommend values of effective mass to be employed in general mathematical cochlear models. In doing so the following factors

expense, if need be, of areas further removed from the source (i.e., areas nearer the upper attachment of Reissner's membrane.)

Satisfactory agreement has resulted from checking the variations of L with distance along the cochlea, relating L to F in each case, against published information. Table 4 and Fig. 8 set out the variations in these variables. There is close agreement between the areas calculated from the selected variables and both the mean cross sectional area of the scala media of 0.19 mm^2 given by Littler⁽⁵⁾ and the value of 0.20 mm^2 , representing a variation from 0.15 to 0.25 mm^2 , given by Wever⁽⁴⁾.

It may also be noted that the dimension h was calculated so as to test the von Békésy implication that the sectional length of Reissner's membrane in cochleas on which he conducted scala media stiffness tests was approximately constant. Results in Table 4 show only 25% variation in h , which remains constant in the apical half of the cochlea. The constant width Békésy apparently observed is calculated as being 1.20 mm . The results in table 5 are calculated for the typical scala media sections as detailed in Table 4 and Figure 8. A mean fluid and cell density of 1.05 was assumed. Results were also obtained for the simple case of a uniform scala media model, having angle α constant at 90° and angle β constant at 45° , and a constant height of 0.633 mm , giving a uniform area of 0.20 mm^2 .

From table 5, it is immediately apparent that the mass for unit area on the basilar membrane of the scala media varies by less than 2.4 times from one end of the cochlea to the other, and that the range of results for the detailed case is only slightly wider than the range for the simple case. As has been concluded elsewhere, the varying width of the basilar membrane is therefore the most significant variable in any effective mass calculation.

The ratio of effective mass per unit length at the helicotrema ($X = 35$) to that at the stapes end ($X = 0$) is slightly greater for excitation $v(x)_1$ than for the excitation case $v(x)_2$. This ratio is about 6 for the simple uniform scala case and 8.5 for the detailed case.

It is now possible to recommend values of effective mass to be employed in general mathematical cochlear models. In doing so the following factors

Table 4.

Typical Geometric Properties of the Scala Media:-

Detailed Case (see Figs. 6 and 8).

Xmm	0	5	10	15	20	25	30	35
from stapes								
α (angle, degrees)	80°	84°	90°	98°	105°	107.5°	100°	90°
n (from $\alpha = \frac{\pi}{2n}$)	1.125	1.071	1.000	0.918	0.857	0.837	0.900	1.000
β (angle, degrees)	65°	60°	55°	50°	45°	40°	35°	30°
F(basilar membrane width, mm)	0.152	0.210	0.269	0.326	0.384	0.442	0.500	0.559
G(distance, mm)	0.35F	0.30F	0.25F	0.20F	0.15F	0.10F	0.05F	0
L(distance, mm)	0.440	0.494	0.510	0.520	0.540	0.600	0.750	0.920
a(height, mm)	0.686	0.724	0.727	0.747	0.738	0.681	0.599	0.532
h(length of Reissner's membrane, mm).	0.755	0.836	0.888	0.972	1.043	1.072	1.052	1.061
A(area of scala media, mm ²)	0.151	0.179	0.186	0.194	0.198	0.207	0.226	0.245

Table 5. Scala Media Effective Mass, computed for the geometrical shapes of both the Detailed and the Simple cases.

SECTION X Position from stapes in mm	Excit- ion $v(x)_1$ or $v(x)_2$	SIMPLE CASE		DETAILED CASE	
		Mass per unit length along cochlea $\frac{gm}{cm}$	Mass per unit area of basilar mem- brane $\frac{gm}{cm^2}$	Mass per unit length along cochlea $\frac{gm}{cm}$	Mass per unit area of basila membrane $\frac{gm}{cm^2}$
0	$v(x)_1$	0.00023	0.0152	0.00018	0.0120
0	$v(x)_2$	0.00020	0.0132	0.00016	0.0108
5	$v(x)_1$	0.00037	0.0176	0.00034	0.0160
5	$v(x)_2$	0.00032	0.0154	0.00030	0.0140
10	$v(x)_1$	0.00052	0.0192	0.00049	0.0182
10	$v(x)_2$	0.00045	0.0166	0.00042	0.0158
15	$v(x)_1$	0.00067	0.0205	0.00061	0.0188
15	$v(x)_2$	0.00058	0.0177	0.00052	0.0150
20	$v(x)_1$	0.00082	0.0215	0.00069	0.0180
20	$v(x)_2$	0.00070	0.0183	0.00057	0.0148
25	$v(x)_1$	0.00098	0.0223	0.00081	0.0183
25	$v(x)_2$	0.00083	0.0188	0.00065	0.0147
30	$v(x)_1$	0.00115	0.0230	0.00112	0.0225
30	$v(x)_2$	0.00095	0.0191	0.00092	0.0184
35	$v(x)_1$	0.00134	0.0240	0.00156	0.0279
35	$v(x)_2$	0.00108	0.0194	0.00131	0.0235

are relevant.

1. The results for the detailed case are assumed to be more accurate.
2. Allowance must be made for the change of velocity patterns $v(u)$ in transformations.
3. A small membrane mass of about $\frac{5}{100}$ of the scala fluid and cell mass must be added to each value.

Figure 9 shows the effective mass per unit length of the scala media plotted graphically for both the $v(x)_1$ and $v(x)_2$ cases, with the derived actual effective mass also plotted. It should be observed that when $\alpha = 107.5^\circ$, at $X = 25\text{mm}$, the $v(x)_1$ function will be sufficiently distorted a form of $v(x)_1$ so as to be similar to function $v(x)_3$, i.e. tangential to the osseous spiral lamina at the limbus end of the basilar membrane and most heavily deformed on the spiral ligament side. Hence, at that point, the true effective mass is considered to be very close to that for $v(x)_1$. Also it is assumed that as function $v(x)_2$ gives smaller effective masses than $v(x)_1$, so will function $v(x)_2$ generally give smaller masses than function $v(x)_3$, due to the shift of the region of maximal excitation. The range of actual effective mass for the scala media, as estimated from these and similar observations, is set out in table 6. These are the values which are used in the final mathematical model of the cochlea. From table 6 it can be seen that as a major simplification, a constant mass per unit area of 0.02 gm/cm^2 would not be an unreasonable approximation. However, the effective mass is expressed more meaningfully as a mass per unit length along the cochlea, and the real influence of the variation of this term can only be illustrated by the effects on cochlea dynamic response.

In principle, however, it would appear from the sharp increase in slope of the curve in Figure 9, showing the variation of estimated effective mass with respect to distance along the cochlea, towards the apical end of the cochlea, that

- a) the mean human cochlea is at least partially adapted for improved amplitude response to low frequency sounds.
- b) cochlea frequency discriminability at the low frequency end of the

Figure No.9

Variation of cochlear partition effective mass per unit length along the length of the cochlea, gm/cm, showing the estimated true values extrapolated from all calculations.

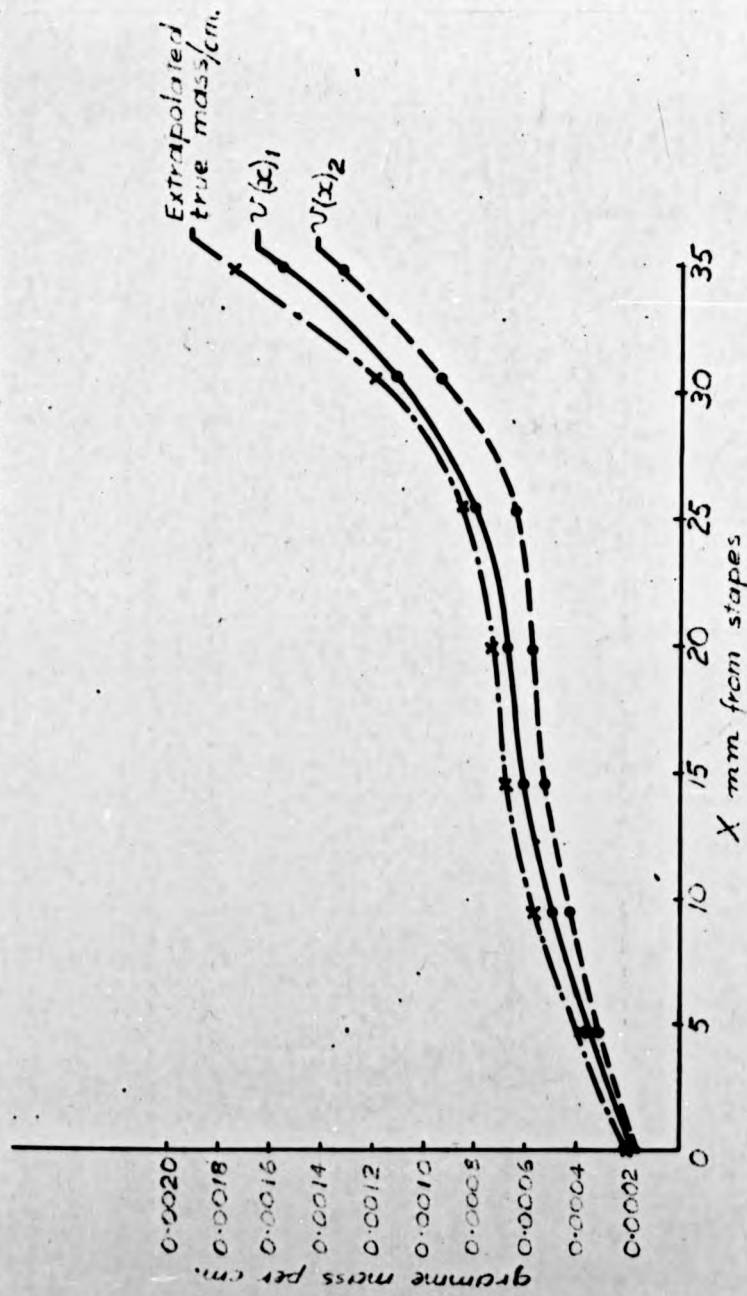


Table 6. Actual effective mass of the typical cochlear partition at various sections along the cochlea, estimate from all results.

X mm from stapes	Mass per unit length along cochlea <u>gm/cm</u>	Mass per unit area of the basilar membrane <u>gm/cm²</u>
0	0.00023	0.0151
5	0.00040	0.0190
10	0.00056	0.0208
15	0.00068	0.0208
20	0.00074	0.0192
25	0.00085	0.0192
30	0.00120	0.0240
35	0.00175	0.0313

audio frequency spectrum (50 to 500 Hz) should be, on this basis alone, better than in other frequency bands.

V. CONCLUSIONS

- a) Effective mass per unit length of the human scala media varies by less than an order of magnitude from one end of the cochlea to the other.
- b) Effective mass per unit area of the basilar membrane varies only by about two times, and could be not unreasonably described as approximately constant at 0.02 gm/cm^2 .
- c) The range of values calculated is considered to be typical and reasonable. The main conditional requirement for using these values in dynamic analyses of cochlear response, and for treating them as being accurate (within 25%) is that they only be employed in dynamic equations of the type mentioned, and then in association with other fluid dynamical equations for the vestibular and tympanic scalae, for the assumption of an infinite potential flow field requires that the scala media fluid be treated as a continuum with the main scalae fluids.
- d) Comparison of these results with those set out in table 1, as used by several investigators, shows that the closest result is that of Hause, whose result was based on a rough estimate, and was not, apparently, the result of particular experimentation, analysis or calculation. Fletcher's result is also surprisingly close, being less than twice as large at the basal end and just over three times larger at the apical end.

Peterson and Bogert's assumption of constant effective mass per unit area appears reasonable, but is almost an order of magnitude too large. The variation suggested and used by Klatt and Peterson is not substantiated.

- e) The actual significance of these results as obtained by the techniques described, as with the effects of other physical parameters of the cochlea for which thorough analyses may be appropriate, can only be assessed in the light of the dynamic response of an integral mathematical cochlea model.

REFERENCES

1. Budde E.
On the Resonance-theory of Hearing
Phys. Zeits., 1917, 18, pp.225-236, 249-260.
2. Wilkinson G. and Gray A.A.
The Mechanism of the Cochlea.
London, Macmillan and Co., Ltd., 1924.
3. von Békésy G.
Experiments in Hearing.
New York, McGraw-Hill Book Co., Inc., 1960.
4. Wever E.G.
Theory of Hearing.
New York, John Wiley & Sons, Inc., 1949.
5. Wever E.G. and Lawrence M.
Physiological Acoustics.
Princeton N.J., Princeton University Press, 1954.
6. Littler T.S.
The Physics of the Ear.
Oxford, Pergamon Press Ltd., 1965, 1st Edition.
7. Ranke O.F.
A Resonance theory involving rectification.
Munich, J. Flehmann, 1931.
8. Ranke O.F.
The Mass-ratio between Membrane and Fluid in the Inner Ear.
Akust. Zeits., 1942, 7, pp.1-11.

9. Ranke C.F.
Theory of Operation of the Cochlea: Contribution to the
hydromechanics of the cochlea.
J. Acoust. Soc. Amer., 1950, 22, pp 772-777
10. Hartridge H. and Banister H.
Hearing II
Foundations of Experimental Psychology
Carl Murchison 1929 p 313
11. Peterson L.C. and Bogert B.F.
A Dynamical Theory of the Cochlea
J. Acoust. Soc. Amer. May 1950, 22, 3, pp 369-381
12. Fletcher H.
On the Dynamics of the Cochlea
J. Acoust. Soc. Amer. Nov. 1951, 23, 6, pp 637-645
13. Zwislocki J.
Theory of the Acoustical Action of the Cochlea
J. Acoust. Soc. Amer. Nov. 1950, 22, 6, pp 778-784
14. Zwislocki J.
Review of Recent Mathematical Theories of Cochlea Dynamics
J. Acoust. Soc. Amer. July 1953, 25, 4, pp 743-751
15. Hause A.D.
Digital Simulation of the Cochlea II
Bell Telephone Labs. Inc., Murray Hill, N.J. Report 1963
(MH - 1276 - ADH)
Summary
J. Acoust. Soc. Amer. Nov. 1963, 35, 11, p 1896
16. Klatt D.H.
Theories of Aural Physiology
Univ. Mich. Commun. Sci. Lab. Report No. 13, Nov. 1964.

17. Klatt D.H. and Peterson G.E.
Re-examination of a Model of the Cochlea.
J.Acoust. Soc. Amer. Jan. 1966, 40, 1, pp.54-61.
18. Johnsson L.G. and Hawkins J.E.
A Direct Approach to Cochlear Anatomy and Pathology in Man.
Archives of Otolaryngology, June 1967, 85, 6, pp.599-613.
19. Anson B.J. and Donaldson J.A.
The Surgical Anatomy of the Temporal Bone and Ear.
Philadelphia. W.B.Saunders Co., 1967.
20. East T.H. and Anson B.J.
The Temporal Bone and Ear.
Springfield, Ill., Charles C. Thomas, 1949.

APPENDIX ITheory of incompressible potential flow.

Consider a three dimensional velocity vector $\bar{w} = \bar{i}u + \bar{j}v + \bar{k}w$

If in a certain fluid field, flow is irrotational,

then spin or vorticity $\nabla \times \bar{w}$, that is, $\text{rot } \bar{w} = 0$

From incompressible continuity equation

$$\nabla \cdot \bar{w}, \text{ that is, } \text{div } \bar{w} = 0$$

$$\text{or } \frac{\partial u}{\partial x} + \frac{\partial v}{\partial y} + \frac{\partial w}{\partial z} = 0$$

A potential ϕ may be defined to exist at all points in the fluid field, if $\text{rot } \bar{w} = 0$, such that

$$\begin{aligned} \bar{w} &= \nabla \phi = \text{grad } \phi \\ \text{i.e. } \bar{i}u + \bar{j}v + \bar{k}w &= \bar{i} \frac{\partial \phi}{\partial x} + \bar{j} \frac{\partial \phi}{\partial y} + \bar{k} \frac{\partial \phi}{\partial z} \\ \therefore u &= \frac{\partial \phi}{\partial x}, \quad v = \frac{\partial \phi}{\partial y}, \quad w = \frac{\partial \phi}{\partial z}. \end{aligned}$$

$$\text{Hence as } \text{div } \bar{w} = 0 \quad \text{i.e., } \nabla \cdot \bar{w} = 0$$

$$\therefore \text{div grad } \phi = 0 \quad \text{i.e., } \nabla \cdot \nabla \phi = 0$$

$$\therefore \text{grad}^2 \phi = 0 \quad \text{i.e., } \nabla^2 \phi = 0$$

$$\text{and } \nabla^2 \phi = \nabla \cdot \nabla \phi = \left(\bar{i} \frac{\partial}{\partial x} + \bar{j} \frac{\partial}{\partial y} + \bar{k} \frac{\partial}{\partial z} \right) \left(\bar{i} \frac{\partial \phi}{\partial x} + \bar{j} \frac{\partial \phi}{\partial y} + \bar{k} \frac{\partial \phi}{\partial z} \right)$$

$$\therefore \nabla^2 \phi = \frac{\partial^2 \phi}{\partial x^2} + \frac{\partial^2 \phi}{\partial y^2} + \frac{\partial^2 \phi}{\partial z^2} = 0$$

For the two dimensional case,

$$\frac{\partial^2 \phi}{\partial x^2} + \frac{\partial^2 \phi}{\partial y^2} = 0, \quad \text{i.e., Laplace's Equation}$$

$$\text{where } \frac{\partial \phi}{\partial x} = u, \quad \frac{\partial \phi}{\partial y} = v$$

Also, if any arbitrary function W of complex variable $x + iy$ is chosen, its real and imaginary parts separately satisfy Laplace's equation.

i.e. if $z = x + iy$ and $W = f(z)$, then W

can be expanded into the form $W = U + iV$ and the quantity U ($= f_1(x, y)$)

then represents one velocity potential for one possible form of 2 dimensional

potential incompressible flow and $V (= f_2(x, y))$ represents another. When the quantity $U (= f_1(x, y))$ is then identified with a velocity potential ϕ for a possible flow then the quantity V is called the stream function ψ for that flow.

$$\text{Consider } W = f(z) = f(x + iy) = \phi + i\psi$$

$$\text{But } \frac{\partial W}{\partial x} = \frac{\partial W}{\partial z} \quad \text{and} \quad \frac{\partial W}{\partial y} = i \frac{\partial W}{\partial z}$$

$$\therefore \frac{\partial W}{\partial x} + i \frac{\partial W}{\partial y} = 0$$

$$\text{But } \frac{\partial W}{\partial x} = \frac{\partial \phi}{\partial x} + i \frac{\partial \psi}{\partial x} \quad \text{and} \quad \frac{\partial W}{\partial y} = \frac{\partial \phi}{\partial y} + i \frac{\partial \psi}{\partial y}$$

$$\therefore \left(\frac{\partial \phi}{\partial x} - \frac{\partial \psi}{\partial y} \right) + i \left(\frac{\partial \psi}{\partial x} + \frac{\partial \phi}{\partial y} \right) = 0$$

$$\therefore \frac{\partial \phi}{\partial x} = \frac{\partial \psi}{\partial y} = u \quad \text{and} \quad \frac{\partial \phi}{\partial y} = - \frac{\partial \psi}{\partial x} = v$$

$$\text{Now } \text{grad } \phi = \bar{i} \frac{\partial \phi}{\partial x} + \bar{j} \frac{\partial \phi}{\partial y} = \bar{i} u + \bar{j} v$$

$$\text{and } \text{grad } \psi = \bar{i} \frac{\partial \psi}{\partial x} + \bar{j} \frac{\partial \psi}{\partial y} = -\bar{i} v + \bar{j} u$$

$$\therefore \text{the scalar product } (\text{grad } \phi) (\text{grad } \psi)$$

$$= (\bar{i} u + \bar{j} v) (-\bar{i} v + \bar{j} u)$$

$$= -u v + u v = 0$$

\therefore grad ϕ is perpendicular to grad ψ .

Since grad ϕ is a vector representing maximum rate of change of ϕ it is perpendicular to ϕ contour lines.

Similarly grad ψ is perpendicular to ψ contour lines

\therefore ϕ and ψ lines are mutually perpendicular

$$\text{and } |\text{grad } \phi| = |\text{grad } \psi|$$

But as $\bar{w} = \text{grad } \phi$, velocity vectors are normal to ϕ constant lines. Thus velocities are parallel to ψ constant lines, which are thus streamlines.

In the direct determination of u and v , either one can find the velocity components for $W = f(z)$ by differentiating an expression for the potential function ϕ , giving

$$u = \frac{\partial \phi}{\partial x}, \quad v = \frac{\partial \phi}{\partial y}, \quad \text{and similarly for } \psi.$$

or the following approach may be used:-

$$\begin{aligned}
 \text{If } W &= f(z) = \phi + i\psi \\
 dW &= \left(\frac{\partial W}{\partial x}\right)_y dx + \left(\frac{\partial W}{\partial y}\right)_x dy \\
 &= \frac{\partial}{\partial x}(\phi + i\psi) dx + \frac{\partial}{\partial y}(\phi + i\psi) dy \\
 &= \left(\frac{\partial \phi}{\partial x} + i \frac{\partial \psi}{\partial x}\right) dx + \left(\frac{\partial \phi}{\partial y} + i \frac{\partial \psi}{\partial y}\right) dy \\
 &= (u - iv) dx + (v + iu) dy \\
 &= (u - iv) dx + i(u - iv) dy \\
 \therefore dW &= (u - iv)(dx + i dy) \\
 \therefore \frac{dW}{dz} &= (u - iv)
 \end{aligned}$$

$$\text{where } W = \phi + i\psi$$

There are many such f functions representing streamline flow patterns coincident with boundaries of useful 2 dimensional shapes.

Consider a simple source or sink, i.e., a singular point of zero area out of which a finite fluid flow emanates in all directions, or into which fluid disappears. Such a source may be described by the following function, in which m is real and constant:-

$$\begin{aligned}
 W &= m \log_e z \quad \text{where } z = x + iy = r e^{i\theta} \\
 \therefore W &= m \log_e (r e^{i\theta}) = m (\log_e r + \log_e e^{i\theta}) \\
 &= m \log_e r + m i \theta
 \end{aligned}$$

But $W = \phi + i\psi$ in the potential field

$$\begin{aligned}
 \therefore \phi &= m \log_e r = m \log_e \sqrt{x^2 + y^2} \\
 \text{and } \psi &= m \theta = m \tan^{-1} \frac{y}{x}
 \end{aligned}$$

m is thus defined as the strength of the source, and the amount of fluid created per sec. is directly proportional to m , flow represented being entirely radial and anti-symmetric.

Now $d\phi = \bar{w} \cdot d\bar{r}$, and as \bar{w} and $d\bar{r}$ are both only radial,

$$\therefore \bar{w} \cdot d\bar{r} = |\bar{w}| |d\bar{r}| = d\phi. \quad \text{Hence } |\bar{w}| = \frac{d\phi}{dr}$$

In above case \bar{w} is radial and at radius r , $\therefore w = \frac{d}{dr} (m \log_e r) = \frac{m}{r}$

APPENDIX II

Solution of the field for specified basilar membrane displacements.

$$\begin{aligned}
 \text{If } W &= f(z) = \phi + i\psi \\
 dW &= \left(\frac{\partial W}{\partial x}\right)_y dx + \left(\frac{\partial W}{\partial y}\right)_x dy \\
 &= \frac{\partial}{\partial x}(\phi + i\psi) dx + \frac{\partial}{\partial y}(\phi + i\psi) dy \\
 &= \left(\frac{\partial \phi}{\partial x} + i \frac{\partial \psi}{\partial x}\right) dx + \left(\frac{\partial \phi}{\partial y} + i \frac{\partial \psi}{\partial y}\right) dy \\
 &= (u - iv) dx + (v + iu) dy \\
 &= (u - iv) dx + i(u - iv) dy \\
 \therefore dW &= (u - iv)(dx + i dy) \\
 \therefore \frac{dW}{dz} &= (u - iv)
 \end{aligned}$$

$$\text{where } W = \phi + i\psi$$

There are many such f functions representing streamline flow patterns coincident with boundaries of useful 2 dimensional shapes.

Consider a simple source or sink, i.e., a singular point of zero area out of which a finite fluid flow emanates in all directions, or into which fluid disappears. Such a source may be described by the following function, in which m is real and constant:-

$$\begin{aligned}
 W &= m \log_e z \quad \text{where } z = x + iy = r e^{i\theta} \\
 \therefore W &= m \log_e (r e^{i\theta}) = m (\log_e r + \log_e e^{i\theta}) \\
 &= m \log_e r + m i \theta
 \end{aligned}$$

But $W = \phi + i\psi$ in the potential field

$$\begin{aligned}
 \therefore \phi &= m \log_e r = m \log_e \sqrt{x^2 + y^2} \\
 \text{and } \psi &= m \theta = m \tan^{-1} \frac{y}{x}
 \end{aligned}$$

m is thus defined as the strength of the source, and the amount of fluid created per sec. is directly proportional to m , flow represented being entirely radial and anti-symmetric.

Now $d\phi = \bar{w} \cdot d\bar{r}$, and as \bar{w} and $d\bar{r}$ are both only radial,

$$\begin{aligned}
 \therefore \bar{w} \cdot d\bar{r} &= |\bar{w}| |d\bar{r}| = d\phi. \quad \text{Hence } |\bar{w}| = \frac{d\phi}{dr} \\
 \text{In above case } \bar{w} &\text{ is radial and at radius } r, \therefore \bar{w} = \frac{d}{dr} (m \log_e r) = \frac{m}{r}
 \end{aligned}$$

APPENDIX II

Solution of the field for specified basilar membrane displacements.

A. Symmetrical displacement.

Considering boundary velocity pattern $v(x)_1$ substituted in equation (7).

$$\begin{aligned} -\alpha g(\alpha) &= \frac{2M}{\pi} \int_{x_1}^{(x_1+f)} ((x-x_1)^2 \cos \alpha x - f(x-x_1) \cos \alpha x) dx \\ &= \frac{2M}{\pi} \left[\left(\frac{(x-x_1)^2}{\alpha} - \frac{2}{\alpha^3} \right) \sin \alpha x + \frac{2(x-x_1)}{\alpha^2} \cos \alpha x - \frac{f(x-x_1)}{\alpha} \sin \alpha x - \frac{f \cos \alpha x}{\alpha^2} \right]_{(x_1)}^{(x_1+f)} \\ &= \frac{2M}{\pi \alpha^3} \left[-2 \sin \alpha(x_1+f) + \alpha f \cos \alpha(x_1+f) + 2 \sin \alpha x_1 + \alpha f \cos \alpha x_1 \right] \quad \text{---(A2-1)} \end{aligned}$$

$$\begin{aligned} \therefore \frac{\pi}{2M} \left(\frac{\partial \phi}{\partial y} \right)_{y=0} &= -2 \int_0^{\infty} \frac{\sin \alpha(x_1+f) \cos \alpha x}{\alpha^3} d\alpha + f \int_0^{\infty} \frac{\cos \alpha(x_1+f) \cos \alpha x}{\alpha^2} d\alpha \\ &\quad + 2 \int_0^{\infty} \frac{\sin \alpha x_1 \cos \alpha x}{\alpha^3} d\alpha + f \int_0^{\infty} \frac{\cos \alpha x_1 \cos \alpha x}{\alpha^2} d\alpha \\ &= - \int_0^{\infty} \frac{\sin \alpha(x_1+f+x)}{\alpha^3} d\alpha - \int_0^{\infty} \frac{\sin \alpha(x_1+f-x)}{\alpha^3} d\alpha + \frac{f}{2} \int_0^{\infty} \frac{\cos \alpha(x_1+f-x)}{\alpha^2} d\alpha \\ &\quad + \frac{f}{2} \int_0^{\infty} \frac{\cos \alpha(x_1+f+x)}{\alpha^2} d\alpha + \int_0^{\infty} \frac{\sin \alpha(x_1+x)}{\alpha^3} d\alpha - \int_0^{\infty} \frac{\sin \alpha(x-x_1)}{\alpha^3} d\alpha \quad \text{---(A2-2)} \\ &\quad + \frac{f}{2} \int_0^{\infty} \frac{\cos \alpha(x-x_1)}{\alpha^2} d\alpha + \frac{f}{2} \int_0^{\infty} \frac{\cos \alpha(x_1+x)}{\alpha^2} d\alpha \end{aligned}$$

Because the α^2, α^3 terms in the denominators are subject to one limit of $\alpha = 0$ it is impossible to compute these infinite definite integrals and it is clearly necessary to determine the limits of the sum of an infinite series.

Consider the first term only, integrating by parts :-

$$\begin{aligned} & - \int_0^{\infty} \frac{\sin \alpha(x_1+f+x)}{\alpha^3} d\alpha = \\ & \left[-\frac{1}{2} \frac{\sin \alpha(x_1+f+x)}{\alpha^2} + \frac{(x_1+f+x)}{2} \frac{\cos \alpha(x_1+f+x)}{\alpha} \right]_0^{\infty} + \frac{(x_1+f+x)}{2} \int_0^{\infty} \frac{\sin \alpha(x_1+f+x)}{\alpha} d\alpha \end{aligned}$$

which now includes two infinite non-integral terms which are expandable in series form, and one finite integral term. These integrals are set out in Appendix IID.

Expanding all eight terms of equation (A2-2) similarly, and adding where possible,

$$\begin{aligned} & \frac{\pi}{2M} \left(\frac{\partial \phi}{\partial y} \right)_{y=0} = \\ & \left[\frac{\sin \alpha(x_1+f+x)}{2\alpha^2} + \frac{\sin \alpha(x_1+f-x)}{2\alpha^2} + \frac{(x_1-x)}{2\alpha} \cos \alpha(x_1+f-x) + \frac{(x_1+x)}{2\alpha} \cos \alpha(x_1+f+x) \right. \\ & \left. - \frac{\sin \alpha(x_1+x)}{2\alpha^2} + \frac{\sin \alpha(x-x_1)}{2\alpha^2} - \frac{(x_1+f-x)}{2\alpha} \cos \alpha(x-x_1) - \frac{(x_1+f+x)}{2\alpha} \cos \alpha(x+x_1) \right] \\ & + \frac{(x_1+x)(x_1+f+x)}{2} \int_0^{\infty} \frac{\sin \alpha(x_1+f+x)}{\alpha} d\alpha - \frac{(x-x_1)(x_1+f-x)}{2} \int_0^{\infty} \frac{\sin \alpha(x_1+f-x)}{\alpha} d\alpha \\ & - \frac{(x_1+x)(x_1+f+x)}{2} \int_0^{\infty} \frac{\sin \alpha(x_1+x)}{\alpha} d\alpha - \frac{(x-x_1)(x_1+f-x)}{2} \int_0^{\infty} \frac{\sin \alpha(x-x_1)}{\alpha} d\alpha \end{aligned}$$

(A simple check on the validity of this expression is that $\left(\frac{\partial \phi}{\partial y}\right)_{y=0}$ is zero at $x = 0$, $x = x_1$, and $x = x_1 + f$. This has been verified). Returning to the general expression, $\frac{\partial \phi}{\partial y}$ (equation 6), substitution from eq.(A2-1) yields

$$\begin{aligned} \frac{\pi}{2M} \left(\frac{\partial \phi}{\partial y}\right) &= \int_0^{\infty} \left(-\frac{e^{-\alpha y} \sin \alpha A}{\alpha^3} - \frac{e^{-\alpha y} \sin \alpha B}{\alpha^3} + \frac{f}{2\alpha^2} e^{-\alpha y} \cos \alpha B \right. \\ &+ \frac{f}{2\alpha^2} e^{-\alpha y} \cos \alpha A + \frac{e^{-\alpha y} \sin \alpha C}{\alpha^3} - \frac{e^{-\alpha y} \sin \alpha D}{\alpha^3} + \frac{f}{2\alpha^2} e^{-\alpha y} \cos \alpha D + \\ &\left. \frac{f}{2\alpha^2} e^{-\alpha y} \cos \alpha C \right) d\alpha \end{aligned} \quad (A2-3)$$

$$\begin{aligned} \text{where } A &= x_1 + f + x, & B &= x_1 + f - x \\ C &= x_1 + x, & D &= x - x_1 \end{aligned} \quad (A2-4)$$

The integral terms of the type $\int_0^{\infty} e^{-\alpha y} (\sin \alpha A) \alpha^{-3} d\alpha$ and of the type $\int_0^{\infty} e^{-\alpha y} (\sin \alpha A) \alpha^{-2} d\alpha$ have been reduced by repeated integration by parts, and are given in Appendix IID.

Substituting similar expressions for these two types of integrals into eq.(A2-3)

$$\begin{aligned} \frac{\pi}{2M} \frac{\partial \phi}{\partial y} &= \left[-\left(\frac{e^{-\alpha y} \sin \alpha A}{2\alpha^2} - \frac{A e^{-\alpha y} \cos \alpha A}{2\alpha} + \frac{y e^{-\alpha y} \sin \alpha A}{2\alpha} \right) - \left(\frac{e^{-\alpha y} \sin \alpha B}{2\alpha^2} - \frac{B e^{-\alpha y} \cos \alpha B}{2\alpha} + \right. \right. \\ &\left. \frac{y e^{-\alpha y} \sin \alpha B}{2\alpha} \right) + \left(\frac{e^{-\alpha y} \sin \alpha C}{2\alpha^2} - \frac{C e^{-\alpha y} \cos \alpha C}{2\alpha} + \frac{y e^{-\alpha y} \sin \alpha C}{2\alpha} \right) - \left(\frac{e^{-\alpha y} \sin \alpha D}{2\alpha^2} - \frac{D e^{-\alpha y} \cos \alpha D}{2\alpha} + \right. \\ &\left. \frac{y e^{-\alpha y} \sin \alpha D}{2\alpha} \right) - \frac{f e^{-\alpha y} \cos \alpha A}{2\alpha} - \frac{f e^{-\alpha y} \cos \alpha B}{2\alpha} - \frac{f e^{-\alpha y} \cos \alpha C}{2\alpha} - \frac{f e^{-\alpha y} \cos \alpha D}{2\alpha} \Big]_0^{\infty} \\ &+ A y \int_0^{\infty} \frac{e^{-\alpha y} \cos \alpha A}{\alpha} d\alpha + \frac{A^2 - y^2}{2} \int_0^{\infty} \frac{e^{-\alpha y} \sin \alpha A}{\alpha} d\alpha + B y \int_0^{\infty} \frac{e^{-\alpha y} \cos \alpha B}{\alpha} d\alpha + \frac{B^2 - y^2}{2} \int_0^{\infty} \frac{e^{-\alpha y} \sin \alpha B}{\alpha} d\alpha \\ &- C y \int_0^{\infty} \frac{e^{-\alpha y} \cos \alpha C}{\alpha} d\alpha - \frac{C^2 - y^2}{2} \int_0^{\infty} \frac{e^{-\alpha y} \sin \alpha C}{\alpha} d\alpha + D y \int_0^{\infty} \frac{e^{-\alpha y} \cos \alpha D}{\alpha} d\alpha + \frac{D^2 - y^2}{2} \int_0^{\infty} \frac{e^{-\alpha y} \sin \alpha D}{\alpha} d\alpha \\ &- \frac{B f}{2} \int_0^{\infty} \frac{e^{-\alpha y} \sin \alpha B}{\alpha} d\alpha - \frac{y f}{2} \int_0^{\infty} \frac{e^{-\alpha y} \cos \alpha B}{\alpha} d\alpha - \frac{A f}{2} \int_0^{\infty} \frac{e^{-\alpha y} \sin \alpha A}{\alpha} d\alpha - \frac{y f}{2} \int_0^{\infty} \frac{e^{-\alpha y} \cos \alpha A}{\alpha} d\alpha \\ &- \frac{D f}{2} \int_0^{\infty} \frac{e^{-\alpha y} \sin \alpha D}{\alpha} d\alpha - \frac{y f}{2} \int_0^{\infty} \frac{e^{-\alpha y} \cos \alpha D}{\alpha} d\alpha - \frac{C f}{2} \int_0^{\infty} \frac{e^{-\alpha y} \sin \alpha C}{\alpha} d\alpha - \frac{y f}{2} \int_0^{\infty} \frac{e^{-\alpha y} \cos \alpha C}{\alpha} d\alpha \end{aligned} \quad (A2-5)$$

First, consider the non integral terms.

These are all zero at the upper limit of $\alpha = \text{infinity}$. For the lower limit,

they become

$$\lim_{\alpha \rightarrow 0} -e^{-\alpha y} \left[\frac{\sin \alpha A}{2\alpha^2} - \frac{y \sin \alpha A}{2\alpha} + \frac{(A-f) \cos \alpha A}{2\alpha} + \frac{\sin \alpha B}{2\alpha^2} - \frac{y \sin \alpha B}{2\alpha} \right. \\ \left. + \frac{(B-f) \cos \alpha B}{2\alpha} - \frac{\sin \alpha C}{2\alpha^2} + \frac{y \sin \alpha C}{2\alpha} - \frac{(C+f) \cos \alpha C}{2\alpha} + \frac{\sin \alpha D}{2\alpha^2} - \frac{y \sin \alpha D}{2\alpha} \right. \\ \left. + \frac{(D-f) \cos \alpha D}{2\alpha} \right] \quad \text{--- (A2-6)}$$

Now consider first term of the expression (A2-6) :-

By expanding the sine term it follows that

$$\frac{1}{2} \frac{\sin \alpha A}{\alpha^2} = \frac{1}{2} \left[\frac{\alpha A}{\alpha^2} - \frac{A^3 \alpha^3}{3! \alpha^2} + \frac{A^5 \alpha^5}{5! \alpha^2} - \dots \right] = \frac{1}{2} \left[\frac{A}{\alpha} - \frac{A^3 \alpha}{6} + \dots \right]$$

In this expansion, as $\alpha \rightarrow 0$, only the first term is non-zero.

Similarly

$$\frac{\cos \alpha A}{\alpha} = \left[\frac{1}{\alpha} - \frac{A^2 \alpha^2}{2! \alpha} + \frac{A^4 \alpha^4}{4! \alpha} - \dots \right] = \left[\frac{1}{\alpha} - \frac{A^2 \alpha}{2} + \dots \right]$$

in which again only the first term is relevant.

Hence the non integral terms of eq. (A2-5) become

$$\lim_{\alpha \rightarrow 0} -\frac{e^{-\alpha y}}{2} \left[\frac{A}{\alpha} - yA + \frac{(A-f)}{\alpha} + \frac{B}{\alpha} - yB + \frac{(B-f)}{\alpha} - \frac{C}{\alpha} + yC - \frac{(C+f)}{\alpha} + \frac{D}{\alpha} \right. \\ \left. - yD + \frac{(D-f)}{\alpha} \right] = \lim_{\alpha \rightarrow 0} -\frac{e^{-\alpha y}}{2} \left[(A+B-C+D) \left(\frac{2}{\alpha} - y \right) - \frac{4f}{\alpha} \right] \quad \text{--- (A2-7)}$$

But from eq. (A2-4) $A + B - C + D = 2f$

hence expression (A2-6) becomes $\lim_{\alpha \rightarrow 0} \left[-\frac{e^{-\alpha y}}{2} (-2fy) \right] = yf$

That is, the sum of the non-integral terms of eq. (A2-4) is yf --- (A2-8)

Secondly consider infinite definite integral terms of type $\int_0^{\infty} \frac{e^{-\alpha w}}{\alpha} \cos \alpha X \, d\alpha$

which, in order to form finite terms, must be combined, yielding terms of the

type $\int_0^{\infty} \frac{e^{-\alpha w}}{\alpha} \sin \alpha Y \sin \alpha Z \, d\alpha$ which equals $\frac{1}{4} \log_e \left(\frac{W^2 + (Y+Z)^2}{W^2 + (Y-Z)^2} \right)$

Collecting such terms from eq. (A2-5) we have

$$y(A - \frac{f}{2}) \int_0^{\infty} \frac{e^{-\alpha y}}{\alpha} \cos \alpha A \, d\alpha + y(B - \frac{f}{2}) \int_0^{\infty} \frac{e^{-\alpha y}}{\alpha} \cos \alpha B \, d\alpha - y(C + \frac{f}{2}) \int_0^{\infty} \frac{e^{-\alpha y}}{\alpha} \cos \alpha C \, d\alpha + y(D - \frac{f}{2}) \int_0^{\infty} \frac{e^{-\alpha y}}{\alpha} \cos \alpha D \, d\alpha$$

which, since $(A - \frac{f}{2}) = (C + \frac{f}{2})$ etc., is equal to

$$-y(A - \frac{f}{2}) \int_0^{\infty} \frac{e^{-\alpha y}}{\alpha} (\cos \alpha A - \cos \alpha C) \, d\alpha + y(B - \frac{f}{2}) \int_0^{\infty} \frac{e^{-\alpha y}}{\alpha} (\cos \alpha B - \cos \alpha D) \, d\alpha \\ = -2y(A - \frac{f}{2}) \int_0^{\infty} \frac{e^{-\alpha y}}{\alpha} \sin \left(\frac{\alpha(A+C)}{2} \right) \sin \left(\frac{\alpha(A-C)}{2} \right) \, d\alpha - 2y(B - \frac{f}{2}) \int_0^{\infty} \frac{e^{-\alpha y}}{\alpha} \sin \left(\frac{\alpha(B+D)}{2} \right) \sin \left(\frac{\alpha(B-D)}{2} \right) \, d\alpha$$

Hence, all the infinite definite integral terms of the type $\int_0^{\infty} \frac{e^{-\alpha w} \cos \alpha X}{\alpha} d\alpha$

$$= -\frac{y}{2} \left(A - \frac{f}{2}\right) \log_e \left(\frac{y^2 + A^2}{y^2 + C^2}\right) - \frac{y}{2} \left(B - \frac{f}{2}\right) \log_e \left(\frac{y^2 + B^2}{y^2 + D^2}\right) \quad (A2-9)$$

Thirdly consider finite terms of type $\int_0^{\infty} \frac{e^{-\alpha w}}{\alpha} \sin \alpha X d\alpha$
which are equal to $\tan^{-1}\left(\frac{X}{W}\right)$ for $X > 0$

Collecting these terms from eq. (A2-5) we have

$$\frac{1}{2} \left[(A^2 - y^2 - Af) \int_0^{\infty} \frac{e^{-\alpha y} \sin \alpha A}{\alpha} d\alpha + (B^2 - y^2 - Bf) \int_0^{\infty} \frac{e^{-\alpha y} \sin \alpha B}{\alpha} d\alpha \right. \\ \left. - (C^2 - y^2 + Cf) \int_0^{\infty} \frac{e^{-\alpha y} \sin \alpha C}{\alpha} d\alpha + (D^2 - y^2 - Df) \int_0^{\infty} \frac{e^{-\alpha y} \sin \alpha D}{\alpha} d\alpha \right]$$

$$= -\frac{(y^2 - AC)}{2} \tan^{-1} \frac{A}{y} - \frac{(y^2 + BD)}{2} \tan^{-1} \frac{B}{y} + \frac{(y^2 - AC)}{2} \tan^{-1} \frac{C}{y} - \frac{(y^2 + BD)}{2} \tan^{-1} \frac{D}{y}$$

Hence $\left(\frac{\partial \phi}{\partial y}\right)$ is given in the case for $v(x)_1$ by

$$\frac{\pi}{2M} \left(\frac{\partial \phi}{\partial y}\right) = yf - \frac{y}{2} \left(A - \frac{f}{2}\right) \log_e \left(\frac{y^2 + A^2}{y^2 + C^2}\right) - \frac{y}{2} \left(B - \frac{f}{2}\right) \log_e \left(\frac{y^2 + B^2}{y^2 + D^2}\right) \\ - \frac{(y^2 - AC)}{2} \tan^{-1} \left(\frac{fy}{y^2 + AC}\right) - \frac{(y^2 + BD)}{2} \tan^{-1} \left(\frac{fy}{y^2 - BD}\right) \quad (A2-10)$$

As shown in section IB

$$\frac{\partial \phi}{\partial x} = \int_0^{\infty} -\alpha g(\alpha) e^{-\alpha y} \sin \alpha x d\alpha$$

and substituting for $-\alpha g(\alpha)$ from eq. (A2-1) it follows that $\frac{\partial \phi}{\partial x}$

is given in the case for $v(x)_1$ by

$$\frac{\pi}{2M} \left(\frac{\partial \phi}{\partial x}\right) = -xf - \frac{(y^2 - AC)}{4} \log_e \left(\frac{y^2 + A^2}{y^2 + C^2}\right) + \frac{(y^2 + BD)}{4} \log_e \left(\frac{y^2 + B^2}{y^2 + D^2}\right) \\ + y \left(A - \frac{f}{2}\right) \tan^{-1} \left(\frac{fy}{y^2 + AC}\right) - y \left(B - \frac{f}{2}\right) \tan^{-1} \left(\frac{fy}{y^2 - BD}\right) \quad (A2-11)$$

APPENDIX IIB - Asymmetrical Displacement $v(x)_2$

The solution to the problem for $v(x)_2 = \Pi \left((x - x_1)^3 - f(x - x_1)^2 \right)$ follows along similar lines. The procedure is as for $v(x)_1$. The details of the mathematics, which is more complex, is presented in abbreviated form.

for velocity pattern $v(x)_2$

$$-\alpha g(\alpha) = \frac{2N}{\pi} \int_{(x_1)}^{(x_1+f)} \left((x-x_1)^3 \cos \alpha x - f(x-x_1)^2 \cos \alpha x \right) dx \\ = \frac{2N}{\pi} \left[\left(\frac{3(x-x_1)^2}{\alpha^2} - \frac{6}{\alpha^4} \right) \cos \alpha x + \left(\frac{(x-x_1)^3}{\alpha} - \frac{6(x-x_1)}{\alpha^3} \right) \sin \alpha x \right. \\ \left. - \left(\frac{f(x-x_1)^2}{\alpha} - \frac{2f}{\alpha^3} \right) \sin \alpha x - \frac{2f(x-x_1)}{\alpha^2} \cos \alpha x \right]_{(x_1)}^{(x_1+f)}$$

$$= \frac{2N}{\pi} \left[\left(\frac{3(x-x_1)^2}{\alpha^2} - \frac{2f(x-x_1)}{\alpha^2} - \frac{6}{\alpha^4} \right) \cos \alpha x + \left(\frac{(x-x_1)^3}{\alpha} - \frac{6(x-x_1)}{\alpha^3} - \frac{f(x-x_1)^2}{\alpha} + \frac{2f}{\alpha^3} \right) \sin \alpha x \right]_{x_1}^{(x_1+f)}$$

$$= \frac{2N}{\pi \alpha^4} \left[(\alpha^2 f^2 - 6) \cos(\alpha(x_1 + f)) - 4\alpha f \sin(\alpha(x_1 + f)) + 6 \cos(\alpha x_1) - 2\alpha f \sin(\alpha x_1) \right]$$

$$\text{Thus } \frac{\pi}{2N} \frac{\partial \phi}{\partial y} = \int_0^{\infty} \left(\left(\frac{f^2}{\alpha^2} - \frac{6}{\alpha^4} \right) e^{-\alpha y} \cos \alpha x \cos \alpha(x_1 + f) - \frac{4f}{\alpha^3} e^{-\alpha y} \cos \alpha x \cos \alpha(x_1 + f) \right. \\ \left. + \frac{6}{\alpha^4} e^{-\alpha y} \cos \alpha x \cos \alpha x_1 - \frac{2f}{\alpha^3} e^{-\alpha y} \cos \alpha x \sin \alpha x_1 \right) d\alpha$$

$$= \frac{f^2}{2} \int_0^{\infty} \frac{e^{-\alpha y} \cos \alpha A}{\alpha^2} d\alpha - 3 \int_0^{\infty} \frac{e^{-\alpha y} \cos \alpha B}{\alpha^4} d\alpha - 3 \int_0^{\infty} \frac{e^{-\alpha y} \cos \alpha A}{\alpha^4} d\alpha + \frac{f^2}{2} \int_0^{\infty} \frac{e^{-\alpha y} \cos \alpha B}{\alpha^2} d\alpha - 2f \int_0^{\infty} \frac{e^{-\alpha y} \sin \alpha A}{\alpha^3} d\alpha$$

$$- 2f \int_0^{\infty} \frac{e^{-\alpha y} \sin \alpha B}{\alpha^3} d\alpha + 3 \int_0^{\infty} \frac{e^{-\alpha y} \cos \alpha C}{\alpha^4} d\alpha + 3 \int_0^{\infty} \frac{e^{-\alpha y} \cos \alpha D}{\alpha^4} d\alpha - f \int_0^{\infty} \frac{e^{-\alpha y} \sin \alpha C}{\alpha^3} d\alpha + f \int_0^{\infty} \frac{e^{-\alpha y} \sin \alpha D}{\alpha^3} d\alpha$$

(12-12)

The integral terms of the type $\int_0^{\infty} \frac{e^{-\alpha y} \sin \alpha A}{\alpha^3} d\alpha$, and

$$\int_0^{\infty} \frac{e^{-\alpha y} \cos \alpha A}{\alpha^2} d\alpha \quad \text{and} \quad \int_0^{\infty} \frac{e^{-\alpha y} \cos \alpha A}{\alpha^4} d\alpha$$

have been reduced by repeated integration by parts to non-integral terms and to residual integrals containing only one order of α in the denominator, and are set out in Appendix IID.

Substituting for these integrals in eq. (A2-12), the thirty four resultant non-integral terms may be collected, and expanded into sine and cosine series, the limits of ∞ and 0 applied, and the resulting terms simplified, giving for

$$\text{the sum of the non-integral terms, } -yf\left(\frac{f}{2} + 2x_1\right) \quad \text{--- (A2-13)}$$

The ten resulting integral terms of type $\int_0^{\infty} e^{-\alpha y} (\cos \alpha A) \alpha^{-1} d\alpha$ may also be

collected, simplified and combined to give

$$\frac{1}{2} \left(\frac{yf^2}{2} + \frac{y}{2} (3A^2 - y^2) - 2Afy \right) \log_e \left(\frac{y^2 + A^2}{y^2 + C^2} \right) + \frac{1}{2} \left(\frac{y}{2} (3B^2 - y^2) + \frac{yB^2}{2} - 2Bfy \right) \log_e \left(\frac{y^2 + B^2}{y^2 + D^2} \right) \quad \text{--- (A2-14)}$$

Lastly, ten integral terms of the type $\int_0^{\infty} e^{-\alpha y} (\sin \alpha A) \alpha^{-1} d\alpha$ may also be

collected, simplified and integrated between the limits to give

$$\left(-\frac{Af^2}{2} - \frac{A}{2} (A^2 - 3y^2) + f(A^2 - y^2) \right) \tan^{-1} \frac{A}{y} + \left(\frac{3}{2} (C^2 - 3y^2) + \frac{f}{2} (C^2 - y^2) \right) \tan^{-1} \frac{C}{y}$$

$$+ \left(-\frac{Bf^2}{2} - \frac{B}{2} (B^2 - 3y^2) + f(B^2 - y^2) \right) \tan^{-1} \frac{B}{y} + \left(\frac{D}{2} (D^2 - 3y^2) - \frac{f}{2} (D^2 - y^2) \right) \tan^{-1} \frac{D}{y} \quad \text{--- (A2-15)}$$

- 41 -

The final expression for $\frac{\pi}{2N} \left(\frac{\partial \phi}{\partial y} \right)$, for $v(x)_2$, is $\frac{\pi}{2N} \left(\frac{\partial \phi}{\partial y} \right) =$

$$-\frac{yf}{2} (4x_1 + f) - \frac{y}{4} (y^2 - 3A^2 + 4Af - f^2) \log_e \left(\frac{y^2 + A^2}{y^2 + C^2} \right) - \frac{y}{4} (y^2 - 3B^2 + 4Bf - f^2)$$

$$\log_e \left(\frac{y^2 + B^2}{y^2 + D^2} \right)$$

$$+ \frac{1}{2} (y^2 (3A - 2f) - AC^2) \tan^{-1} \left(\frac{fy}{y^2 + AC} \right) + \frac{1}{2} (y^2 (3B - 2f) - BD^2) \tan^{-1} \left(\frac{fy}{y^2 - BD} \right)$$

(a2-16)

Similarly, $\frac{\pi}{2N} \left(\frac{\partial \phi}{\partial x} \right)$ for $v(x)_2$ is equal to :-

$$\int_0^{\infty} e^{-\alpha y} \left(\left(\frac{f^2}{\alpha^2} - \frac{6}{\alpha^4} \right) \sin \alpha x \cos \alpha (x_1 + f) - \frac{4f}{\alpha^3} \sin \alpha x \sin \alpha (x_1 + f) \right. \\ \left. + \frac{6}{\alpha^4} \sin \alpha x \cos \alpha x_1 - \frac{2f}{\alpha^3} \sin \alpha x \sin \alpha x_1 \right) d\alpha \\ = \frac{f^2}{2} \int_0^{\infty} \frac{e^{-\alpha y} \sin \alpha A}{\alpha^2} d\alpha + 3 \int_0^{\infty} \frac{e^{-\alpha y} \sin \alpha B}{\alpha^4} d\alpha - 3 \int_0^{\infty} \frac{e^{-\alpha y} \sin \alpha A}{\alpha^4} d\alpha - \\ \frac{f^2}{2} \int_0^{\infty} \frac{e^{-\alpha y} \sin \alpha B}{\alpha^2} d\alpha \\ - 2f \int_0^{\infty} \frac{e^{-\alpha y} \cos \alpha B}{\alpha^3} d\alpha + 2f \int_0^{\infty} \frac{e^{-\alpha y} \cos \alpha A}{\alpha^3} d\alpha + 3 \int_0^{\infty} \frac{e^{-\alpha y} \sin \alpha C}{\alpha^4} d\alpha + \\ 3 \int_0^{\infty} \frac{e^{-\alpha y} \sin \alpha D}{\alpha^4} d\alpha - f \int_0^{\infty} \frac{e^{-\alpha y} \cos \alpha D}{\alpha^3} d\alpha + f \int_0^{\infty} \frac{e^{-\alpha y} \cos \alpha C}{\alpha^3} d\alpha$$

The thirty four resultant non-integral terms, when treated as previously, eventually simplify and reduce to $\frac{fx}{2} (4x_1 + f)$

The ten $\int_0^{\infty} \frac{e^{-\alpha y} \cos \alpha A}{\alpha} d\alpha$ terms reduce, combine and simplify to

$$\frac{1}{4} (y^2 (3A - 2f) - AC^2) \log_e \left(\frac{y^2 + A^2}{y^2 + C^2} \right) - \frac{1}{4} (y^2 (3B - 2f) - BD^2) \log_e \left(\frac{y^2 + B^2}{y^2 + D^2} \right)$$

Lastly the ten $\int_0^{\infty} \frac{e^{-\alpha y} \sin \alpha A}{\alpha} d\alpha$ terms collect and simplify more directly

to four arc tangent terms as previously:-

$$\frac{y}{2} (y^2 - 3A^2 + 4Af - f^2) \tan^{-1} \left(\frac{A}{y} \right) - \frac{y}{2} (y^2 - 3C^2 - 2Cf) \tan^{-1} \left(\frac{C}{y} \right)$$

$$- \frac{y}{2} (y^2 - 3B^2 + 4Bf - f^2) \tan^{-1} \left(\frac{B}{y} \right) - \frac{y}{2} (y^2 - 3D^2 + 2Df) \tan^{-1} \left(\frac{D}{y} \right)$$

Thus final expression for $\frac{\pi}{2H} \left(\frac{\partial \phi}{\partial x} \right)$ for $v(x)_2$ is:- $\frac{\pi}{2H} \left(\frac{\partial \phi}{\partial x} \right)$

$$= \frac{fx}{2} (4x_1 + f) + \frac{1}{4} (y^2 (3A - 2f - AC^2) \log_e \left(\frac{y^2 + A^2}{y^2 + C^2} \right) - \frac{1}{4} (y^2 (3B - 2f) - BD^2) \log_e \left(\frac{y^2 + B^2}{y^2 + D^2} \right)$$

$$+ \frac{y}{2} (y^2 - 3A^2 + 4Af - f^2) \tan^{-1} \left(\frac{fy}{y^2 + AC} \right) - \frac{y}{2} (y^2 - 3B^2 + 4Bf - f^2) \tan^{-1} \left(\frac{fy}{y^2 - BD} \right)$$

(A2-17)

APPENDIX IIC - Asymmetrical Displacement Function $v(x)_3$

It can be shown similarly that the solution for the input function

$$v(x)_3 = P \left(- (x - x_1 - f)^3 - f (x - x_1 - f)^2 \right) \text{ yields}$$

- 43 -

$$-\alpha g(\alpha) = \frac{2P}{\pi \alpha^4} \left[6 \cos \alpha (x_1 + f) + 2\alpha f \sin \alpha (x_1 + f) + (\alpha^2 f^2 - 6) \right. \\ \left. \cos \alpha x_1 + 4\alpha f \sin \alpha x_1 \right] \quad \text{----- (A2-18)}$$

giving

$$\frac{\pi}{2P} \left(\frac{\partial \phi}{\partial y} \right) = \frac{-yf}{2} (4x_1 + 3f) + \frac{y}{4} (y^2 - A(3A - 2f)) \log_e \left(\frac{y^2 + A^2}{y^2 + C^2} \right) + \\ \frac{y}{4} (y^2 - B(3B - 2f)) \log_e \left(\frac{y^2 + B^2}{y^2 + D^2} \right) \\ - \frac{1}{2} (y^2 (3A - f) - A^2 C) \tan^{-1} \left(\frac{fy}{y^2 + AC} \right) - \frac{1}{2} (y^2 (3B - f) + B^2 D) \tan^{-1} \\ \left(\frac{fy}{y^2 - BD} \right) \quad \text{----- (A2-19)}$$

and

$$\frac{\pi}{2P} \left(\frac{\partial \phi}{\partial x} \right) = \frac{x f}{2} (4x_1 + 3f) - \frac{1}{2} (y^2 (3A - f) - A^2 C) \log_e \left(\frac{y^2 + A^2}{y^2 + C^2} \right) + \\ \frac{1}{4} (y^2 (3B - f) + B^2 D) \log_e \left(\frac{y^2 + B^2}{y^2 + D^2} \right) \\ - \frac{y}{2} (y^2 - A(3A - 2f)) \tan^{-1} \left(\frac{fy}{y^2 + AC} \right) + \frac{y}{2} (y^2 - B(3B - 2f)) \tan^{-1} \left(\frac{fy}{y^2 - BD} \right) \\ \text{----- (A2-20)}$$

APPENDIX II D - Solution of Integrals

$$\begin{aligned} \underline{a.} \quad & \frac{\int_0^{\infty} \frac{e^{-xy} \sin x A}{x^2} dx}{dx} \\ &= -\frac{e^{-xy} \sin x A}{x} - y \int_0^{\infty} \frac{e^{-xy} \sin x A}{x} dx \\ & \quad + A \int_0^{\infty} \frac{e^{-xy} \cos x A}{x} dx \end{aligned}$$

$$\begin{aligned} \underline{b.} \quad & \frac{\int_0^{\infty} \frac{e^{-xy} \cos x A}{x^2} dx}{dx} \\ &= -\frac{e^{-xy} \cos x A}{x} - y \int_0^{\infty} \frac{e^{-xy} \cos x A}{x} dx \\ & \quad - A \int_0^{\infty} \frac{e^{-xy} \sin x A}{x} dx \end{aligned}$$

$$\begin{aligned} \underline{c.} \quad & \frac{\int_0^{\infty} \frac{e^{-xy} \sin x A}{x^3} dx}{dx} \\ &= \frac{(dy-1) e^{-xy} \sin x A}{2x^2} - \frac{A}{2x} e^{-xy} \cos x A \\ & \quad + \frac{y^2-A^2}{2} \int_0^{\infty} \frac{e^{-xy} \sin x A}{x} dx - Ay \int_0^{\infty} \frac{e^{-xy} \cos x A}{x} dx \end{aligned}$$

$$\begin{aligned} \underline{d.} \quad & \frac{\int_0^{\infty} \frac{e^{-xy} \cos x A}{x^3} dx}{dx} \\ &= \frac{A}{2x} e^{-xy} \sin x A + \frac{(dy-1) e^{-xy} \cos x A}{2x^2} \\ & \quad + Ay \int_0^{\infty} \frac{e^{-xy} \sin x A}{x} dx + \frac{y^2-A^2}{2} \int_0^{\infty} \frac{e^{-xy} \cos x A}{x} dx \end{aligned}$$

Continued next page

APPENDIX II D Continued

$$\begin{aligned}
 \underline{e.} \quad & \frac{\int_0^{\infty} \frac{e^{-dy} \sin dA}{d^4} dd}{=} \\
 & = (e^{-dy} \sin dA) \left[-\frac{(y^2 - A^2)}{6d} + \frac{y}{6d^2} - \frac{1}{3d^3} \right] \\
 & + (e^{-dy} \cos dA) \left[\frac{Ay}{3d} - \frac{A}{6d^2} \right] \\
 & + \frac{y(3A^2 - y^2)}{6} \int_0^{\infty} \frac{e^{-dy} \sin dA}{d} dd \\
 & + \frac{A(3y^2 - A^2)}{6} \int_0^{\infty} \frac{e^{-dy} \cos dA}{d} dd
 \end{aligned}$$

$$\begin{aligned}
 \underline{f.} \quad & \frac{\int_0^{\infty} \frac{e^{-dy} \cos dA}{d^4} dd}{=} \\
 & = (e^{-dy} \sin dA) \left[-\frac{Ay}{3d} + \frac{A}{6d^2} \right] \\
 & + (e^{-dy} \cos dA) \left[-\frac{(y^2 - A^2)}{6d} + \frac{y}{6d^2} - \frac{1}{3d^3} \right] \\
 & + \frac{A(A^2 - 3y^2)}{6} \int_0^{\infty} \frac{e^{-dy} \sin dA}{d} dd \\
 & + \frac{y(3A^2 - y^2)}{6} \int_0^{\infty} \frac{e^{-dy} \cos dA}{d} dd
 \end{aligned}$$

ELASTICITY OF THE COCHLEAR PARTITION

Chapter 4

Contents

Introduction	Page 4- 1
I Cochlear Partition Stiffness Data	Page 4- 6
I a. Experimental Data	Page 4- 6
I b. Review	Page 4-12
II Analysis of Pressure-Deflected Membranes	Page 4-20
II a. No Resistance to Bending	Page 4-20
II b. Small Deflections with Bending Moment	
Resistance	Page 4-26
III Analysis of Pin-Deflected Membranes	Page 4-28
IV Application of Pressure-Stiffness Data	Page 4-41
V Application of Point-Load Stiffness Data	Page 4-51
V a. Bekesy Hair-Probe Data	Page 4-51
V b. Berendes Point-Load Stiffness Data	Page 4-55
VI Discussion of Partition and Basilar Membrane	
Elasticities	Page 4-57
VII Conclusions	Page 4-60
VIII References	Page 4-62

INTRODUCTION

For any dynamic analysis of the human cochlea, and for the design of both physical and mathematical models of the cochlea, some assumptions have to be made about the way in which the cochlear partition deflects, deforms or displaces when subject to a pressure unbalance between its two surrounding fluid ducts or scalae.

In the initial theories, e.g. the Helmholtz resonance theory, it was always assumed that the membranes dividing the vestibular and tympanic scalae were under a state of constant transverse tension, very much higher at the stapes end of the cochlea than at the helicotrema end, and that as in piano strings, the loci of maximum response for any pure tone excitation in the surrounding fluid was primarily dependent upon the length and tension of the membranes constituting the cochlear partition. Since the length variation is only three or four times, and as it was difficult to see how the membranes would respond in modes higher than the fundamental without upsetting the theory, it was assumed that the tension variation was of the order of several thousand times in order to accommodate the known human audio frequency range.

Before the relatively-recent introduction of composite vibratory partition/fluid mechanics-of-main-scalae-theories, other investigators produced theories, often substantiated more verbally than mathematically, in which cochlear partition tensions and stiffnesses played small part, and in which either the neural processes were endowed with phenomenal capabilities or the bone or (in some incomprehensible way) fluid column elasticities permitted a limited degree of mechanical frequency discrimination.

In the present state-of-the-art, cochlear partition elasticities still appear to be discussed by some writers in the same breath as partition tensions, while other writers, who do not confuse them quite so obviously, introduce equations, definitions, constants and simplifications which, when examined, imply a return to the old theories of stretched, vibrating strings. Whatever form of the Bekesy experimental stiffness data they choose to insert in their calculations, whether it be volumetric, superficial or discontinuous pin loaded stiffness data, the formulae used by some investigators demonstrate a belief that the functions relating forces and pressures to displacements and displacement volumes are necessarily (and conveniently) linear.

Many of these investigators have at the same time apparently accepted, if not come to terms with, Bekesy's conclusions that, like all other fibrous, membranous structures in a static and unpressurised condition in the human body, the static basilar membrane is not in a state of tension. Or at least, any normal residual tension existing is biological in nature, being primarily for the growth and maintenance of the characteristic regular transverse fibrous layers, and, in the mechanical and functional sense, being insignificantly small and quite unable to give rise to significant basilar membrane stiffness variations of the order of 100 fold from the basal to the apical end (100 times variation being the magic number usually assumed).

The purpose of this paper is, at least in part, to draw attention to the mechanics of pressure-deflected membranes, which, if such membranes are normally not in a state of tension when in the mean or rest position, implies non linear systems.

At the beginning it must be said that the outstanding experiments of von Békésy on cochlear partition stiffness and elasticity, completed some 30 years ago, were then, and remain today unique, authoritative and quite invaluable. However the insufficiencies of the experimental data must cast some uncertainty on some of the quantitative values calculated in this paper and demands for improved accuracy can only be met by new, advanced cochlear experimentation.

Since many investigators appear to have applied the classical von Békésy stiffness experimental data directly to their dynamic equations of cochlear partition motion, an application which the writer considers, in several cases, to be highly suspect, both the typical form of the relevant equations and the appropriate experimental data are described here.

In the simplest case of a massive body suspended by a linear elastic element

$$f = k \cdot x$$

where f is the deforming force, k is a constant stiffness (force/unit displacement) and x is the displacement of the body from the rest position.

In most natural situations, the system subject to deformation, i.e. the elastic element, is not linear. That is, the force deforming it is not, over the whole range of deformation, directly proportional to the deformation. This situation may be described by making k some function of the deformation. Then,

$$f = k(x) \cdot x$$

or more generally,

$$f = k(x)$$

For example, in a composite spring system, where increasing resistance to deformation is encountered as the deformation proceeds, one could find

$$k(x) = Ax + Bx^2 + Cx^3 + \dots$$

where A, B, C, ... are all constants independent of x.

Such a system when subject to rapid time-dependent disturbances, instead of to a static force f , can be described as follows in an equation where the force F is required to balance three different effects. The single degree-of-freedom system

$$F = M \frac{d^2x}{dt^2} + c(x) \frac{dx}{dt} + k(x)$$

which this equation represents, of effective mass M , requires a force to accelerate the massive part, a force to oppose the frictional effect and a force to produce the elastic deformation. In the equation $c(x)$ is some dissipating function which may include fluid damping and friction (in a simple case when c is independent of x , c is a viscous friction coefficient) and $k(x)$ represents the restraining forces due to the displacement of the body causing a deformation of the elastic element.

Now this equation describes only the motion of an isolated massive element of the system. When such an equation is to be used to describe the dynamic motion of a body whose mass is distributed integrally with its elasticity the terms in the equation become more complicated. However, the deformation term $k(x)$ may remain unchanged, assuming that the forcing function F is applied in some known way to the elastic element and that the response of the element is being examined at only one section at a time. So this stiffness term, being just one of the terms in the dynamic equation, may be the same as in the static force equation.

In the case of a system with more than one degree of freedom, for example a membrane, having two natural dimensions and being deflected in a third orthogonal direction, the static force equation

$$F = k(x, y, z)$$

describes the deflection, z , of a certain point (x, y) due to a force F at that point. Similarly the equation

$$F = k'(x, y, x', y', z)$$

describes the deflection z of a certain point (x, y) due to a force F at some other known point (x', y') . Clearly, the use of pressures instead of forces is convenient when dealing with membranes, and depending upon the size of area $(x' - x)$, $(y' - y)$ over which the pressure acts, and the location of this area with respect to the point (x, y) whose pressure/deflection stiffness function is known, an equation could be written

$$P(x', x'', y', y'', z(x, y)) = k''(x, y, z, x', x'', \dots)$$

Similarly, a volumetric stiffness could perhaps be deduced, in which the relationship between a pressure acting in some defined area of the membrane and the volume displacement of some area of the membrane as a result of this pressure is defined.

It is generally inadmissible to replace a point load stiffness constant of the type $k'(x, y, x', y', z)$ by a point load stiffness constant of the type $k(x, y, z)$, which has a different meaning, and at the same time assume equality of the two different constants. It is equally inadmissible to generally interchange point load stiffness constants of the type $k(x, y, z)$ with volumetric displacement pressure stiffness constants such as $k''(x, y, z, x', y', y'', \dots)$.

Unfortunately, this has been done by more than one cochlear investigator without any attempt to co-relate these two independent functions. (See Review section Ib. following).

I. COCHLEAR PARTITION STIFFNESS DATA

Ia. Experimental Data

In 1947 a paper⁽¹⁾ by von Békésy appeared on which is based a large part of the study of cochlear theory. The first part of the paper is devoted to a description of experiments and apparatus for measuring variations in phase of vibrations occurring in the cochlea. The second part (very appropriately) begins by considering non-linearity in the vibration of the cochlear partition, and Békésy observes that his measurements show that with increasing amplitude of vibration the cochlear partition becomes stiffer. He also points out that the measured mechanical changes in the cochlear partition lie in a direction which would explain the expected lowering in pitch with an increase in loudness. This latter effect is, he says, well known in musical circles for pure tones of less than 800Hz (whether musicians can produce pure tones in this frequency range without harmonics is an interesting question). Békésy finally concludes that the mechanical non-linearities he measured were not likely to cause subjective pitch changes for other than very loud sounds, and that such pitch changes as do occur for amplitude changes in quieter sounds must be caused by neural rather than mechanical processes.

Despite this not-altogether-convincing statement, he did consider the one effect most relevant to the subject of non-linearity in the cochlear partition:- the absence or presence of permanent residual tension in the cochlear partition.

In a neat and simple experiment, he was able to bore out the bone surrounding the spiral ligament of one portion of a human cochlea and, with the aid of a probe, release any residual cochlear partition and basilar membrane tension and also slightly compress the scala media.

Absolutely no effect on the partition dynamic response could be observed. Hence Bekey reaffirmed his conclusion that the basilar membrane is not under tension.

It is natural therefore that the remainder of this 1947 paper should be devoted to an examination of the variations in stiffness of the basilar membrane, and to an attempt to examine physically the other membranes and structures to determine whether all of these membranes move integrally, allowing the partition to be considered as an entity, and to establish which components govern the stiffness of the partition.

He demonstrated and confirmed that all structures and membranes constituting the scala media and organ of Corti vibrate wholly in phase, so that it is reasonable to consider the cochlear partition as a single structure. He goes on to describe and supply graphical data from experiments in which he measured the resistance to deformation of each membrane due to a single point load. It is this which, based on a very simple conception of a pin or a hair deflecting an elastic membrane, has probably never been used in the way in which Bekey clearly intended and in fact stated it should be used - for the calculation of elastic modulus of the membranes. Although several analyses of cochlear dynamics are open to severe criticism for having misused this data it must be pointed out that the data is incomplete unless each membrane is assumed to have a wholly linear force/deformation or pressure/volume-displacement characteristic. Presumably most investigators have assumed this, which implies that a one hundred fold range of point load/maximum-deflection stiffness in the basilar membrane implies at least an 100 fold range of pressure/volume stiffness. Unfortunately no such co-relation necessarily exists and the equations of the system must be carefully solved

in order to convert a range in one stiffness system to a range in another.

The difficulty with Bekeasy's data arises because even in the membrane with large initial tension, so large that the added tension due to its deflection under load is negligible, a single discontinuous point load p_1 , in the centre, say, of a membrane of certain width, may produce a deflection of x , but a point load $2p$, on the same membrane will not cause a deflection of $2x_1$ (although it will approximate to it if x_1 is small). Hence the ratio p_1/x_1 is a function of p_1 or x_1 . The membranes under consideration, for which Bekeasy had shown no tension or little tension to be present, will thus behave with even less linearity, and hence, for any ratio of p/x or x/p a value of x or p is required to make the so called stiffness term meaningful.

Consequently, for each set of data used, a value of p has been deduced by the writer, allowing membrane moduli of elasticity to be calculated for the three sections along the cochlea at 10, 20 and 30mm, these being the sections for which Bekeasy supplied pin stiffness data.

What Bekeasy did was to use pieces of human hair, as straight as possible, varying in length from 3 to 10mm, fastened at one end to a small stick or needle probe. These hairs were fine tactile stimulus hairs presumably from the back of the human hand or wrist, and their property in common with all elastic columns, of always buckling under the same longitudinal crippling load, was employed to ensure the transmission of a known maximum force for each hair/stick assembly. By choosing hairs of different diameters and lengths a wide range of steady forces was applied to the membranes of the cochlea.

For each load, the depth of the impression of the hair, i.e. the deflection of the membrane under that point load, was measured microscopically. Bekeasy's intention was that the resultant stiffness

values, expressed as centimetres deflection per dyne force, should be reduced to the elastic modulus of the membrane by measuring, in the same way, a specimen of homogeneous material with a known modulus. Such a direct reduction is valid only when complete geometric similarity exists between the specimen and the membrane and there is a 1:1 scale ratio, this being the only scale factor at which dynamic similarity can be ensured. This implies building up membranes of the same modulus and testing them microscopically over the same widths of 0.1 to 0.5mm, which is not a useful proposition. The other alternative, of evaluating elastic moduli analytically has been attempted and is described in this chapter.

In another earlier paper, first published in 1941, von Békésy⁽²⁾ discusses the ratios of tensions in the transverse and longitudinal directions and he makes much of the point that an axi-symmetric deflection pattern results from the distortion of a uniformly tensed membrane by a pin load applied normal to the membrane, while the ratio of the major to minor axes of elliptical isoclines and deflection contours characteristic of a non-uniformly tensed membrane under a point load deformation is a measure of the ratio of tensions in the two orthogonal dimensions of the membrane. Unfortunately neither he nor other cochlear investigators since have bothered to analyse and evaluate non-uniformly tensed membrane point load displacements mathematically. Such calculations illustrate how relatively insensitive this test is to tension differences in homogeneous membranes. For the case of the distinctly non-homogeneous basilar membrane, which apparently acts more like a plate than a membrane on the side adjacent to the osseous lamina, such data as Békésy presents are of limited use; e.g. a ratio of 1:2 for the axes of the deformed area under point load deformation near to the stapes.

However, Bekeesy's observations and arguments concerning the lack of tension in the undeformed basilar membrane are very convincing (except perhaps, his statement that "the claim that the transverse fibres of the basilar membrane are especially well developed cannot be substantiated"). A formula for a plate in bending is presented by Bekeesy which includes for the stiffening effects of the arch of Corti and of the tectorial and reticular membranes, linked by stereocilia, and on the osseous lamina side (i.e. the arcuate zone) the plate model is probably reasonable. However, on the spiral ligament side, in the pectinate zone, which includes most of the width of the basilar membrane, the structure apparently has only small bending resistance. Thus, the plate bending formula introduced by Bekeesy becomes seriously inaccurate when applied to the whole basilar membrane width for other than small deflections because it cannot include direct stresses due to increased lengths of curved paths. Bekeesy's static basilar membrane stiffness experiments involved large deflections.

The short section of this 1941 paper dealing with the static elasticity of the cochlear partition contains data possibly more vital than any other to the problems of cochlear mathematical modelling. Although this data is again misleading and does not constitute his actual experimental results, it is so important for the estimation of membrane moduli and partition stiffness that it is essential to re-interpret it.

In these classic experiments, Bekeesy opened the oval window of each of his cochlea specimens and pressurised the cochlea via the round window. He opened the scalae at various sections from the helicotrema to near the stapes, one at a time, sealing the scalae on the helicotrema side of the opening on each occasion. The specimen

in each case was immersed in saline or tap water, and the displacement of the intact cochlear partition was measured and noted at each opening in the lumen for known pressure "heads" of water acting across the partition. These pressures were selected so as to induce a maximum displacement of the cochlear partition at each section of about 10 microns, which was a convenient deflection for microscopic observation and measurement.

Unfortunately, although very different heads of water (calculated herein to be of the order of 5 to 500 mm.) were required to produce this 10 micron maximum deflection at all of the sections considered, (with corresponding varying widths and stiffnesses of basilar membrane), the results are "normalised" to linear and volumetric partition displacements for 1 cm. pressure of water. As before, this has apparently been done assuming absolute linearity of partition stiffness, that is, assuming that if a pressure h_1 induces a maximum partition displacement of d_1 , then $10h_1$ induces a displacement of $10d_1$. If the partition acts like a single highly stressed membrane then for moderate displacements this is approximately true, but if the partition can be analysed as a single unstressed, elastic membrane, at least over half of its width, then the bending plate model will be seriously inaccurate for other than small deflection ranges. Fortunately, both a "stiffness" term and a displacement are calculable for each set of data and ignoring the comment that the assumed, reduced values illustrate an elasticity variation of one hundred fold from stapes to helicotrema, which cannot be inferred from the data in this form, the actual experimental data can be deduced.

Several authors have estimated values and variations of tension of the basilar membrane and some have discussed elasticities of this and other membranes of the cochlear partition. As far as is known, only Berendes⁽³⁾, other than von Békésy, has produced experimental data for basilar membrane stiffness. It was, in fact, Békésy⁽²⁾ who drew attention to Berendes' work, suggesting that the Berendes technique for measuring the deformation at only one cochlea section of the basilar membrane by using a blunt rod to apply a point load to the centre of the basilar membrane was invalid. In fact the Berendes data, though very limited, is presented adequately and has been used with little difficulty in the calculations which follow. The only doubts concerning this data arise from some uncertainty of the sections along the cochlea and basilar membrane to which his three sets of data refer.

Berendes built a compact item of apparatus in which a light hair spring rotated a shaft carrying a lever arm and a membrane-engaging pin. By calibrating the rotation of two shafts via minute light-reflecting mirrors he was able to plot directly the force exerted by the pin on the basilar membrane as the membrane deflected, thus giving an ideal hysteresis type record of point load versus deflection as load was applied and removed. How his technique compares with Békésy's hair test regarding experimental accuracy is difficult to judge, but certainly his apparatus, though doubtless difficult to apply to all points of the cochlea, lends itself to the requirements of data extraction.

Ib. Review

In the literature there is a complex array of cochlear partition stiffness and elasticity data. Nearly all the authors whose theories of cochlear action have been published have used

different ranges of stiffness values and many authors have added to the confusion by mis-quoting the values of others. Although the cochlear partition equations of motions into which these stiffness data are substituted are virtually the same in all cases, the dimensions of the chosen, invariably linear, stiffness coefficients have not been consistent.

In table 1 is summarized the data used by a number of authors, all of which is based, at least indirectly, on the work of von Békésy. Some explanation is given of how the Békésy results, in the form in which they were published, have come to be used, and, where it can be deduced, an outline of how each investigator derived or modified his chosen data is presented.

TABLE 1 COCHLEA PARTITION STIFFNESSES
AS USED BY SEVERAL INVESTIGATORS

Sectional position along cochlea:-	Near Stapes	10mm.	20mm.	30mm.	Near Helicotrema
1. Békésy hair test data dyne/cm.		2.1×10^4	1.4×10^3	3.1×10^2	
2. Békésy pressure test data dyne/cm ³	1.5×10^8	2.7×10^7	7.5×10^6	2.0×10^6	1.6×10^6
3. Békésy pressure test data dyne mm/cm ⁵	2.2×10^{10}	4.5×10^9	1.3×10^9	3.4×10^8	1.6×10^8
	2.2×10^9	4.5×10^8	1.3×10^8	3.4×10^7	1.6×10^7
4. Fletcher (based on 1) dyne/cm	1.0×10^5	1.8×10^4	1.4×10^3	2.5×10^2	70
5. Fletcher/Zwislocki. (based on 4) dyne/cm ⁴		2.1×10^9	7.7×10^7	2.4×10^6	
6. Fletcher/Klatt (based on 4) dyne/cm ²	1.0×10^5				70

Continued

Sectional position along cochlea:-	Near Stapes	10mm.	20mm.	30mm.	Near Helicotrema
7.Hause (Force/displacement) /area: dyne/cm ³	1.0x10 ⁹	5.0x10 ⁷	2.5x10 ⁶	1.2x10 ⁵	2.8x10 ⁴
8.Hause/Klatt. (based on 7) dyne/cm ²	1.0x10 ⁹				3.0x10 ⁴
9.Klatt "stiffness/unit membrane length" Dyne/cm ²	3.0x10 ⁵				20
10.Klatt and Peterson (based on 9) dyne/cm ²	3.0x10 ⁴				20
11.Bekesy/Zwislocki. (based on 3) dyne/cm ⁴		5.0x10 ⁸	1.2x10 ⁸	3.4x10 ⁷	
12.Bekesy/Klatt & Peterson dyne/cm ²	1.0x10 ³				40
13.Guelke, (based on 3) dyne/cm ⁵		5.0x10 ⁸	1.3x10 ⁸	5.3x10 ⁷	
14.Zwislocki (based on 3) dyne/cm ⁴	5.0x10 ⁹	1.1x10 ⁹	2.3x10 ⁸	5.3x10 ⁷	2.3x10 ⁷
15.Zwislocki by Hause (based on 14) dyne/cm ³		1.1x10 ⁹	2.5x10 ⁸	5.5x10 ⁷	
16.Peterson & Bogert (based on 1) dynes/cm ³		2.3x10 ⁸	1.8x10 ⁷	2.5x10 ⁶	
17.Peterson & Bogert/ Zwislocki (based on 16) dynes/cm ⁴		7.0x10 ⁹	7.5x10 ⁸	8.0x10 ⁷	

1) Bekesy⁽¹⁾ hair or pin test.

Data is given in dynes/cm; the force exerted by a straight hair on or near the centre of the basilar membrane per unit displacement of the basilar membrane at the position of this point load.

2) Bekesy⁽²⁾ pressure test.

Linear displacement data is dynes/cm³, the pressure acting across the cochlear partition per unit maximum deflection of the partition due to this pressure at the section considered, assuming that a linear relationship exists between the pressure and deflection. The data was reduced by Bekesy (for publication) to a pressure of 1cm. of water or 981 dynes per cm², and at each point along the cochlea, both a volumetric displacement (per 1mm. of distance along the cochlea in cm³) of the partition and an alleged corresponding maximum linear displacement of the partition in cm. are given. So it is possible to evaluate a second pressure-per-unit-displacement term from the volumetric displacement, by dividing the volume by, say, $\frac{2}{3} \times 0.1 \times b$, where b is the local width of the basilar membrane, (or of the cochlear partition), 0.1 is the 1mm. of length along the cochlear for which the Bekesy volumetric displacements are calculated and $\frac{2}{3}$ is a membrane shape constant.

3) Bekesy's pressure test.

Volumetric displacement data in dynes/cm⁵ per unit length of the cochlea. Assuming that the cochlear partition displays a linear pressure-volumetric displacement relationship, as indeed all authors have assumed and, considering the steps Bekesy took to reduce his pressure-test experimental data to the form in which it is presented, the least incorrect way in

which to use the pressure test data is as a pressure per unit volumetric displacement in dynes/cm⁴.

- 4) Fletcher⁽⁴⁾ used the hair test stiffness data, 1), directly and equated that stiffness to the force acting on a square surface of the partition, of side equal to the width of the basilar membrane at the section considered, per unit mean displacement of that square surface due to that force.
- 5) Zwislocki⁽⁵⁾ re-expressed Fletcher's data in terms of pressure per unit volumetric displacement for purposes of comparison with his own and other data. Thus he correctly divided Fletcher's data by the cube of the width of the basilar membrane, obtaining data in dynes/cm⁴ which, not surprisingly, bears no relation to data 3).
- 6) Klatt⁽⁶⁾ compared his own data with Fletcher's and other data, and simply re-expressed Fletcher's data, presented logically if inappropriately in dynes/cm, as dynes/cm². By what argument he did this remains uncertain.
- 7) Hause⁽⁷⁾ presented his data, which was probably based on Bekesy's pressure test data, in the form of partition stiffness per unit area of basilar membrane. His figures display a stapes-to-helicotrema variation of an order of magnitude greater than Bekesy's figures. His variation from basal to apical end follows the law $10^9 \cdot e^{-3X} \cdot \text{dyne/cm}^3$. (X cm. being the distance from the oval window).
- 8) Klatt for purposes of comparison re-expressed Hause's data in different units, the justification for which again remains uncertain.

- 9) Klatt's analysis of the deformation of a membrane and his defence of his stiffness formulae contains three errors, and it is not worthwhile to review his work closely. He has equated his linear stiffness constant k to $\frac{p b}{8 w_{\max}}$, where p is the pressure acting on the cochlear partition at some section, b is the width of the basilar membrane and w is the maximum linear deflection of the basilar membrane at that section. The value he uses for k at the stapes end of the cochlea agrees closely with the Bekesy pressure test data reduced in this way but at the apical end it would appear that his value of k is several hundred times smaller than the value which, by the method he suggested, can be derived from Bekesy's data. However, it may be that he has based his range of values of k on re-arranged Bekesy data, extracted and re-converted to approximate more nearly what he estimates to be Bekesy's original experimental data.
- 10) Klatt and Peterson⁽⁸⁾ have published a cochlear dynamic analysis based on Klatt's paper, employing the same principles for estimation of partition stiffness. Data is again given in dynes/cm² but the range of values of k from the basal to the apical end is reduced by one order of magnitude, the stapes value being one tenth of the value given in 9). It is implied in the text that this is intended to be based on Bekesy's pressure test data. This is open to question.
- 11) Zwislocki accurately refers to data 3) and quotes it with correct dimensions.
- 12) According to Klatt and Peterson's definition, $k = \frac{p b}{8 w_{\max}}$, the Bekesy pressure-test data gives either $k = 3 \times 10^5$ dynes/cm²

at stapes and $k = 6 \times 10^3$ at apex or $k = 4 \times 10^5$ dyne/cm² at stapes and $k = 2 \times 10^3$ at apex. However, they quote the data in one of Bekeasy's papers as yielding $k = 10^3$ dyne/cm² at stapes and $k = 40$ at apex, which range is needed to validate their own chosen range at the apical end of the cochlea.

- 13) Guelks⁽⁹⁾ has used data for analogous volume compliance in his apt and useful electrical transmission line analogue of cochlear dynamics. The reciprocal of his compliance, with units of dyne/cm⁵, shows a variation along the cochlea according to the formula $\frac{1.355X}{1.96 \cdot 10^9}$ and is closely in agreement with Bekeasy data 3 in dynes/cm⁴.
- 14) Zwislocki's own data is closely related to data 3), but is increased by a factor ranging from about 2.2 at the basal end to 1.5 at the apex.
- 15) According to Hause, a private communication from Zwislocki suggests that Hause's exponential formula for stiffness variation would be a more satisfactory approximation (? to the Bekeasy data) if the exponential term in $k = 10^9 e^{-3X}$ was amended to be $e^{-1.5X}$. Such a variation in fact describes Zwislocki's data 14.
- 16) Peterson and Bogert⁽¹⁰⁾ based their stiffness data on the hair test data, 1), and calculated an effective stiffness term in the form of pressure per unit mean linear displacement of the basilar membrane at the section considered. To do this the authors apparently assumed, in effect, that the point hair load on the membrane was equivalent to a pressure distributed over an area of 0.01 sq.mm.

17) In order to compare Peterson and Bogert's data, 16), with his own data, Zwislocki needed to divide by the width of the basilar membrane at corresponding positions. In fact he divided by a mean basilar membrane width throughout of about 0.03cm.

It will be apparent from the foregoing brief notes that only Zwislocki's treatment of Bekesy's data appears to be intelligent. Despite this, however, it is probable that none of the ranges of data displayed in Table 1 can be employed with confidence. Bekesy's reduction of his own experimental readings to the data which has been published is based upon a number of uncertain premises including pressure displacement linearity and small deflection theory. It is therefore considered desirable to look again at partition and membrane statics from first principles, considering cases for both small and large deflections.



FIGURE 1

STATIC ANALYSIS OF THE COCHLEA
 SHOWING THE EFFECTS OF
 SMALL DEFLECTIONS

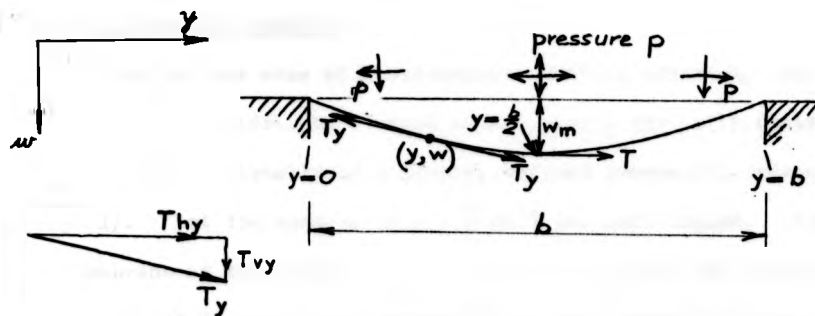
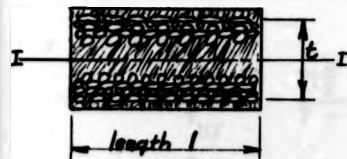


FIGURE 1.

GENERAL ANALYSIS OF LONG RECTANGULAR MEMBRANES WITH LARGE DEFLECTIONS CAUSED BY UNIFORM HYDROSTATIC PRESSURES



MEMBRANE OR PLATE SECTION -
EFFECTIVE THICKNESS t

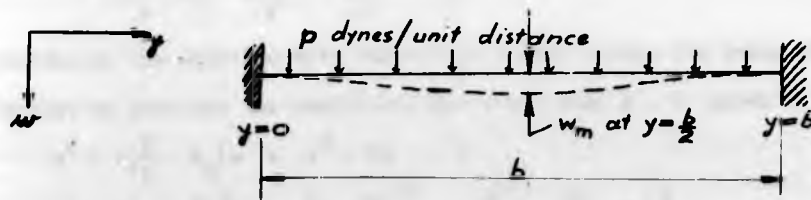


FIGURE 2.

UNIFORM CLAMPED MEMBRANE OR PLATE OFFERING ELASTIC RESISTANCE TO BENDING AND SUBJECT TO SMALL DEFLECTIONS

II ANALYSIS OF PRESSURE-DEFLECTED MEMBRANES

IIa. No Resistance to Bending

Consider the case of a rectangular uniform membrane, long compared to its width, b , clamped at all edges, initially unstressed, and deflected statically by a steady, uniform hydrostatic pressure, p , (Fig. 1). Let the tension at $y = \frac{b}{2}$ be T per unit length. Consider the membrane at the point (y, w) . Let the vertical and horizontal components of the membrane tension T_y per unit length at this point, be T_{vy} and T_{hy} respectively. Assuming symmetry about the centre line $y = \frac{b}{2}$, and equating vertical forces on an element of membrane of unit length,

$$T_{vy} = \frac{pb}{2} - py = p\left(\frac{b}{2} - y\right)$$

Equating horizontal forces

$$T_{hy} = T - p(w_m - w)$$

where the maximum deflection of the membrane at the mid point

$y = \frac{b}{2}$ is w_m

$$\therefore \frac{T_{vy}}{T_{hy}} = \frac{p\left(\frac{b}{2} - y\right)}{T - p(w_m - w)} = \left(\frac{\partial w}{\partial y}\right)_y$$

$$\therefore \frac{T - pw_m}{p} \frac{\partial w}{\partial y} + w \frac{\partial w}{\partial y} = \frac{b}{2} - y$$

integrating the equation with respect to y and setting the integration constant to zero for the condition that $w = 0$ when $y = 0$, gives

$$w^2 + 2\left(\frac{T}{p} - w_m\right)w + y^2 - by = 0 \quad (1)$$

$$\left[w - \left(w_m - \frac{T}{p}\right)\right]^2 + \left[y - \frac{b}{2}\right]^2 = \frac{b^2}{4} + \left(\frac{T}{p} - w_m\right)^2$$

which is the equation of a circle, centre $\left\{\frac{b}{2}, \left(w_m - \frac{T}{p}\right)\right\}$ and radius $\frac{T}{p}$.

Now $T_y^2 = T_{vy}^2 + T_{hy}^2$

$$\therefore T_y^2 = T^2 + p^2\left(w_m^2 + \frac{b^2}{4} - \frac{2Tw_m}{p}\right) + p^2\left(w^2 + 2\left(\frac{T}{p} - w_m\right)w + y^2 - by\right)$$

Hence, from equation (1),

$$T_y^2 = T^2 + p^2\left[w_m^2 - \frac{2Tw_m}{p} + \frac{b^2}{4}\right] \text{ which is independent of both } w \text{ and } y.$$

But from equation (1), at the point of maximum deflection, i.e., at point $(\frac{b}{2}, w_m)$ it can be seen that $w_m^2 - \frac{2Tw_m}{p} + \frac{b^2}{4} = 0$. Hence, $Ty^2 = T^2$ at all values of y .

That is, the tension in the membrane is constant across the whole section. This conclusion, and the observation that the shape of the membrane is circular depend only on the membrane being unable to support any bending moment, and both conclusions apply regardless of the size of the deflection. Subject to these same assumptions, it is only when just the horizontal component of membrane tension is constant over the span, or when the loading is wholly normal to the undeflected position of the membrane that a parabolic shape (as assumed by some investigators) can be shown to exist. For example, if, in the above derivation,

$$T_y = T = \text{constant}$$

then

$$\frac{\partial w}{\partial y} = \frac{p}{T} (b/2 - y)$$

and

$$w = -\frac{p}{2T} (y^2 - by)$$

which is parabolic. When w is small, this shape is indistinguishable from a circular arc, as also are several other shapes, including half wave sine functions. Note that when w is small, the assumption on which the above analysis is based, that the membrane is unable to support bending moments, may not be realistic.

For the case being considered the length of the stretched and deflected membrane above is the length of the circular arc in Fig. (1)

$$= \frac{T}{p} \cdot 2\sin^{-1}\left(\frac{b/2}{T/p}\right).$$

Now as T is the uniform tension per unit length of the membrane, if t is the thickness of the membrane then the stress at any and every

point in the section is T/t . That is, strain = $\frac{T}{Et}$ where E is the modulus of elasticity for the membrane material at that section. But from equation 2,

$$\frac{T}{p} = \frac{1}{8w_m} (b^2 + 4w_m^2)$$

Defining a parameter R to be the ratio of width of membrane to the maximum deflection of the membrane at its centreline, ($R = \frac{b}{w_m}$), it follows that the radius $\frac{T}{p} = \frac{b}{8R} (R^2 + 4)$. Hence strain at any point in the section of the membrane

$$\frac{T}{Et} = \frac{pb}{8REt} (R^2 + 4)$$

But also, strain = $\frac{\text{length of arc} - b}{b}$

$$\therefore \frac{pb}{8REt} (R^2 + 4) = \frac{2T}{bp} \sin^{-1}\left(\frac{bp}{2T}\right) - 1$$

$$\text{Therefore } \frac{pb}{2Et} = \sin^{-1}\left(\frac{4R}{R^2 + 4}\right) - \frac{4R}{R^2 + 4}$$

Expressing this as a series in $\frac{4R}{R^2 + 4}$ we have

$$\frac{pb}{2Et} = \frac{4R}{R^2 + 4} + \frac{\left(\frac{4R}{R^2 + 4}\right)^3}{6} + \frac{\left(\frac{4R}{R^2 + 4}\right)^5}{40} + \frac{\left(\frac{4R}{R^2 + 4}\right)^7}{336} + \dots - \frac{4R}{R^2 + 4}$$

In his pressure tests of the cochlear partition, for which data this analysis is prepared, Bekesy notes that the maximum linear displacement which he applied to the cochlear partition at any section was 0.01mm. At the stapes end, for a basilar membrane width of 0.10mm, which is slightly less than normal, this would indicate a maximum R value for the whole pressure test of ten, assuming for the most severe case that the basilar membrane was subject to the maximum deflection of the partition. At all other points, R would thus have been greater than 10. Therefore the error then introduced into the value for $\frac{pb}{2Et}$ by ignoring terms higher than the second in the expansion for the inverse sine in equation (3) is 6%. This is the maximum error which

could be encountered because it is not feasible in static pressure test data for R to have a value less than ten as such deformations would destroy the cochlear partition. Furthermore the magnitude of the error falls approximately as the cube power of the increase in R. For R = 100, the error diminishes to 0.006%.

$$\text{Thus } \frac{4R}{R^2 + 4} \approx \sqrt[3]{\frac{6pb}{2Et}} \quad (4)$$

If R were to be calculated from given values of $\frac{pb}{2Et}$, then the error resulting from the above truncation would be not more than 2% for R = 10.

In its normal response the cochlea would never generate an R value less than about 100 (as calculated from Bekesy measurements at a sound intensity of 140dB), and taking note of the likely accuracy of the Bekesy results after interpolation, it is suggested that the use of the equation (4) is wholly accurate. Nevertheless in order to evaluate Et from static test data, in which conditions of low R may apply, equation (3) has been used. Therefore no inaccuracy has been involved in calculating Et values from the static pressure test data in which the ratio of w_{\max} to b may approach $\frac{1}{20}$ or $\frac{1}{10}$.

$$\text{Now let } \sqrt[3]{\frac{3pb}{Et}} \equiv z$$

Then

$$4R = z(R^2 + 4)$$

$$\therefore R^2 - \frac{4}{z}R = -4$$

$$\therefore R = \frac{2}{z} (1 \pm \sqrt{1 - z^2})$$

As $p \rightarrow 0$, $z \rightarrow 0$, therefore $R \rightarrow \frac{2}{0}$ or $\frac{0}{0}$. For second value of R,

consider, by L'hospital's rule,

$$\lim_{z \rightarrow 0} \frac{\frac{d}{dz}(2 - 2\sqrt{1 - z^2})}{\frac{d}{dz} \cdot z} = \lim_{z \rightarrow 0} \left(\frac{2z}{\sqrt{1 - z^2}} \right) = 0$$

Hence since R should approach ∞ , take first value of R

$$\begin{aligned} \therefore R &= \frac{2}{z} (1 + \sqrt{1 - z^2}) \\ \therefore w_m &= \frac{bz}{2(1 + \sqrt{1 - z^2})} \\ \therefore \frac{w_m}{p} &= \frac{b \sqrt[3]{\frac{3b}{p^2 Et}}}{2(1 + \sqrt{1 - (\frac{3pb}{Et})^{2/3}})} \end{aligned} \quad (5)$$

This equation follows directly from equations (3) and (4) and, if the single membrane representing the cochlear partition, and the basilar membrane are normally unstressed when at rest, the relation also follows from equation (1).

Equation (5) clearly indicates non-linear behaviour in the variation of the maximum partition or membrane displacement with pressure. As the equation is free of error for all values of R obtaining in the natural dynamic case, the assumptions being that the cochlear partition may be considered as an untensed rectangular elastic membrane clamped at its edges, and that this membrane has no resistance to bending, it will have to be simplified with minimum loss of accuracy to a form appropriate to an equation of motion. Non-linear stiffness terms in dynamic equations are invariably associated with either difficult exact solutions of such equations, or inconvenient approximate solutions, and before attempting either it is necessary to express the stiffness component in a form such as

$$p = Aw + Bw^2 + Cw^3 + \dots$$

Rewriting equation (5),

$$8 w_m^3 \left(1 + \sqrt{1 - \left(\frac{3pb}{Et} \right)^{2/3}} \right)^3 = b^3 \frac{3pb}{Et}$$

$$\therefore 8w_m^3 \left[1 + \left(1 - \left(\frac{3pb}{Et} \right)^{2/3} \right)^{3/2} + 3 \left(1 - \left(\frac{3pb}{Et} \right)^{2/3} \right) + 3 \left(1 - \left(\frac{3pb}{Et} \right)^{2/3} \right)^{3/2} \right] = b^3 \frac{3pb}{Et}$$

Expanding the terms in brackets on the left hand side in binomial series:

$$8w_m^3 \left[1 + 1 - \frac{3}{2} \left(\frac{3pb}{Et} \right)^{2/3} + \frac{3}{8} \left(\frac{3pb}{Et} \right)^{4/3} + \frac{1}{16} \left(\frac{3pb}{Et} \right)^2 + 3 - \frac{3}{2} \left(\frac{3pb}{Et} \right)^{2/3} - \frac{3}{8} \left(\frac{3pb}{Et} \right)^{4/3} - \frac{3}{16} \left(\frac{3pb}{Et} \right)^2 + 3 - 3 \left(\frac{3pb}{Et} \right)^{2/3} + \dots \right] = b^3 \frac{3pb}{Et}$$

$$\therefore 8w_m^3 \left[8 - 6 \left(\frac{3pb}{Et} \right)^{2/3} - \frac{1}{8} \left(\frac{3pb}{Et} \right)^2 - \frac{3}{32} \left(\frac{3pb}{Et} \right)^{8/3} \dots \right] = b^3 \frac{3pb}{Et} \quad (6)$$

It can easily be shown that for all values of R the third and fourth etc. terms on the left hand side of equation 6 are insignificant. For a value of R of the order of one hundred, omission of the second term also causes an error of 0.04% in R. Omission of the same term for R of the order of ten gives rise to an error of 4% in R.

$$\therefore \frac{64}{R^3} = \frac{3pb}{Et}$$

$$\therefore p = \frac{64}{3} \cdot \frac{Et}{b^4} \cdot w_m^3 \quad (7)$$

This equation can be used for the normal dynamic case and be included as a cubic stiffness term in the equations of cochlear partition motion. It is interesting to observe in the derivation of equation (7) successively from equations (5) and (3) etc., that subject to the assumptions made, no linear component of pressure stiffness appears.

IIb. Small Deflections - Bending Moment Resistance

Consider the case of an elastic plate or membrane, initially unstressed, subject to small deflections and offering full normal elastic resistance to bending moments. Let the rectangular plate have unit length and width b between its two clamped fixed ends, and be subject to a uniform hydrostatic pressure of p dynes per unit area, which, considering its unit length, indicates a distributed load of p dynes per unit sectional (span) distance. (Fig.2).

Then from consideration of its bending moment diagram and the principles of elastic bending,

$$w_m = \frac{p}{384} \frac{b^4}{EI}$$

where w_m is the maximum deflection of the plate or membrane at $y = \frac{b}{2}$, E is the elastic modulus of the material and I is the second moment of area of the section subject to bending.

For a simple rectangular section of unit length l and effective thickness t , for bending about the neutral axis $I - I$ (See Fig.2),

$$I = \frac{l t^3}{12}$$

Hence

$$w_m = \frac{12p b^4}{384 E t t^2}$$

$$\text{or } p = \left(\frac{32 E t t^2}{b^4} \right) w_m \quad (8)$$

That is, the membrane obeys a simple, linear pressure displacement relationship. This relationship may only remain an adequate description of the mechanics of a deformed plate or membrane when deflections are so small that no resistance to deformation arises due to axial strain, when the true length of the deformed membrane becomes sufficiently in excess of its initial span b .

In the case of an initially untensed elastic membrane subject to an increasing deflection, it is clear that the linear equation

(8) will apply when deflections remain very small, while the non-linear equation (7) will apply when deflections become large enough to significantly stretch the membrane in which situation the linear stiffness effects of equation (8) become insignificant. The only other analysis concerning membrane static deformations which could conceivably be introduced is the well known three dimensional elemental theory approach which yields a three dimensional Laplace's equation, or for a long uniform rectangular membrane, its two dimensional equivalent. This in turn gives a sine wave membrane deflection shape and a linear pressure vs. displacement relationship, but this type of analysis depends wholly on an assumption of a permanent uniform tension stress throughout the membrane, which is a wholly illegitimate assumption in this case.

It seems reasonable in the general case to combine these two types of equations, one a so-called membrane equation, and the other an elastic plate equation, as is frequently done in the theory of plates and shells and thick and thin cylinders, giving

$$P = \frac{Et}{b} \left(32 t^2 + \frac{64}{3} w_m^2 \right) w_m \quad (9)$$

Note that these two components become of equal importance when $w_m = \sqrt{\frac{3}{2}} t$. As w_m increases beyond this range, the non linear component rapidly predominates.

III. ANALYSIS OF PIN-DEFLECTED MEMBRANES

In order to estimate the range of moduli of elasticity of the basilar membrane from the data contained in Bekeasy's 1947 paper⁽¹⁾, an analysis is given for the general case of a discontinuous single load F , acting axisymmetrically on a uniform, circular, elastic membrane. The membrane has no initial stress, and when $F = 0$ it lies flat. The membrane is clamped at its outer radius r_2 , and is assumed to be held in firm contact with the central deflecting pin of radius r_1 throughout the area $0 \leq r \leq r_1$. Thus it is, in effect, also clamped at radius r_1 , (See Fig.3) The membrane is assumed to be sufficiently deflected so that small displacement solutions are not valid, and that linear, plate-bending mechanics are both invalid and irrelevant: that is, the membrane is assumed to offer no bending moment resistance. The membrane is assumed to not be subject to deflections gross enough to invalidate Hooke's law for the material. A maximum radial angle of inclination of the membrane in the region of the deflecting pin of 30° to 45° is considered acceptable to these assumptions.

Let the deflection of the membrane at any radius r , where $r_1 < r < r_2$, be w and the radial (or meridional) slope of the membrane at that point be $\tan \theta = \frac{dw}{dr}$. Let the maximum deflection of the membrane at the pin, that is, from the centre to radius r , be w_m . (See Fig.3).

At radius r , let the membrane radial tension per unit length and the membrane radial strain be Q and ϵ_r respectively, and the circumferential tension per unit length and the circumferential (or tangential) strain be P and ϵ_θ respectively. Let E , t and ν denote membrane elastic modulus, thickness and Poisson's ratio respectively, and assume that an element of deflected membrane

of radial length δr , and true meridional length $\delta r / \cos \theta$, at radius r , was formerly, when $F = 0$, of radial length δr^1 , and at radius r^1 .

Then

$$\epsilon_r = \frac{1}{\delta r} (Q - P) = \frac{\frac{\delta r}{\cos \theta} - \delta r^1}{\delta r^1} = \frac{\delta r}{\delta r^1} \frac{1}{\cos \theta} - 1$$

and

$$\epsilon_\theta = \frac{1}{\delta r} (P - Q) = \frac{r - r^1}{r^1} = \frac{r}{r^1} - 1$$

(10)

Note that ϵ_θ is zero at $r = r_1$ and $r = r_2$

Consider the equilibrium of a small element lying in the plane of the deflected membrane at radius r (See Fig.4). If the element subtends an angle $\delta \phi$ when viewed radially, that is, vertically from above, then resolving forces in the plane of the element,

$$Q r \delta \phi - (Q + \delta Q) (r + \delta r) \delta \phi + 2P \frac{\delta r}{\cos \theta} \frac{\delta \phi \cos \theta}{2} = 0$$

which gives

$$P = \frac{d}{dr} (rQ) = Q + r \frac{dQ}{dr}$$

(11)

By considering the equilibrium of the vertical forces, i.e. the applied force F , at any annular ring of radius r , it follows that

$$F = Q 2 \pi r \sin \theta$$

(12)

Note in these basic equations (10), (11) and (12), that P , Q and θ are all functions of r .

As a solution to this apparently simple problem does not appear in the literature, it was assumed that no exact solution was possible by other than numerical methods. Also, the appropriate experimental data from which cochlear membrane elasticities are to be extracted is particularly poor, and does not warrant solutions of great accuracy. Therefore, several alternative means to solving the problem were considered.

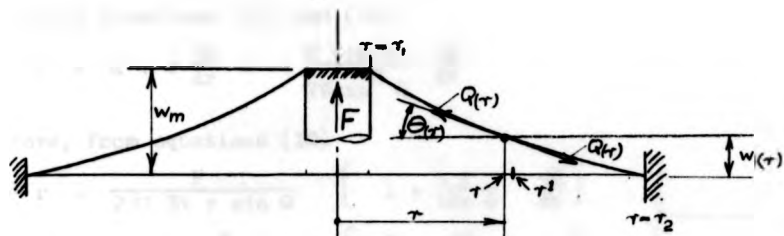


FIGURE NO. 3. CIRCULAR MEMBRANE DEFLECTED BY CONCENTRIC POST

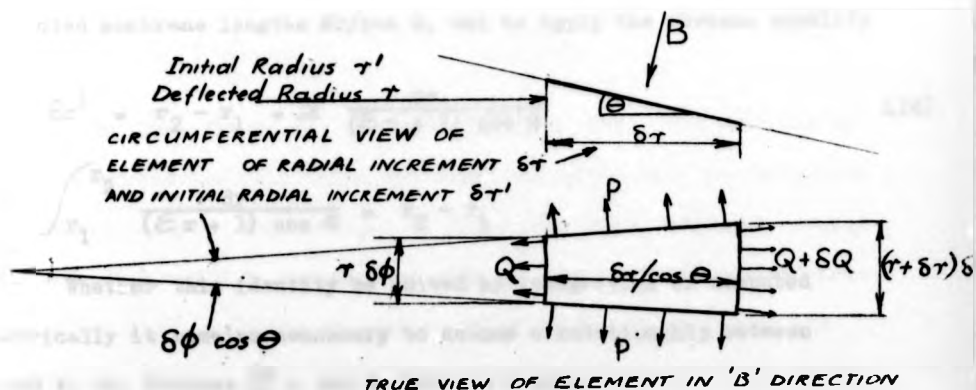


FIGURE NO. 4. ELEMENT OF CIRCULAR DEFLECTED MEMBRANE

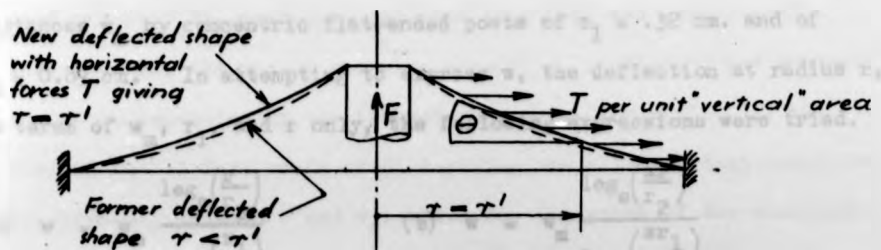


FIGURE NO. 5

DEFLECTED CIRCULAR MEMBRANE IN WHICH CIRCUMFERENTIAL STRAIN IS ZERO

Method 1

From equations (11) and (12),

$$P = Q + r \frac{dQ}{dr} = - \frac{F \cos \theta}{2\pi \sin^2 \theta} \frac{d\theta}{dr}$$

Therefore, from equations (10)

$$\left. \begin{aligned} \epsilon_r &= \frac{F}{2\pi E t r \sin \theta} \left[1 + \frac{r}{\tan \theta} \frac{d\theta}{dr} \right] \\ \epsilon_c &= \frac{-F}{2\pi E t r \sin \theta} \left[\frac{r}{\tan \theta} \frac{d\theta}{dr} + \nu \right] \end{aligned} \right\} \quad (13)$$

It would appear that the direct way to employ the ϵ_r equation (13) is to derive the former unstressed length Sr^1 of each of the small elemental deflected membrane lengths $Sr/\cos \theta$, and to apply the obvious equality that

$$\sum \delta r^1 = r_2 - r_1 = \sum \frac{\delta r}{(\epsilon_r + 1) \cos \theta} \quad (14)$$

or

$$\int_{r_1}^{r_2} \frac{dr}{(\epsilon_r + 1) \cos \theta} = r_2 - r_1$$

Whether this identity be solved by integration or computed numerically it remains necessary to assume a relationship between θ and r , or, because $\frac{dw}{dr} = \tan \theta$, between w and r .

In order to discover a general relationship between w and r , a series of simple tests were made in which three uniform, initially untensed, circular rubber diaphragms of $r_2 = 7.45$ cm. $E = 20 \times 10^6$ dyne/cm² and t of 0.027 cm, 0.017 cm. and 0.006 cm. respectively were deflecting varying distances w_m by concentric flat-ended posts of $r_1 = .32$ cm. and of $r_1 = 0.89$ cm. In attempting to express w , the deflection at radius r , in terms of w_m , r_1 , and r only, the following expressions were tried.

$$(a) \quad w = w_m \frac{\log_e \left(\frac{r}{r_2} \right)}{\log_e \left(\frac{r_1}{r_2} \right)} \quad (b) \quad w = w_m \frac{\log_e \left(\frac{ar}{r_2} \right)}{\log_e \left(\frac{ar_1}{r_2} \right)}$$

$$(c) \quad w = w_m \frac{\log\left(\frac{r_2^2 + a}{r_1^2 + a}\right)}{\log\left(\frac{r_2^2 + a}{r_1^2 + a}\right)} \quad (a = r_1, a = 2r_1, a = 3r_1)$$

$$(d) \quad \frac{r - r_1}{r_2 - r_1} = \frac{\log\left(\frac{w + w_0}{w_m + w_0}\right)}{\log\left(\frac{w_0}{w_m + w_0}\right)} \quad (w_0 = \text{constant})$$

$$(e) \quad w = w_m \frac{\log\left(\frac{r + a}{r_2 + a}\right)}{\log\left(\frac{r_1 + a}{r_2 + a}\right)} \quad \text{best } a = \frac{2r_2}{w_m}$$

$$(f) \quad w = w_m \left(\frac{r_2 - r}{r_2 - r_1}\right)^n \quad n = \frac{3}{2} \text{ etc.}$$

The best fit to all of the deflection shapes was obtained by use of expression (e), which was also reasonably easy to manipulate mathematically. Three values of Poisson's ratio were used, namely $\nu = 0, 0.2$ and 0.4 , and sets of data of F vs w_m were inserted into equation (13). Taking an initial value of E_t , and dividing the radial distance $r_2 - r_1$ into 1000 intervals, equation 14 was tested numerically via a short digital computer programme, and a new value of E_t interpolated from the residue. Despite this being a slowly converging method of solution, the interpolation for E_t was easily accelerated, and after about six substitutions and re-trials, a good value of E_t , certainly accurate to 0.01%, was established. Nevertheless, the method was time consuming, inelegant, and subject to the inaccuracies of the assumed expression for $w(r)$. It was also an inefficient means of discovering the all-important non-linear relationship between F and w_m , which was the point of the exercise. Knowing that this approach was possible, if unattractive, for the calculation of E_t from F vs w_m data, alternative methods were examined in an effort to seek less indirect expressions.

Method 2

The expressions for ϵ_r and ϵ_c in equations (10) may be combined through the linear strain compatibility relationships,

$$\text{From } \frac{dr}{dr^1} = (\epsilon_r + 1) \cos \theta$$

$$\text{and } \epsilon_c = \frac{r}{r^1} - 1$$

it follows that

$$\frac{d\epsilon_c}{dr^1} = \frac{1}{r^1} \left[(\epsilon_r + 1) \cos \theta - 1 - \epsilon_c \right] \quad (15)$$

By making the appropriate substitutions for ϵ_c , ϵ_r and $\frac{d\epsilon_c}{dr^1}$, the following exact equation may be obtained, giving Q in terms of θ and r ; the prime denoting differentiation with respect to r ,

$$Q''r^2 = Et - Q \left(\nu + \frac{r \theta'}{\tan \theta} \right) - \frac{\left[Et - Q \left(\nu + \frac{r \theta'}{\tan \theta} \right) \right]^2}{\cos \theta \left[Et + Q \left(1 + \frac{\nu r \theta'}{\tan \theta} \right) \right]} + (2 - \nu) Q \left(1 + \frac{r \theta'}{\tan \theta} \right) \quad (16)$$

From equation (12), this may be rewritten to give a non-linear second order differential equation in either θ or Q as a function of r . Unfortunately no convenient solution appears possible.

Method 3

Alternatively, the linear strain compatibility relationships having been applied to yield equation (15), it is with a minimum of error that the approximation $r = r^1$ may be employed, giving

$$\frac{d\epsilon_c}{dr} = \epsilon_c' = \frac{1}{r} \left[(\epsilon_r + 1) \cos \theta - \epsilon_c - 1 \right] \quad (17)$$

Substituting for ϵ_r and ϵ_c , and making a valid small angle approximation for θ , that

$$\cos \theta = 1 - \frac{1}{2} \sin^2 \theta$$

the following approximate equation in $Q(r)$ results:-

$$Q''Q^2r^4 + 3Q'Q^2r^3 = QN(1 - \nu) - Q'r^2N + NEt \quad (18)$$

At first sight a convenient solution for Q would appear to be $Q = \frac{a}{r^2} + b$, but such a simple solution can neither satisfy equation (18) nor preserve the essential non-linearity of the L.H.S. of that equation. This simple expression for Q also corresponds with expression (c) in Method 1 for $w(r)$, which did not provide a satisfactory fit to the experimental deflection curves.

Equation (18) may be solved by the use of Bessel or Hankel functions, but this approach was not favoured.

Method 4

From equations (11) and (12) respectively:-

$$P = (rQ)'$$

$$\text{and } (rQ)' = -\frac{F}{2\pi} \frac{\cos \theta}{\sin^2 \theta} \theta'$$

where the prime denotes differentiations with respect to r .

Assuming, as is intuitively clear, that θ' is always negative for positive θ , then it follows that

$$P > 0 \text{ for all } r.$$

Also assume that E_c is always negative, that is, $r < r^1$. (the conditions under which this assumption is justified are set out under Method 5).

$$\text{Hence, if } E_c < 0$$

then from equation (10) for E_c ,

$$\downarrow Q > P$$

$$\therefore \downarrow^2 Q > \downarrow P$$

Hence, from equation (10) for E_r ,

$$\frac{Q(1-\nu^2)}{Et} < E_r < \frac{Q}{Et} \quad (19)$$

Thus, for $\nu < \frac{1}{2}$, inequality (19) defines reasonably close upper and lower bounds for E_r , which converge as ν decreases.

Clearly, the lower bound is appropriate to the situation when $\epsilon_0 = 0$

$$\text{that is } \frac{r}{r_1} = 1$$

$$\text{in which case } \frac{dr}{dr_1} = 1$$

$$\text{and } \epsilon_r = \sec \theta - 1$$

Using a small angle approximation for θ ,

$$\text{that } \sin \theta = \theta \quad (-4\% \text{ error at } \theta = 30^\circ)$$

$$\text{and that } \sec \theta = 1 + \frac{\theta^2}{2} \quad (-1\frac{1}{2}\% \text{ error at } \theta = 30^\circ)$$

it follows that, as a first approximation

$$\epsilon_r = \sec \theta - 1 = \frac{\theta^2}{2} \quad (-11\% \text{ error at } \theta = 30^\circ)$$

Substituting Q from equation (12) into the inequality (19);-

$$\frac{F(1-\nu^2)}{\pi Et} < \theta^3 r < \frac{F}{\pi Et}$$

For $-\frac{dw}{dr} = \tan \theta \rightarrow \theta$, it follows from

$$w = - \int \theta dr$$

that at the lower bound

$$w = - \int \frac{3\sqrt{F(1-\nu^2)}}{\pi Et} \int \frac{dr}{r^3}$$

which, inserting the boundary condition that $w(r_2) = 0$, gives

the following approximate inequality

$$\frac{3}{2} \sqrt{1-\nu^2} \frac{3}{2} \sqrt{\frac{F}{\pi Et}} (r_2^{2/3} - r^{2/3}) < w < \frac{3}{2} \sqrt{\frac{F}{\pi Et}}$$

$$\cdot (r_2^{2/3} - r^{2/3}) \quad (20)$$

Note that for $\nu = \frac{1}{2}$, the limit factor becomes 0.91

and for $\nu = \frac{1}{4}$, " " " " 0.98

The relationship expressed in inequality (20), although it is a first order approximation only, describes the general cubic relation between F and w_m , given when $r = r_1$. It is more accurate towards the lower bound.

Method 5

It was assumed in method 4 that r was always less than the initial element radius r^1 . If that is generally the case, then the superimposition of a uniform outward radial pressure, acting on each element of the deflected membrane, should restore each deflected element radius r to its initial value of r^1 . Let this horizontal pressure per unit vertical area of deflected membrane be T , acting on each element so as to ensure that $r = r^1$. (See Fig.5)

Hence equations (10) become

$$\left. \begin{aligned} \epsilon_{\theta} &= \frac{1}{Et} (P - \nu Q) = \frac{r}{r^1} - 1 = 0 \\ \text{giving } P &= \nu Q, \text{ and as } \frac{dr}{dr^1} = 1, \\ \epsilon_r &= \frac{Q}{Et} (1 - \nu^2) = \frac{dr}{dr^1} \frac{1}{\cos \theta} - 1 = \sec \theta - 1 \end{aligned} \right\} \quad (21)$$

When the equilibrium of forces acting on any element of membrane in the plane of the element is considered, equation (11) is replaced by the following relationship,

$$P = Q + rQ' + Tr \delta r \sin \theta \quad (22)$$

Equation (12) remains unaltered, and in differentiating equation (12) with respect to r ,

$$\text{from } Q = \frac{F}{2\pi} \left(\frac{1}{r \sin \theta} \right)$$

it is seen that

$$Q' = -Q \left(\frac{\theta'}{\tan \theta} + \frac{1}{r} \right)$$

Hence from equation (22)

$$\begin{aligned} Tr \delta r \sin \theta &= P - Q - rQ' \\ &= Q(\nu - 1 + r \frac{\theta'}{\tan \theta} + 1) \\ Tr \delta r \sin \theta &= Q(\nu + r \frac{\theta'}{\tan \theta}) \\ \text{But } \epsilon_r &= \frac{Q}{Et} (1 - \nu^2) = \sec \theta - 1 = \frac{1 - \cos \theta}{\cos \theta} \\ \therefore Q &= \frac{Et (1 - \cos \theta)}{(1 - \nu^2) \cos \theta} = \frac{F}{2\pi} \frac{1}{r \sin \theta} \end{aligned} \quad (23)$$

Putting $y = \frac{F(1 - \nu^2)}{2\pi Et}$ it follows that

$$y = r \tan \theta - r \sin \theta$$

Differentiating with respect to r , it can be shown that

$$\theta' \left(r \cos \theta - \frac{r}{\cos^2 \theta} \right) = \tan \theta - \sin \theta$$

$$\therefore \frac{\theta'}{\tan \theta} = \frac{1}{r} \frac{\cos^2 \theta}{(\cos^3 \theta - 1)} (1 - \cos \theta)$$

and substituting this expression back into equation (23) the following exact equation in θ may be used to check the sign (and direction) of the imposed pressure T :-

$$T r \delta r \sin \theta = Q \left[\nu + \frac{\cos^2 \theta (1 - \cos \theta)}{(\cos^3 \theta - 1)} \right] \quad (24)$$

For example, when $\theta = 30^\circ$ and $\cos \theta = \frac{\sqrt{3}}{2}$

$$T r \delta r \sin \theta = Q(\nu - 0.286)$$

that is, T is in the assumed direction, outwards, provided that $\nu > 0.286$, and when $\nu = 0.286$, $T = 0$. As θ increases, this lower limit of ν decreases. The case for $\theta \rightarrow 0$ may be studied by small angle approximations, as follows:-

$$\epsilon_r = \frac{Q}{Et} (1 - \nu^2) = \frac{1 - \cos \theta}{\cos \theta} = \frac{\theta^2}{2 - \theta^2} \quad (\text{error} + 3\% \text{ at } \theta = 30^\circ)$$

$$\therefore Q = \frac{Et}{1 - \nu^2} \left(\frac{\theta^2}{2 - \theta^2} \right) = \frac{F}{2\pi} \frac{1}{r\theta} \text{ when } \theta = \sin \theta$$

$$\therefore r\theta^3 = y(2 - \theta^2) \quad (25)$$

Differentiating with respect to r , it is seen that

$$\frac{\theta'}{\theta} = \frac{-\theta}{3r\theta + 2y} = - \frac{(2 - \theta^2)}{r(6 - \theta^2)}$$

From equation (23), putting $\theta = \tan \theta$

$$\begin{aligned} T r \delta r \sin \theta &= Q \left(\nu + r \frac{\theta'}{\theta} \right) \\ &= Q \left(\nu - \frac{2 - \theta^2}{6 - \theta^2} \right) \\ &= Q \left(\nu - \frac{1 - \frac{\theta^2}{2}}{3 - \frac{\theta^2}{2}} \right) \end{aligned} \quad (26)$$

Equation (26) shows that as $\theta \rightarrow 0$, the direction of T will be as assumed, that is, outwards, provided that $\nu > \frac{1}{3}$. When $\nu = \frac{1}{3}$, then in the case of small deflections, $T = 0$ and hence $r = r^1$.

It also follows that the assumption made in Method 4, that $\epsilon_0 < 0$, and $r < r^1$, is valid provided that $\nu > \frac{1}{3}$ in the case of small deflections, and $\nu > (\frac{1}{3} - \alpha)$ in the case of larger deflections (from equation 24), the small number α increasing as the deflection increases.

It should be noted at this point that ν for the basilar membrane is very roughly estimated at about 0.40. On the basis of its typical fibrillary arrangements, in which fibrous bundles are located within dense, mechanically inert matter, one would expect to model the basilar membrane using soft rubber sheeting, or some synthetic fibrous substance. Values of Poisson's ratio for a variety of such materials, extracted from a number of published tables of mechanical properties of substances are in table 2 below.

TABLE 2 Poisson's Ratio for Various Materials

Polymethylmethacrylate	Poisson's ratio = 0.40
Vulcanized rubber	0.40
Nylon	0.40
Polystyrene	0.35 - 0.40
Polytetra fluorethylene	0.40
Polyethylene	0.40
Soft rubber	0.50

Finally, the approximate relationship of w , w_m and F given in inequality (20) may now be checked using, instead of the small angle approximations

$$\sec \theta - 1 = \frac{1}{2}\theta^2 \quad \text{and} \quad \tan \theta = \theta,$$

the more accurate expressions

$$\sec \theta - 1 = \frac{\theta^2}{2 - \theta^2} \quad \text{and} \quad \tan \theta = \frac{2\theta}{2 - \theta^2}$$

From equation (25)

$$\theta = \left(\frac{\Delta}{r}\right)^{\frac{1}{2}} (2 - \theta^2)^{\frac{1}{2}}$$

$$\text{But } \frac{dw}{dr} = -\tan \theta = \frac{-2\theta}{2 - \theta^2}$$

$$\begin{aligned} \therefore \frac{dw}{dr} &= -2 \left(\frac{\Delta}{r}\right)^{\frac{1}{2}} (2 - \theta^2)^{-\frac{3}{2}} \\ &= -2 \left(\frac{\Delta}{r}\right)^{\frac{1}{2}} \left[2 - \left(\frac{\Delta}{r}\right)^{\frac{1}{2}} (2 - \theta^2)^{\frac{1}{2}} \right]^{-\frac{3}{2}} \end{aligned}$$

This may be expanded by the binomial theorem to give the following expression, in which only the first two terms of this rapidly converging series are considered:-

$$\begin{aligned} \frac{dw}{dr} &= -2 \left(\frac{\Delta}{r}\right)^{\frac{1}{2}} \left[2^{-\frac{3}{2}} + \frac{2}{3} (2)^{-5/3} \left(\frac{\Delta}{r}\right)^{\frac{1}{2}} (2 - \theta^2)^{\frac{1}{2}} + \dots \right] \\ &= -2 \left(\frac{\Delta}{r}\right)^{\frac{1}{2}} \left[2^{-\frac{3}{2}} + \frac{1}{3} \left(\frac{\Delta}{r}\right)^{\frac{1}{2}} \right] \\ \therefore \frac{dw}{dr} &= -\left(\frac{2\Delta}{r}\right)^{\frac{1}{2}} - \frac{2}{3} \left(\frac{\Delta}{r}\right) \quad \text{to a second order of approximation.} \end{aligned}$$

Integrating with respect to r ,

$$w = -\frac{1}{2} (2\gamma)^{\frac{1}{2}} r^{\frac{3}{2}} - \frac{2}{3} \gamma \log_e r + c$$

and the boundary conditions that $w = w_m$ at $r = r_1$, and $w = 0$ at $r = r_2$ give

$$w = w_m \left(\frac{r_2^{\frac{3}{2}} - r^{\frac{3}{2}} + \frac{2}{9} (2\gamma)^{\frac{1}{2}} \log_e \left(\frac{r_2}{r}\right)}{r_2^{\frac{3}{2}} - r_1^{\frac{3}{2}} + \frac{2}{9} (2\gamma)^{\frac{1}{2}} \log_e \left(\frac{r_2}{r_1}\right)} \right) \quad (27)$$

$$\text{where } \gamma = \frac{F(1 - \nu^2)}{2\pi Bt}$$

$$\text{and } w_m = \frac{1}{2} (2\gamma)^{\frac{1}{2}} (r_2^{\frac{3}{2}} - r_1^{\frac{3}{2}}) + \frac{2}{3} \gamma \log_e \left(\frac{r_2}{r_1}\right) \quad (28)$$

Note that in the practical case $\gamma < 1$.

For example, if $r_2 = 8$, $r_1 = 1$, then w_m as a function of y is typically as follows:-

y	w_m	Ratio $\frac{w_m}{r_2 - r_1}$
1	7.0	1.0
$\frac{1}{2}$	6.7	0.95
$\frac{1}{16}$	3.1	0.44

Hence, considering the required accuracy of these expressions omission of the logarithmic terms in equations (27) and (28) is clearly permissible for all cases except those involving very large deflections.

It is also worth mentioning that equation (27) was tested against experimental data mentioned in Method 1, and the relationship between w and r given by equation (27) matched the experimental relationships considerably better than did expression (e).

The only problem remaining in the use of the relations derived in Methods 4 and 5 concerns the fact that Bekesy's pin stiffness data naturally involves the deflection of a long rectangular sections of membrane rather than circular membranes.

Several laboratory tests were therefore conducted in order to obtain a simple relationship between the pin force required to produce a certain deflection in a clamped, untensed circular membrane and the pin force required to produce the same deflection in a long, narrow rectangular clamped membrane, also initially untensed. This particular approach was abandoned when it was noticed, in the course of the tests, that for a reasonably wide range of deflections, and including the natural non-linear effects, that a long, narrow, clamped, rectangular membrane, of width, b ,

displayed very nearly the same load vs. deflection characteristic when loaded by a single pin at its centre-line as did a clamped circular membrane of diameter $\frac{4}{3} b$. It was considered that under the circumstances this relationship was adequate by which to convert a set of pin stiffness data for a rectangular membrane of a certain width to its circular membrane equivalent.

IV APPLICATION OF PRESSURE STIFFNESS DATA

The only quantitative data based on experiments in which uniform hydrodynamic static pressures have deflected the cochlear partition is presented in Bekegy's paper⁽²⁾ which is discussed earlier in this paper.

In order to understand the writer's interpretation of this data, it is important to recall that Bekegy reported that over the whole length of the cochlea, when subject to large deflections, the partition deformed like an elastic rod, free at one end and fixed at the other ~~side~~. The lower extension of Reissner's membrane moved with almost maximum partition amplitude. The basilar membrane, being narrower than Reissner's membrane and stiffer on the limbus side, presumably displayed the actual maximum partition amplitude of deformation at a point about two-thirds of the width of the basilar membrane from the limbus on the spiral ligament side. Due to the near constant width of Reissner's membrane, and the tapering width of the basilar membrane, the maximum basilar membrane displacement is, by inference, only slightly greater than the maximum Reissner's membrane displacement at the apical end, and is several times greater at the basal end.

The implication of Bekegy's observations is that only the outer half or two-thirds of the basilar membrane, that is the pars Pectinata, on the spiral ligament side, can reasonably be considered to deform under relatively large pressure loads like a membrane. The inner third of the structure and membrane, that is the arcuate sone emanating from the limbus spiral adjacent to the bony lamina, clearly deflects like a beam cantilevered at one end. It is therefore considered reasonable to assume that in this arcuate sone, the basilar membrane and the reticular lamina, which are relatively

rigidly separated by the arch of Corti and the cellular structures, are analogous to a double-flanged beam, and in this manner will invariably present a large, linear restraining moment of resistance to any tendency to deformation of the partition.

It is probable that the support afforded by the tectorial membrane, which is known to be relatively strongly resistant to forces parallel to the basilar membrane and in the direction of the spiral ligament via the cilia and hair cells to the reticular lamina, reinforces this moment of resistance. However, beyond the outer leg of the arch of Corti and further towards the spiral ligament than the outermost hair cells, where the tectorial/reticular membranes cannot stiffen the structure, the basilar membrane in this pectinate zone must bear pressure loads unaided.

Iurato⁽¹¹⁾ and others have demonstrated the nature of the well defined transverse fibres lying in two strata which constitute the main characteristic of the basilar membrane in the pars pectinata. Such discoveries may be well appreciated by those more mathematical or mechanical investigators who would ascribe to physiological membrane systems certain definite physical properties such as elasticity. For the biological membrane is normally conceived as a well ordered, electrically non-conducting, cellular complex, studied in the domains of molecular science rather than the science of load bearing structures.

That the density of these fibrous layers of the pectinate zone has been observed in electron microscope sections of the basilar membrane to increase in sections approaching the basal end of the cochlea from the apex also encourages the mechanical theory that these fibres are the basis for any variation in elastic behaviour of the basilar membrane which may be deduced from

macroscopic experiments. It appears reasonable to assume that for small deflections, these double fibrillary arrangements in the pectinate zone allow the membrane to deflect linearly, like a plate.

A formula describing, with as much accuracy as Bekeesy's rather qualitative data permits, the gross displacement of the basilar membrane under relatively heavy pressure loading is

$$w = A(y^3 - by^2) \quad (29)$$

where A is a numerical factor, w is the displacement of the section at some distance y from the beginning of the basilar membrane at the limbus side, and b is the width of the membrane from its attachment at the limbus to the end of the arcuate zone at the spiral ligament.

As is illustrated in Fig. 6-2, this function, and the actual shape noted by Bekeesy, approximates very closely indeed in the region

$$\frac{2b}{3} \leq y \leq b$$

to a circular shape whose radius for values of R (where $R = \frac{b}{w_m}$) greater than ten is within a few percent of the radius, T/P , predicted by Equation (1). In view of this it is reasonable to perform all non-linear stiffness calculations on the assumption that, in the region $\frac{b}{3} \leq y \leq b$, the basilar membrane can be treated as a pure elastic membrane in the mathematical sense.

For small deflections, linear stiffness calculations should also be based upon the same outer zone width, $\frac{2}{3}b$, of the membrane, because the linear stiffness of the partition and basilar membrane in the arcuate zone, that is, the inner $\frac{1}{3}$ of the width, must be orders of magnitude in excess of the simple membrane linear stiffness in the pectinate zone.

In the approximating function (29), since the factor A is dependent upon pressure, it follows that associated with any deflection in whatever way the pars tecta/tectorial membrane mechanics demand, there must be always a stretching due to deformation of the "pure" membrane in the pectinate zone, which may be represented mathematically as the outer two thirds of the basilar membrane. Therefore the following analyses consider both linear and non-linear stiffness components existing in the outer $\frac{2}{3}$, or pectinate zone, only. Now instead of presenting his actual experimental readings, namely, a pressure and a volume displacement at a certain section, Bekesy presented reduced data, all at the same pressure;— reduced on the assumption of a wholly linear law relating displacements to pressures. This data must therefore be re-converted to its original form for use in non-linear elasticity calculations. Note that Bekesy's data must be classified large displacement data.

In order to estimate w_{MAX} from Bekesy's volume displacement data for the cochlear partition consider:

$$\begin{aligned} \text{Volume per unit length, } V &= \int_0^b w \, dy \\ &= A \left[\frac{y^3}{3} - \frac{y^4}{4} \right]_0^b = \frac{g}{16} b \cdot w_m \end{aligned}$$

Therefore, assuming relatively large displacements, the maximum basilar membrane displacement is

$$w_m = \frac{16}{9} \frac{V}{b} \quad (30)$$

The actual data presented by Bekesy is given in Table 3.

~~From Fig. 3~~ It is inferred that Reissner's membrane remains in an approximately straight line during pressure deflections of the cochlear partition, and assuming a straight line span for the same membrane in its rest condition, it follows that if h is the length

of this span, and d_m is the maximum normal displacement of Reissner's membrane, then $\frac{1}{2} d_m h$ is its volume displacement V per unit length. On this basis h is tabulated in column 5 of Table 3. Column 3 is Bekesy's volume displacement data and column 4 is the right hand ordinate of Bekesy's graphically displayed data, which he labelled "maximum displacement of the cochlear partition for a pressure of 1cm of water". In view of the fact that Bekesy observed that both the span of Reissner's membrane at each section and the form of its displacement under different pressures were approximately constant along the cochlea, it is reasonably certain that the constant quotient calculated at all sections in column 5 is no accident, but was assumed by Bekesy in calculating his "maximum displacement of the cochlear partition" values, and that these values are actually calculated maximum displacements of Reissner's membrane, d_m , not true experimental data.

Assuming that deflections in the plane of the bony shelf and basilar membrane are restricted to the width of the basilar membrane only, the maximum deflection w_m for the latter may be calculated by Equation (3) for each of the data sets given in Table 3 and is presented in column 6.

TABLE 3

Volume displacements and maximum point displacements of the cochlear partition for a pressure of 1 cm. water: Bekesy⁽²⁾

(1)	(2)	(3)	(4)	(5)	(6)
Section Distance from stapes	Typical width of basilar membrane	Volume displacement per cm.	Alleged maximum displacement of partition	Span of Reissner's membrane	Maximum displacement of basilar membrane
X(mm)	b(cm)	V(ccs/cm)	d_m (cm)	$h = \frac{2V}{d_m}$ (cm)	w_m (cm)
5	.0211	9.4×10^{-7}	1.6×10^{-5}	0.118	7.92×10^{-5}
10	.0269	2.3×10^{-6}	3.75×10^{-5}	0.122	15.20×10^{-5}
20	.0384	7.8×10^{-6}	1.3×10^{-4}	0.120	36.1×10^{-5}
30	.0500	2.9×10^{-5}	4.8×10^{-4}	0.120	103.1×10^{-5}
34	.0547	6.0×10^{-5}	1.0×10^{-3}	0.120	195.0×10^{-5}

Examination of table 3 and its inherent assumptions indicates that simple laws of fluid continuity would tend to demand that the basilar membrane should deflect about five times as much as a linear-deflecting Reissner's membrane near the basal end and about twice as much at the apex. Hence it may be concluded that either the observations made by Bekesy that the lower extension of Reissner's membrane moved with almost maximum partition amplitude only applies to the apical end of the cochlea, or the assumption that Reissner's membrane remains in a straight line is seriously in error, or that under the abnormally large static pressures evidently applied to the cochlea to produce displacements of 1×10^{-3} cm, the bony shelf itself deflected by more than an insignificant amount, such a deflection permitting a reduction in the value calculated on the basis of continuity for w_m . Whichever it is it is clear that the right hand ordinate values of "maximum displacement of the cochlear partition" given by Bekesy are unreliable as such, but may well provide approximate values for the maximum displacement of Reissner's membrane. It is also worthy of

note that none of the investigators mentioned in Section I and Table I of this chapter admit to having used these right-hand ordinate values.

Table 4 displays the re-converted Bekesy data in its probable original form. In view of the possible deflection of the bony shelf at high pressures, a "spread factor", K, allows for an effective increase in width of the deflecting area. In effect, the effective width of the basilar membrane is increased by this factor only for the calculation by Equation 30 of the actual maximum deflection of the basilar membrane corresponding to the volumetric displacement given for a pressure of 1 cm. of water.

TABLE 4

Interpolation of Bekesy data (n in Table 3) to a form for which the maximum deflection of the basilar membrane at each section is 10 = 0.001 cm.

(1)	(2)	(3)	(4)	(5)	(6)	(7)
Section distance from stapes	V	Basilar membrane width	Spread factor	w at 981 dynes/cm ² pressure (cm)	Pressure to give w _m of 0.001 cm.	
(mm)	(ccs/cm)	b(cm)	K	$\frac{w}{m} = \frac{16 V}{9 Kb}$	cm. water	dynes/cm ²
5	9.4×10^{-7}	0.0211	1.30	0.610×10^{-4}	0.001	16082
10	2.3×10^{-6}	0.0269	1.20	1.266×10^{-4}	$\frac{0.610 \times 10^{-4}}{7.90} = 16.39$	7749
20	7.8×10^{-6}	0.0384	1.15	3.138×10^{-4}	3.19	3126
30	2.9×10^{-5}	0.0500	1.10	9.375×10^{-4}	1.07	1046
34	6.0×10^{-5}	0.0547	1.10	17.71×10^{-4}	0.56	554
5	9.4×10^{-7}	0.0211	1.60	0.494×10^{-9}	20.24	19858
10	2.3×10^{-6}	0.0269	1.33	1.139×10^{-4}	8.78	8613
20	7.8×10^{-6}	0.0384	1.05	3.441×10^{-4}	2.91	2851
30	2.9×10^{-5}	0.0500	1.00	10.312×10^{-4}	0.97	951
34	6.0×10^{-5}	0.0547	1.00	19.503×10^{-4}	0.51	503

The model of the scala media on which elasticity calculations are based thus contains an imaginary membrane of width $\frac{2}{3} b$. There is little doubt that a single membrane model is justifiable in the basal region of the cochlea where the basilar membrane is known to possess an elasticity orders of magnitude higher than any other single membrane or structure in the partition. Bekesy also observed that the gelatinous cellular mass above the basilar membrane noticeably increased the rigidity of the partition and the membrane at the apical end, and that if these cellular structures and Reissner's membrane were brushed aside, the displacement of the basilar membrane at the apex for the same fluid pressure in the scala vestibuli was almost doubled. It is therefore to be expected that while the basilar membrane probably remains the most elastic component at the apical end, the stiffness of the partition is significantly affected by the other structures, and another factor S is introduced giving an estimate of the increase in the deflection of the basilar membrane when the effects of the remainder of the partition are removed. For example, if $S = 1.5$ in say, the third turn of the cochlea, then for no increase in static pressure, the free basilar membrane will deflect 1.5 times the deflection obtaining when the partition was intact.

The calculation of values for E_t from this interpolated data is via equation (9), allowing for both linear and hard spring stiffness effects, and also by equation (4). This latter alternative was included partly for cases when deflections are so large that non linear effects predominate. It was also included so as to examine values of E_t resulting from neglect of the linear term when it is theoretically significant but when the plate bending model may have broken down by virtue of the low R ratio to prevailing at the stapes end.

Reference was made to many publications in order to obtain reliable values for t for equations (8) and (9). Based on Iurato⁽¹¹⁾ and Engstrom⁽¹²⁾, the following values were selected to represent t , where t is considered as the effective thickness of the load-bearing structure comprising the basilar membrane in the pectinate zone; t was selected from photographs of electron-microscope sections as the overall distance from the top of the well developed upper fibril layer to the bottom of the well developed lower fibrillary bundle, and t does not include the overall cellular depth of the membrane.

Section distance from stapes, X.(cm)	t - thickness
stapes end	2.5 = 2.5×10^{-4} cm.
2.0 cm.	5.5 = 5.5×10^{-4} cm.
3.4 cm.	7.8 = 7.8×10^{-4} cm.

Therefore, equation (9), when adapted to an effective membrane width of $\frac{2}{3}b$, becomes

$$P = \frac{Et}{\left(\frac{2}{3}b\right)^4} \left(32 t^2 + \frac{64}{3} w_m^2 \right) w_m$$

That is,

$$P = \frac{Et}{b^4} (162 t^2 + 108 w_m^2) w_m \quad (31)$$

$$\therefore P = \frac{Et}{b^4} \left(\frac{\tau}{10^5} + 108 w_m^2 \right) w_m$$

when τ is given by

$$\tau = 10.0 - 2.56 X, \text{ where } X \text{ is in cm,}$$

this expression being the simplest, and not the least accurate, means by which to present the above relationship between X and t .

Therefore

$$Et = \frac{P b^4}{\left(\frac{10 - 2.56 X}{10^5} + 108 w_m^2 \right) w_m} \quad (32)$$

Where X cm. is the distance of the section considered from the basal end of the cochlea.

TABLE 5

Calculation of Et from data of table 4 for both the basilar membrane and for the single membrane at the location of the basilar membrane which represents the whole cochlear partition.

(Basilar membrane maximum deflection at each section of 0.001 cm.)

(1) Section distance from stapes X cm.	(2) Pressure giving $w = .001$ cm in $\frac{w}{s}$ dynes/cm ²	(3) Relaxation factor for basilar membrane $\frac{w}{s}$	(4) (5) Non-Linear Et values (Equation 4) Et dynes/cm.		(6) (7) Linear and non-linear Et values (Equation 32) Et dynes/cm.	
			whole partition	basilar membrane	whole partition	basilar membrane only
0.5	16082	1.00	30110	30110	16330	16330
1.0	7749	1.00	38040	38040	22250	22250
2.0	3126	1.25	63400	32590	43350	24990
3.0	1046	1.75	60720	11440	49830	10550
3.4	554	1.90	46140	6790	40990	6480
0.5	19858	1.00	37180	37180	20160	20160
1.0	8613	1.05	42280	39800	24730	22370
2.0	2851	1.30	57820	26440	39530	20610
3.0	951	1.85	55200	8820	45300	8180
3.4	503	2.00	41810	5290	37220	5060

TABLE 6

Calculation of Et from table 3 data for both the basilar membrane and for the single membrane representing the whole cochlear partition, assuming Reissner's membrane maximum deflection at each section of 0.001 cms. (using formula $w_m = \frac{16}{9Kb} (\frac{1}{2} \times d_m \times r_m)$ where $d_m = 0.001$ cms., and $r_m =$ mean span of Reissner's membrane = 0.120cms.)

(1) Section distance from stapes Xcm.	(2) Tabulated (Bekesy) maximum displot. of Reissner's membrane d_m (cm)	(3) Assumed spread factor K	(4) Actual max. displot. of Basilar membrane when $d_m = 0.001$ cm. w_m (cm)	(5) Pressure to give maximum Reissner's displot. of 0.001 cm. dynes/cm ²	(6) (7) Et calculated from non-linear equation (4) only	
					Basilar membrane	whole partition
0.5	1.6×10^{-5}	1.30	3.9×10^{-3}	63290 (S = 1.0)	2680	2680
1.0	3.75×10^{-5}	1.20	3.3×10^{-3}	25820 (S = 1.0)	4020	4020
2.0	1.3×10^{-4}	1.15	2.4×10^{-3}	7550 (S = 1.25)	5930	11310
3.0	4.8×10^{-4}	1.10	1.95×10^{-3}	2040 (S = 1.75)	3160	16410
3.4	1.0×10^{-3}	1.10	1.75×10^{-3}	981 (S = 1.90)	2230	14880
0.5	1.6×10^{-5}	1.40	3.65×10^{-3}	63290 (S = 1.0)	3210	3210
1.0	3.75×10^{-5}	1.33	2.95×10^{-3}	25820 (S = 1.0)	5370	5370
2.0	1.3×10^{-4}	1.10	2.5×10^{-3}	7550 (S = 1.30)	4620	9850
3.0	4.8×10^{-4}	1.00	2.1×10^{-3}	2040 (S = 1.70)	2610	12360
3.4	1.0×10^{-3}	1.00	1.95×10^{-3}	981 (S = 1.95)	1560	11160

V. APPLICATION OF POINT LOAD STIFFNESS DATA

Va. Bekesy's Hair Deflection Data⁽¹⁾

The purpose of this section is to calculate values of basilar membrane elastic modulus - thickness product, E_t , at the three sections along the cochlea for which Bekesy supplied experimental data.

The most pertinent of Bekesy's observations are:-

1. The probe used to apply a point load to the basilar membrane was a straight human tactile-sense hair, from 3.0 to 10.0 mm. long, apparently taken from the wrist. The portion of hair used in each test crippled in the sense of an elastic column when required to transmit more than a certain axial load.
2. The basilar membrane, at each of the three test sections, 10, 20 and 30 mm. from the stapes, when subject to a number of point load applications across its width, showed itself to be most sensitive in the pectinate zone. In this regard, Bekesy's data support the theory discussed in section IV of this chapter, for maximum deflection to uniform point load applications across the span occurred at about $2/3$ of the membrane width from the limbus side.
3. Of the four component membranes in the scala media, Reissner's and the tectorial membranes showed the smallest resistance to normally-directed point loads. The reticular lamina, stiffened and supported by the arch of Corti and the cellular structures of the arcuate zone, proved to offer more resistance to point loads than did the basilar membrane at the 30 mm. section. This experimental result is in accord with observations⁽²⁾ on which the calculation of E_t

(in section IV) for the basilar membrane only was based.

Table 5 results suggest that in the apical region, the elasticity of the single effective partition membrane is several times that of the basilar membrane alone.

4. Bekesy's data⁽¹⁾ for the basilar membrane only is summarized in table 7. It is clear that, considering the extreme non-linear character of the model for point load membrane stiffness, and the necessary use of equation (28) in order to calculate values of E_t , table 7 data is practically meaningless unless an addition data column, giving either forces or displacements, is included.

TABLE 7

Summary of Bekesy hair test data⁽¹⁾ for the basilar membrane

Section: Distance from stapes - cm.	Minimum resistance to point loads occurring at about two thirds of span of the basilar membrane	
	cm/dyne	mgf/mm
1.0	4.80×10^{-5}	2.1×10^3
2.0	7.15×10^{-4}	1.4×10^2
3.0	3.25×10^{-3}	3.1×10

Consider an elastic column of length L , and of circular section, diameter D , fixed at one end and pin jointed at the other, having a modulus of elasticity e . The appropriate crippling load P_{cr} is

$$P_{cr} = \frac{\pi^2 E I}{\left(\frac{L}{\sqrt{2.05}}\right)^2}$$

$$= \frac{2.05 \pi^2 E D^4}{32 L^2}$$

$$\therefore P_{cr} = \frac{C D^4}{L^2} \quad \text{where } C \text{ is a constant.}$$

In order to determine a representative value of C for human tactile hairs, a mini-project involving sample-data analysis was

launched in which, regardless of religion, colour, age or academic ability, a large variety of departmental wrists were plucked of a few hairs which were then measured and tested for buckling using a fine Oertling 0.0001 to 100 gramme force electronic balance. The large and rather arbitrary selection of tactile hairs obtained varied in diameter from 0.0007" (0.0178 mm.) to 0.0014" (0.0356 mm.). From results of table 8, the value of C chosen was

$$C = 500 \text{ mgf}(\text{mm})^2/(\text{inch thou.})^4$$

$$= 1.2 \times 10^9 \text{ dyne/mm}^2$$

TABLE 8

Summary of Results of Buckling tests on human wrist hairs

Per mgf	D thousandths of inches	L mm.	$C = \frac{P_0 L^2}{D^4}$
15	1.1	7.0	502
50	1.25	4.9	492
40	0.95	3.0	442
88	1.0	2.45	528

Hairs used by Beksy varied in length from 3 to 10mm., which, with the above diameter variation, gives a possible range of crippling loads of from 1 to 200 dynes. It may be assumed that at the stiffest, 10mm. section, in order to provide a basilar membrane displacement large enough to measure accurately, the shortest and thickest hairs were used. It is also suspected that, due to his having to use hairs 1cm. long (straight tactile hairs of this length being less common) at the 30mm. section, Beksy may have found difficulty in producing sufficiently light, repeatable crippling forces at the apical end.

The reliability of this somewhat devious attempt to estimate the loads applied by human hairs of various dimensions, unfortunately made

necessary by Bekesy's data omissions, may be assessed by examination of table 9.

TABLE 9

Calculation of Et for basilar membrane only, based on Bekesy⁽¹⁾ hair-loaded data and using the approximate form of equation (28),

namely;
$$Et = \frac{F(1 - \sqrt{2}) r_2^2 (1 - K^{\frac{2}{3}})^3}{\pi (\frac{2}{3})^3 (w_m)^3} \quad \text{where } K = \frac{r_1}{r_2}$$

Equivalent diameter of membrane	Length of hair	Diameter of hair	Load Per = F	w_m	Et
cm.	mm.	mm.	dynes.	cm.	dynes/cm.
At Section 10mm. from stapes, where b = 0.0269 cm. and pin stiffness = 4.8×10^{-5} cm/dyne.					
.0269	3.00	0.02875	91	4.37×10^{-3}	82,800
.0359	3.00	0.02875	91	4.37×10^{-3}	170,600
.0269	3.00	0.0300	106	5.08×10^{-3}	60,000
.0359	3.00	0.0300	106	5.08×10^{-3}	124,200
.0269	3.00	0.0325	145	6.96×10^{-3}	30,300
.0359	3.00	0.0325	145	6.96×10^{-3}	63,400
At Section 20mm. from stapes, where b = 0.0384 cm. and pin stiffness = 7.15×10^{-4} cm/dyne.					
.0384	7.50	.02125	4.35	3.11×10^{-3}	29,800
.0512	7.50	.02125	4.35	3.11×10^{-3}	58,100
.0384	7.00	.0225	6.15	4.40×10^{-3}	14,700
.0512	7.00	.0225	6.15	4.40×10^{-3}	32,900
.0384	7.00	.0250	9.37	6.70×10^{-3}	6,200
.0512	7.00	.0250	9.37	6.70×10^{-3}	11,950

Continued

necessary by Bekesy's data omissions, may be assessed by examination of table 9.

TABLE 9

Calculation of Et for basilar membrane only, based on Bekesy⁽¹⁾ hair-loaded data and using the approximate form of equation (28),

namely;
$$Et = \frac{F(1 - \sqrt{2}) r_2^2 (1 - K^{\frac{2}{3}})^3}{\pi (\frac{2}{3})^3 (w_m)^3} \quad \text{where } K = \frac{r_1}{r_2}$$

Equivalent diameter of membrane <u>cm.</u>	Length of hair <u>mm.</u>	Diameter of hair <u>mm.</u>	Load Per = F <u>dynes.</u>	w_m <u>cm.</u>	Et <u>dynes/cm.</u>
At Section 10mm. from stapes, where b = 0.0269 cm. and pin stiffness = 4.8×10^{-5} cm/dyne.					
.0269	3.00	0.02875	91	4.37×10^{-3}	82,800
.0359	3.00	0.02875	91	4.37×10^{-3}	170,600
.0269	3.00	0.0300	106	5.08×10^{-3}	60,000
.0359	3.00	0.0300	106	5.08×10^{-3}	124,200
.0269	3.00	0.0325	145	6.96×10^{-3}	30,300
.0359	3.00	0.0325	145	6.96×10^{-3}	63,400
At Section 20mm. from stapes, where b = 0.0384 cm. and pin stiffness = 7.15×10^{-4} cm/dyne.					
.0384	7.50	.02125	4.35	3.11×10^{-3}	29,800
.0512	7.50	.02125	4.35	3.11×10^{-3}	58,100
.0384	7.00	.0225	6.15	4.40×10^{-3}	14,700
.0512	7.00	.0225	6.15	4.40×10^{-3}	32,900
.0384	7.00	.0250	9.37	6.70×10^{-3}	6,200
.0512	7.00	.0250	9.37	6.70×10^{-3}	11,950

Continued

Table 9 cont'd.

Equivalent diameter of membrane	Length of hair	Diameter of hair	Load Per = F	w_m	Et
cm.	mm.	mm.	dynes.	cm.	dynes/cm.
At Section 30mm. from stapes, where $b = 0.0500$ cm., and pin stiffness = 3.25×10^{-3} cm/dyne.					
.0500	10.00	.01875	1.46	4.75×10^{-3}	5,410
.0667	10.00	.01875	1.46	4.75×10^{-3}	10,200
.0500	10.00	.0200	1.89	6.14×10^{-3}	3,170
.0667	10.0	.0200	1.89	6.14×10^{-3}	6,040
.0500	10.00	.02125	2.42	7.83×10^{-3}	1,930
.0667	10.00	.02125	2.42	7.83×10^{-3}	3,640

It is clear that the diameter of the hair selected to probe the membrane has a great effect on the force that may be applied, and from equation (28), while the diameter of the hair as such does not have a great effect, the deflection w_m of the membrane, which is an indirect function of the strength of the hair, is a variable to which the resultant value of Et is very sensitive.

Also note that two values for the diameter of the circular membrane, whose resistance to point load deformation is equivalent to that of the rectangular membrane, are tried for each data set; in one case the circular membrane has a diameter b , obtained from $\frac{4}{3} \times \frac{2}{3} \times b$ when the pectinate zone only is considered, and in the second case the diameter is simply $\frac{4}{3} \times b$, where b is the total span of the basilar membrane.

Vb. Berendes point load stiffness data⁽³⁾

By means of the fine hair-spring instrument mentioned in Section Ia, Berendes⁽³⁾ has provided quantitative graphical data showing the relationship between point load deflection of the basilar membrane and the force applied. This data is reproduced in Fig. 8. Although it is not quite clear to

which sections of the cochlea the three plots refer, or what diameter pins Berendes used to deflect his membranes (it seems that one shouldn't expect too much from mechano-physiologic data!) the treatment of this clearly displayed graphical data is a relief after the problems of applying the Bekesy data.

The approximately cubic form of the force vs. deflection characteristic shown in Berendes' data agrees very well indeed with the relationship predicted by equation (28).

Berendes' script refers to a basilar membrane width of 0.2 mm. near to one of his test sections, and therefore it is assumed that the "stiffest" curve (c) in Fig.8 refers to the 10 mm. section, or near to it. As table 10 shows, values of Et calculated from Fig. 8(c) data agree reasonably with values calculated from the Bekesy data at the 10mm. section. Note that effects of various pin sizes are shown in table 10. As pin sizes diminish, the effect of changes of pin diameter become less. Included in table 10 are calculated Et values assuming that Fig. 8(b) applies to the 20 mm. section, or near to it, and that Fig. 8(a) applies about the 30mm. section.

TABLE 10

Calculation of Et for basilar membrane from Berendes' data (See Fig.8)

for $r_2 = \frac{b}{2}$ only

Figure reference	Circular membrane equivalent dia. = b (cm)	Pin Diameter $2r_1$ (mm)	Load F (dynes)	w_m (mm)	Et dynes/cm
8c	.0269	.03	12.0	.029	37,000
8c	.0269	.01	12.0	.029	57,000
8c	.0269	.005	12.0	.029	65,000
8c	.0269	.03	5.0	.020	46,500

Continued

Table 10 Cont'd

Figure Reference	Circular membrane equivalent dia. = b (cm)	Pin Diameter $2r_1$ (mm)	Load F (dynes)	w_m (mm)	Et dynes/cm
8b	.0384	.03	8.2	.049	12,700
8b	.0384	.03	2.0	.030	13,400
8a	.0500	.03	6.7	.070	6,700
8a	.0500	.03	2.0	.047	6,600

VI. DISCUSSION OF PARTITION AND BASILAR MEMBRANE ELASTICITIES

From tables of results of calculations for Et in sections IV and V, and from the anatomical etc. data available, it now remains to approve a range of values for Et most likely to apply in a human cochlea.

None of the data on which the calculations are based can be considered satisfactory, and it is surprising that the results are so relatively close. Despite all the difficulties involved in computing Et from the incomplete hair test data, it is expected that the values given in tables 9 and 10 are within a factor of two or three of the real values. Certainly they display a more realistic trend, with higher values of Et towards the stapes, than do the values in tables 5 and 6 which were based upon interpolations of Bekesy's apparently extrapolated pressure test data. These values from table 5 are probably more correct towards the apical end, because errors due to confusion about Bekesy's maximum partition deflection of 0.001 cm. and pressure of 1cm. of water must be minimized in this region. At the same time, there may be serious errors of observation, experimentation etc. in Bekesy's pressure test data, which may have been recognized as such by Bekesy, who, it must be remembered, conducted these tests some time before he renewed his attempts to measure partition stiffness and conducted the hair-probe experiments.

It seems to be a very good compromise to admit that at the 30mm. section, the value of E_t for the basilar membrane is between 5000 and 10,000 and for the whole partition (when considered as a single membrane) is between 40,000 and 50,000 dynes/cm. At the 10 mm. section, the pin test data suggests that the value of E_t for basilar membrane lies around ten times that obtaining at the 30 mm. section.

This order of variation is confirmed by a study of the anatomical and physiological information available concerning depths and sectional areas of basilar membrane pectinate zone fibrillary layers. It appears from Iurato's⁽¹¹⁾ section photographs that over half of the length of the cochlea, from about the 13 mm. section to about the 30 mm. section, the area of the fibril bundles decreases by about 6 or 7 times, suggesting an overall variation from stapes to helicotrema of 13 times. As previously described, the effective membrane thickness, t , which displays an overall variation from one end of the cochlea to the other of over 3 times, may be expected to vary over half the cochlea length by at least 1.5 times.

In view of these details, the trends arising in the point-load data and the absolute values of E_t yielded for the apical region by the pressure stiffness data, a variation in E_t for the basilar membrane of from about 4,000 dynes/cm at the helicotrema to about 150,000 dynes/cm at the stapes, that is about $37\frac{1}{2}$ times variation, is considered likely.

For the single elastic membrane having all of the characteristics of the basilar membrane but with an elasticity equivalent to that of the whole cochlear partition, it is suggested that a reasonable range of values of E_t is from 160,000 dynes/cm at the stapes to 20,000 dynes/cm at the helicotrema, that is, about 8 times variation.

Hence, expressed as a linear variation with distance, X cm, from the stapes, the value of the elastic parameter E_t of the ideal single

membrane, of effective width of two thirds of that of the basilar membrane, representing the whole cochlear partition, is given by

$$Et \text{ dynes/cm} = 160\,000 - 40\,000 X \quad (33)$$

From equations 31 and 32 it is now possible to write the general relationship giving the cochlear partition deforming pressure, P , as a function of the maximum displacement, w_m , of the partition, at any section X cm along the cochlea from the stapes:-

$$P = \frac{Et}{b^4} \left[\tau \times 10^{-5} (w_m) + 108 (w_m)^3 \right] \text{ dynes/cm.}^2 \quad (34)$$

where $Et = 160\,000 - 40\,000 X$ dynes/cm.

$$b = \text{width of basilar membrane at section } X \\ = 0.0152 + 0.0116 X \text{ cms. (described elsewhere)}$$

$$\tau = (10.0 - 2.56 X) \text{ sq. cms.}$$

and X is in cms.

The resulting linear and non linear stiffness components may be evaluated in order to compare with data used by other authors - see table 1, section I.

$$\text{Writing } P = \sigma w_m + \psi (w_m)^3$$

then σ and ψ at five sections are set out in table 11 below, from which it is seen that the overall variation in stiffness of the cochlear partition is about 10,000 times for the linear component and 1,000 times for the non-linear.

TABLE 11

Cochlear partition linear and non-linear stiffness coefficients.

Section X cm.	Linear coefficient σ dynes/cm ³	Non-linear coefficient ψ dynes/cm ⁵
0	3.00×10^8	3.24×10^{14}
1.0	1.73×10^7	2.51×10^{13}
2.0	1.80×10^6	3.97×10^{12}
3.0	1.49×10^5	6.91×10^{11}
3.5	2.06×10^4	2.23×10^{11}

VII. CONCLUSIONS

As past generations of cochlear theorists have all considered wholly linear cochlear partition systems, despite the evidence supporting the generally accepted belief that the principal elastic component, the basilar membrane, is not in a state of tension in its undisturbed state, semi-mathematical models for both the linear and non-linear pressure-deflection relationships for the cochlear partition have been built up from first principles.

It is agreed that in the arcuate zone of the basilar membrane, the cellular and membranous structures of the organ of Corti may together form a stiffened structure capable of exerting moments of resistance to bending of the cochlear partition. Thus, any future analysis based on this anatomical complex, and supported by adequate physiological and geometric data, may well demonstrate a new linear component in the static deflection vs. pressure relationship for the basilar membrane, and for the cochlear partition. Nevertheless, the deflection shapes observed by von Békésy for the pressure-loaded partition, together with data giving point-load stiffnesses across the span of the basilar membrane, support the ideal mechanical membrane hypothesis inferred from the basilar membrane. That is, that in the outer pectinate zone the membrane is both more elastic in nature and, compared with the inner arcuate zone, has limited resistance to bending moments.

Having accepted such a hypothesis and the consequent deformation relationship for the outer zone of the basilar membrane, (in which zone occurs the maximum deflection per unit pressure of the partition, which parameter is the present object of the calculations) it is difficult to see how a stronger linear relationship in the inner zone can appreciably

affect the pectinate zone function, on which depend the stiffness characteristics of the whole partition.

Values of Et , the modulus of elasticity E multiplied by an effective thickness t of membrane, in dynes/cm., have been computed for both the basilar membrane in its pectinate zone and for the single perfect membrane representing the whole partition and of width equal to that of the pectinate zone of the basilar membrane. This has been done for the basilar membrane for three independent collections of somewhat unreliable data, but the possibility of good agreement between these different sets of data has been demonstrated.

Although every effort has been made to employ the limited data available as effectively as possible, it is possible that the values selected as being representative of elasticity are too large.

It is clear that new cochlear partition experimental stiffness data is required and that a sound grasp of the bio-mechanical principles on which the cochlea and scala media must eventually be modelled is necessary before experiments to yield the correct data can be designed. It is expected that pressure test experiments will be repeated in the future, and that they will be based on Berendes' and Bekeasy's classical techniques. It is hoped that such tests will be designed to explore the elasticities and non-linearities of individual membranes and components of the organ of Corti, and, for the dynamic as well as the static case, the nature of the stiffness of the whole scala media.

The type of data offered by Berendes, by whom force vs. deflection curves were displayed, may well be considered essential to future examinations of cochlear partition stiffness relationships.

Note that the only data set in Table 1, section Ib (page 4-13) which is in reasonable agreement with the estimated linear stiffness coefficients of Table 11 section VI is that of Hause.

VIII REFERENCES

1. **The Variation of Phase Along the Basilar Membrane with Sinusoidal Vibrations.**
G. von Békésy
Jnl. Acoust. Socy. Am. Vol. 19. No.3. May 1947. pp.452 - 460
2. **On the Elasticity of the Cochlear Partition**
G. von Békésy
Akustische Zeitschrift Vol.6. 1941. pp.265 - 278
republished in
Jnl. Acoust. Socy. Am. Vol.20. No.3 May 1948. pp. 227 - 241
3. **Die Spannung der menschlichen Basilarmembran**
Berendes
Zeits. Hals-, Nas, und Ohrenheilk Vol.36 1934. pp.338 - 342
4. **On the Dynamics of the Cochlea**
H. Fletcher
Jnl. Acoust. Socy. Am. Vol.23 No.6 Nov.1951. pp. 637 - 645
5. **Review of Recent Mathematical Theories of Cochlear Dynamics**
J. Zwislocki
Jnl. Acoust. Socy. Am. Vol.25 No.4 July 1953 pp.743 - 751
6. **Theories of Aural Physiology**
D.H. Klatt
Univ. Mich. Communications Sciences Lab. Report No.13. 1964
7. **Digital Simulation of the Cochlea**
A.D. Hause
Bell Telephone Labs. Inc. Report MH-1276-ADH, 1963
also Jnl. Acoust. Socy. Am. Vol. 35 1963. p.1896
8. **Re-examination of a Model of the Cochlea**
K.H. Klatt and G.E. Peterson
Jnl. Acoust. Socy Am. Vol. 40. No.1 Feb. 1966. pp.54 - 61

9. **An explanation of the Travelling Wave Theory of Hearing**
R. Guelke
Med. & Biol. Engng. Vol. 4. pp. 349 - 356. Pergamon 1966.
10. **A Dynamical Theory of the Cochlea**
L.C. Peterson and B.P. Bogert
Jnl. Acoust. Socy. Am. Vol.22 No.3 May 1950. pp.369 - 381.
11. **Functional Implications of the Nature and Submicroscopic Structure of the Tectorial and Basilar Membranes.**
S. Iurato
Jnl. Acoust. Socy. Am. Vol. 34. No.9. Sept. 1962. Part 2.
pp. 1386 - 1395
12. **The Structure of the Basilar Membrane**
H. Engstrom
Acta Oto-Rhino-Laryngologica Belgica Vol. 9. 1955. pp.531 - 539

Also

The Ultrastructural Organization of the Organ of Corti.....

H. Engstrom.

Exptl. Cell. Research. Suppl.5. 1958 pp. 460 - 492

PHYSICAL MODELS OF THE COCHLEA

Chapter 5.

Contents

	Introduction	Page 1
I	Review of Previous Cochlear Model Investigations	Page 6
Ia.	Bekesy	Page 6
Ib.	Tonndorf	Page 9
II	Design of Cochlear Models	Page 14
IIa.	General	Page 14
IIb.	Cochlear Geometry	Page 14
1)	Length	Page 14
2)	Basilar Membrane Width	Page 15
3)	Scalae Sectional Areas	Page 16
4)	Windows	Page 17
IIc.	Properties of Cochlear Components	Page 18
IIId.	Dimensional Analysis for Dynamic Similarity	Page 19
III	Detailing, Manufacture, Assembly and Experimentation	Page 27
IIIa.	Model Geometry Detail	Page 27
IIIb.	Manufacture	Page 29
IIIc.	Assembly	Page 32
IIId.	Experimentation	Page 34
IV	Results of Physical Cochlear Model Experiments	Page 39
V	Discussion of Results of Model Tests	Page 43
Va.	Phase effects	Page 43
Vb.	Place and Amplitude effects	Page 45
Vc.	Comments on Effects of Variables	Page 48
Vd.	Other Tests	Page 50
VI	Conclusions	Page 53
VII	References	Page 56

INTRODUCTION

Several successful attempts to construct and to experiment with physical cochlear models have been reported since the turn of the century. (1,2,3,4,5,6,7) Most of these models have been designed with some degree of dynamic similarity to actual cochleas and all investigators involved in this aspect of inner ear research have identified travelling wave vibratory motion in their cochlear model partitions.

The cochlear model studies pioneered by Ewald⁽¹⁾ in 1903, which were based on limited anatomical data, were much improved upon by Wilkinson^(2,3) in 1922, whose experiments stimulated von Békésy⁽⁴⁾ to investigate at first hand the nature of the human cochlear response.

Before engaging in the detail of review, model design, experimentation and physical cochlear model results, it is particularly helpful to consider the two completely complementary and integrated principles of operation which make the mammalian cochlea so efficient a mechanical frequency analyser. Consider first the mechanics of its fundamental component, the membranous labyrinth or cochlear partition.

The basilar membrane (or a single membrane whose stiffness is equivalent to that of the whole partition) may be considered as a long, narrow, elastic element, not in a state of permanent tension, with clamped, tapering edges, its width increasing by 4 to 5 times from the basal or stapes end to the distal (apical or helicotrema) end. Consider this membrane immersed in water and rather heavily damped as it is excited by a general, transverse sound pressure field, acting normal to the plane of the membrane.

Within the range of pure tone sound frequencies to which this membrane responds, it may be seen to display crude spatial frequency discrimination, with lower frequency tones causing a maximum amplitude of vibration response

at the wider end, and an increase of frequency causing the region of maximum amplitude to move towards the narrower end. Because of the membrane being heavily damped, the responding region is broad, and at the lowest frequencies in the range to which it responds, the whole membrane may be observed to be vibrating.

At any intermediate frequency travelling waves occur and almost one half wave length, i.e. π radians, of the membrane transverse travelling wave may be observed at any instant, this wave being spread broadly along the membrane. This response pattern may also be complicated by the appearance of higher order modes of membrane vibration than the fundamental.

Now consider the hydrodynamics of the cochlear bony labyrinth, when rigid boundaries, namely, the walls of the two scalae, are applied to the fluid field surrounding the partition.

The former mechanics of the membrane have not been disturbed, but the manner of excitation of the partition is quite unlike the former case. At whichever point sound is introduced to the liquid in the scalae, the propagation of pressure wave motion is dependent only upon the requirements (or equations) for continuity of fluid and equilibrium of forces acting upon each element of fluid. Clearly the impedance of the channel boundaries has a strong effect on both continuity and force relationships. For a wholly rigid walled tube, i.e. of infinite impedance, the equations are simplified, and only geometrical (sectional area, length and end condition) variations, viscosity, density, and compressibility effects are relevant to the nature of the pressure distributions arising due to pressure wave propagations and fluid particle motions. When part of the boundary of the tube is subject to its own equation of motion it follows that the pressure propagation relationship at any section along either scala is primarily a

function of all of the complex boundary impedances at other sections. In the cochlea, where the same compliant membrane forms the same boundary, but in opposite senses, for the two adjacent scalae, the instantaneous cyclic pressure differential across the partition at any section X causes the partition at that section to vibrate with a certain amplitude and phase, and this motion may, in turn, induce,

- a) a pressure differential at the adjoining section $X + \delta X$ which is significantly greater than that obtaining in the case of a rigid walled duct
- b) a significant phase delay in the induced pressure differential at the adjacent section.

Hence, due to this complex hydrodynamic action by which the cyclic pressure differentials, which excite the partition at each point along the cochlea, change in both amplitude and phase depending upon the previously excited response of the partition, several notes can be made about basilar membrane dynamic behaviour, compared with the case for a simple, transverse sound field:-

- a) For pure tone excitation, excited regions may be less broad, particularly on the helicotrema side of an area of maximal stimulation of the membrane
- b) Such points of maximum amplitude response may be at different locations to those obtaining for uniform pressure excitation
- c) Travelling waves will display phase differentials larger than π radians, which effect may assist the wave-form, place and frequency sensory processes
- d) If sound be introduced at the basal end, i.e. adjacent to the region of the partition responding to the highest frequencies,

then only fundamental modes of membrane vibration can be excited. Acoustic power will be absorbed and scalae pressure differential propagations will be diminished by the first region of membrane undergoing major excitation in its fundamental mode, and distal along the cochlea, subsequent sections of membrane capable of a higher mode harmonic response at the stimulating frequency cannot be sufficiently excited to respond.

It would therefore appear that in any attempt to model the cochlea, the following physical properties and characteristics are relevant; cochlear scalae geometry, size and shape, perilymph density, compressibility and viscosity, round and oval window areas and impedances, cochlear partition mass, damping, stiffnesses and effective widths, and the manner in which sound is introduced into the system. The hydrodynamical aspects of cochlear modelling being rather more daunting than the pure mechanics of the isolated partition, provided of course that some means are found by which to estimate the physical properties of the partition and its components, it was decided to design and execute a physical model experimental programme which would principally examine the effects of those variables most relevant to the hydrodynamic nature of the cochlea; particularly scala geometry, size and shape and also the fluid properties.

In such an experimental investigation, however, there are certain problems to be faced before design of models can begin, and these include:-

- a) doubt as to the actual ranges of physical properties appropriate to human cochleas, and uncertainties as to which properties or parameters, if any, may not vary widely from person to person.
- b) difficulty in simultaneous matching of a number of dimensionless parameters required for complete dynamic similarity of models, including

- difficulty with choice of materials.
- c) design of models so as to ensure accurate measurement of the dynamic response of inaccessible membranes, fluid motions, etc.
 - d) manufacture and assembly of the ranges and shapes of models ideally required.
 - e) means of measurement and adjustment of physical properties of components.

With regard to these five points, little help may be gleaned from the literature on physical cochlear models, largely because of the qualitative nature of all other investigations. No cochlear model investigator has reported a formal range of values for partition elasticity (or mass and damping) as used in his model. Possibly because of the difficulties involved in reducing his own data, Bekeasy⁽⁴⁾ abandoned attempts to build enlarged dynamically similar cochlear models in favour of life-sized models, using the same techniques to test the stiffness of model membranes as he used to measure, "in vitro", human cochlear partition stiffnesses.

The model designs of both Bekeasy and Tonndorf^(5,6,7) were geometrically crude with scalae sectional shapes represented by rectangular passages. Bekeasy's work mainly defined the essential elements of the cochlear arrangement, while Tonndorf, showing little interest in the effects of controlled variations in scalae, membrane or fluid properties, made a large number of visual and photographic studies of cochlear response to time dependent input signals. There is no doubt that Tonndorf's cochlear model researches have added to the modern appreciation of the role of the cochlea as a hydrodynamic frequency discriminator, and that adaption and development of his techniques could prove a most rewarding research topic. As he and Bekeasy are the only reputable and rigorous cochlear model researchers remaining at this time, and their studies are pertinent to this report, their work is discussed in review. However, the programme of cochlear

modelling initiated by the writer is supplementary to Bekesy's and Tonndorf's researches.

I REVIEW OF PREVIOUS COCHLEAR MODEL INVESTIGATIONS

Ia. Bekesy⁽⁴⁾

Appreciating the need to scale dynamic parameters for the design of similar models of other than unit geometric scale factor, Bekesy in 1928 defined two dimensionless numbers which, he claimed, were adequate for complete similarity. Other writers invariably requote these two parameters, which are-

$$\frac{\rho f L^2}{\mu} \quad \frac{\mu^2 \epsilon}{\rho L^4}$$

where μ and ρ represent dynamic viscosity and density of cochlear fluid, respectively,

f = frequency, L = characteristic length and ϵ = volumetric pressure stiffness per unit length of the cochlear partition, that is

$$\epsilon = \frac{\text{volume displacement per unit length}}{\text{deforming pressure}}$$

$$= \left[\frac{L^3 T^2}{N} \right]$$

Influenced by the prevailing belief that cochlear partition membranes derived their stiffness from residual tension forces, Bekesy first argued that due to difficulties in matching the stiffness ϵ , similar cochlear

models could not be constructed for length ratios of model to human cochlea greater than about 4. Although no quantitative data was given Bekesy did report observations made on a four times natural size, glass sided model of an "unwound" cochlea, the straightening of the spiral cochlea whorls being reasonable because of the existence of unspiraled cochleas in several species, e.g. the anteater. A hardened rubber solution model partition was cast on a lightly tapering metal frame and cemented into his rectangular glass channel, and an electromagnetically driven tuning fork excited a plunger in a model oval window. A rubber-covered secondary opening performed the functions of a round (scala tympani) window.

By means of floating particles of metal foil, Bekesy identified vibrating areas of his rubber partition with adjacent fluid eddies. As the eddies were easier to observe, he noted their shift towards the stapes following increases in membrane stiffnesses, and, when optimum membrane thicknesses were better established by trial and error, he was able to view microscopically the movements of fine carbon particles distributed on the membrane. A rotating disc provided a stroboscopic effect which permitted close observation of regular travelling wave motions in his model partitions. Note that these experiments with models followed the similar studies by Wilkinson and preceded his own human cochlear "in vitro" experiments.

In 1942 Bekesy published the qualitative results of a more critical series of experiments in which he apparently used natural sized metal-and-glass cochlear models. As geometrically similar models these bore only a functional resemblance to the cochlea, but model partition stiffnesses were similar to those for, and measured by the same means as, human basilar membranes and cochlear partitions. Although these measured stiffness values as published by Bekesy remain somewhat obscure, it is probable that

his models were, as regards partition stiffness, better representations of human cochlear than any other models since.

The following points summarise Bekesy's results , for which no quantitative data was given:-

- a) the elasticity of the round window had no effect on partition response.
- b) the length of the model had no effect on partition response within most of the normal (scaled) audible frequency range.
- c) oval window impedance did not affect the partition response.
- d) increase of depth of either channel did not affect spatial frequency discrimination achieved by the partition.
- e) a substantial decrease of depth of either channel, if arranged in the length of channel between the stapes and the distal end of the region of maximum vibration of the partition, always broadened the responding region and moved this region towards the stapes.
- f) a change of position of the vibrating, fluid-exciting source from the stapes to the centre of a channel or to its distal end had no effect on apparent partition frequency response.
- g) removal of all fluid from the lower (tympani) channel caused the region of maximum partition vibration to shift towards the proximal (stapes) end.
- h) removal of fluid from one channel on both sides of the responding region of the partition, but not adjacent to the region of vibration, had no effect on the position of this region along the partition.
- i) an increase of fluid (perilymph) viscosity caused the vibrating region to shift towards the stapes.
- j) the position along the partition of the centre of the eddy coincided with the position of maximum amplitude of the partition at every frequency.

k) when a viscous mass representing the scala media was added to the rubber membrane representing the partition, the mass and damping increase caused the locus of maximum partition vibration to shift towards the stapes.

Ib. Tonndorf.

Since 1957 Tonndorf has published several papers (including refs. 5,6,7) dealing mainly with fluid motion in cochlear models. His models were similar to Bekesy's, about five times size and made of transparent plastic. Frames supporting cochlear partitions were interchangeable so that various membranes could be tested, and these partitions were usually of rubber cement impregnated with reflectant aluminium particles. Models were stimulated by a loud-speaker unit connected to the oval window by a closed air-filled coupler. Rubber model membranes were reported to have an exponential stiffness gradient, and Tonndorf expressed this gradient in terms of the membrane stiffness ratio at the two ends, which was about 10 to 1. It is not clear whether this is due to a variation in thickness and/or elasticity of his material, or whether it is a nett partition stiffness taking into account the increasing width of the model basilar membrane. It is, in fact, believed that these model membranes were uniform.

Tonndorf's models responded with observable travelling waves in the applied frequency range 10 to 500 Hz. Observations were assisted by the use of a stroboscope and a dissecting microscope of magnification 10 to 40 times.

In his 1957 paper⁽⁵⁾ Tonndorf observed motions of fluid-suspended reflecting particles. He noted that in the oval window region, fluid was in a state of longitudinal wave motion with particle amplitudes directly

corresponding to oval window displacements (after allowing for sectional area differences). Progressing along a model stimulated by pure tones in the apical direction, a transversal vector appeared in the motions of fluid particles adjacent to the partition, making these orbits elliptical, while particles near to the solid walls of the scalae retained a linear, non-trachoidal motion. All particles, regardless of their position, moved in their orbits with the same angular direction and speed.

The transversal axis of particle orbits attained a maximum near the place of partition maximum amplitude and then both axes lost amplitude rapidly. Principal axes of all elliptic orbits were noted to lie either longitudinally or normal to the partition, indicating the presence of only two mutually perpendicular particle velocity vectors. Tonndorf also noted a progressive phase lag for particle position in elliptic orbits which accumulated with increase of distance along the partition from the stapes. This angle apparently corresponded with the increasing phase lag of the vibrating partition. Particle motion in the scala tympani was observed to lag by about 180° behind scala vestibuli fluid particle motion.

At high levels of sound intensity fluid eddies appeared in both scalae, their effect on particle motions suggesting a direct imposition of steady eddy velocities on oscillating particle orbits. Tonndorf studied the dependence of eddy velocity on sound frequency and intensity, and likened the inclinations and instabilities of particle orbits in the vicinity of eddies to surf due to a shallow water wave incident on a sloping beach. He also prepared two additional models with which to test hypotheses concerning deep (short wave length) vs. shallow water waves. One model contained an un-naturally deep scala in which fluid was excited by sound at varying depths, while the other model scala was only a few millimetres deep. As

in his previous model experiments, he was able to demonstrate the absence of deep water waves by means of his fluid particle observations; the transversal diameter of elliptical particle orbits clearly diminished with depth or distance from the vibrating partition and longitudinal wave velocities of particles were not influenced by variations in frequency. Both of these points imply shallow water wave motion; and the second point was also substantiated by subsequent observations by Tonndorf of model response to complex signal excitation, when phase relationships between component waves remained constant along the scales. In this later series of experiments, it was discovered that in response to complex harmonic signals, higher harmonic wave motion was simply superimposed upon that of the fundamental, retaining the phase relationships present in the original disturbance; the harmonic wave effects are carried with the fundamental until eliminated by low-pass filter action.

In his 1962 paper ⁽⁶⁾ Tonndorf pointed out that the acoustic law defined in 1843 by Ohm, who first considered Fourier frequency analysis as the principal analytic function of the ear, had remained virtually unchallenged, especially since its endorsement in 1863 by Helmholtz. The techniques to which this reference refers include Fourier expansion series, for the analysis of steady-state periodic sounds, and Fourier integrals for the case of short-lasting sounds including aperiodic transients. Fourier transforms, for example, may be applied to determine the effect of a transmission system, with a certain frequency response characteristic, upon a particular signal.

Tonndorf argued that in addition to the frequency analysis of sounds by spatially arranged responses along the cochlear partition and within the scala media, there are other conditions when it is probable that the cochlear elements recognize the purely temporal features of an auditory disturbance.

The semi-quantitative results he obtained in a long and well-conceived series of cochlear model tests supported his thesis that, even in the mechanical domain, along a time-frequency continuum the response of the cochlea to sinusoidal signals represents one extreme, of a pure Fourier (frequency) analysis, and the response to sharp transients represents the other extreme, approaching a pure time (wave-form) analysis. Thus responses to all other signals arrange themselves between these two extremes.

Illustrating this original thesis, Tonndorf performed model experiments in which partition responses were photographed under optical magnifications for a great variety of input disturbances to models, including pure tones, complex combinations of pure tones (already mentioned), various transients, periodically repeated pulses, random noises, amplitude and frequency modulated signals and beating, mistuned consonances. His observations for transients only are briefly discussed:-

Systematic application of signals in the form of impulses and, more frequently, gradual step-functions of various time constants, were made. Although such signals were aperiodic at the cochlear model entrance, their response pattern along the less than critically damped partition consisted of short duration travelling waves. The primary time-domain response of the partition to a step-function consisted of the first time derivative, a pulse, which was synchronized with the signal. Subsequently, with model windows at rest, a secondary response continued during which the partition travelling bulge achieved a maximum amplitude some distance along the model. The time duration of the travelling bulge increased gradually and continually with distance, and the shape of the pulse (ratio of bulge amplitude to time duration) remained unaltered up to the place of maximal amplitude, thereafter broadening and flattening.

This behaviour is typical of a low-pass filter system and can be predicted from superposition of the Fourier transform of the pulse upon the frequency characteristic of the system in question. In fact an electrical cochlear analogue by Peterson and Bogert⁽¹¹⁾ was designed on this basic assumption of a mechanical analogue of a low-pass filter system in which bandwidth decreases continually with distance, *c.f.*, a tapered transmission line. Peterson and Bogert and Guelke⁽¹²⁾ have both employed the transmission line analogy to assist in the formulation of mathematical cochlear models. Both the shape of the travelling bulge and the location of the place of maximum partition amplitude were seen to be functions of the time constant of the original step function signal. Tonndorf compared a plot of time constant *vs.* distance for step function inputs with a similar plot for steady state pure tone inputs, the frequencies of which corresponded to the inverse time constants of the first set of signals. The two curves were parallel and fairly close.

Hence he re-affirmed his point that in the case of transient signals, the cochlea performs a time analysis as well as a frequency analysis.

Although the models designed by the writer are considerably larger than Tonndorf's models and particularly lend themselves to an examination of the time responses of their cochlear partitions to various aperiodic and complex signals, no attempt has yet been made to emulate Tonndorf's outstanding researches other than for a few simple observations.

II DESIGN OF COCHLEAR MODELS

Ila. General.

The models designed by the writer were intended to supplement the established qualitative model test data, particularly as regards the hydrodynamics of the cochlea. Better substantiated dynamic similarity was intended, and models and associated apparatus were required to ensure that accurate quantitative data on partition response could be obtained. A range of nine different models was designed, of which there was only time to manufacture and test seven, in order to introduce and to exceed a variety of explicit geometrical variations which might be expected in a range of human cochleas. Materials were selected in an attempt to match and vary, within the probable range of normal human variations, the physical properties of the cochlear partition and the cochlear fluid perilymph.

Although the scope and precision of this programme of research constituted a departure from previous cochlear model studies, the general comparative approach was similar in that the effect of each change of variable was assessed by comparing the responses of models containing these changes. Accuracy was also required in order to test the response of a mathematical model of a physical model.

Iib. Cochlear Geometry.

(1) Length

Both Littler⁽⁸⁾ and Wever⁽¹³⁾ refer to measurements by Wever and others which gave mean lengths of the spiral channels of human cochleas of between 31 and 33 mms., whereas several other authors including Fletcher⁽¹⁴⁾, Peterson and Bogert⁽¹⁵⁾ and also Bekesy⁽⁴⁾ constantly refer to lengths of 35 and 36 mm. A mean human cochlea length of 3.5 cms. from the oval window to

the apical end of the helicotrema was assumed for this study.

(2) Basilar Membrane Width

Table 1 shows the ranges of basilar membrane width accepted by a number of authors. The first three references (4, 13 and 18) are more authoritative as those investigators actually made measurements of human cochlea dimensions. Range A given at the bottom of the table was accepted for the design of the writer's cochlea models. However, more recent examination of additional data by Wever (13,8) prompted consideration of a slightly increased range of basilar membrane widths, which is given as range B. Range B widths are all 1.20 times range A widths and have been used in all other sections of the writer's work, including the mathematical cochlear model in chapter 6. The distinction between these two ranges is not important, and had not most cochlear models already been manufactured at the time of the re-examination of the data, range A would have been abandoned. Note that detailed basilar membrane width measurements show a slightly curved, exponential plot of width vs. distance from stapes and a maximum width occurring not at the distal end of the cochlea but at some 5% to 8% of the cochlea length from the apex. Thus range A probably provides a closer apical-area average width, but range B, while being more in error at the apex, gives a better linear approximation to membrane width as a function of distance from the stapes over the remainder of the cochlea.

TABLE I.

Width of the Basilar Membrane

<u>Investigator</u>	<u>Width at basal end (cm.)</u>	<u>Width at apex (cm.)</u>
Bekesy ⁽⁴⁾	0.01	0.05
Wever ⁽¹³⁾	0.012	0.048
Wever ⁽⁸⁾	0.008	0.042 to 0.065
Wrightson and Keith ⁽¹⁸⁾	0.016	0.052
Little ⁽⁸⁾	quotes Wever - 6.25 fold variation	
Wilkinson and Gray ⁽¹⁷⁾	0.016	0.052
Fletcher ⁽¹⁴⁾	0.01	0.05
Peterson and Bogert ⁽¹⁵⁾	0.0190	0.0516
Zwislocki ⁽¹⁶⁾	0.016	0.055
Retzius (1884) ⁽⁸⁾	0.021	0.036
<u>Range A</u>	0.0127	0.0466
	i.e., $b = (0.0127 + 0.00967.X) \text{ cm.}$	
<u>Range B</u>	0.0152	0.0558
	i.e., $b = (0.0152 + 0.0116.X) \text{ cm.}$	

(3) Scalae Sectional Areas and Diameters.

Information on variations of sectional areas of the scala vestibuli and the scala tympani has been collated from the data of Wever⁽¹³⁾, Zwislocki⁽¹⁶⁾ and Keith⁽¹⁸⁾. The other cochlear theorists have used an assortment of values for scalae areas, and only the range used by Peterson and Bogert⁽¹⁵⁾ is mentioned for comparison, whose area A for both scalae, at any section X cm. from the stapes is given by $A = (0.029 - 0.005.X) \text{ cm}^2$.

Each of the sets of experimental data above clearly shows that while the usual linear taper simplifications describing the reduction in either area

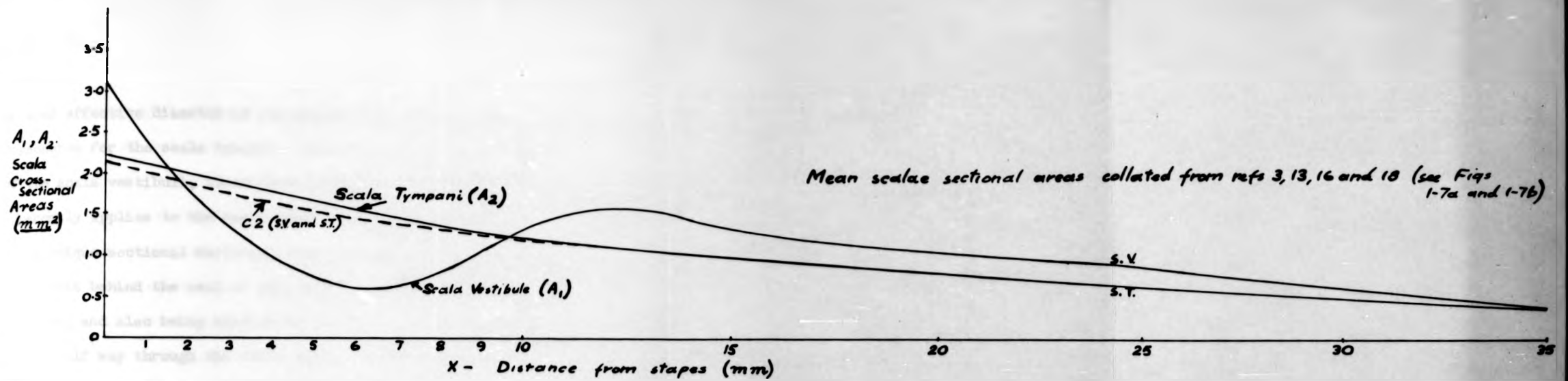


FIGURE 5-1.a.

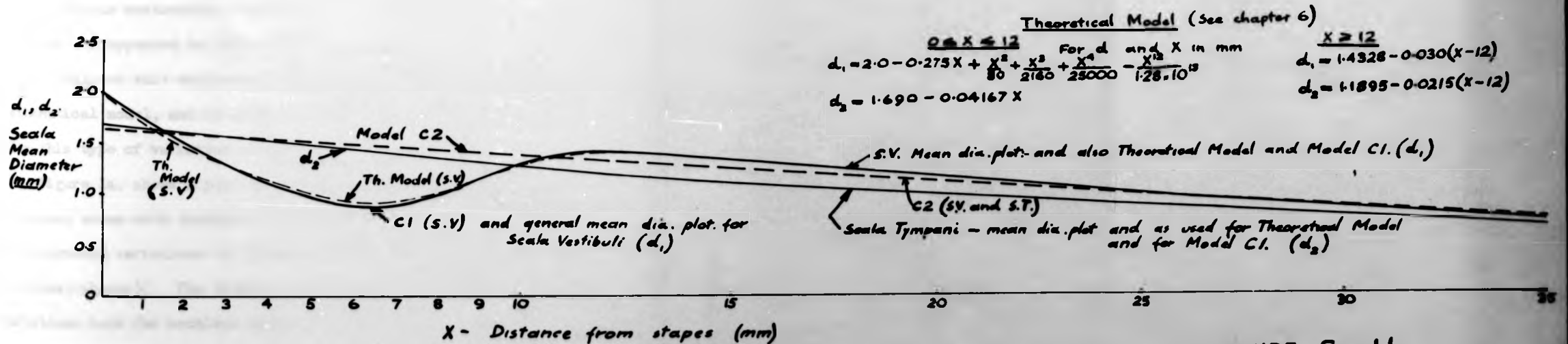


FIGURE 5-1.b.

Scalae Vestibuli and Tympani sectional areas and equivalent mean diameters for human cochleas and for cochlear models

window is about 2 to 2.5 mm², and the area of the stapes footplate, is about 3.0 to 3.5 mm², although Keith gave an area range of 1.65 to 3.75 mm². The area of the oval window is about 0.2 mm² according to Keith

or mean effective diameter of the scalae with distance from the stapes is reasonable for the scala tympani, and is also reasonable for the apical end of the scala vestibuli, it can not describe the "necking" function which apparently applies to the basal half of the scala vestibuli. For this duct has a unique sectional variation with distance, its area being effectively large just behind the oval window, where perilymph passages lead to the vesicles, and also being subject to a definite minimum of sectional area almost half way through the first turn. With further distance from the stapes, the area increases to a second maximum just before the end of the first turn, and subsequently decreases towards the apex in an approximately linear manner. As this unique contraction and dilation of vestibular scala areas with initial distance has appeared in three sets of independent data, it was not considered wise to neglect this variation, and it has therefore been included in the mathematical model, and in order to determine its effect, if any, experimentally this type of variation of area was tested in the physical model programme.

Figure 1a. shows a plot of typical variation of scalae mean cross sectional areas with distance from the stapes, and Figure 1b. shows the corresponding variations of scalae diameters (calculated assuming circular sectional shapes). The dashed lines in Fig. 1a. show the scaled area variations used for cochlear models C1 and C2 and the dashed line in Fig. 1b. shows the effective diameter variation used in continuum form in the mathematical model.

(4) Windows.

According to Bekey⁽⁴⁾, Keith⁽¹⁸⁾ and Littler⁽⁸⁾ the area of the round window is about 2 to 2.5 mm², and the area of the stapes footplate, is about 3.0 to 3.5 mm², although Keith gave an area range of 1.65 to 3.75 mm². The area of the helicotrema opening is about 0.1 to 0.2 mm² according to Keith and Littler.

Iig. Properties of Cochlear Components

Dimensions of components have been discussed above, and cochlear partition effective stiffness and mass variations have constituted the theme of chapters 4 and 3 respectively. Damping functions and details for the cochlear partition and the basilar membrane are not known, but it would appear from consideration of the scala media fluid flow patterns resulting from deflection of the cochlear partition (see Chapter 3) that liquid shearing forces induced by moving boundaries, constrictions and scala media component motions suggest a classic case of (heavy) simple viscous damping.

Bekesy paid a great deal of attention to cochlear partition damping, and discussed the almost historic results of Helmholtz and others whom, he said, estimated that the partition showed a logarithmic decrement of $\xi = 0.1$. It is probable that Helmholtz's definition of log. decrement was more in line with the modern definition than was Bekesy's, rather implying that $\log. \xi = 0.1$. giving $\xi = 1.1$. Bekesy's own extensive but rambling analysis of damping suggested a value of $\log. \xi$ of between 1.4 and 1.8, which gives a ratio of actual viscous damping constant c to critical viscous damping constant c_c of approximately 1 to 10. As none of the analyses or experiments involved seem particularly pertinent, an intuitive value for c/c_c of about 0.5 to 1 is suggested and the matter is left for further investigation in chapter 6. In the practical case of physical modelling of the cochlea, it is not possible to control model partition damping conditions to any significant extent (without detailed modelling of the microstructures of the organ of Corti) other than by controlling the viscosity of the fluids in which model partition membranes are immersed.

The physical properties of perilymph are shown in table 2. Peterson and Bogert's values for dynamic viscosity, μ , density ρ , and speed of sound,

α , in perilymph are, like values used by other cochlear theorists, based on values actually measured by Bekesy, and the writer has used a similar range for both physical and mathematical model design. However a recently discovered N.A.S.A. publication by Steer et al⁽¹⁹⁾ gives a new set of values for physical properties of labyrinthine fluids. These latter values are considered more authoritative than Bekesy's but the former values as used by the writer have not yet been corrected.

TABLE 2.

Physical Properties of Cochlear Fluids at 37°C

<u>Reference</u>	<u>Density</u> <u>gm/cc.</u>	<u>Viscosity</u> <u>centi-poise</u>	<u>Speed of</u> <u>sound; cm/sec.</u>	<u>Temperature</u> <u>Coefficient</u> <u>of Viscosity</u>
Bekesy ⁽⁴⁾	1.034	1.97	-	-
Peterson and Bogart ⁽¹⁵⁾	1.00	2.00	1.43×10^5	-
Steer et al ⁽¹⁹⁾	1.00	0.802	-	- 2.3% per °C
Perilymph	(accuracy \pm 2%)			
Steer et al	1.00	0.852	-	- 2.4% per °C
Endolymph	(accuracy \pm 2%)			

IId. Dimensional Analysis for Dynamic Similarity

Adequate geometric and kinematic similarity is obtained in cochlear models by the construction of the two principal scales in straightened form, separated by a single tapering membrane representing the cochlear partition, and with elastic scaled windows at the basal end of each scale, in one of which a rocking stapes excites the enclosed liquid. Dynamic similarity may

be achieved by matching the component and materials physical and mechanical properties so as to ensure similar relationships between all of the internal forces involved in the models to those obtaining in the human cochlea. The partition response, excited by pressure waves and particle motions in the surrounding fluid, is determined by the following independent variables:-

L	characteristic length	[L]
f	frequency, cycles per second	[T ⁻¹]
ρ	perilymph density, gm/cc.	[M L ⁻³]
μ	perilymph viscosity, c.g.s. units or poise	[M L ⁻¹ T ⁻¹]
α	speed of sound in perilymph cm/sec.	[L T ⁻¹]
Et	modules of elasticity multiplied by membrane thickness, dynes/cm.	[M T ⁻²]
m	mass per unit area of membrane gm/cm ²	[M L ⁻²]

A set of dimensionless numbers containing convenient arrangements of these seven variables may be calculated. For example, taking ρ , L and μ to be convenient variables by which to link scalae fluid properties with partition elasticity Et;

$$\text{let } \Pi_1 = \rho^a \mu^b L^c Et$$

$$\therefore \Pi_1 = M^a L^{-3a} M^b L^{-b} T^{-b} L^c M T^{-2}$$

equating indices for M,

$$0 = a + b + 1$$

similarly,

$$0 = -3a - b + c \quad \text{and} \quad 0 = -b - 2$$

Hence $b = -2$, $a = 1$ and $c = 1$

$$\text{giving } \pi_1 = \frac{L^2 \rho f}{\mu}$$

Similarly for the other three independent dimensionless parameters

$$\pi_2 = \frac{\rho L a}{\mu}$$

$$\pi_3 = \frac{\rho L E t}{\mu^2}$$

and the fourth term to emerge from this treatment with ρ , L and μ as basic variables is

$$\pi_4 = \frac{\rho L}{m}$$

which gives a ratio between fluid and partition inertia forces. The influence of m may be better appreciated by arranging the partition dynamical variables together, e.g. $\pi_5 = \frac{f^2 L^2 m}{E t}$.

Et

The numerical value for each π term must ideally be the same for the model as for the human cochlea. If the variables are arranged as ratios,

$$\text{e.g. } f_R = f \text{ model} / f \text{ cochlea}$$

$$L_R = L \text{ model} / L \text{ cochlea} \quad \text{etc.,}$$

then $\pi_{1R}, \pi_{2R}, \dots = 1$, that is

$$\frac{L_R^2 \rho_R f_R}{\mu_R} = 1, \quad \frac{\rho_R L_R a_R}{\mu_R} = 1 \quad \text{etc.}$$

The first approach to the design of model variables involves selecting a preferred value for any one or two variables and deciding whether subsequent parameter matching can be produced with materials available. As the π_1 and

Π_2 terms were considered to be most important, and the Π_3 and Π_5 terms less important, based upon less certain data, and probably difficult to match, a number of values for L_p of 5, 10 and 15 were tried to ascertain their effects on other variables, remembering the limitations of some of these variables; for example, the compressibility parameter a and the density ρ do not vary much for liquids likely to be used at room temperatures, and in using a single elastic membrane to represent the cochlear partition, its surface density m will be so closely linked to its elastic parameter E_t as to make the $\frac{m}{E_t}$ component of the Π_5 term very inflexible to manipulation and adjustment. The frequency factor f_R imposes further limitations; it is not convenient to attempt to vibrate large models which are supported on microscope platforms, benches etc. below about 10 Hz, or, considering the normal ranges of power of electromagnetic vibrators and power amplifiers and frequency limits of stroboscopes, above about 3 kHz. As the audio-frequency range for the cochlea lies between about 50 Hz and 20 kHz, these requirements suggest an optimum frequency factor f_R of between $1/4$ and $1/20$.

Finally, the following parameter values and materials were selected:-

$$L_p = 12.0 \quad , \quad f_R = 0.100$$

and using an aqueous glycerol mixture, of 74% by weight of glycerol at 17.5°C ,

$$\rho_{\text{model}} = 1.21 \text{ gm/cc. giving } \rho_R = 1.21,$$

$$\mu_{\text{model}} = 0.343 \text{ poise giving } \mu_R = 17.40,$$

$$a_{\text{model}} = 1.71 \times 10^5 \text{ cm/sec. giving } a_R = 1.196.$$

$$\text{Hence } \Pi_{1R} = 1.00 \quad \text{and} \quad \Pi_{2R} = 1.00,$$

that is, the two dimensionless parameters concerned only with scales fluid mechanics were well matched.

Matching of Π_3 and Π_5 was difficult. A very wide range of latex and synthetic rubber sheeting, cured under different conditions and with

different additions was purchased and tested for elastic modulus and density. Most of this rubber sheeting lost its elastic properties quickly with exposure to either air or aqueous glycerol solutions, and changed its characteristics hysteretically following simple strain. Nor was it able to withstand, without considerable creep and loss of elasticity, periods of cyclic tension. However, one small rubber research and development company accepted the challenge and, at great inconvenience to themselves, experimented with various additives and produced an ample supply of well cured, dense latex sheeting containing additives to preserve and implement elasticity, and this material has proved to be reliable and satisfactory. The same firm was able to supply this sheeting in a number of different thicknesses from 0.0015" to 0.025" and also to a difficult specification for which sheeting in 48" widths increased in thickness uniformly from 0.002" to 0.020" over a length of 16".

These rubber membranes used in models possessed the following properties, (subscript M refers to models) where the thickness t in cm. is re-expressed as t_1 in thousandths of inches (inch thou)

$$E_M = 21.0 \cdot 10^6 \text{ dynes/cm}^2.$$

$$Et_M = 21.0 \cdot 2.54 \cdot 10^6 \cdot 10^{-3} \cdot t_1 = (53340 \cdot t_1) \text{ dynes/cm.}$$

$$\rho_M = (0.0035 \cdot t_1) \text{ gm/cm}^2.$$

Table 3. shows the numbers calculated for π_{3R} and π_{5R} using any of three different rubber thicknesses, 0.003", 0.0075" and 0.020" at any three different sections X cms. along the cochlea from the stapes (at either end and centrally). As above, subscripts M refer to model values, subscripts C to the human cochlea. When π_{3R} is unity the relationships between fluid dynamics forces involving fluid inertia and viscosity effects in the scalae and the fluid pressure forces required to overcome membrane elastic effects

will be the same in the model as in the cochlea. These relationships must exercise considerable influence upon general scalae hydrodynamic response and vice versa. When the parameter representing "internal" membrane dynamics only, $\pi_{\frac{5}{2}}$ is unity, the relationships between membrane inertia and membrane elastic forces for the model are similar to those in the human cochlear partition.

In table 3, π_R numbers very close to unity are ringed, and those within a factor of 2 or 3 of unity are surrounded by broken rings.

TABLE 3.

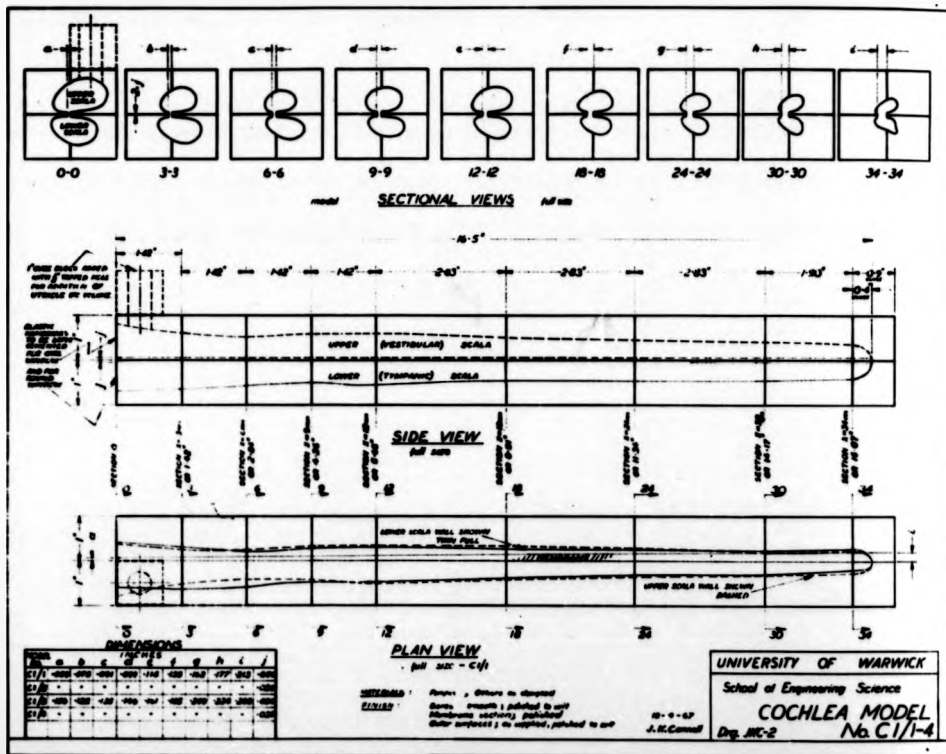
Dimensionless parameters $\pi_{\frac{3}{2}}$ and $\pi_{\frac{5}{2}}$ for cochlear models.

Distance from } stapes (cm.)	$X_c = 0$ $X_M = 0$	$X_c = 1.75$ $X_M = 21.0$	$X_c = 3.5$ $X_M = 42.0$
Et_0 (dyne/cm.)	160000	90000	20000
m_0 (gm/cm ²)	0.015	0.020	0.031
$t_1 = 3, t = 0.0076$ cm., $Et_M = 160,000, m_M = 0.0105$			
$\pi_{\frac{3}{2}}$	0.048	0.085	(0.384)
$\pi_{\frac{5}{2}}$	(0.992)	(2.351)	16.40
$t_1 = 7\frac{1}{2}, t = 0.0191$ cm., $Et_M = 400,000, m_M = 0.0263$			
$\pi_{\frac{3}{2}}$	0.120	(0.220)	(0.959)
$\pi_{\frac{5}{2}}$	(1.217)	(2.340)	16.37
$t_1 = 20, t = 0.0508$ cm., $Et_M = 1,006,700, m_M = 0.0700$			
$\pi_{\frac{3}{2}}$	(0.300)	(0.540)	(2.414)
$\pi_{\frac{5}{2}}$	(0.936)	(2.220)	15.48

The following notes summarize table 3. results:-

- 1) All thicknesses of rubber sheeting provide excellent similarity for membrane "internal" dynamics (parameter Π_{5R}) at the stapes end of the model, and reasonable similarity up to the mid-point of the model.
- 2) Mass and elasticity characteristics for this type of rubber do not permit any matching of cochlear partition dynamics (parameter Π_{5R}) at the apical end of the model.
- 3) Only the medium thickness rubber allows a close match for fluids-membrane combined dynamical similarity (parameter Π_{3R}) at the apical end of models. Rubber sheeting of this type would have to be as much as 1 mm. thick to match this parameter at the mid-point of models, and 2 or 3 mm. thick for complete similarity at the basal end, in which case, when assembled in a 12 times full size cochlear model, seated over an unsupported span at the stapes end of only $1\frac{1}{2}$ mm., it could not possibly be considered as a model membrane.
- 4) As diagonal arrows indicate, the most satisfactory compromise is a membrane of tapering thickness, being about 0.003" thick at the helicotrema and 0.015" to 0.020" thick at the stapes end. For this choice of membrane, matching of the parameter Π_{3} , describing similarity between fluid forces disturbing the fluid and driving the membrane, is consistent over the length of the cochlear model, while parameter Π_{5} is exactly matched around the stapes end.
- 5) A similar consistency in Π_{3} but with exact matching of Π_{5} nearer to the centre may clearly be achieved by reducing all thicknesses by about 50%, i.e., by use of rubber tapering from about 0.002" at the apex to 0.014" at the stapes. This was, in fact, attempted for all cochlear models.

- 6) Most models were also assembled with uniform thickness rubber membranes of about 0.007" for an additional series of tests in order to simulate the effect of close matching of π_3 at the apical end.



III DETAILING, MANUFACTURE, ASSEMBLY AND EXPERIMENTATION

IIIa. Model Geometry Detail

Having decided upon model scales, sizes and approximate shapes, and upon the need for a general design of model to allow extraction of accurate quantitative information on the vibration of the membrane representing the cochlear partition, it was then necessary to decide upon the means by which such measurements could be made along the whole length of each model without interfering with its response. Tests were conducted using built-up earphone diaphragms on which vibrating, protruding membranes were inspected under microscopes, metrology profile projectors and metrology measuring machines using 10 to 200 times magnifications and phase-controlled incident and direct stroboscope illumination. A trial model was then roughly constructed in which a membrane was clamped between two highly polished blocks of perspex, a square sided, polished walled passage having been milled out of the seating face of each block so as to allow the membrane to move and vibrate within this gap. With the clamped membrane in the vertical plane, and vibrated by a horizontal plunger, stroboscopic light directed from various angles and an observer looking vertically downwards at the perspex-membrane interface through a microscope, it was very easy to locate the side to side membrane excursions provided that the two horizontal perspex surfaces between the membrane and the microscope were square-cornered, very flat and highly polished. Although machining and polishing operations were likely to be rather time consuming, the techniques were found to be relatively simple, and it was decided to incorporate this method of viewing membrane motions into the design of all models. (Also see Figure 8.)

Figures 2 to 7 inclusive show the final detailed design of the perspex models, whose principal features are summarized as follows:-

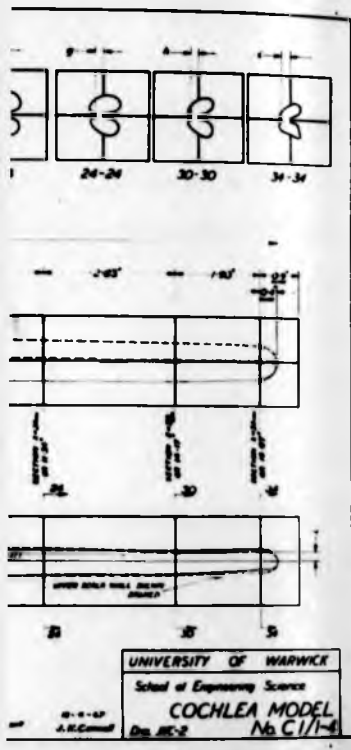


Fig 5-2

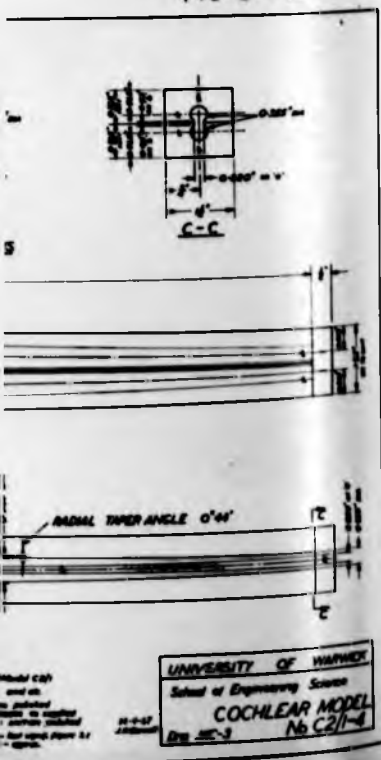


FIG 5-3

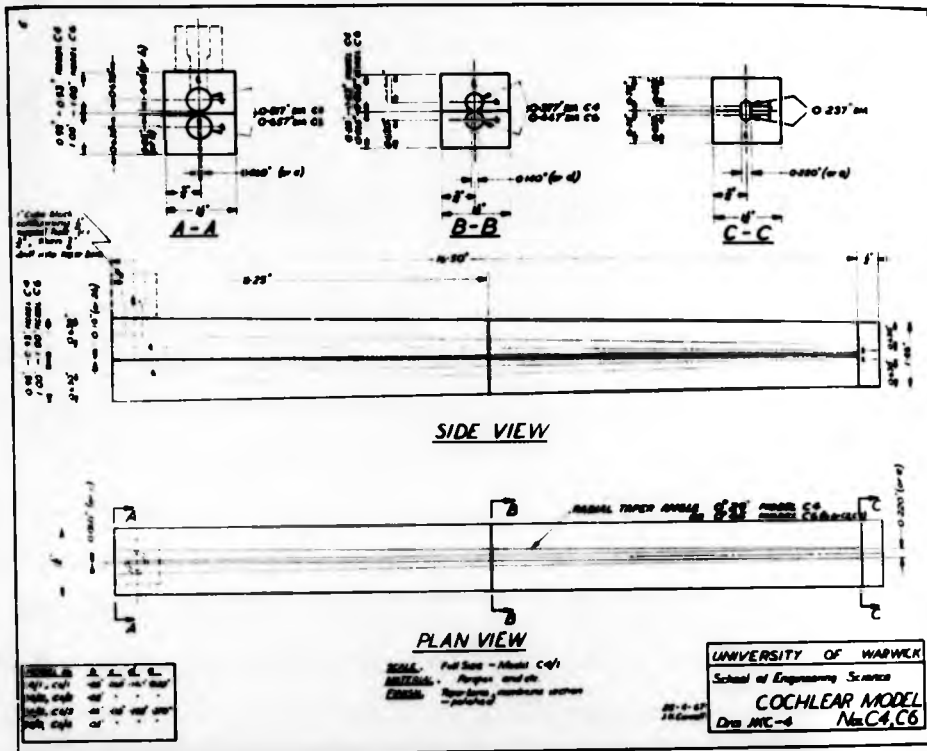


Fig. 2.

Fig. 3.

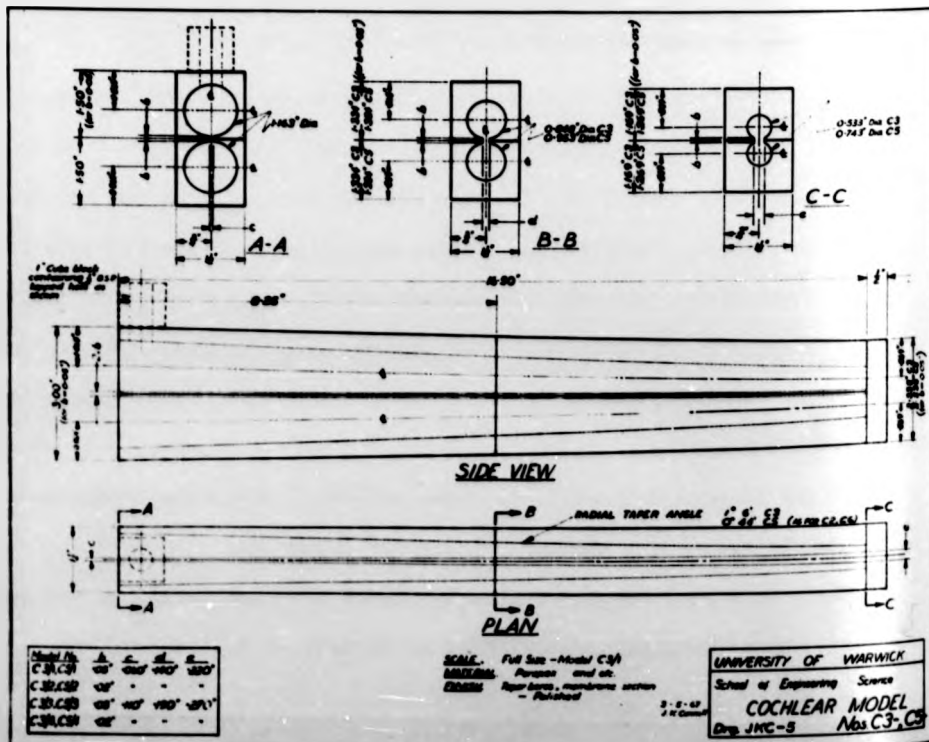
Fig. 4.

Fig. 5.

Fig. 5.

Fig. 6.

Fig. 7.



T
const
in sec
C 2.
simply

FIG 5-5

Fig. 2. Model C 1. Introduces actual scala sectional shapes and typical scala sectional area variations, including "necking" of the scala vestibuli - known as the "true" model, this was shaped by hand.

Fig. 3. Model C 2. Linear taper approximation of model C 1. Both scalae identical. Drilled and taper-reamed, contains circular sections - known as the "average" model. Two of these models were built, the second containing a considerably wider membrane slot. The first "average" model was designated C 2/A, the second wider slot model C 2/C.

Fig. 4. Model C 4. Diameters at each section are $\frac{2}{3}$ ds of corresponding diameters of model C 2. Thus sectional areas are uniformly $\frac{4}{9}$ ths of those of C 2. Identical scalae. Called the "small" model.

Fig. 5. Model C 3. (Not made). Diameters at each section are $\frac{3}{2}$ times corresponding diameters of C 2.

Fig. 5. Model C 5. At the basal end, diameter is $\frac{3}{2}$ times that of C 2. Same diametral taper as C 2. Identical scalae. Known as the "large" model.

Fig. 6. Model C 7. (Not made). Circular sections, taper-reamed, with two dissimilar scalae, machined to be as similar as possible to C 1.

Fig. 7. Model C 8. Drilled and cylindrically-reamed, non-tapered, identical scalae, having the average sectional area of model C 2 - known as the "straight" model.

Thus the shaped model C 1 is the basic cochlear model. The model C 2, constitutes an approximate, simplified form of C 1 with no uneven variations in scala vestibuli area and C 8 is a much simplified, cylindrical form of C 2. Models C 2, C 5 and C 6 all employ the same diametral taper, and simply introduce sectional area size effects.

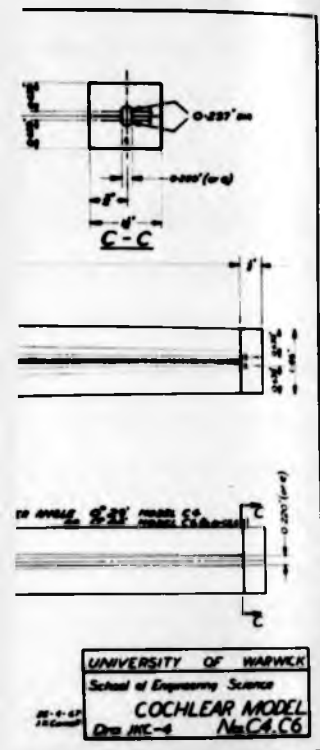


FIG 5-4

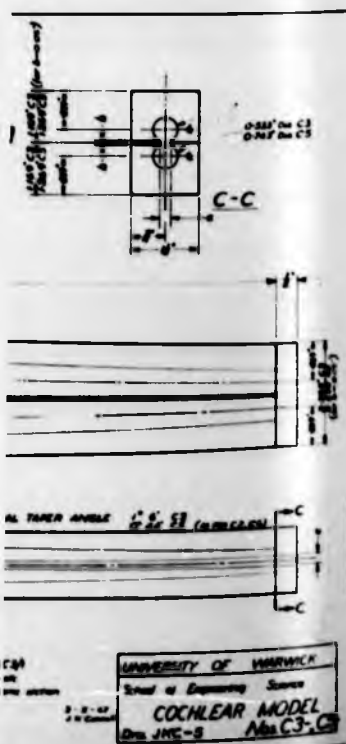


FIG 5-5

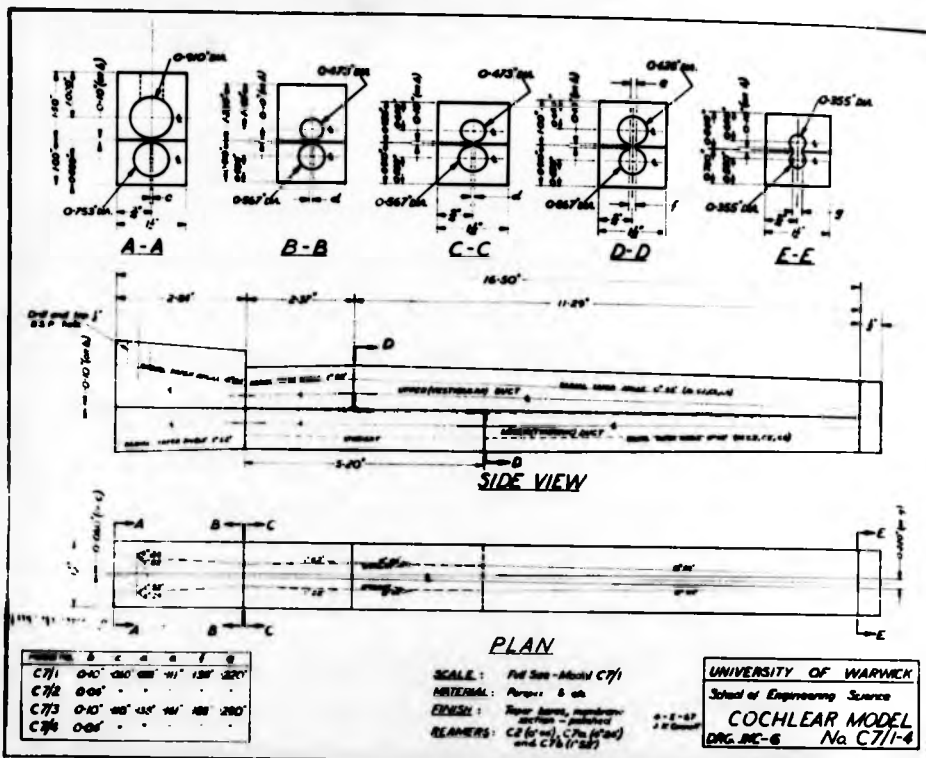


FIG 5-6

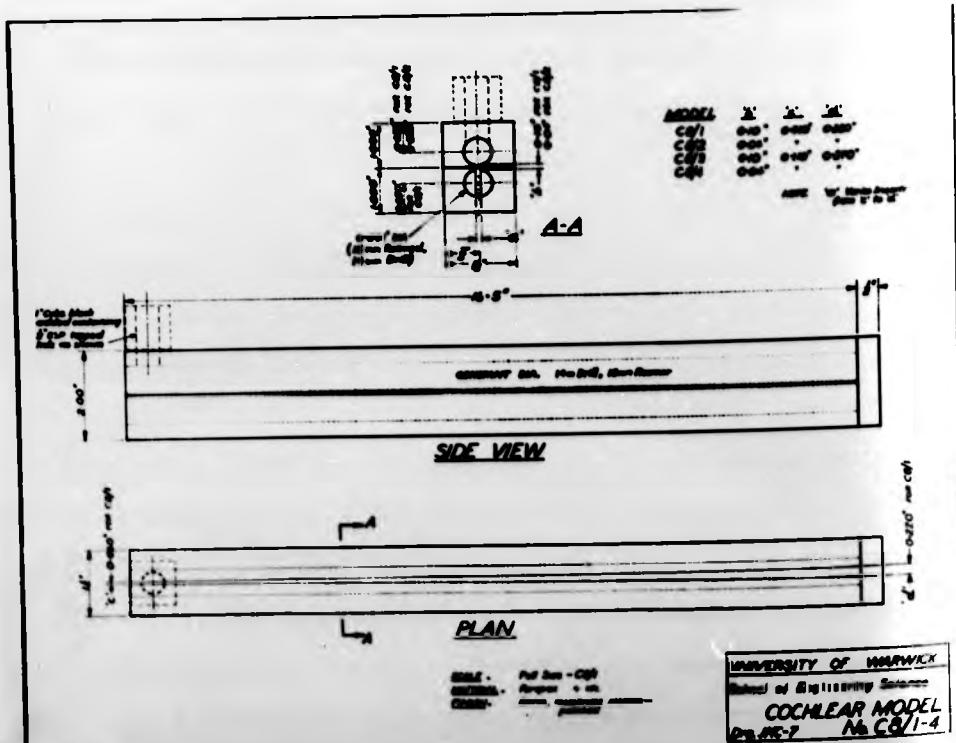


FIG 5-7

Model C 4, being not much smaller than C 6, displays a distinctly smaller scalae diametral taper than C 6 but has the same apical-end diameter. Hence the geometric variations introduced by these seven (or nine) models include

- 1) scalae shapes
- 2) scalae sizes
- 3) scalae sectional area vs. distance-along-the-cochlea functions
- 4) identical scalae vs. unequal scalae effects.

IIIb. Manufacture

Models were initially blocked from 1" or 1½" sheets of clear I.C.I. perspex and were cut and shaped to approximate dimensions, each half of each model being prepared in two separate sections.

In the case of all models but C 1, holes were bored in preparation for reaming, whereas for C 1 each half of the model was divided into 6 sections 2" to 3" long and bored holes were opened slowly by arduous, hand grinding and filing until the required scalae shapes were obtained. Several taper reamers had to be manufactured for models C 2, C 4, C 5 and C 6, which posed particular problems as reaming had to be carried out on a continuous 16° taper hole. After a few failures it was found necessary to construct the reamers in two half lengths with an arrangement for subsequently locking the halves together.

Reamers were initially taper turned from stock silver steel and, taking care to leave adequate metal for the screw-locking arrangement and stud location, were parted centrally. Fluted teeth were then milled on the

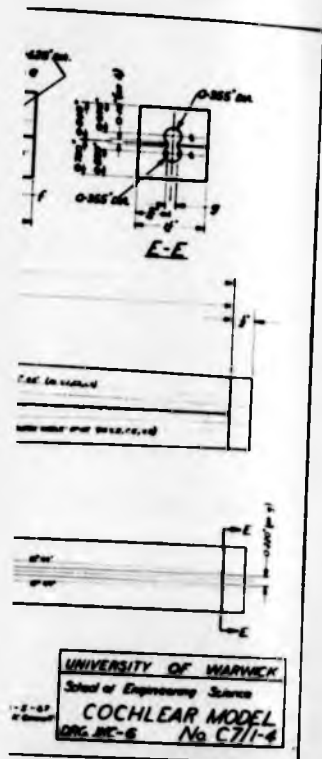


FIG 5-6

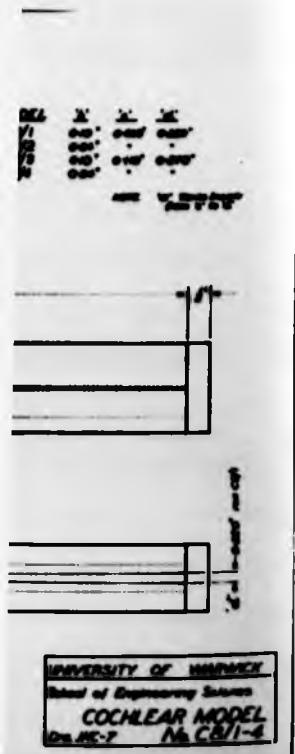


FIG 5-7

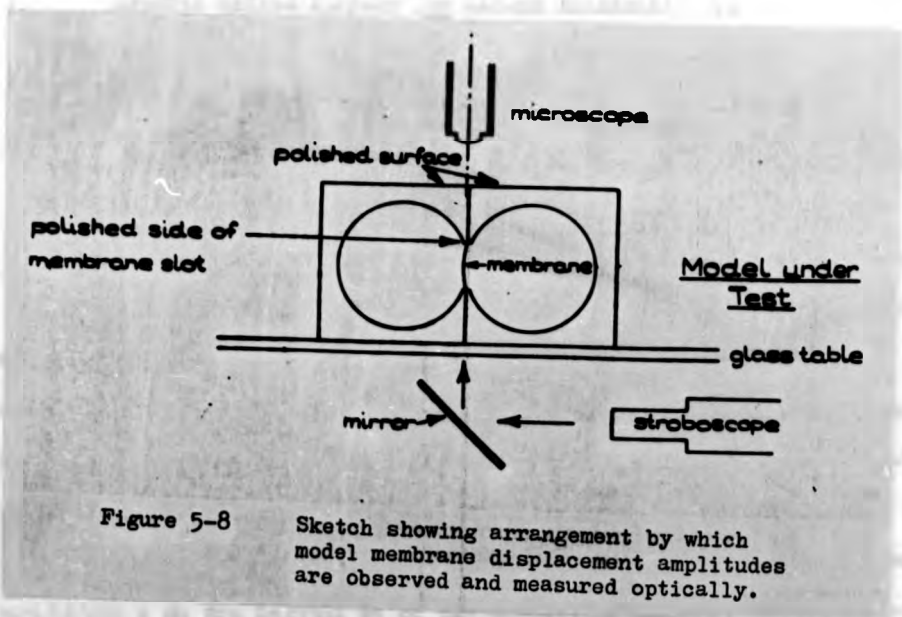


Figure 5-8 Sketch showing arrangement by which model membrane displacement amplitudes are observed and measured optically.

reame
 small
 halve
 machi
 from
 finia
 ream
 ream
 lubri
 flex
 and
 para
 flut
 each
 when
 half
 asse
 dime
 mill
 tabl
 adju
 for
 The
 len
 the

reamer bodies, with six flutes on the larger reamers and four on the smaller ones. This operation had to be performed with reamers in two halves because of limitations in the distance of traverse of the milling machines available. Reamers were deep surface hardened by an oil quench from cherry-red heat, and in the final operation they were ground and finished to the exact cutting angle demanded by experience with perspex reaming, and to the required sharpness.

Stepped holes were bored in the perspex blocks in preparation for reaming, and during the hand-reaming process water was found to be the best lubricant. Rotating steel burrs and later felt cones, driven by a flexible shaft drive motor, were used to smooth the newly reamed taper holes and bore polishing was completed using chamois leather impregnated with paraffin and liquid metal polish, wrapped around a blank reamer or non-fluted taper steel bar. One of these blank reamers was constructed for each taper angle involved, and was also used as an accurate locating device when, in the next stage of manufacture, the separate sections of each model half were assembled and cemented together.

A steel jig for slot-milling was built in which was secured the assembled model-half after it had been accurately shaped to its final dimensions along one face, which was then used as a datum for the slot-milling operation. One end of the jig was then bolted to the horizontal table of a vertical milling machine, and the opposite end of the jig was adjusted using clock gauges until the perspex block was exactly in position for the taper slot milling operation, using peripherally-cutting slot drills. The tapering membrane slot having been milled down one side (over the entire length of the model but in two stages), the jig was re-adjusted to subtend the opposite taper milling angle and the opposite side of the slot was

Model under
Test

glass table

troboscope

by which
amplitudes
optically.

... with the larger reservoir and four in the
 ... The operation had to be performed with reservoir in two
 ... in the distance of reservoir of the milling
 ... were deep surface polished by an oil spray
 ... and in the final operation they were ground and
 ... by experiment with papers
 ... to the required sharpness.



Figure 5-9 View of (clean room) perspex model polishing rig.

... of a vertical milling machine, and the opposite end of the rig was
 ... until the perspex block was steady in position
 ... being partially-cutting and drilling
 ... also having been milled down one side (over the entire
 ... the rig was re-adjusted to subside
 ... the opposite side of the rig was

milled
 width
 halve
 order
 until
 all f
 were
 half
 surf
 surf
 lubr
 "wet
 rein
 obta
 day
 a ch
 read
 to c
 para
 chan
 con
 gra
 fur
 the

milled. Perspex plug gauges were made to aid workshop checking of slot widths, and were subsequently found to be invaluable for locating model halves exactly opposite each other during model assembly.

With the difficult milling operation completed, (figure Q 1 outlines the order of the machining errors which, unfortunately, were not suppressed until several models had been milled) each model half was lightly planed on all four surfaces until required dimensions and acceptable surface flatnesses were obtained.

The succeeding stage of manufacture involved polishing. Each model half was clamped between two plain 1" strips of perspex with the outer viewing surface exposed, and the protective strips arranged flush with this machined surface. The clamped assembly was worked to and fro upon 4' long, water lubricated, 400 gauge and later 600 gauge carborundum paper surfaces, this "wet and dry" polishing paper being supported by a smooth, flat plate of reinforced glass. When completely flat surfaces and sharp corners were obtained, usually after about three changes of carborundum paper and a half day's rubbing, the clamped assembly was transported to a clean room where a chamois leather surface, stretched over another flat glass plate, was in readiness for the final stage of surface polishing. The chamois was found to cut most smoothly and reliably when loaded with a mixture of filtered paraffin and metal polish. The model half assembly was polished on this chamois surface for at least three hours, care being taken to ensure a continually moist clean surface. A scratch occurring because of a five grain of silica, for example, was in three cases severe enough to require a further application of 600 gauge carborundum paper in order to re-prepare the surface. Figure 9 shows a clean room rig used for perspex polishing.

Polishing of the square side of the milled membrane slot through which



Figure 5-10 Preparation of rubber sheets for selection of strips of rubber for insertion in models. Rubber strips were selected on the basis of correct thickness and stiffness (and elasticity) variations.



Figure 5-11 Testing of stiffness and elasticities of rubber membranes. The deflections of loaded pins acting on rubber membranes were measured via the balance-arm device shown in order to (a) check the variations in stiffness of various rubber membranes loaded in this manner, (b) make an experimental check on the theory for concentric-pin-loaded circular rubber membranes, as developed in chapter 4, section III. (c) compare the stiffnesses of pin-deflected circular membranes of various diameters with stiffnesses of pin-deflected rectangular membranes of various widths.

micro
tratio
time o
projec
of per
to pro
Again
requir
from
thin,
was o
that
as po
cont
ment
could

III

con
A de
con
rota
nag
mod
rub

microscope observations were to be made required even more care and concentration, although, with success, this part of the polishing work was not as time consuming. Similar gauge carborundum paper was clamped around a thin, projecting horizontal metal plate, and two carefully machined square blocks of perspex were fixed above and below this slot polishing projection so as to provide a right-angled wall against which to slide the polished block. Again two or three changes of the 600 gauge "wet-and-dry" paper were required before the slot wall was sufficiently square-cornered and free from machining marks. The wet carborundum paper was then replaced by a thin, clean sheet of paraffin-loaded chamois leather and the model slot wall was quickly and firmly polished to a very fine finish. It was imperative that this final chamois-polishing stage be completed with as little rubbing as possible in order to retain the sharp surface corners. Tests were made continually on the amount of distortion involved in making optical measurements through the two polished perspex surfaces, and practically no distortion could be detected in any model finally accepted for experimentation.

IIIc. Assembly

As the drawings (figs. 2 to 7) show, the cubic filling block was cemented on to the basal end of the scala vestibuli half of each model. A delicate perspex bracket for support of the rocking model stapes was also cemented in place, and the machined perspex stapes itself, containing a rotating, 4 B.A. tapped pin into which the driving link from an electromagnetic vibrator was later screwed, was assembled. The two halves of any model were thoroughly cleaned, inside and out, and a preselected length of rubber membrane, measured and marked for thickness and elasticity variations,

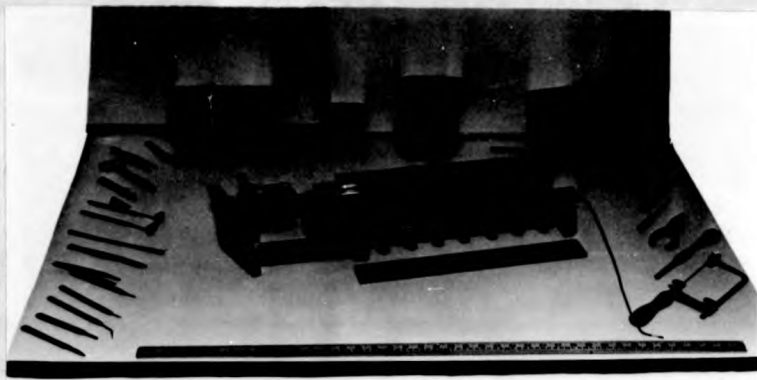


Figure 5-12 Assembly of model in steel frame.



Figure 5-13 Mixing of model perilymph solution to obtain the correct dynamic viscosity.

(see P
tympan
rubber
subse
damage
for th
assem
to re
provi
vibra
unifo
optio
betwe
exact
gauge
were
In th
aque
corre
The
in o
of t
lowe
esca
comp

(see Figs. 10 and 11) was laid in position upon the lower half (scala tympani) of the model. The width of the membrane was adjusted to avoid any rubber protruding from the model when the halves were clamped together, as subsequent removal of such rubber with a sharp knife or razor blade sometimes damaged the outer polished surface. Openings were also made in the rubber for the helicotrema and also in order to clear any upper and lower half assembly locating pins which had previously been fitted.

A very strong steel frame (see Fig. 12) was then cleaned and adjusted to receive the model. These steel frames were constructed in an effort to provide maximum rigidity and support for the assembled model and its electric vibrator mechanism, and also in order to clamp the two halves of each model uniformly together across the rubber membrane joint without interfering with optical viewing along the model. The model was then clamped in this frame, between both steel and perspex protective strips, the two halves being exactly located relative to their common membrane slot by locating plug gauges and permanent pins.

Oval and round window membranes, usually of 0.010" rubber sheeting, were cemented into place, and the model stapes cemented to the oval window. In the last stage of model assembly, which was also the most awkward, the aqueous glycerol solution, mixed with precise parts by weight and with correct viscosity (see Fig. 13), was slowly poured into the model scala. The helicotrema opening had to be considerably larger than the scale demanded in order to allow the viscous perilymph solution to flow from the stapes end of the upper scala down to the apical end, through the opening into the lower scala, and down to the round window while, at the same time, air could escape via the same pathway. Fluid loading did not prove to occupy much time compared with the "de-bubbling" process. It was shown to be quite essential

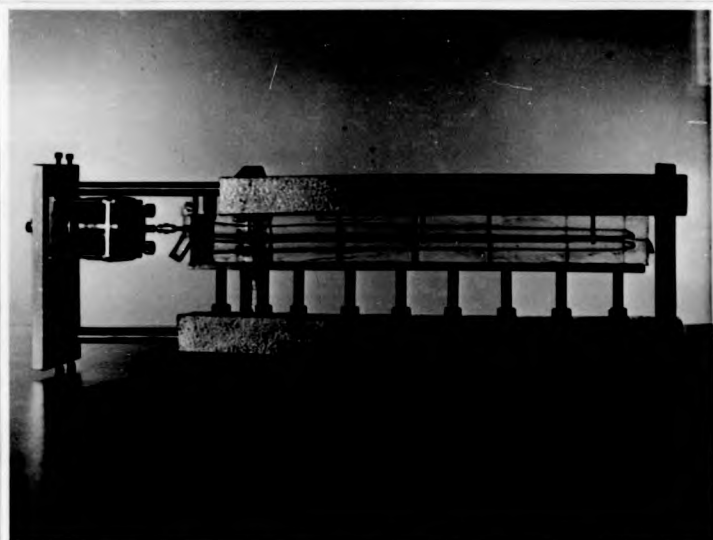


Figure 5-14 Model C1 assembled in steel test frame and prepared for experimentation.

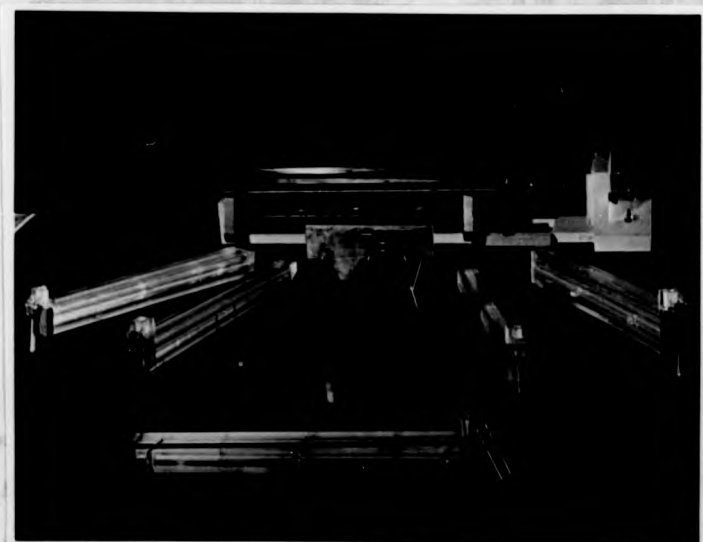


Figure 5-15 View of all cochlear models manufactured up to this time, showing two models assembled and prepared for testing.

to any model cochlear partition response that entrained air bubbles should not occupy more than 1 or 2 cubic millimeters of volume. Therefore there was no alternative to long periods of lifting the heavy (36 lb.) assembly from side to side, gently tapping and inclining the fluid columns in order to expel even the minute air bubbles. Sometimes leaks were discovered at this stage and model assembly and even model machining stages had to be repeated. Another problem concerned the membrane; in clamping of the two halves together, the untensed rubber normally compressed slightly, bulging the membrane perhaps one or two tenths of a millimeter into either scala. This was helpful, as it made membrane viewing very much easier and more accurate, but in the event that the membrane bulged to one side at one position and to the opposite side elsewhere, a false microscope reading was obtained at the "cross-over" point. Therefore care had to be taken in the clamping stage, before round and oval windows were in place, to deflect the membrane uniformly. Subsequently when the model was almost filled with liquid, a sharp blow to the steel frame or an impulse at the stapes would either straighten a non-uniformly bulging membrane, or make it worse. However, a satisfactorily and completely assembled model, when cleaned and fine-polished, was dry, stable and well-protected, and had a rather impressive appearance! (see figures 14 and 15).

III.d. Experimentation

Cochlear model experiments were conducted in The University of Warwick School of Engineering Science metrology room, and the experimental arrangement is shown in figure 18. The principal component of apparatus was an S.G.I.P. Societe Genevoise M.U.214 B, Universal Measuring Machine which, in addition



Figure 5-16 Close-up side view of S.G.I.P. Universal Measuring Machine, showing measuring microscope head, traverse vernier microscopes and traversing glass table on which models are mounted for examination.

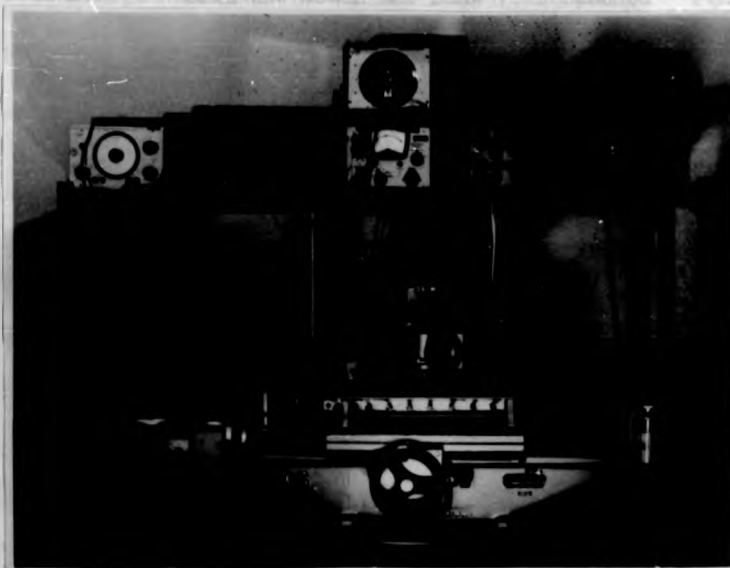


Figure 5-17 View of microscope bench and apparatus

to having an excellent range of microscopes with various objective magnifications, convenient 2 to 5 cm. working distances, and with several types of calibrated graticules, offers a 40 cm. uni-directional traversing table (see fig. 16). Its microscope mounting also transverses in the other two orthogonal directions, and on all three axes the illuminated scales read direct to $0.5\mu\text{m}$. Handwheels and fine-movement screws give complete control of the three-directional traverse accuracy of this instrument, which has a glass table attachment and a light-source collimating tube running forward from behind the machine, reflecting light upwards through the glass table.

Models were placed upon this glass table (see fig. 17) so oriented that upon traversing the carriage in the (40 cm. range)'x' direction, the membrane joint of each model, being longitudinally oriented in the vertical plane, remained exactly below the objective lens. A stroboscope lamp fitting and sleeve was designed and manufactured to allow substitution of stroboscopic for normal monochromatic illumination. Associated apparatus and equipment included an Advance A.F. signal generator type JIB with continuous output signal level control, a Derritron 20 WLF valve power amplifier with continuous gain control and various output impedance terminals, and a control panel containing 1A, 5A, and 15V AC meters, an adjustable rheostat of 0-25 ohms, fuses and multiple terminals. A Dawe type 1208A Variphase control unit with its input signal direct from the 600 ohm high impedance terminals of the signal generator controlled a Dawe type 1202D transistor Strobotorch, from which high voltage leads were taken to the stroboscope lamp fitting in the S.G.I.P. measuring machine. A two-channel oscilloscope was used to monitor the amplitude and wave-form of various signals, including the supply to the electromechanical vibrator driving the

model stapes, and also to check the wave-form of the frequency modulated signal generated by a Wayne Kerr type B 721 B vibration amplitude meter and its capacitance probe, the latter being clamped very closely to a copper strip cemented to the model stapes assembly. Figure 18 gives an early view of the experimental rig and equipment at the beginning of the experimental phase.

Frequencies of excitation of the model stapes were adjusted at the signal generator, the input power to the vibrator was set by use of the amplifier gain control and small adjustments to the amplitude of stapes vibration were made by use of the control panel rheostat, which was also of use for matching the input impedance of the vibrator. The stroboscope phase controller permitted adjustment of either phase or constant flashing difference frequency (up to 2 Hz). Phase measurements were accurate to about $\pm 1\frac{1}{2}^{\circ}$. In making an examination of cochlear partition response at any point along the cochlea, a stroboscope difference frequency of about 1 Hz was very convenient by which to check whether or not there was any response visible through, for example, the 87 x magnification S.&I.P. goniometric microscope. With a zero difference frequency, the phase was adjusted until the microscope-viewed element of partition arrived at the scala vestibuli side extreme of its travel, a graticule hair-line was aligned with the partition image, and the measuring machine y scale reading noted. The stroboscope phase was again adjusted (through about 180°) to move the partition image maximally to the scala tympani side, and the y scale reading corresponding to the re-adjusted graticule hair reference was again noted. The y scale reading difference gave the peak-to-peak partition amplitude at that point and the latter phase angle, if considered relative to maximum inward motion of the stapes, gave the relative phase of the membrane vibration. As the stapes phase angle also had to be measured in this optical manner, it was convenient

to measure stapes peak-to-peak amplitudes optically at the same time, and to use the Wayne-Kerr vibration meter only to check wave forms.

In the complete testing of the frequency response of a model, the following steps were taken:-

- 1) The upper frequency limit was scanned, and a basal end response of 1 kHz was usually found to be the upper limit beyond which any membrane amplitudes became too small to measure.
- 2) With frequency set to, say, 1 kHz, the stapes amplitude was set to some reasonable, low level (for example, 0.010 mm.).
- 3) Oval window and, if possible, round window amplitudes and phases were measured (models were intended to be sufficiently fluid filled that both windows bulged outwards slightly, partly in order to observe their motions and partly in order to prevent air leaks).
- 4) Starting at 1 cm. from the stapes, partition amplitudes and phases were recorded at 1 cm. steps along the model until no further response was evident.
- 5) In the regions of greatest membrane activity, additional measurements were made at $\frac{1}{2}$ and even $\frac{1}{4}$ cm. steps.
- 6) The examination was then repeated for pure tones of 800, 600, 400, 200, 100, 50, and when appropriate, 25 and 15 Hz frequency, and on each occasion that the frequency was re-set, stapes amplitudes were also adjusted as required, care being taken not to overheat the vibrator, over-excite the model, or damage the valuable measuring machine.

Although a few modifications to the above straightforward experimental approach were introduced for some model tests, and other less formal experiments were also conducted, these quantitative measuring techniques were in general most satisfactory, and the experimental arrangement—apparatus, equipment and models—proved to be efficient and extremely reliable.

It may be noted that this complete programme of physical cochlear model research was particularly inexpensive regarding equipment, materials and apparatus, use being made of existing departmental equipment and facilities at all times. However, two and a half man years of working time were required in order to prepare drawings, manufacture and assemble the models and to develop and test experimental techniques. Model manufacture occupied the technician involved for 15 months, and model polishing and finishing required a further 4 months of both his time and that of the writer, who also supervised model manufacturing. Model assembly and experimentation also occupied 6 months of the writer's time, and several months of the time of the metrology room technician.

In all some 3000 microscope readings made on the S.G.I.P. measuring machine occupied the machine for almost 200 hours of actual use.

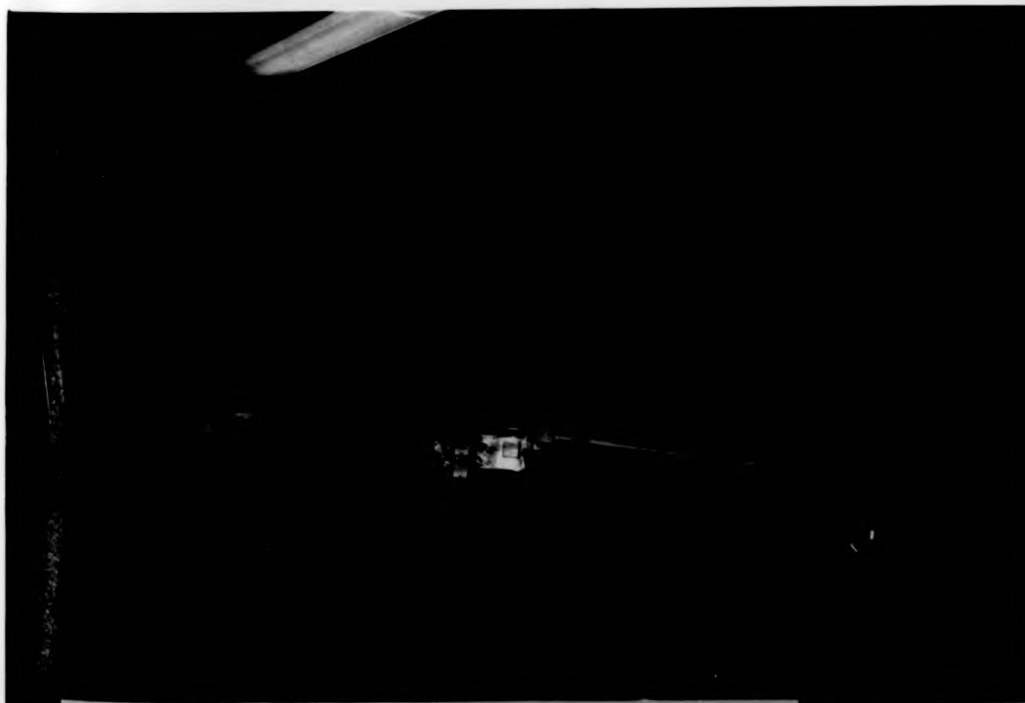


Figure 5-18. General view of experimental rig.

Note that the model here shown to be under test is assembled and clamped by an earlier procedure which was later replaced by the steel frame mounting assembly.

IV RESULTS OF COCHLEAR PHYSICAL MODEL EXPERIMENTS

Sixteen full tests were conducted on the seven cochlear models manufacture, and results for each test, excepting test no. 3, are given graphically on Figures R1, R2, R⁴ etc. to R16. As the information forthcoming from these experiments is presented infinitely more efficiently by graphical plots rather than by pages of verbal description only brief notes are presented to accompany these results, and table 4 summarizes the tests. Note that four different rubber membrane types were used, categorized in Figure Q2 as RM1, which was of uniform thickness, and RM2, RM3 and RM⁴, all of which were tapered. Figure Q1 shows to what extent the membrane slot widths in each model departed from the designed values.

Tests using pre-tensed rubber membranes in models were always less satisfactory than tests for which membranes were inserted in models without any permanent tension, partly because oscillating membranes were more difficult to view when moving to and fro across the main joint of the model, and partly because it was almost impossible to insert tensed membranes into models while maintaining a state of uniform strain in the rubber. No results are given for test No. 3, for which the membrane for model C2A was initially tensed, being set at the time of clamping of model halves together with 6% initial strain, and for which the model was also filled with water, viscosity 0.011 poise, rather than with the modelled perilymph solution of aqueous glycerol, of viscosity 0.341 poise. The response of the membrane was particularly violent at frequencies between 25 and 200 Hz, and after only 10 minutes of exposure to very moderate vibration intensity levels, the membrane split and collapsed in two areas. During this short time the membrane was clearly observed to be vibrating with a very complex wave form, with the first and second harmonics of the applied pure tone being generated on the basal half of

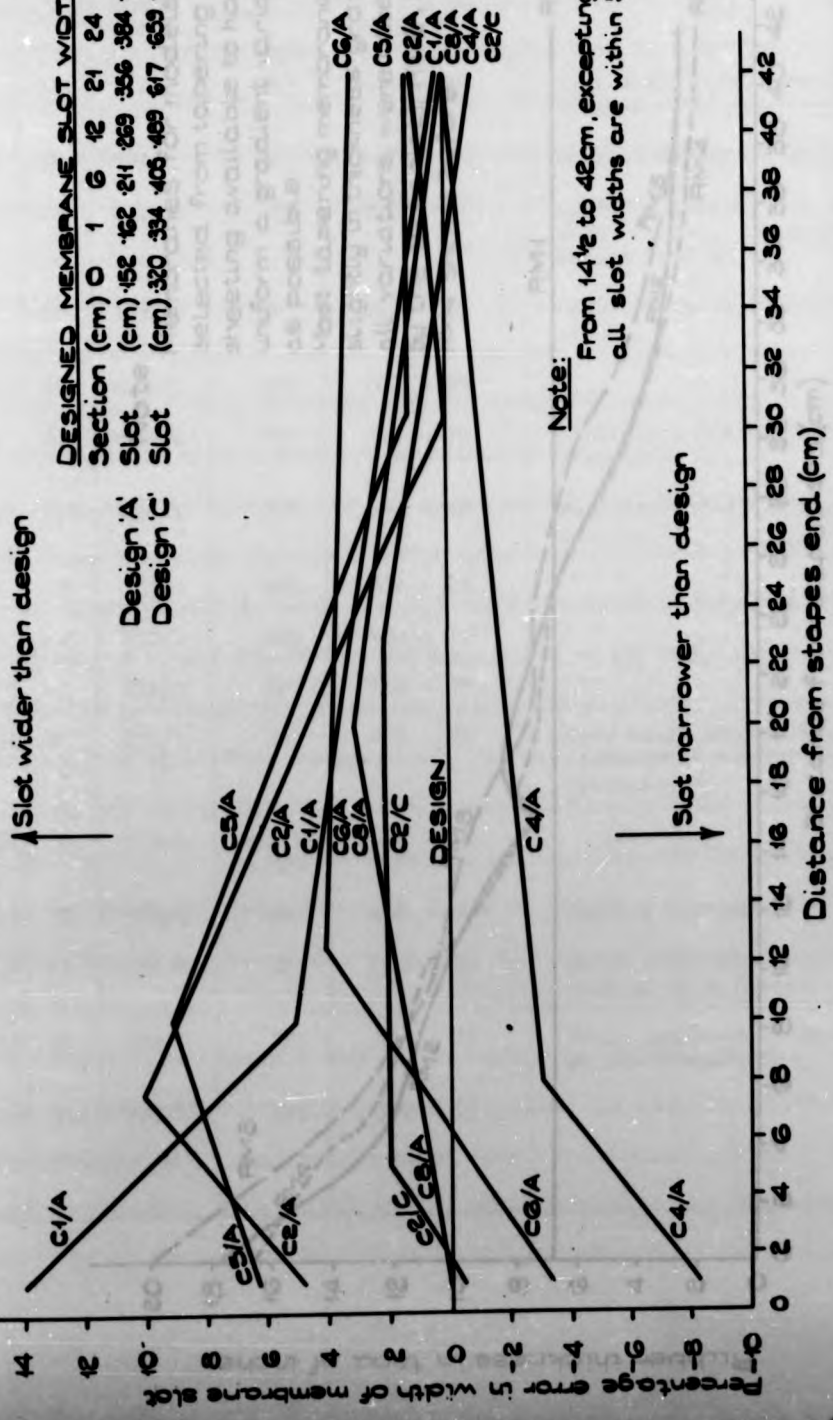


FIGURE Q1

ERRORS IN MANUFACTURE OF MODEL MEMBRANE SLOTS.

Desaru G (cm) 250 224 192 168 144 120 96 72 48 24 0
 Desaru Y (cm) 105 105 105 105 105 105 105 105 105 105 105
 Desaru Z (cm) 0 1 2 3 4 5 6 7 8 9 10 11

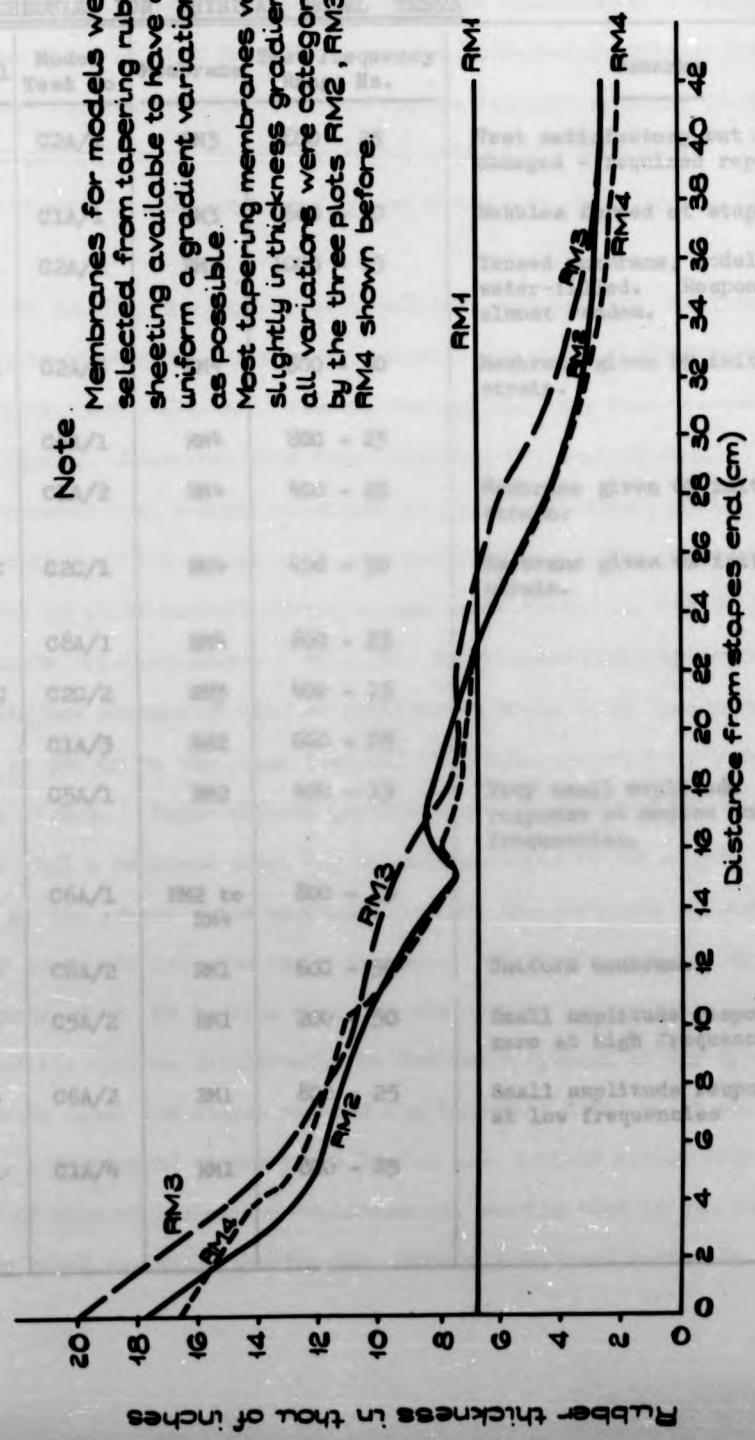
DESIGNED MEMBRANE SPEC. MODEL

120x 100x 100x

Test No.	Model	Notes
1	02	
2	02	
3	02	
4	02	
5	02	
6	02	
7	02	
8	02	
9	02	
10	02	
11	02	
12	02	
13	02	
14	02	
15	02	
16	02	

Note: Membranes for models were selected from tapering rubber sheeting available to have as uniform a gradient variation as possible.

Most tapering membranes varied slightly in thickness gradient but all variations were categorized by the three plots RM2, RM3 and RM4 shown before.



RUBBER MEMBRANE THICKNESS FIGURE Q2

Fig. No.	Model	Test
1	C2A	C2A
2	C1	C1
3	C2A	C2A
4	C2A	C2A
5	C1	C1
6	C2C	C2C/1
7	C8	C8A/1
8	C2C	C2C/2
9	C1	C1A/3
10	C5	C5A/1
11	C6	C6A/1
12	C8	C8A/2
13	C5	C5A/2
14	C6	C6A/2
15	C1	C1A/4

Note Membranes for models were selected from tapering rubber sheeting available to have as uniform a gradient variation as possible. Most tapering membranes varied slightly in thickness gradient but all variations were categorized by the three plots RM2, RM3 and RM4 shown before.

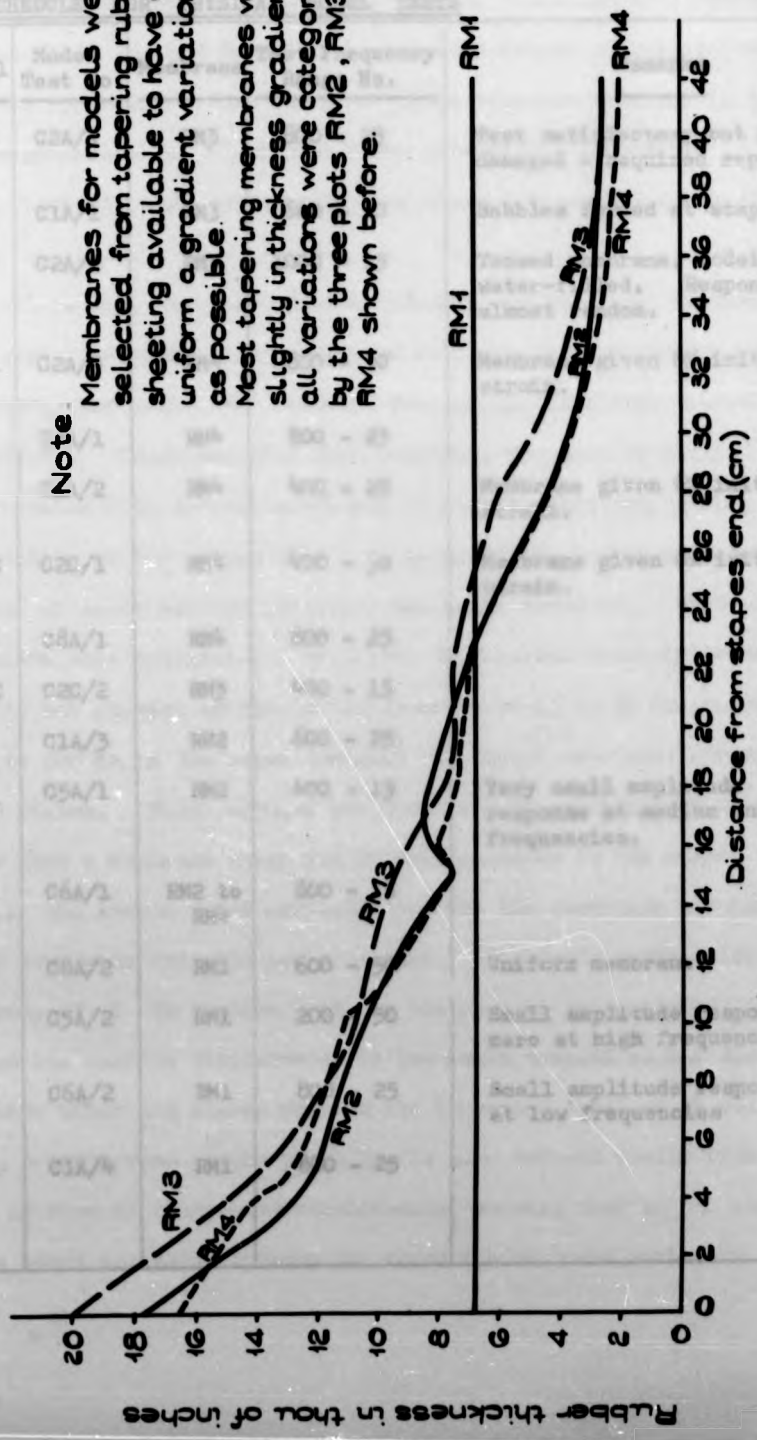


FIGURE Q2
RUBBER MEMBRANE THICKNESS

TABLE 4.

SCHEDULE FOR PHYSICAL MODEL TESTS

Test No.	Fig. No.	Model	Model Test No.	Membrane	Test Frequency Range Hz.	Remarks
1	R1	C2A	C2A/1	RM3	600 - 25	Test satisfactory but model damaged - required repolish.
2	R2	C1	C1A/1	RM3	600 - 50	Bubbles formed at stapes leak.
3	-	C2A	C2A/2	RM3	1000 - 15	Tensed membrane, model water-filled. Response almost random.
4	R4	C2A	C2A/3	RM4	800 - 50	Membrane given 6% initial strain.
5	R5	C4	C4A/1	RM4	800 - 25	
6	R6	C1	C1A/2	RM4	400 - 25	Membrane given 6% initial strain.
7	R7	C2C	C2C/1	RM4	400 - 50	Membrane given 6% initial strain.
8	R8	C8	C8A/1	RM4	800 - 25	
9	R9	C2C	C2C/2	RM3	400 - 15	
10	R10	C1	C1A/3	RM2	600 - 25	
11	R11	C5	C5A/1	RM2	400 - 15	Very small amplitude response at medium and high frequencies.
12	R12	C6	C6A/1	RM2 to RM4	800 - 15	
13	R13	C8	C8A/2	RM1	600 - 50	Uniform membrane.
14	R14	C5	C5A/2	RM1	200 - 50	Small amplitude response zero at high frequencies.
15	R15	C6	C6A/2	RM1	800 - 25	Small amplitude response at low frequencies
16	R16	C1	C1A/4	RM1	800 - 25	

SCHEDULE FOR TESTS

Test No.	Model	Test No.	Test No.	Test No.
1	ASD	ASD	ASD	ASD
2	ASD	ASD	ASD	ASD
3	ASD	ASD	ASD	ASD
4	ASD	ASD	ASD	ASD
5	ASD	ASD	ASD	ASD
6	ASD	ASD	ASD	ASD
7	ASD	ASD	ASD	ASD
8	ASD	ASD	ASD	ASD
9	ASD	ASD	ASD	ASD
10	ASD	ASD	ASD	ASD
11	ASD	ASD	ASD	ASD
12	ASD	ASD	ASD	ASD
13	ASD	ASD	ASD	ASD
14	ASD	ASD	ASD	ASD
15	ASD	ASD	ASD	ASD
16	ASD	ASD	ASD	ASD

the model. The mean relative amplitude of partition vibration with respect to the stapes was about 25, and from later tests with tensed membranes (tests 4, 6 and 7) it was appreciated that the near random response obtained in test 3, with the intense generation of "overtone," was primarily a result of decreased fluid viscosity and, consequently, of minimal viscous damping of the partition.

On figures B1 to B16, the peak of each relative amplitude vs. distance-from-stapes frequency response curve is marked with the appropriate frequency in Hz. In some cases, two peaks were recorded for any one pure tone vibration signal at the stapes. Sometimes when this occurred, the test at that frequency was repeated with a lower amplitude of stapes vibration, giving a check on the veracity of the former plot as a means of specifying the section along the cochlea at which maximum partition amplitude occurred. Tests 2, 4 and 11 illustrate this situation. At higher frequencies model G5 scarcely responded at all, but at each of the low frequencies of 15 to 50 Hz (corresponding to 150 to 500 Hz in the human cochlea) this model responded strongly in at least two places. These effects are discussed in section V of this chapter. Note that a membrane phase lag of zero relative to the stapes indicates that as the stapes moved maximally inwards the partition membrane moved maximally downwards into the scala tympani. Similarly a phase lag of Θ at a frequency of f Hz implies that, at the section being viewed, the membrane reached its maximum displacement in the scala tympani at Θ radians, or $(\Theta/2\pi f)$ seconds after the stapes reached its innermost limit of travel.

Similarly, a zero round window phase lag is also defined wholly from the expedient point of view of continuity requirements, meaning that as the stapes and oval window moved maximally inwards the round window moved maximally outwards.

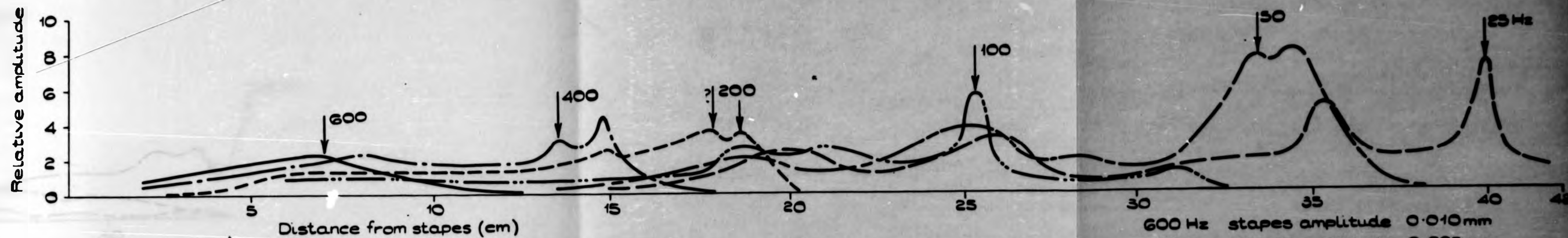
A most interesting point which should be made in this section is that the phase vs. distance plot for each pure-tone frequency test invariably shows a sudden change of gradient and a short plateau either directly in line with the maximum amplitude peak or slightly on the helicotrema side of the peak. In the earliest tests this effect was considered to be due to experimental error, and later due to phase controller malfunction. However, these locally uneven rate of change of phase effects were found to be genuine, and may be due to fluid dynamic effects stimulated by the large, local partition amplitude, or even to a Rankine, deep-water wave effect (see chapter 2 section IV).

Alternatively, they may be due to the rubber membrane-surrounding fluid viscous damping properties, which, unlike the scala media of the human cochlea, suggest less than critical damping in which case large changes of phase of the membrane response will occur local to the region of maximum membrane amplitude.

This effect was very regular, and sometimes proved to be of use in deciding which of two similar amplitude peaks represented a bona fide maximum response section.



Figure 11



TEST No.1 MODEL C2A/1

- 600 Hz stapes amplitude 0.010mm
- 400 Hz stapes amplitude 0.025mm
- 200 Hz stapes amplitude 0.019mm
- 100 Hz stapes amplitude 0.010mm
- 50 Hz stapes amplitude 0.008mm
- 25 Hz stapes amplitude 0.005mm

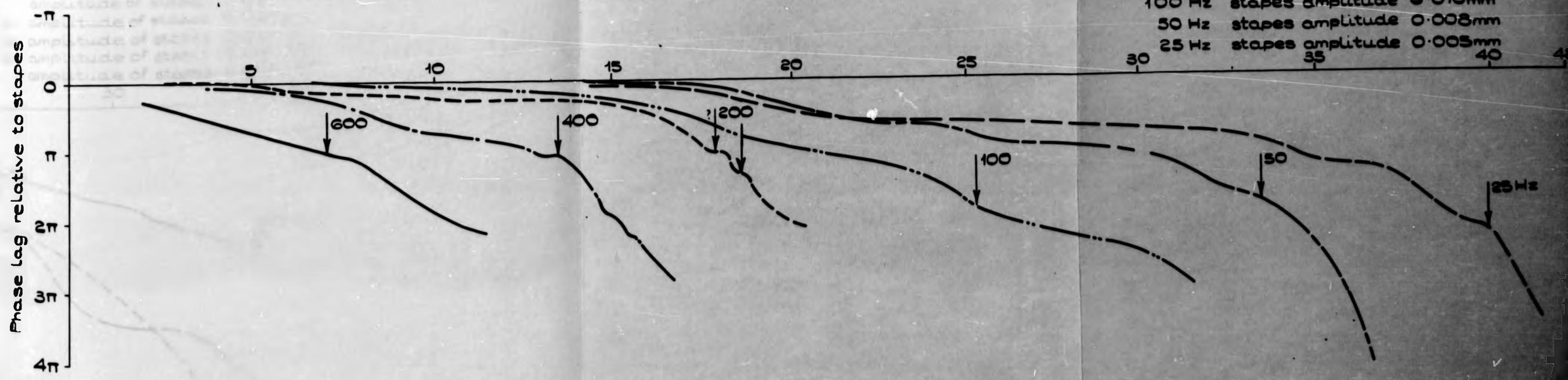
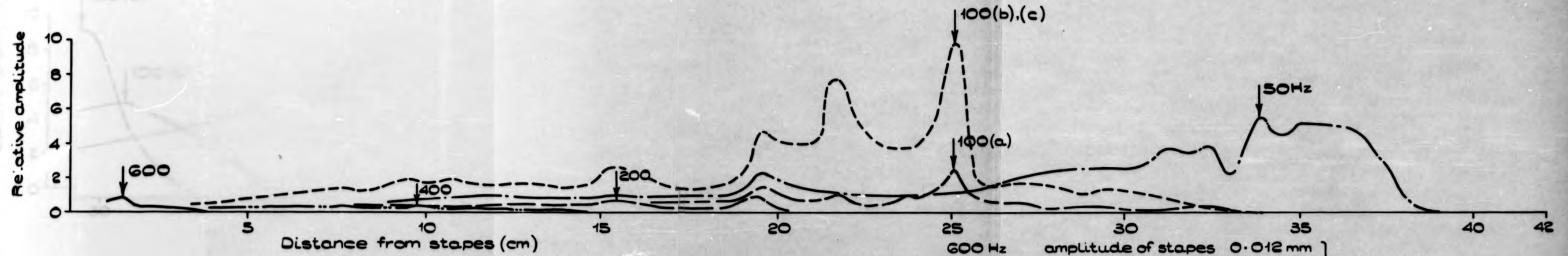


Figure R1



TEST No. 2 MODEL C1/A

600 Hz	amplitude of stapes	0.012 mm	} with bubble gradually developing
400 Hz	amplitude of stapes	0.025 mm	
200 Hz	amplitude of stapes	0.060 mm	
100 Hz (a)	amplitude of stapes	0.040 mm	} bubble removed, model refilled
100 Hz (b)	amplitude of stapes	0.027 mm	
100 Hz (c)	amplitude of stapes	0.025 mm	— test repeated 1 hour later
50 Hz	amplitude of stapes	0.010 mm	

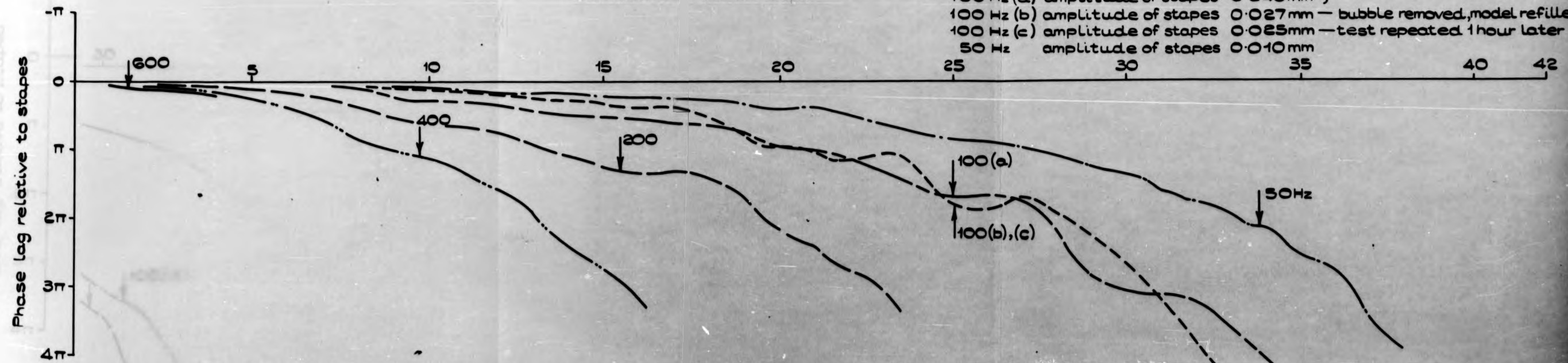
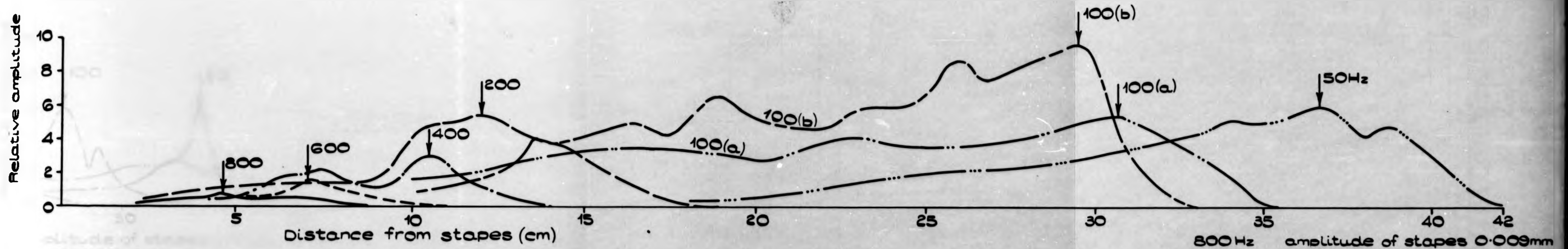


Figure R2



TEST No. 4 MODEL C2/A

- 800 Hz amplitude of stapes 0.009mm
- 600 Hz amplitude of stapes 0.004mm
- 400 Hz amplitude of stapes 0.016mm
- 200 Hz amplitude of stapes 0.039mm
- 100 Hz(a) amplitude of stapes 0.040mm
- 100 Hz(b) amplitude of stapes 0.007mm
- 50 Hz amplitude of stapes 0.007mm

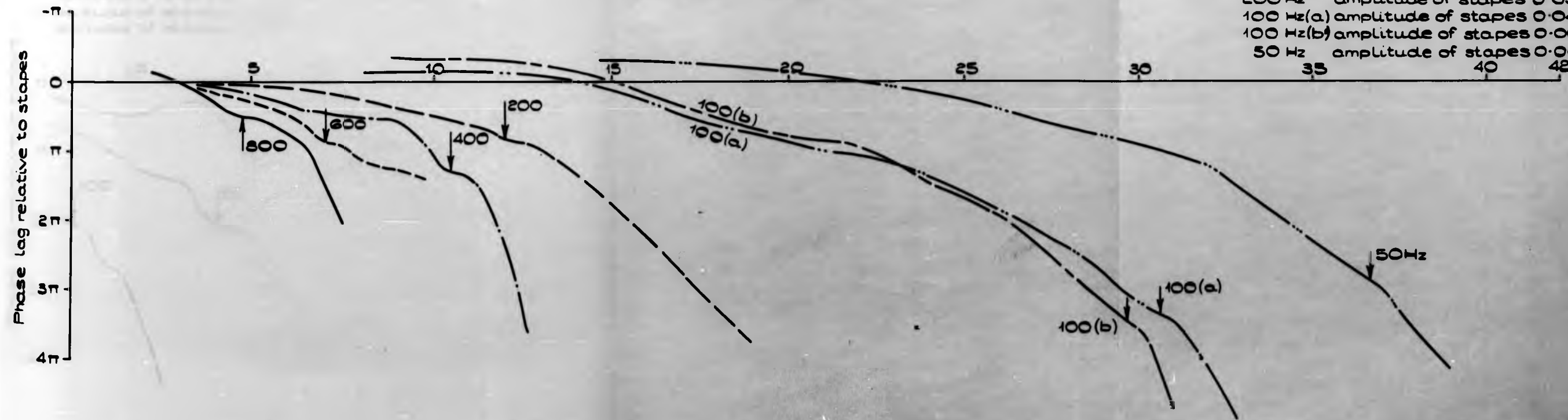


Figure R4

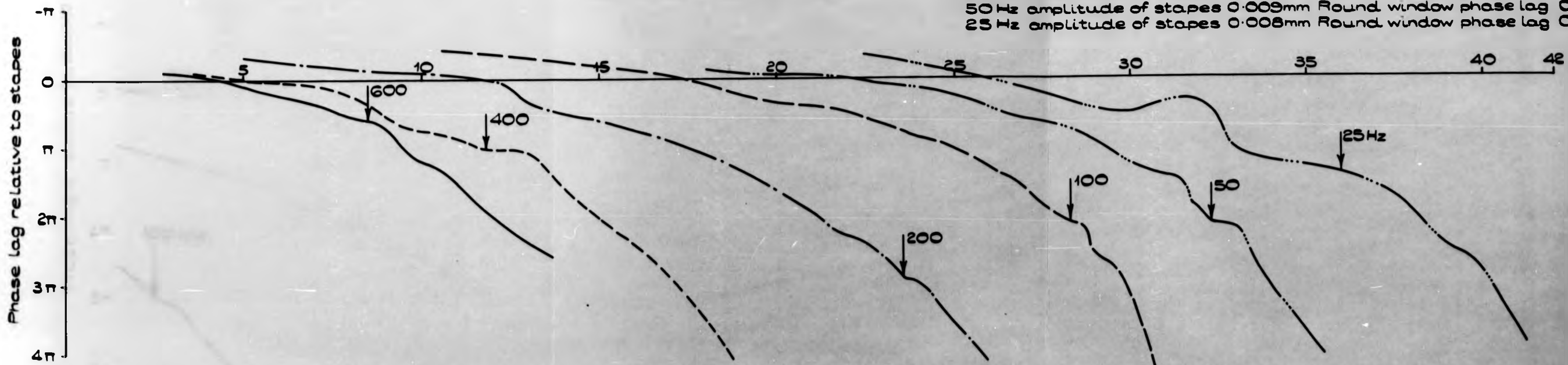
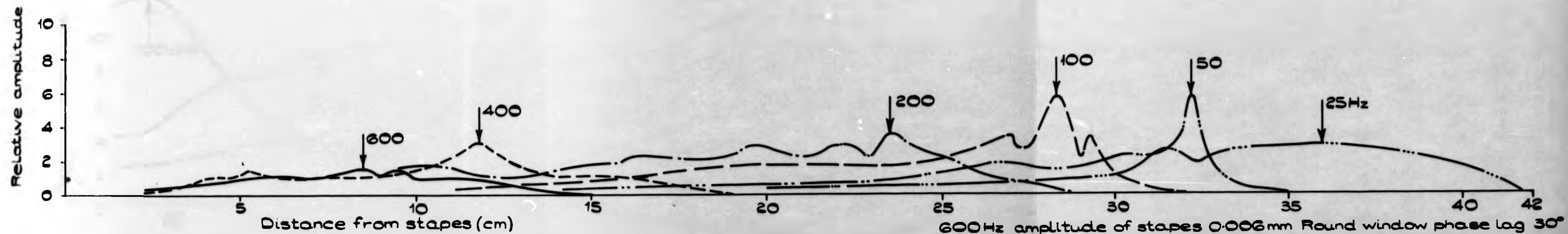
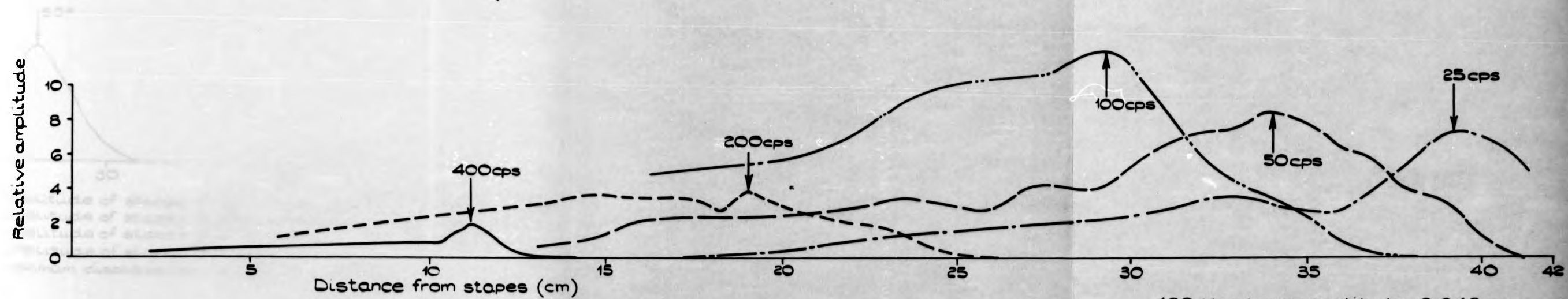


Figure R5



TEST No. 6 MODEL C1A/2

400 Hz stapes amplitude 0.040 mm
 200 Hz stapes amplitude 0.030 mm
 100 Hz stapes amplitude 0.017 mm
 50 Hz stapes amplitude 0.005 mm
 25 Hz stapes amplitude 0.005 mm

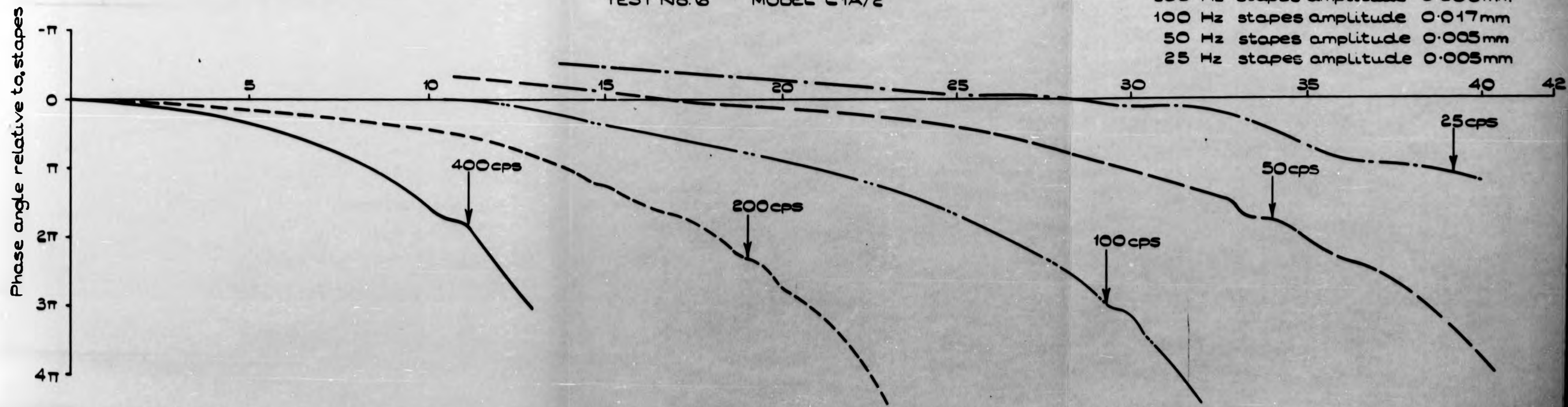
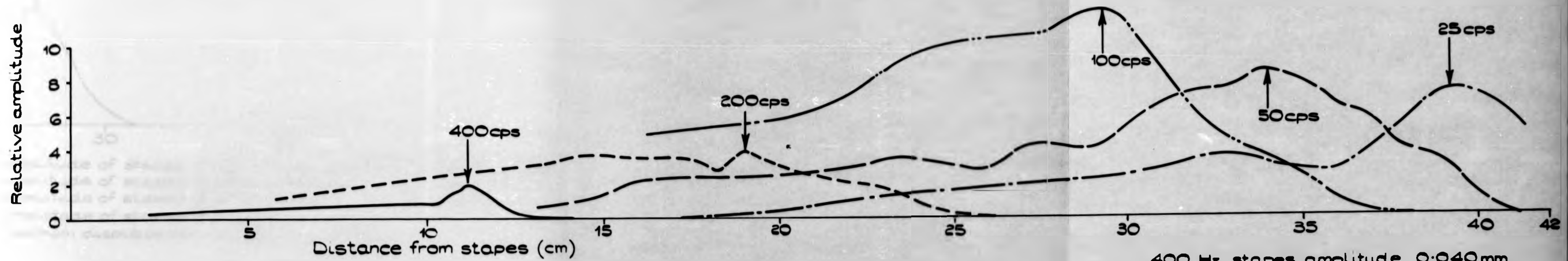


Figure R6



TEST No. 6 MODEL C1A/2

400 Hz stapes amplitude 0.040mm
 200 Hz stapes amplitude 0.030mm
 100 Hz stapes amplitude 0.017mm
 50 Hz stapes amplitude 0.005mm
 25 Hz stapes amplitude 0.005mm

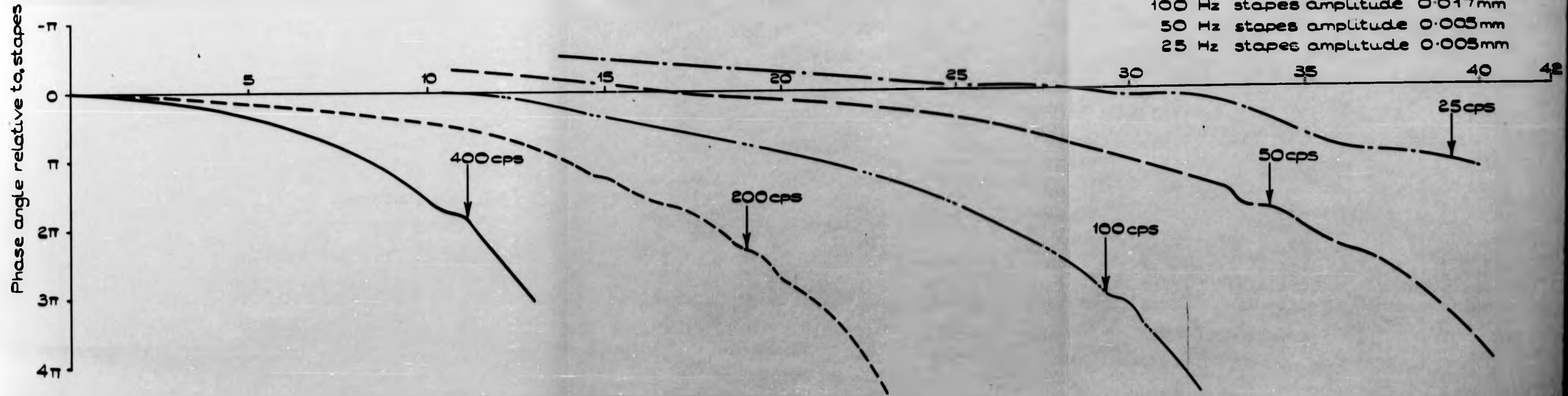


Figure R6

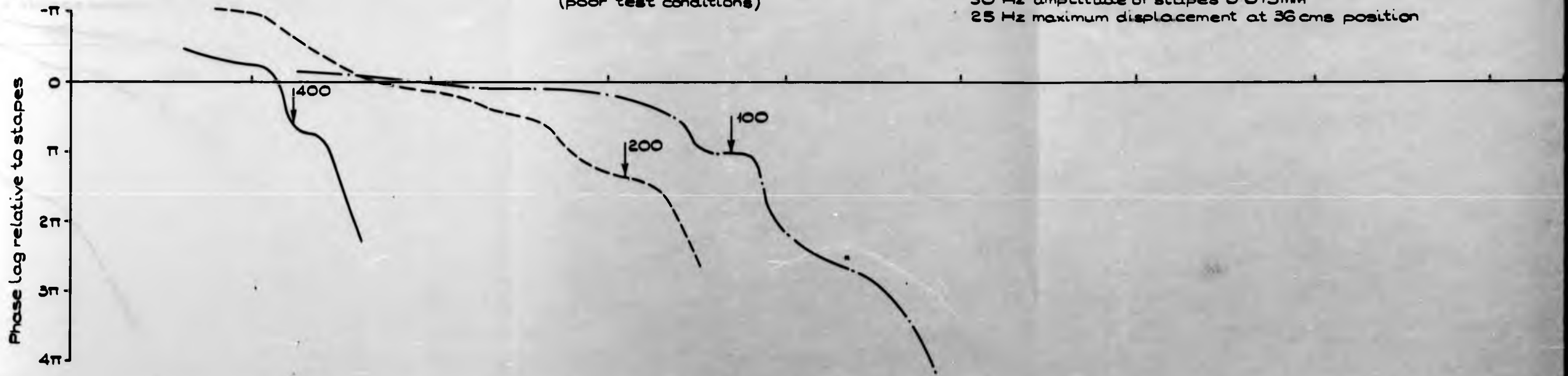
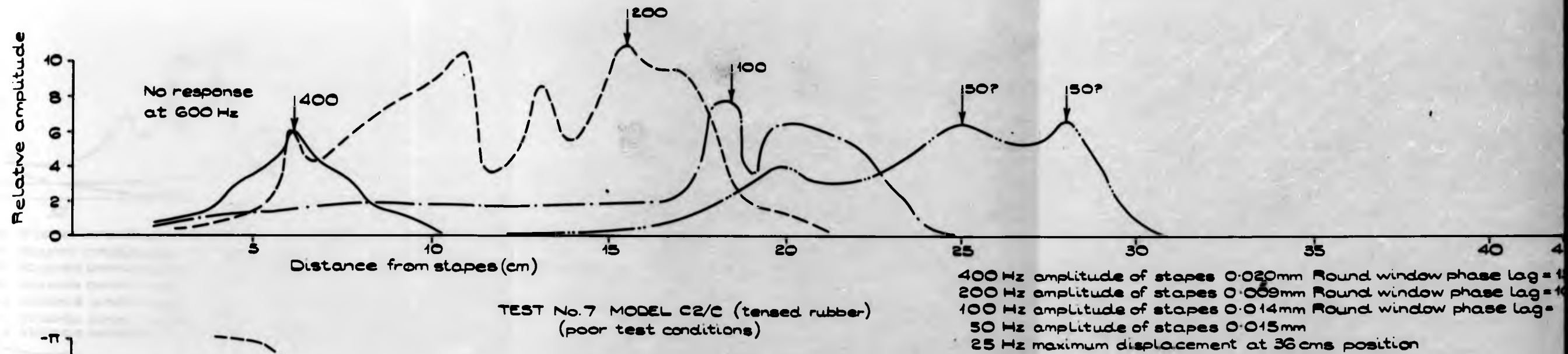
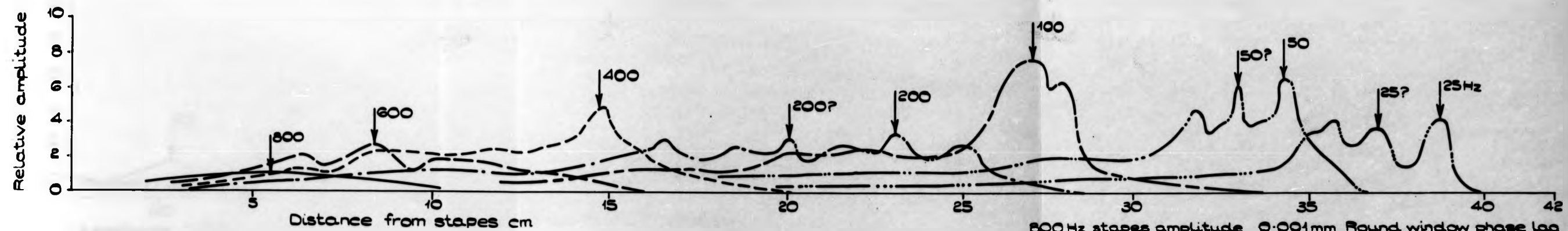


Figure R7

Figure R11

uniform membrane. Hence it seems clear that a cochlea containing a membrane with a strongly decreasing elastic modulus towards the apical end is most



TEST No. 8 MODEL C8/A

800 Hz stapes amplitude 0.001mm Round window phase lag 1
 600 Hz stapes amplitude 0.003mm Round window phase lag 3
 400 Hz stapes amplitude 0.006mm Round window phase lag 4
 200 Hz stapes amplitude 0.012mm Round window phase lag 9
 100 Hz stapes amplitude 0.012mm Round window phase lag 9
 50 Hz stapes amplitude 0.005mm Round window phase lag 2
 25 Hz stapes amplitude 0.005mm Round window phase lag 2

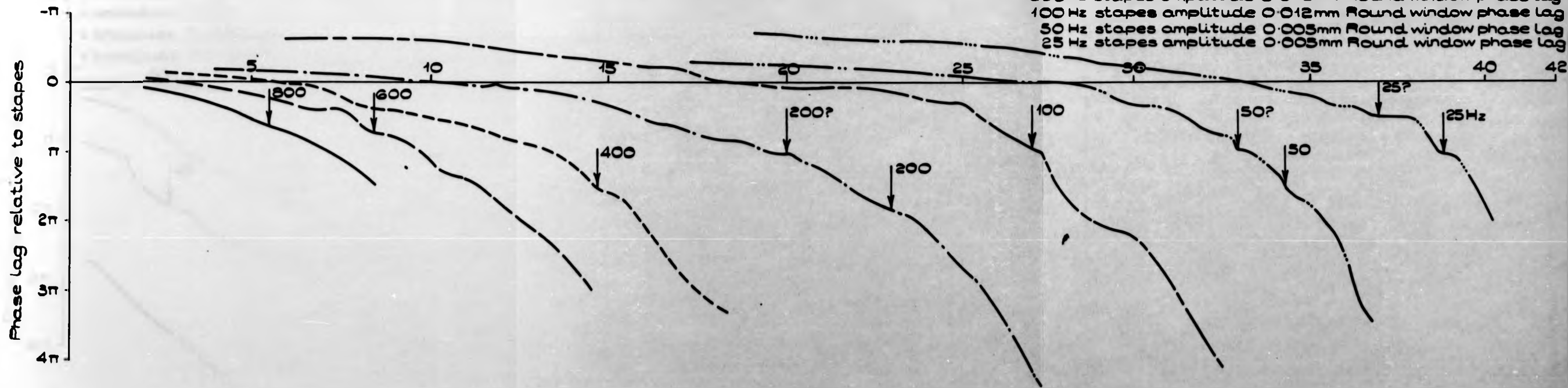


Figure R8

Figure R11

uniform membrane. Hence it seems clear that a cochlea containing a membrane with a strongly decreasing elastic modulus towards the apical end is most

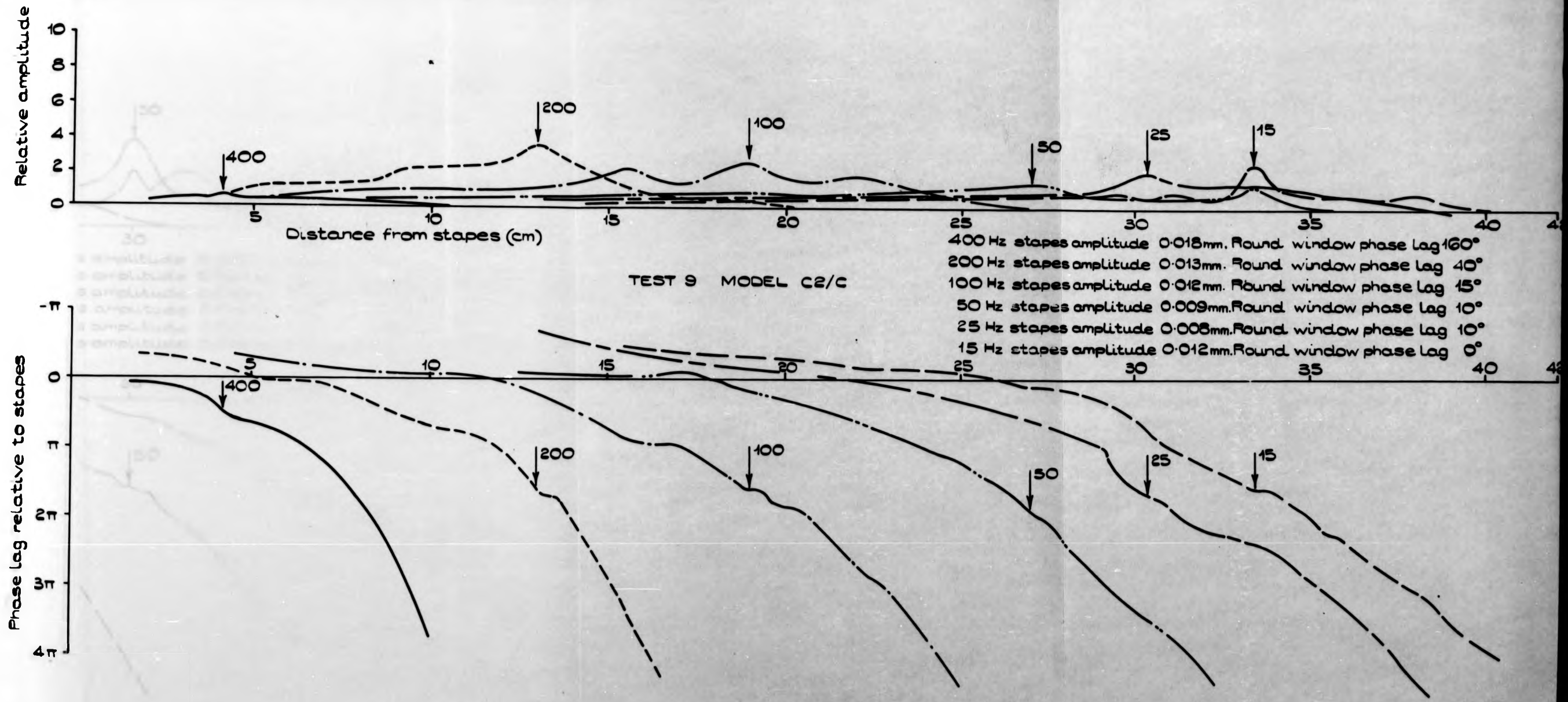


Figure R9

Figure R11

uniform membrane. Hence it seems clear that a cochlea containing a membrane with a strongly decreasing elastic modulus towards the apical end is most

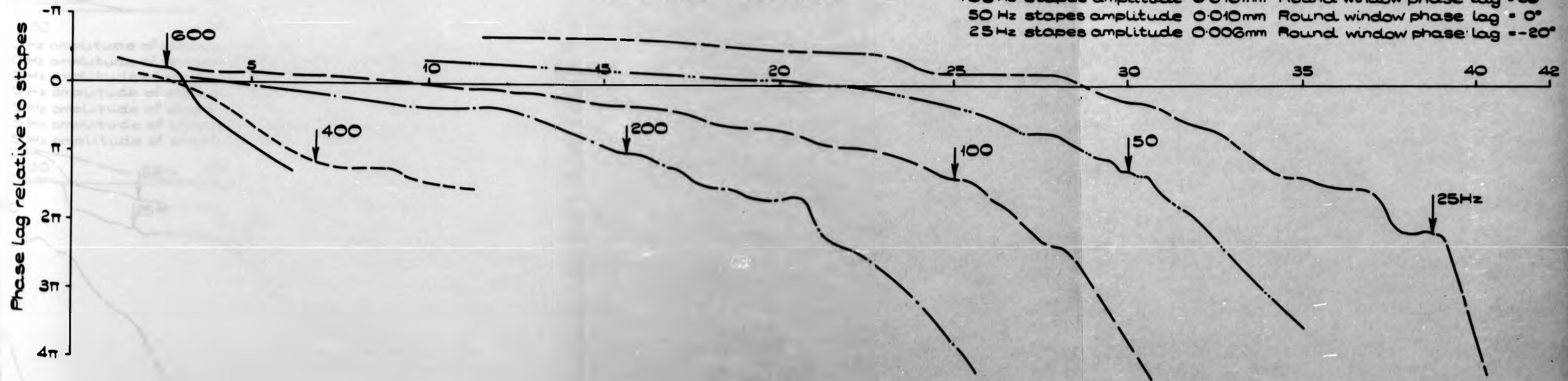
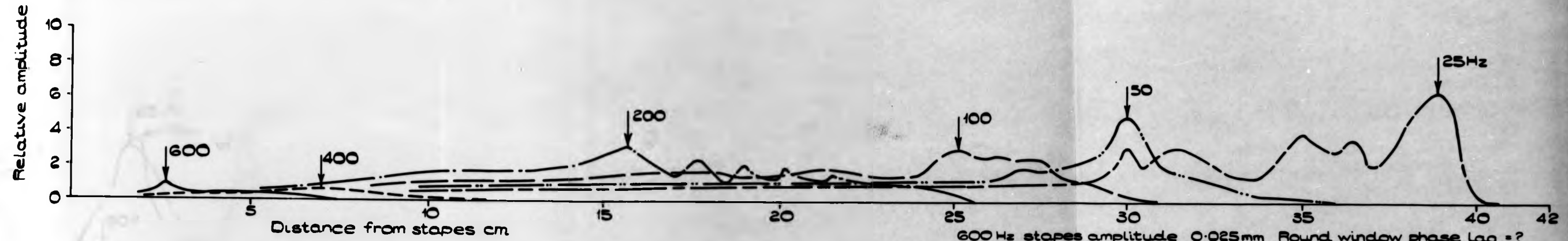
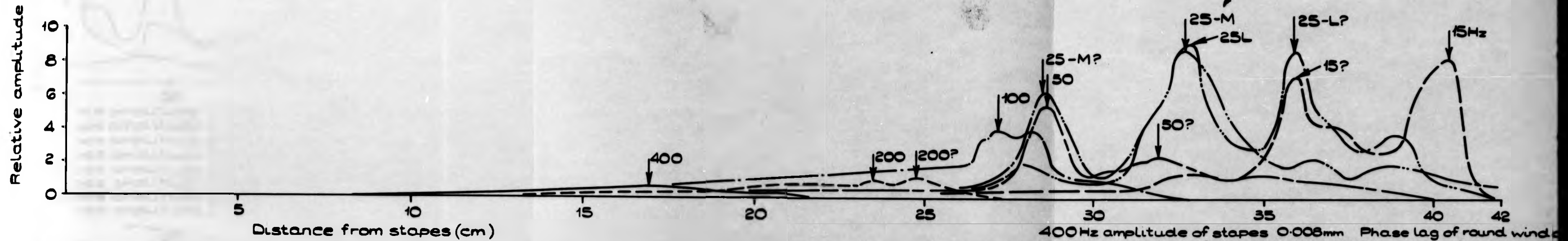


Figure R11

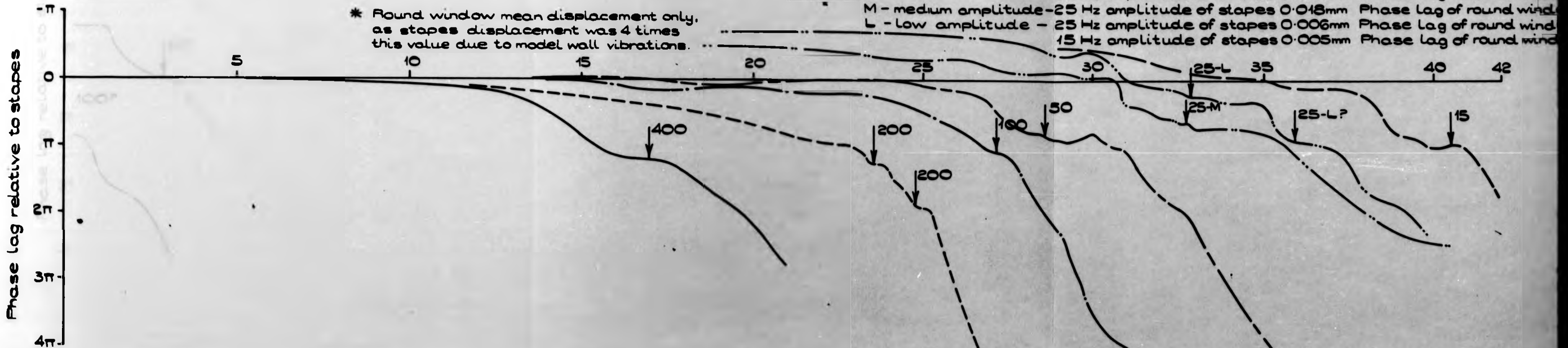
uniform membrane. Hence it seems clear that a cochlea containing a membrane with a strongly decreasing elastic modulus towards the apical end is most

Figure R10



TEST No.11 MODEL C5/A

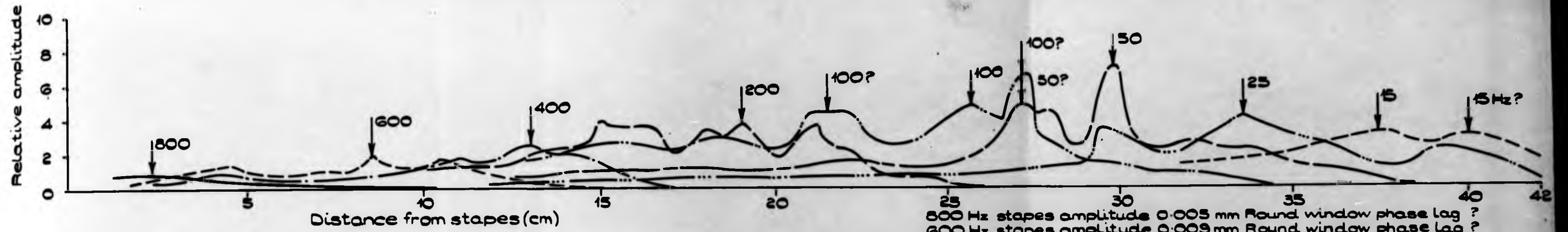
400 Hz amplitude of stapes 0.006mm Phase lag of round window
 200 Hz amplitude of stapes 0.020mm *Phase lag of round window
 100 Hz amplitude of stapes 0.005mm*Phase lag of round window
 50 Hz amplitude of stapes 0.012mm Phase lag of round window
 M - medium amplitude - 25 Hz amplitude of stapes 0.018mm Phase lag of round window
 L - low amplitude - 25 Hz amplitude of stapes 0.006mm Phase lag of round window
 15 Hz amplitude of stapes 0.005mm Phase lag of round window



* Round window mean displacement only, as stapes displacement was 4 times this value due to model wall vibrations.

Figure R11

uniform membrane. Hence it seems clear that a cochlea containing a membrane with a strongly decreasing elastic modulus towards the apical end is most



TEST No.12 MODEL C6/A

- 800 Hz stapes amplitude 0.005 mm Round window phase lag ?
- 600 Hz stapes amplitude 0.009 mm Round window phase lag ?
- 400 Hz stapes amplitude 0.012 mm Round window phase lag 140°
- 200 Hz stapes amplitude 0.009 mm Round window phase lag 100°
- 100 Hz stapes amplitude 0.010 mm Round window phase lag 20°
- 50 Hz stapes amplitude 0.010 mm Round window phase lag 10°
- 25 Hz stapes amplitude 0.006 mm Round window phase lag 0°
- 15 Hz stapes amplitude 0.004 mm Round window phase lag -10°

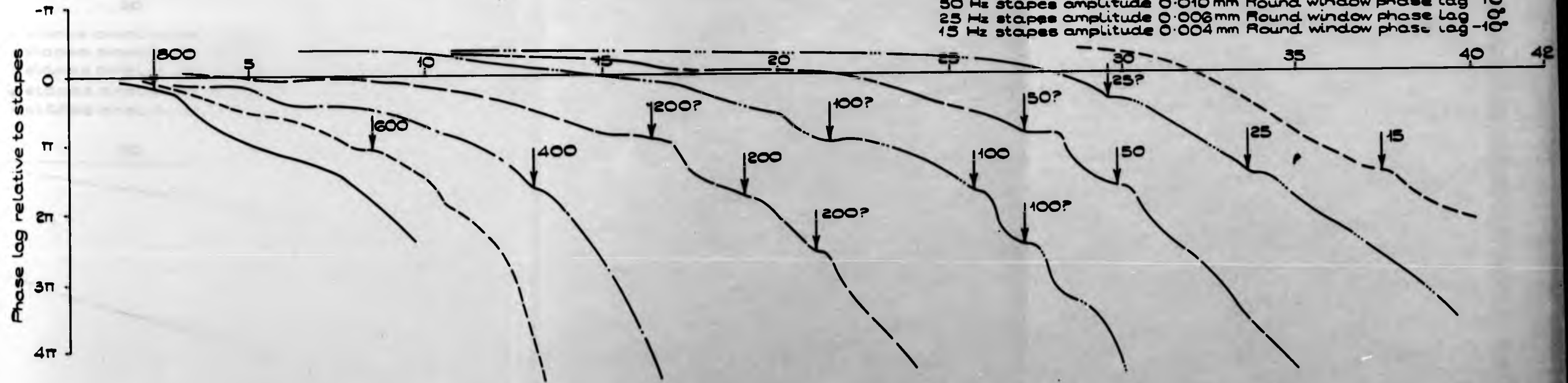
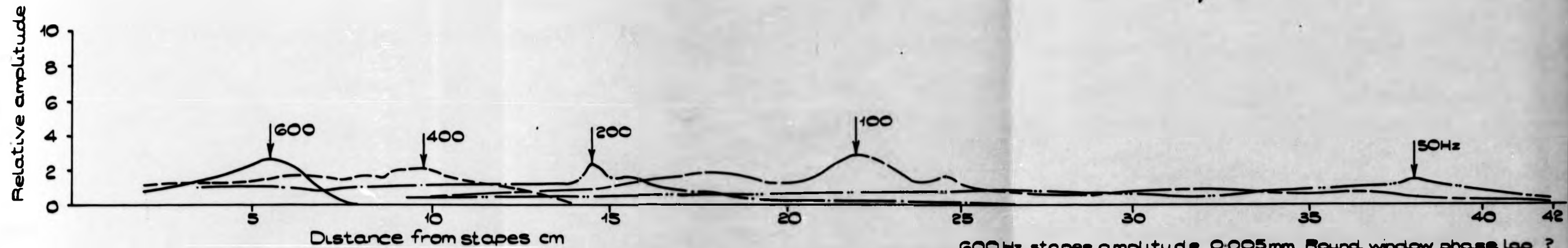


Figure R12

Figure R13

Figure R14

uniform membrane. Hence it seems clear that a cochlea containing a membrane with a strongly decreasing elastic modulus towards the apical end is most



TEST No. 13 MODEL C8/A

600 Hz stapes amplitude 0.005 mm Round window phase lag ?
 400 Hz stapes amplitude 0.014 mm Round window phase lag ?
 200 Hz stapes amplitude 0.029 mm Round window phase lag 45°
 100 Hz stapes amplitude 0.033 mm Round window phase lag 5°
 50 Hz stapes amplitude 0.042 mm Round window phase lag 10°

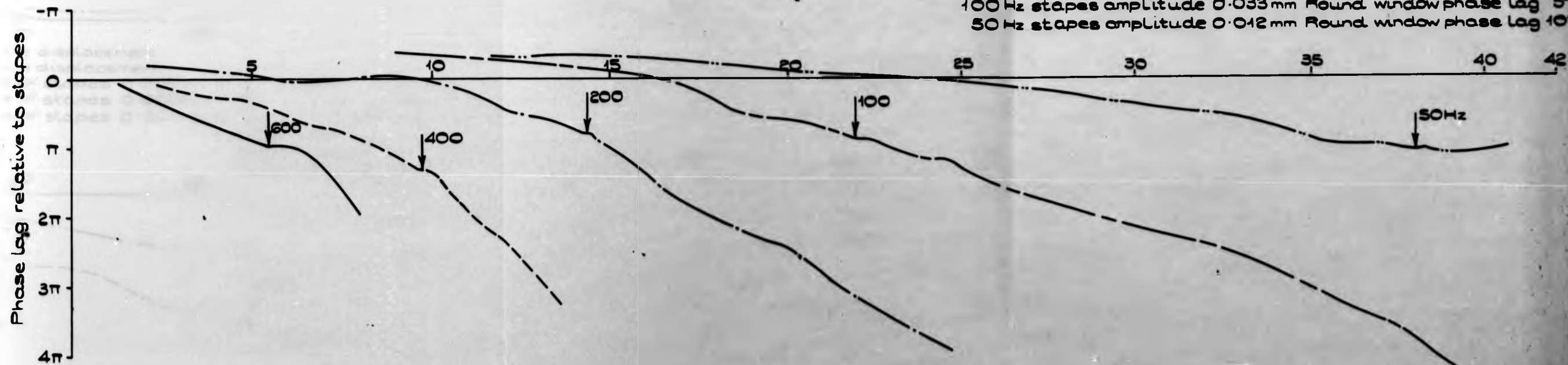
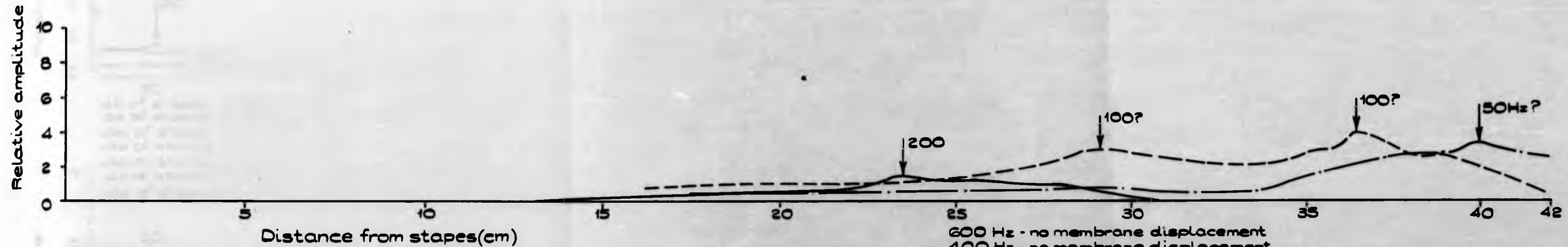


Figure R 13

uniform membrane. Hence it seems clear that a cochlea containing a membrane with a strongly decreasing elastic modulus towards the apical end is most



TEST No. 14 MODEL C5/A

200 Hz - no membrane displacement
 400 Hz - no membrane displacement
 200 Hz - amplitude of stapes 0.003 mm * Round window phase lag 150°
 100 Hz - amplitude of stapes 0.003 mm * Round window phase lag 150°
 50 Hz - amplitude of stapes 0.004 mm * Round window phase lag 100°

Note - Test repeated with model under reduced pressure and response found to be identical.

* Stapes effective amplitude derived from round window amplitude, the former being about 4 times the latter.

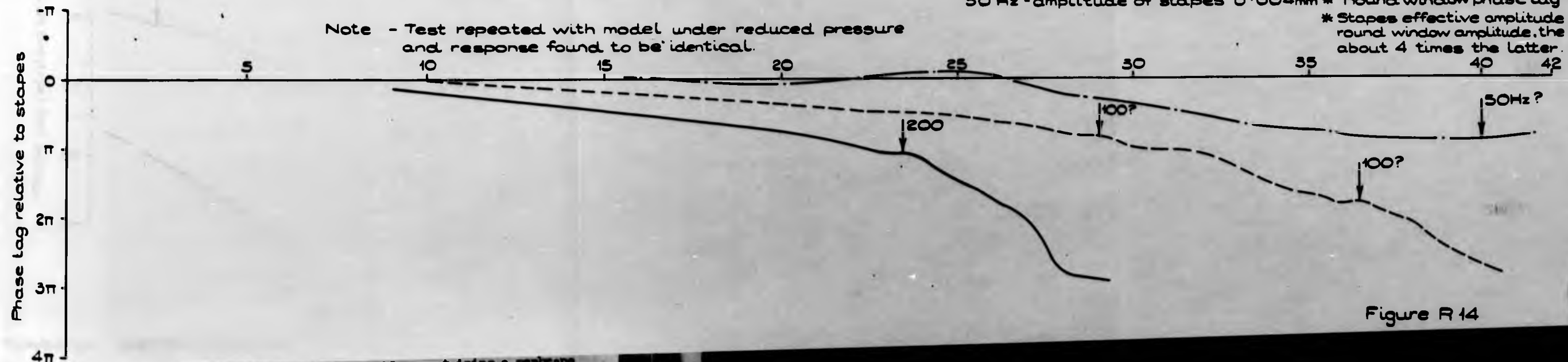
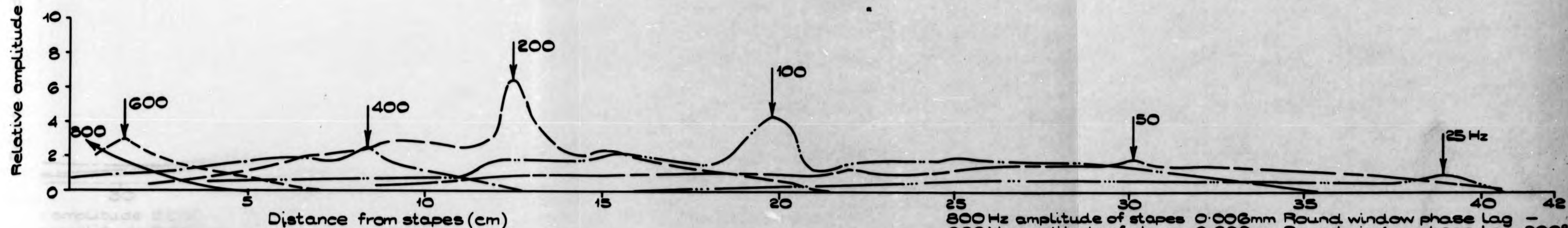


Figure R 14

uniform membrane. Hence it seems clear that a cochlea containing a membrane with a strongly decreasing elastic modulus towards the apical end is most



TEST No. 15 MODEL CG/A

800 Hz amplitude of stapes	0.006 mm	Round window phase lag	-
600 Hz amplitude of stapes	0.009 mm	Round window phase lag	200°
400 Hz amplitude of stapes	0.011 mm	Round window phase lag	60°
200 Hz amplitude of stapes	0.012 mm	Round window phase lag	45°
100 Hz amplitude of stapes	0.009 mm	Round window phase lag	10°
50 Hz amplitude of stapes	0.008 mm	Round window phase lag	0°
25 Hz amplitude of stapes	0.012 mm	Round window phase lag	0°

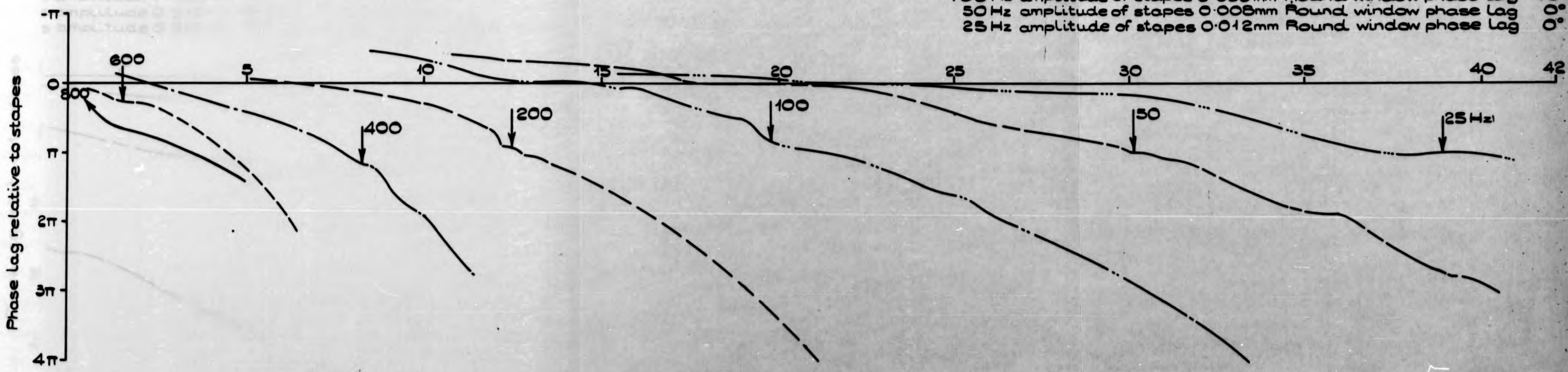
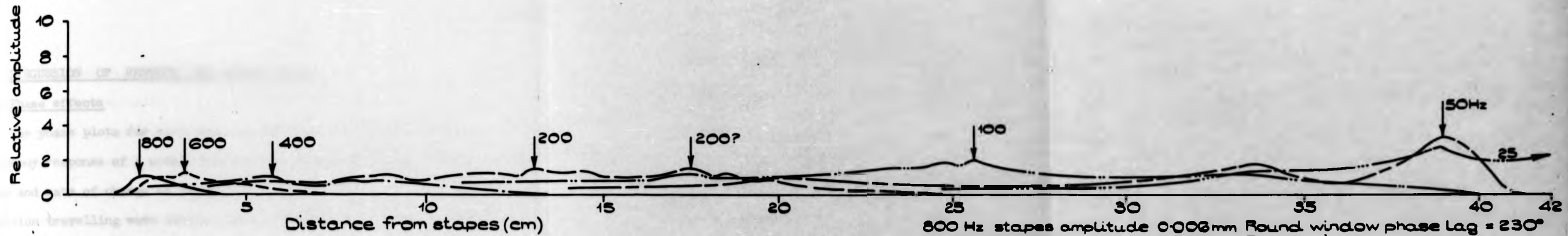


Figure R 15

respectively. Note that in tests Nos. 15 to 18 each model contained a uniform membrane. Hence it seems clear that a cochlea containing a membrane with a strongly decreasing elastic modulus towards the apical end is most

observed in the high frequency region of the cochlea



800 Hz stapes amplitude 0.008 mm Round window phase lag = 230°
 600 Hz stapes amplitude 0.008 mm Round window phase lag = —
 400 Hz stapes amplitude 0.008 mm Round window phase lag = 150°
 200 Hz stapes amplitude 0.010 mm Round window phase lag = 55°
 100 Hz stapes amplitude 0.009 mm Round window phase lag = 30°
 50 Hz stapes amplitude 0.012 mm Round window phase lag = 10°
 25 Hz stapes amplitude 0.012 mm Round window phase lag = 0°

TEST No. 16 MODEL C1/A

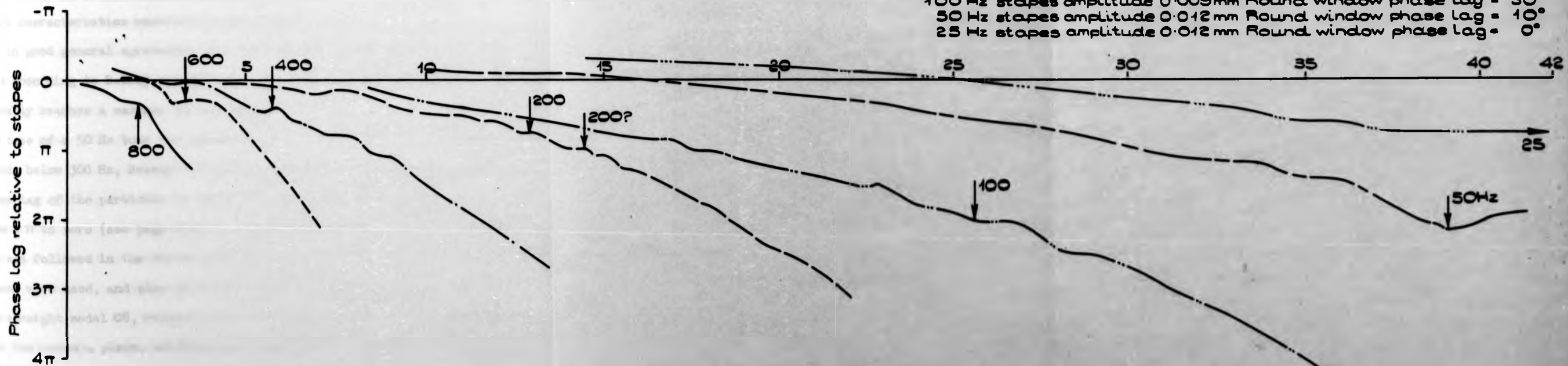


Figure R 10

also constant in the case of tests Nos. 13 and 14 for membrane to membrane
 respectively. Note that in tests Nos. 13 to 16 each model contained a
 uniform membrane. Hence it seems clear that a cochlea containing a membrane
 with a strongly decreasing elastic modulus towards the apical end is most

Y DISCUSSION OF RESULTS OF MODEL TESTS

Ya. Phase effects

The phase plots for each test are no less distinguishing a feature of the frequency response of a model than are the amplitude envelope curves, and both phase and rate of change of phase with distance characteristics describe partition travelling wave shapes, etc., rather more explicitly than do the envelope characteristics.

The model phase results illustrate that even the low frequency, apical-end phase characteristics recorded by von Bekesy, with which these model results are in good general agreement, are not independent of amplitude. Note also that according to Bekesy the relative phase angle between partition and stapes probably reaches a maximum in the case of an 100 Hz sound of about π , while in the case of a 50 Hz tone the phase angle does not reach $\pi/4$. In fact, for sounds below 300 Hz, Bekesy's figures show that as frequency decreases the phase lag of the partition at the point of maximum amplitude also decreases from 2π to zero (see page 2-15.) This trend is not always so for the models, but was followed in the three tests Nos. 4, 6 and 7 in which pre-tensed membranes were used, and also in tests Nos. 5 and 8, using the small model C4 and the straight model C8, respectively, with tapered rubber membranes in each. Note that when a plain, uniform rubber membrane was fitted into model C8, in test No. 13, the phase angle occurring at each maximum amplitude section was constant for all frequencies. This similarly applied to model C5 in test 14, and the phase lag occurring at the low frequency maximum amplitude points was also constant in the case of tests Nos. 15 and 16 for models C6 and C1 respectively. Note that in tests Nos. 13 to 16 each model contained a uniform membrane. Hence it seems clear that a cochlea containing a membrane with a strongly decreasing elastic modulus towards the apical end is most

likely to show the low frequency phase trend observed by Bekesy. Note that a model test frequency of 25 Hz is equivalent to 250 Hz in an actual cochlea.

There are no results available describing phase vs. distance characteristics at the high frequency, basal end of the human cochlea. All tests except Nos. 11 and 14 for model C5 and test No. 13 for C8 show that as the stapes is approached the membrane relative phase angle occurring at the point of maximum amplitude response decreases towards zero. Another interesting feature describing the travelling wave, which is relevant to sharpness of sensory hair cell frequency discrimination, is the slope of the phase plot, (or the rate of change of phase lag with respect to distance along the cochlea) at the place of maximum amplitude and between this point and the place of extinction of the travelling wave on the apical side. Results of uniform membrane (RM1) tests Nos. 13 to 16 all showed a very steep phase plot slope for high frequencies, and a slope of about zero at the low frequency end. Models C1 and C2 with untensed tapering membranes showed, in tests Nos. 1, 2 and 10, the opposite effect, with maximum slope and therefore smallest partition travelling wave length occurring at low frequencies. Other models with tapering membranes gave a less specific trend. Note that Bekesy's result in this respect (see Fig. 6 in Chapter 2) shows no clear trend.

In general, the model results indicate that partition travelling wave motion is sharp and well-developed in the high frequency region of the cochlea. Note. Observations reported more recently by Perlman⁽⁹⁾ and Diestel⁽¹⁰⁾ on travelling wave motion in the partition of human cochleas are concerned with basal end response. These papers are very interesting but do not appear to be referred to by other authors and have not been reviewed here because of the absence of any quantitative or critical qualitative frequency response data. They do, however, suggest that phase-varying partition waves, i.e. travelling waves, do occur and can be observed in the high frequency, proximal region of the cochlea.

Vb. Place and Amplitude Effects

In nearly all of the results, the place at which the partition membrane vibrates with maximum amplitude can be seen quite clearly. Due to the model manufacturing and experimental techniques, experimental observations were always clear and measurements accurate, so that experimental error as such cannot explain the apparent proximity of two peaks for one response curve, or the lack of a well defined amplitude maximum, both of which situations occasionally occur in Figs. R1 to R16. Normal model response in the case of the large model C5, which has rather thin walls, was partly interfered with by the independent dilational vibration of the model walls, a situation which was discovered by the use of accelerometer probes coupled to vibration measuring equipment. This mode existed in most models, but other than for C5, amplitudes involved were practically insignificant.

Uneven clamping of membranes may have resulted in some unexpected variations in membrane properties, but this was carefully avoided as much as possible. However, two other effects which come into the category of manufacturing errors are known to affect actual membrane responses. Figure Q1 shows the membrane slot width errors. Thus in comparing the high frequency response results of model C1, for example, with results for model C4, it must, unfortunately, be borne in mind that in the basal region the membrane in C1 was up to 22% wider than in C4. Hence it may be assumed that if model C1 responded well to a frequency f Hz near to the stapes, then with the same slot width as C4 it would probably have responded to a higher frequency of $1.2f$ to $1.4f$ at the same section.

Figure Q2 shows the un-evenness of the tapering rubber membrane thicknesses. Although the most linear sections of the tapering rubber sheeting supplied were used in the models, some discontinuities were unavoidable, e.g., membranes

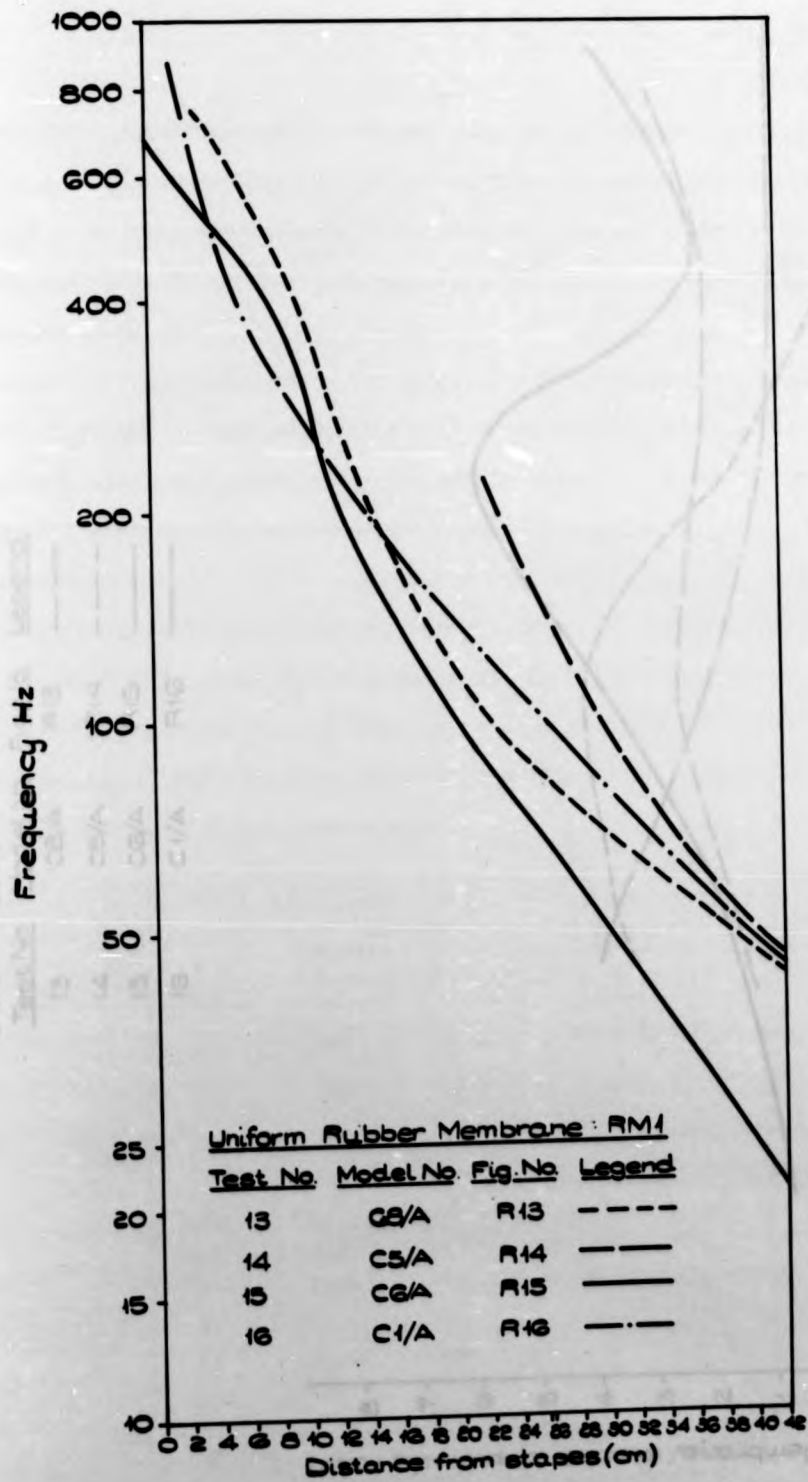
RM2 and RM4 at 15 cms. from the stapes. One of the reasons for including the uniform membrane tests Nos. 13 - 16 was in order to ensure that certain trends in model responses, particularly place effects, were correctly ascribed to hydrodynamic effects arising from geometric variations and were not caused by unevenness of membranes.

Figures S1 to S7 summarize the place effects obtained in the results of Figures R1 to R16. That is, each of the seven figures whose number carries an S prefix outlines the relationship between frequency and place along the cochlea at which maximum amplitude response of the partition occurred for that frequency.

Figures T1 to T4 and T7 summarize amplitude ratio effects. That is, each of the five T prefix number figures roughly outlines the relationship between model partition maximum amplitude ratio, relative to stapes amplitudes, and frequency. The following schedule shows how these summary curves, based on Figures R1 to R16, are arranged.

SCHEDULE OF SUMMARY FIGURES S1 to S7 and T1 to T4 and T7

<u>For Place Effects - S prefix.</u>	<u>For Amplitude Effects - T prefix.</u>	<u>Membrane Type</u>	<u>To show functional effects of:-</u>	<u>Model Tests involved</u>
S1	T1	RM1	Geometric Variations	Nos. 13 - 16
S2	T2	RM2	Geometric Variations	Nos. 10 - 12
S3	T3	RM3	Geometric and Membrane Width Variations	Nos. 1, 2, 9
S4	T4	RM4	Geometric Variations	Nos. 5, 8, 12
S5	-	RM4 (Tensed)	Geometric and Membrane Width Variations	Nos. 4, 6, 7
S6	-	Various	Membrane tension	Nos. 6,7,9,10
S7	T7	RM1, RM4	Membrane thickness	Nos. 8,12,13,15

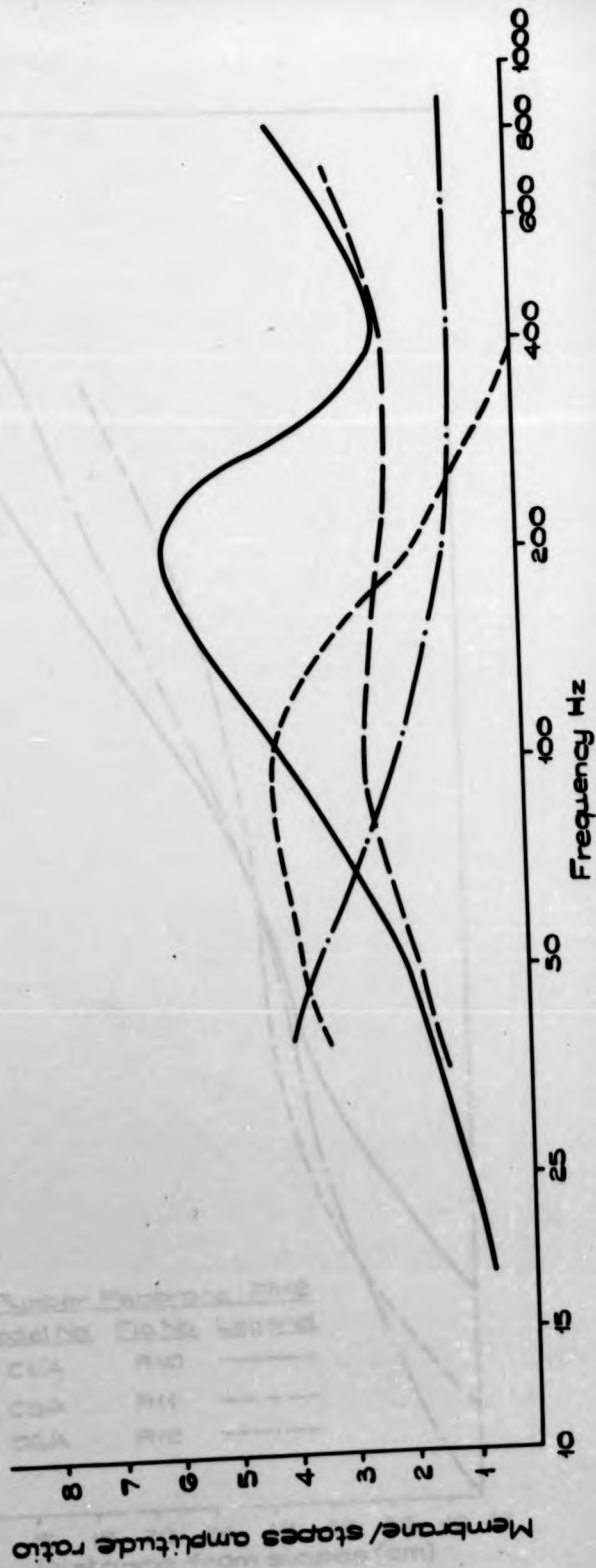


EFFECTS OF COCHLEAR SCALA GEOMETRY: FIGURE S1

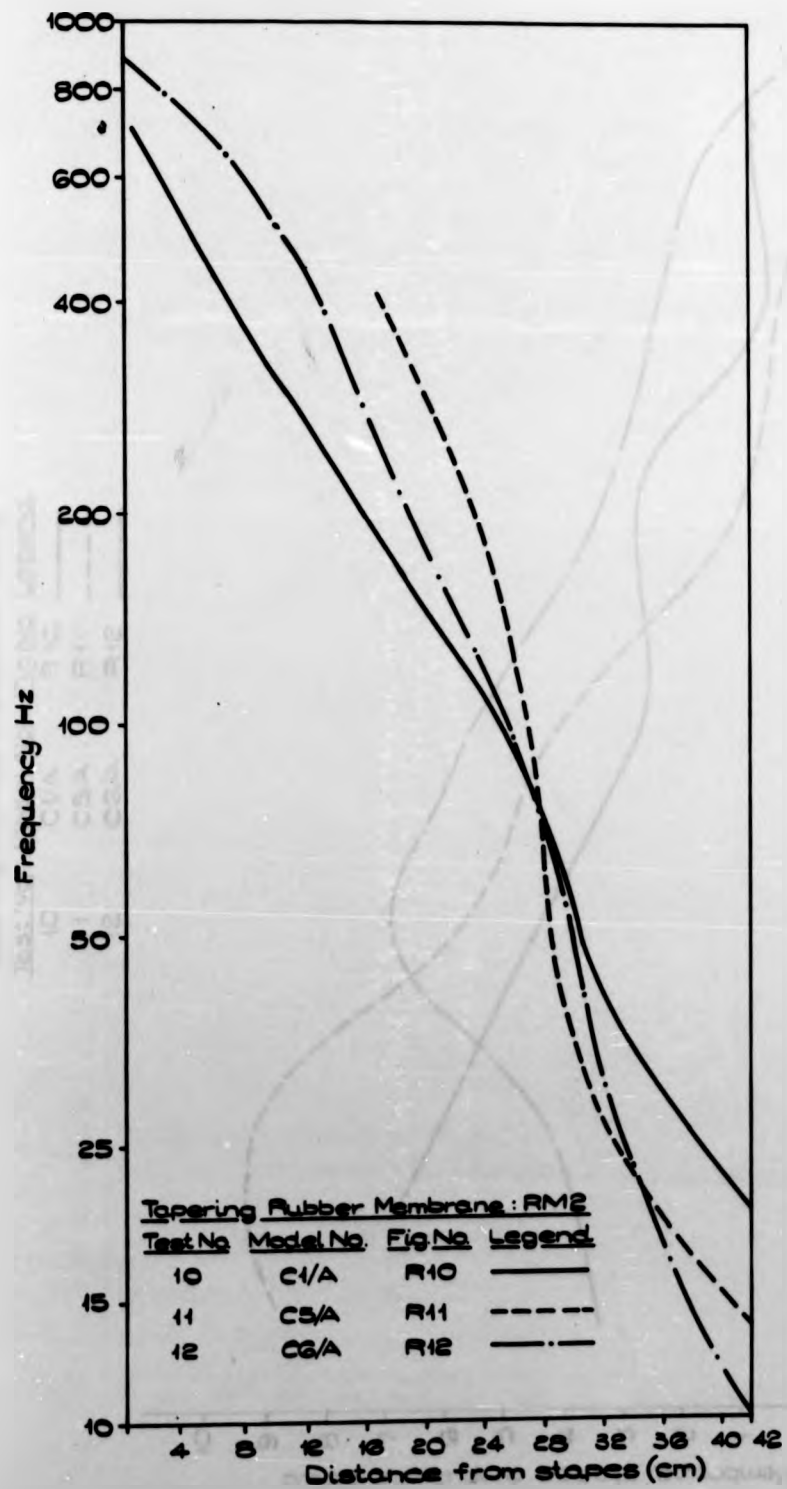


Uniform Rubber Membrane : RM1

Test No	Model No	Fig No	Legend
13	C8/A	R13	---
14	C5/A	R14	- - - -
15	C6/A	R15	— — — —
16	C1/A	R16	— · — · —



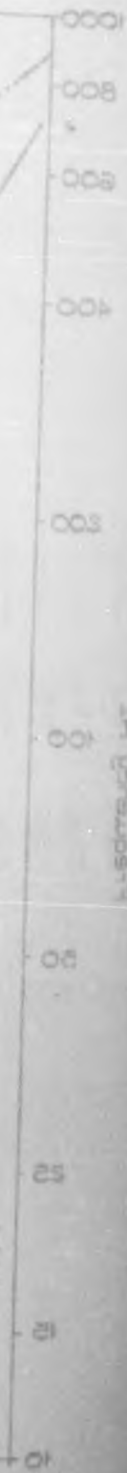
EFFECTS OF COCHLEAR SCALA GEOMETRY : FIGURE T1



EFFECTS OF COCHLEAR SCALA GEOMETRY: FIGURE S2

Tapering Rubber Membrane
 Test No. Model No. Evg No Legend

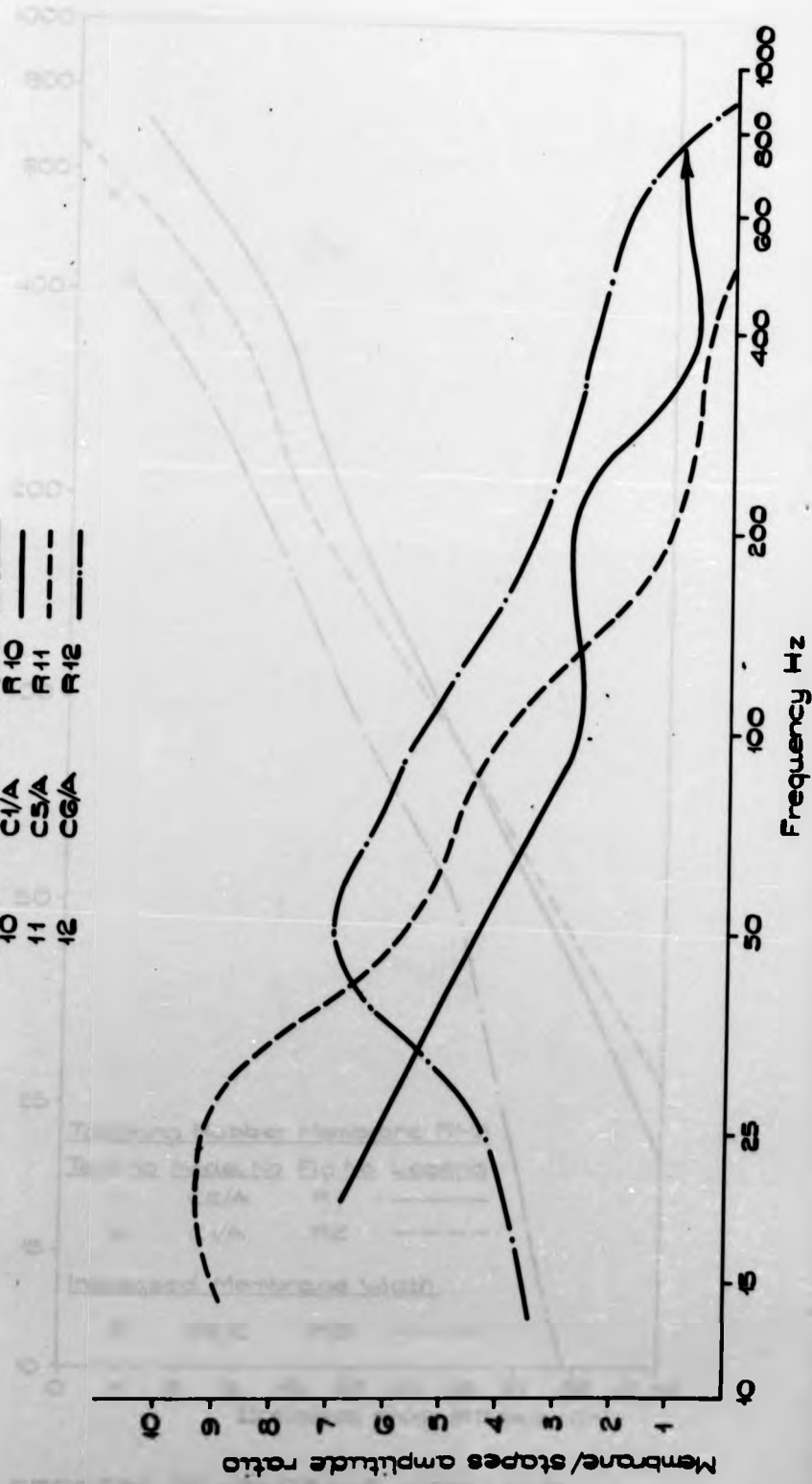
10	C1/A	R10	—
11	C5/A	R11	- - -
12	C6/A	R12	· · ·



Tapering Rubber Membrane: R12

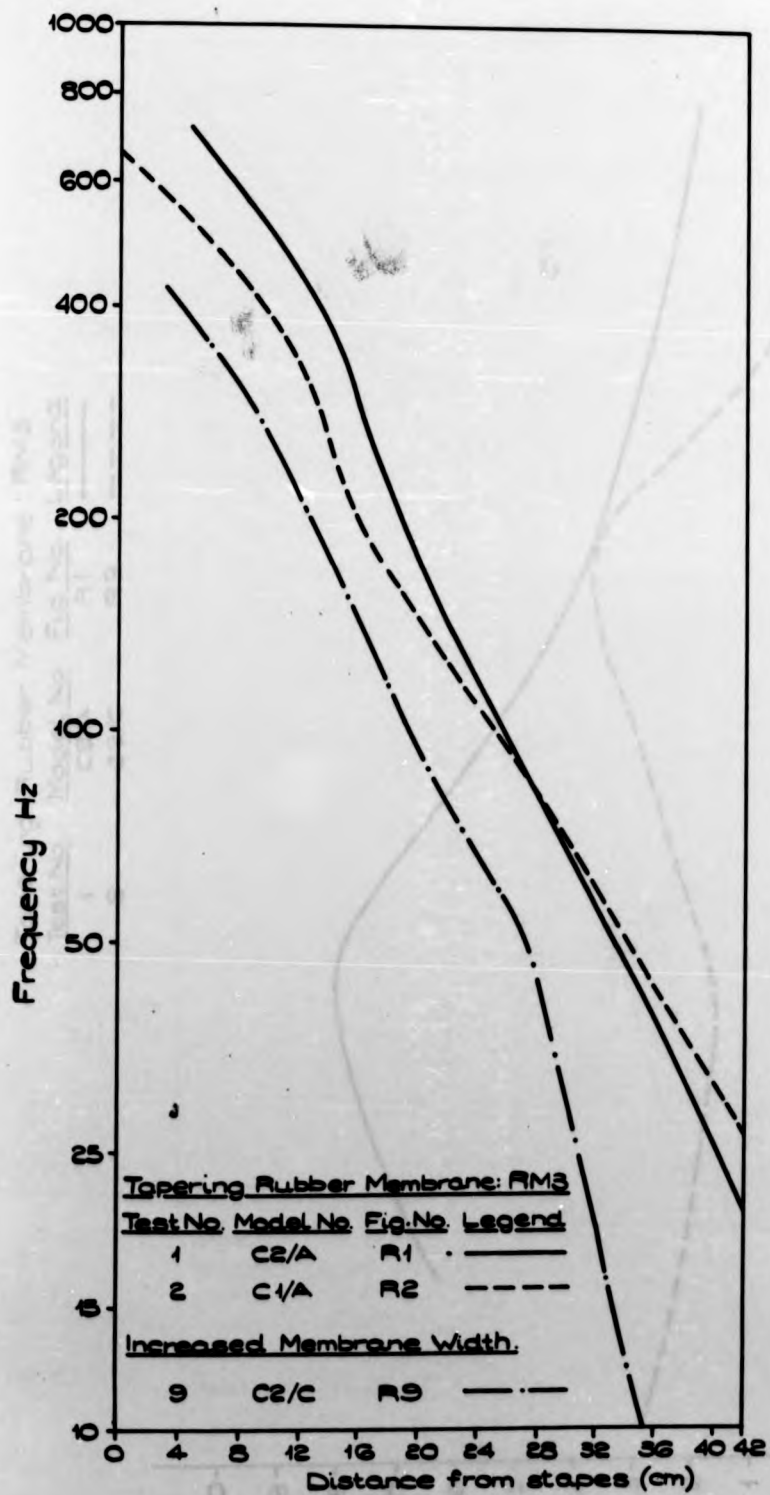
Test No. Model No. Evg No Legend

10	C1/A	R10	—
11	C5/A	R11	- - -
12	C6/A	R12	· · ·



EFFECTS OF COCHLEAR GEOMETRY :

FIGURE T2



EFFECTS OF MEMBRANE WIDTH AND
OF COCHLEAR SCALA GEOMETRY : FIGURE 53



Tapering Rubber Membrane : RM3

Test No.	Model No.	Fig. No.	Legend
1	CS/A	R1	—
2	CS/A	RS	—
3	CS/C	RS	---

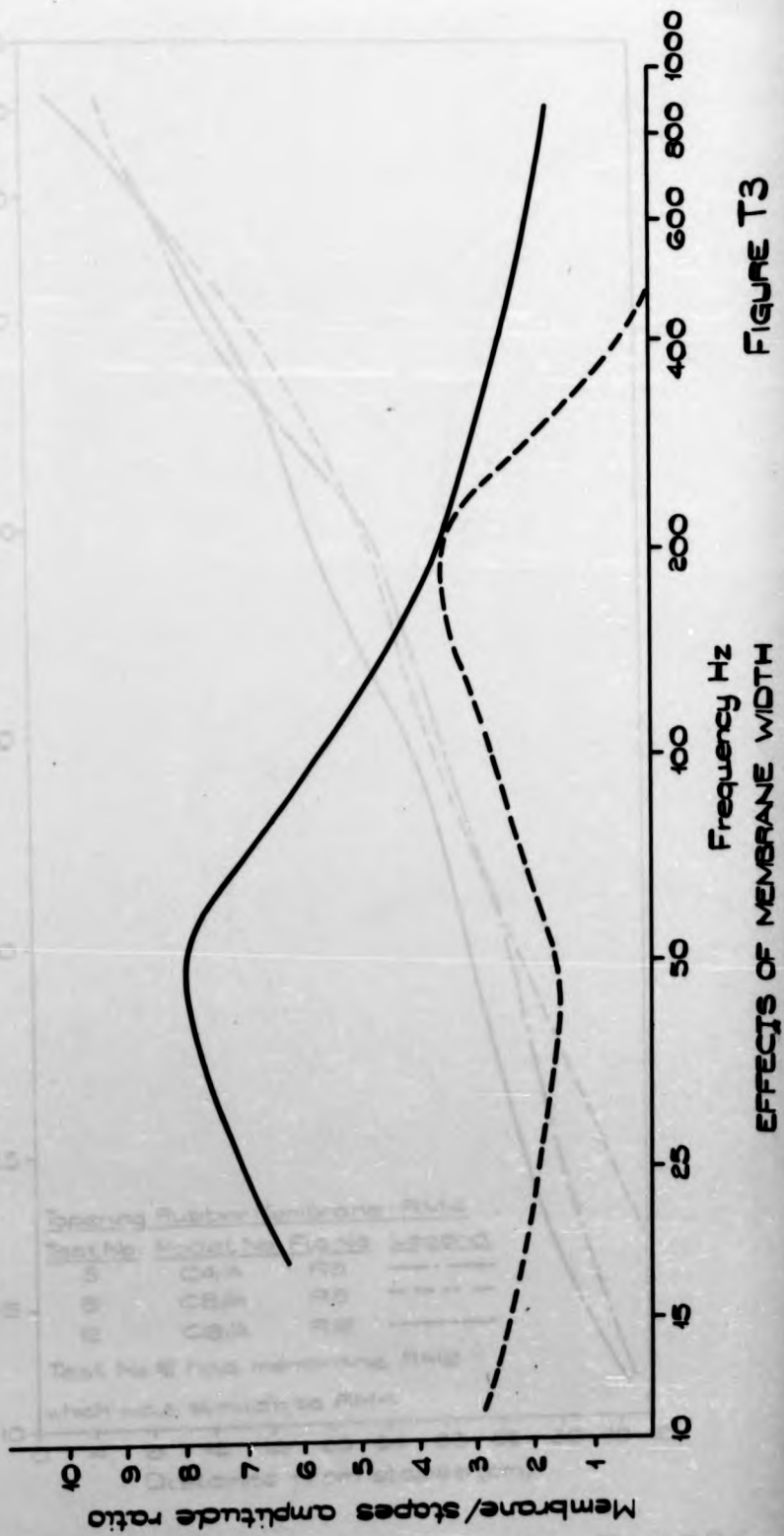
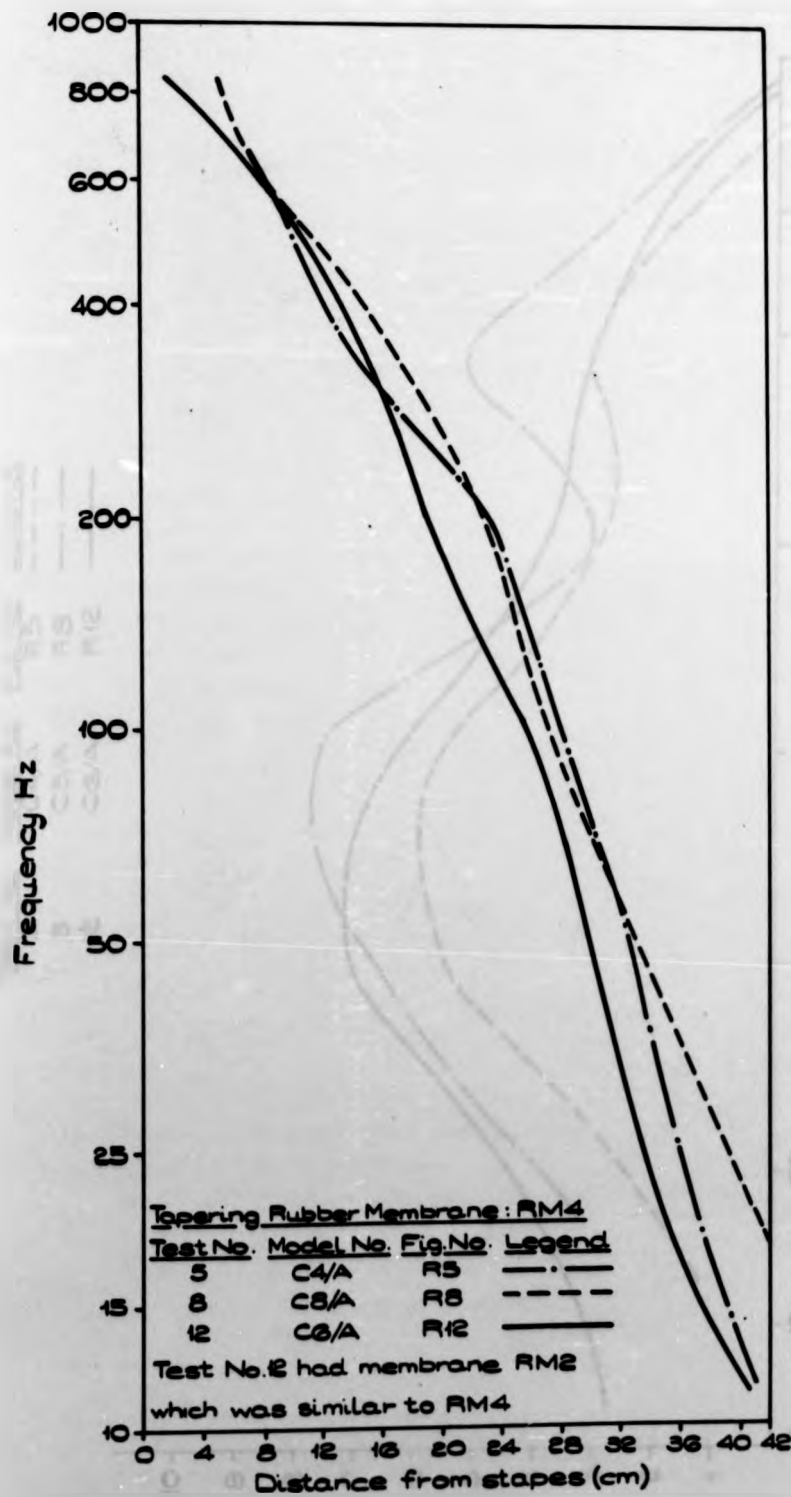


FIGURE T3



EFFECTS OF COCHLEAR SCALA GEOMETRY: FIGURE S4



Tapering Rubber Membrane: RM 4

Test No. Model No. Fig. No. Legend

5 C4/A R5 ---

8 C8/A R8 -.-

12 C6/A R12 —

For model C4/A
membrane
tension side
left during
test only over
the region
10 to 50 cps

Tapering Rubber Membrane
5% initial strain
Test No. Model No. Fig. No. Legend
4 C4/A R4 ---
6 C6/A R6 -.-
Increased membrane width
7 C8/A R7 —

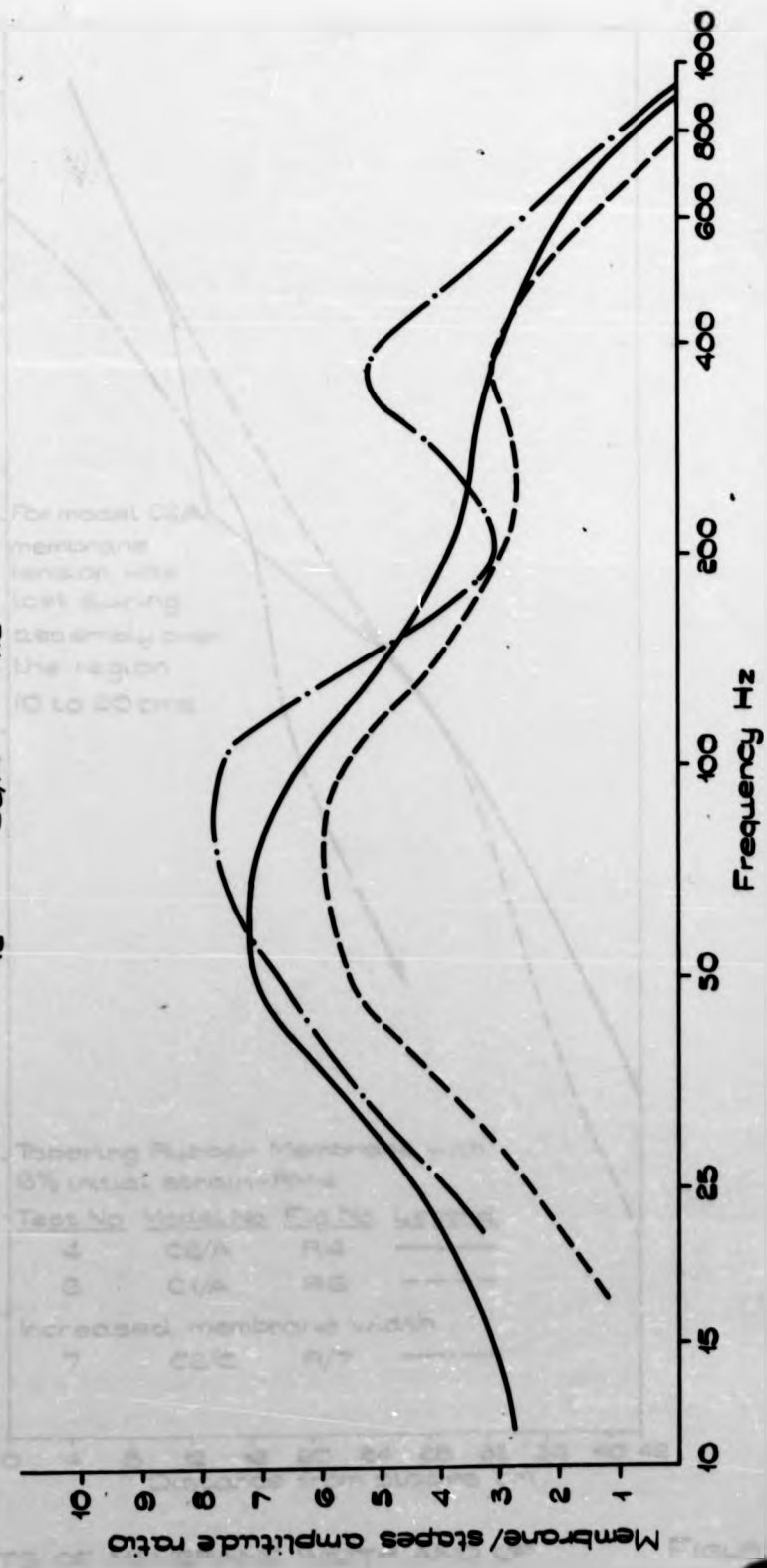
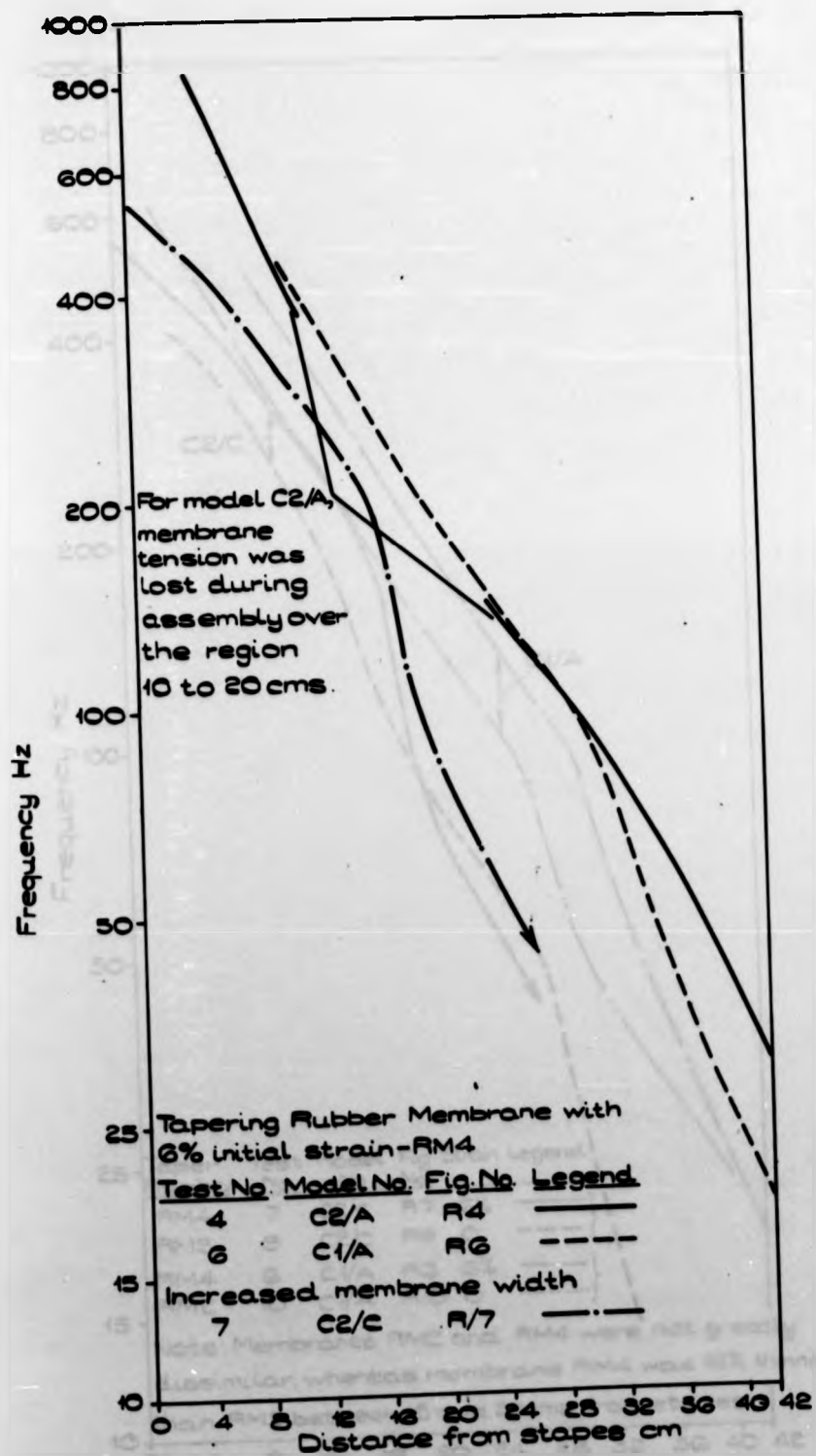


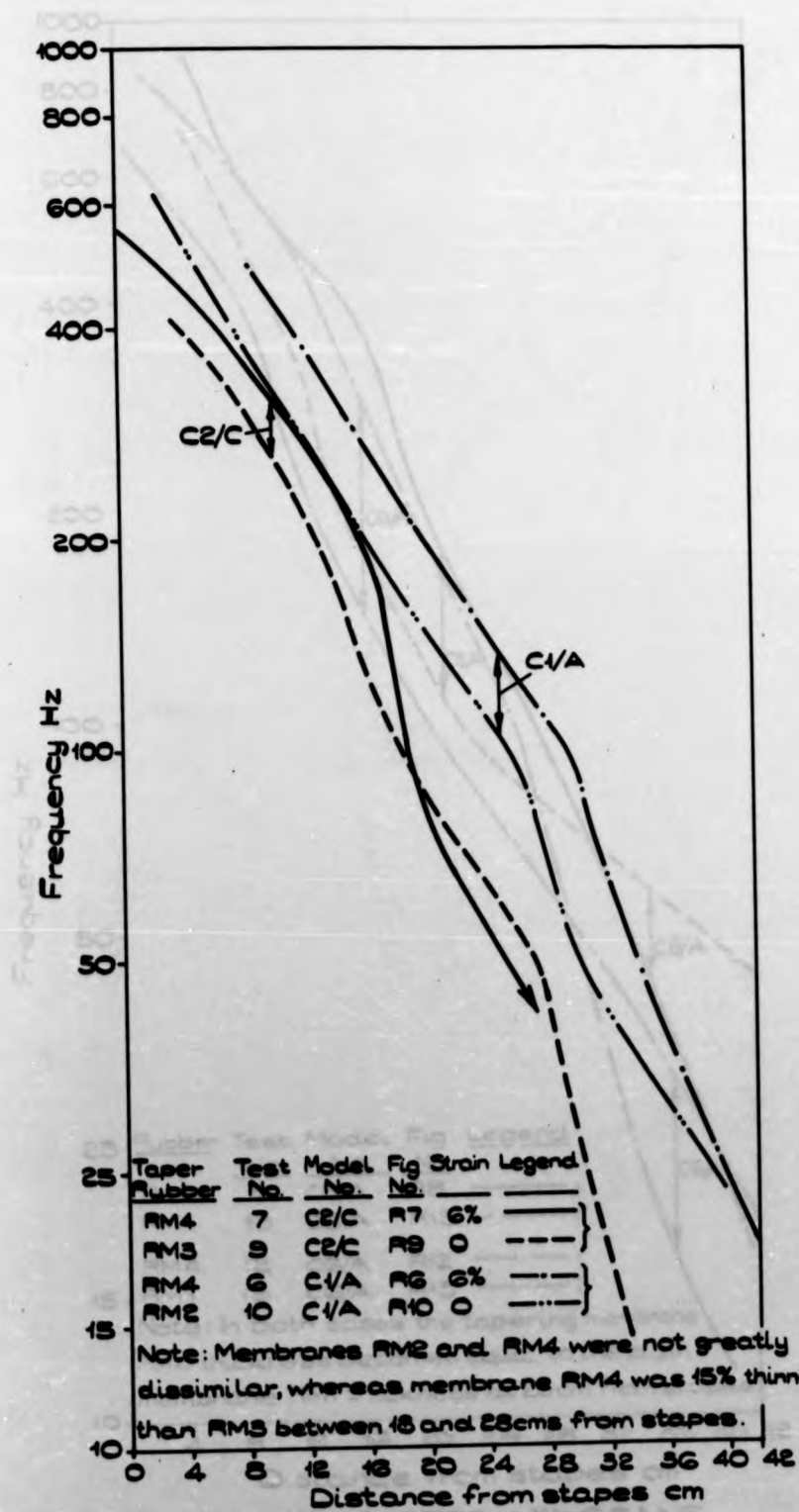
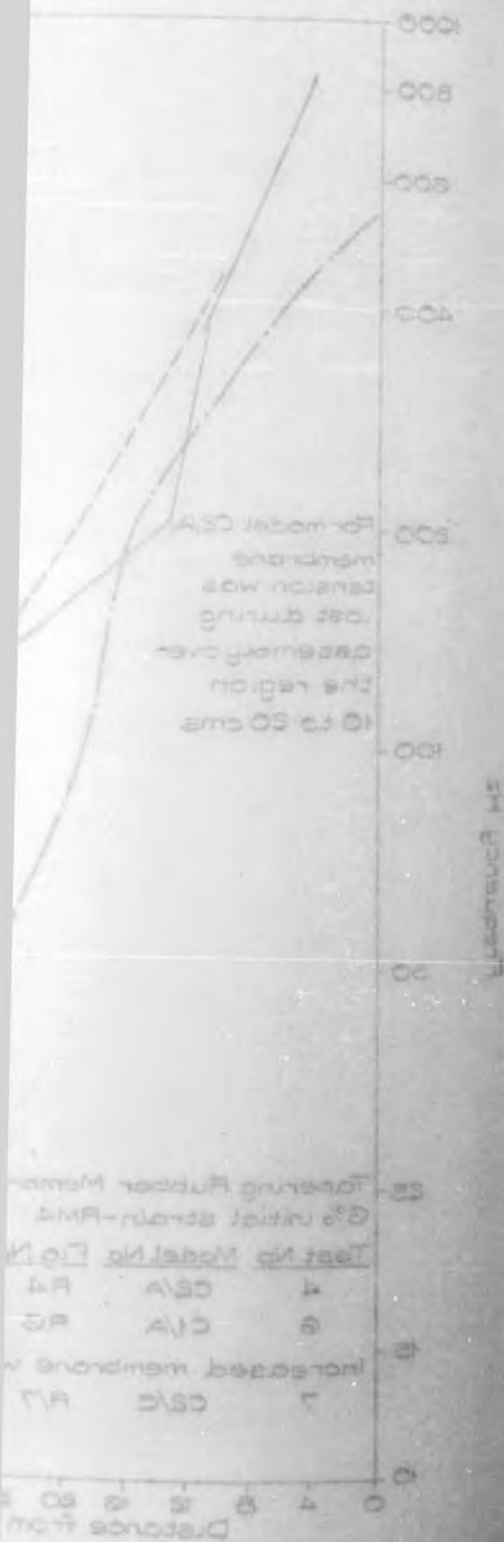
FIGURE T4

EFFECTS OF COCHLEAR SCALA GEOMETRY :

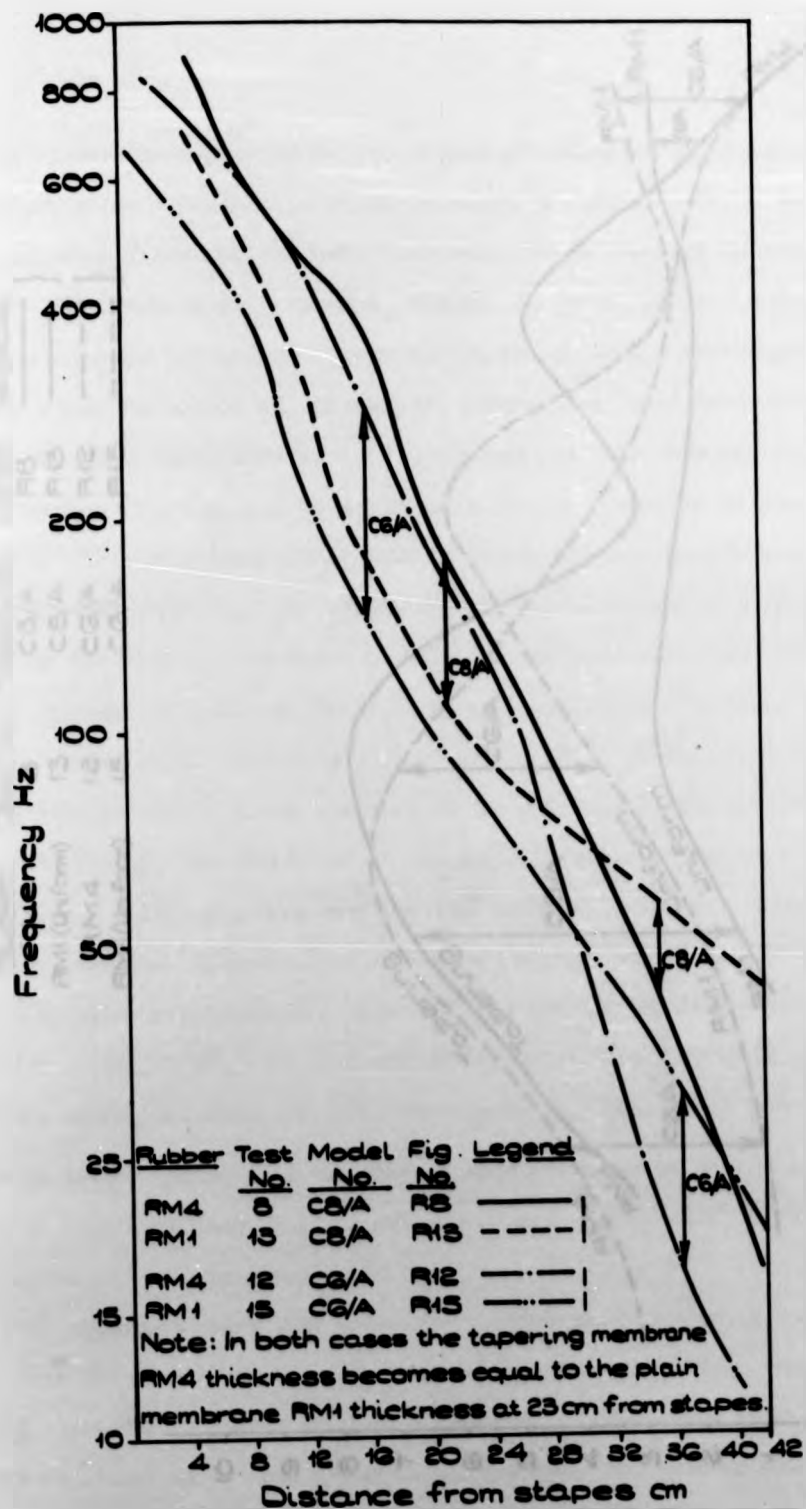


EFFECTS OF MEMBRANE WIDTH AND OF COCHLEAR SCALA GEOMETRY-TENSED MEMBRANES:

FIGURE S5



EFFECTS OF MEMBRANE TENSION: FIGURE 56



EFFECTS OF RUBBER MEMBRANE THICKNESS VARIATIONS:

FIGURE S7

These figures present some of the effects of changes of size and shape of model scalae, width variations of membrane slots, membrane thickness variations and some effects of tensing the model membranes, and a detailed discussion of each figure is unnecessary. However, figures S1 and T1 are discussed briefly in order to indicate how certain trends may be recognized. From Figure S1, it is at once clear that model C6, in test 15, responds to lower frequencies than do any of the other three models. This, however, is only true as regards place. Figure T1 shows that C6 and C8 both display a smaller maximum amplitude at the appropriate places than do models C5, or, particularly, C1.

Fig. T1 also shows that the amplitude response of C6 and C8 increases strongly for the highest frequencies, while the membrane amplitude maxima for C1 do not increase as frequency rises, but remain approximately equal to the stapes amplitude, still showing no sign of decreasing. Model C5, however, is unable to provide any amplitude response at all for frequencies greater than 400 Hz, even though, from Figure S1, there is ample space in the basal half of the model for a travelling wave envelope and amplitude maximum. Model C6, for example, despite its increasing amplitude response at 600 to 800 Hz, is prevented by place requirements from responding with an amplitude maximum to frequencies above 700 Hz. It is therefore apparent from Figures S1 and T1 that, even before making allowance for its over-machined membrane slot (see Figure Q1), model C1 is better suited than the other 3 models considered to a sustained response at high frequency, e.g., 1 kHz and above, whereas model C6 has the best-balanced low frequency response.

A very important point thus arises in examining and comparing the effects of geometric and component variations on cochlear model response; that both place and amplitude responses must be inspected. A model with an excellent amplitude relationship at some interpolated frequency but with no place for its

response, (or vice versa) must be considered to have an inadequate response at that frequency. Considering the ear's remarkable natural characteristics of adaption, such ill-conditioning of two functions of its response must be unlikely in nature.

Vc. Comments on Effects of Variables

1) Geometry.

The large-bore model, C5, invariably compares poorly with the other models, for although its response to low frequencies is reasonable, but ill conditioned, it does not respond at all to high frequencies. As is shown in Figures S1 and S2, the partition in the very wide basal half of this model seems to be impossible to stimulate. The small-bore models C4 and C6, particularly the latter, have a well matched amplitude and phase response at high frequencies, (see Figs. S4 and T4) and although the sectional area of the scalae of these two models is identical at the apical end, model C6 performs rather better at lowest frequencies.

This is an effect due to bore taper, the taper angle of the scalae of model C6 being the same as that for C2. In figures S1 and T1, S2 and T2 and S4 and T4, in all of which results for model C6 are involved, it is interesting to note that in each case the small model C6 performs most satisfactorily at low frequencies.

Model C2C, with a membrane slot of approximately twice the normal width, is compared with the "average" model C2A in figures S3 and T3, and in figure S5, and as is expected this model displays an excellent low frequency response, approaching about 5 Hz minimum frequency at the helicotrema. Model C2C is, however, unable to respond at frequencies above 500 Hz.

While the shaped model C1 compares well with other models at high frequencies, there is no very clear trend to be observed in comparing its

response with that of model C2, the design for which was intended to approximate to the model C1 design but without the basal-end scala vestibuli sectional constriction. In figure S3 the high frequency place response of model C2 is superior to C1, although when reference is made to both amplitude and place details for high frequencies, from figures R1, R2 and R10, it is seen that these two response characteristics are considerably better-conditioned for C1 than for C2, or for the other models. To summarize these comments concerning geometry and size, it appears from considerations of the very poor overall response of the large model, the somewhat truncated response of the straight model C8, and the fact that model C6 performed better than the smallest model C4 and best of all models in the low frequency range, that the best-conditioned and most extensive overall frequency response would have been obtained from a slightly smaller-bore version of the shaped model C1 (containing the correctly designed membrane slot width).

2) Rubber thickness.

Figures S7 and T7 show clearly the effect of rubber membrane thickness variations; the uniform membrane RM1, being thicker and therefore having higher elastic modulus in the apical region than the tapered RM4, did not permit either of models C8 or C6 to respond as well to low frequency stimuli as they did when fitted with the tapering membrane.

In the stapes region, although the thinner (RM1) membrane resulted in considerably larger amplitude ratios, the two models responded to higher frequencies with well-conditioned place and amplitude responses when fitted with the thicker but more elastic tapering membrane. Hence the apparent effect of a thicker, homogeneous membrane was not a mass effect but an increase in elasticity.

3) Rubber tension.

The trends discussed above involving comparisons between models were only

slightly changed by the test results for the three models which were fitted with pre-tensed membranes (compare figures S5 and S3). Figure S6 is rather surprising in that it shows a very much smaller shift of place of vibration amplitude maxima for tensed as against untensed membranes than might be expected from the imposition of such a relatively vast (6%) initial strain. However, as may be seen when figures R7 and R9 are compared, or R6 and R10, amplitudes of vibration of tensed model membranes are, particularly in the mid-frequency range, dramatically increased beyond amplitudes obtained using untensed membranes. This effect is, however, misleading, for similarly large vibration amplitudes could be obtained using better "tuned" untensed membranes with elastic properties more suited to the requirements of dynamic similarity.

Vd. Other Tests

Experiments similar in style and intention to those performed by Tonndorf were not attempted except for three simple tests, which are discussed below.

1) On switching the control panel power supply to the vibrator on and off, and at the same time observing through a microscope the motions of the membrane at the maximally responding section appropriate to the steady pure tone being applied, it was possible to obtain a rough idea of how much time elapsed between switch-on and the achievement of steady state vibration conditions of the membrane, and in what time all transients disappeared after switch-off. For a vibrator frequency of 100 cps., this time interval was certainly less than the writer's own manual response time of 0.2 secs., and was estimated at about 50 to 100 m.secs. The switched-on sound, being audibly generated by the vibrator and stapes, was recognized (and detected by an actual cochlea) before it was seen as a steady membrane motion, and if the model scaled frequency factor is

1/10, it would be expected that the corresponding time interval for the human cochlea, during which all cochlear transient response is dissipated, is about 5 to 10 m.secs. This figure seems to be reasonably in line with the neurological and subjective data available.

2) Various approximate step-function and impulse disturbances were applied to the stapes, firstly by means of an adjacently mounted, tightly compressed steel spring which was suddenly released, secondly by colliding the bob of a swinging pendulum with the stapes, and thirdly by flicking the stapes by hand. The last approach clearly generated a "travelling bulge" in the apical region of the model which displayed a maximum amplitude at the helicotrema, but it was more difficult to observe by eye the fast travelling wave which developed and was mainly dissipated in the basal half of the model following a very sharp impulse. It was intended to take photographs through the microscope of these transients, but this has not yet been done. Using these 12 times size models, with their necessarily greater time constants than the 4 times size models used by Tonndorf, it would be very instructive to design a similar series of cochlear time-analysis tests to his.

3) During several tests when the membrane amplitude response at one test frequency, f Hz, seemed to display a secondary peak at a section to which the membrane had already responded maximally when excited at frequency $2f$ Hz, (see figures R1, R2, R10, R11 and R12) it was concluded that harmonics were being generated mainly by membrane nonlinear mechanics within some models at the power intensity levels applied.

In order to make sure of this conclusion, and also to examine the effects of externally produced, simple complex sounds, on two occasions the outputs of two signal generators, each with separate amplifiers, were taken to the multiple input terminals of the control panel. With a 100 Hz signal and a

200 Hz signal, both of equal (and low) current exciting the vibrator and stapes, the complex travelling wave response was viewed with the stroboscope on manual control and was seen to match exactly the observations described by Tonndorf. Two clear peaks were observed; one at the section already proven to respond maximally to 200 Hz, and a second separate peak at the 100 Hz section. The microscope was focussed on some fine liquid-borne fibres of soft, shredded (toilet) paper which had been left in one model after cleaning, and these fibres displayed almost classic single-looped lissajous figures for fluid particle motions between the stapes and the 200 Hz stimulated membrane section. Between that section at the 100 Hz maximum amplitude station the fibres oscillated in elliptical orbits, and a little beyond the 100 Hz region there were no fluid movements.

This test, performed on models C1 and G2A during tests Nos. 2 and 1 greatly assisted in the recognition of internally-generated multiples of the applied fundamental signal.

These observations of model behaviour, showing that, especially for high sound intensities and large membrane displacements, the necessarily non-linear, vibrating partition not only generates its own harmonics but also performs a Fourier frequency analysis on the resulting complex signals, are particularly significant to a better understanding of some of the principal subjective phenomena of hearing.

VI. CONCLUSIONS

As it was suspected from the absence of any similar experimental accounts or data in the literature, the design, construction and testing of physical cochlear models to yield quantitative data is an arduous and difficult business, and assembling and interpreting the data satisfactorily can also become a formidable task. However, despite some disappointment with the limited degree of model partition membrane similarity which was obtained, the models performed well, and the experimental technique and apparatus, including the basic unit, the universal measuring machine/microscope, was a delight to use.

Detailed comments are included in the previous section, but other conclusions and observations pertinent to better comprehension of the nature of cochlear response, are enumerated below:-

- 1) Due to scalae fluid dynamics, the response of the apical end of the cochlea, that is, cochlear response to low frequencies, depends not only on the dynamics of the partition at the apical end but upon partition motion and response over the whole length of the cochlea.
- 2) The amplitude envelope defining the limits of vibratory motion of the cochlear partition at the basal end of the cochlea, i.e. for high frequencies, does not appear to be as sharply peaked as the envelope of the low frequency amplitude response, but is restricted to a considerably smaller region of activity along the cochlea.

Travelling wave motion in the basal region of the cochlea is at least as well developed as it is in the apical region, and together with the observation that the high frequency amplitude envelope is compressed compared with the response at low frequency, it follows that mechanical frequency discrimination at high frequencies is as sharp as for intermediate and lower frequencies.

- 3) Geometric variations have a profound effect on refined cochlear frequency

response, and it would seem that the mean shape and sectional dimensions of the human cochlea, after making allowance for the reduction in size of the two fluid ducts by membranous and ligament structures lining the inside of the bony labyrinth, and for a mean cochlea length of 3.5 cms., offer an optimum design for the amplitude and place frequency response it is required to perform.

4) In the sense of the Tonndorf experiments, simple tests also suggested that the cochlea is capable of performing an analysis on signals specified wholly by time, rather than by frequency. The ability of the cochlear models to perform a spatial Fourier frequency analysis on complex tones was demonstrated. This fact, and the ~~reals~~ of the cochlear hydrodynamics in this regard, is of supplementary benefit to the whole research programme, as the mathematical model has, up to the present, only been designed to analyse pure tones.

5) From considerations of the physical model test results, the degree of complete similarity obtaining in the models, and the trends of the results summary figures, it appears that the range of values for the variation of the elastic parameter $E.t$ (modulus of elasticity multiplied by membrane thickness) calculated in chapter 4 for the cochlear partition is very reasonable. It was clear, for example, that had the calculated value for partition $E.t$ at the stapes been modelled correctly instead of at $\frac{1}{3}$ rd of its theoretically similar value (see table 3 section II d.), high frequency model cochlear responses would have even more closely approached the scaled equivalent of the known upper frequency limit of the human cochlea. Also, as it was pointed out in discussing low frequency phase effects, a substantially greater range of model $E.t$ values in model cochlear partitions would have brought apical end results more in line with measurements recorded by Bekesy.

Model membrane response and damping effects indicated that human cochlea values for perilymph viscosity, on which the viscosity of the aqueous glycerol

solution was based, were consistent with other cochlear response and physical properties data.

6) Results of figure R11, for model C5, and particularly results for test no. 4, using model C2 with a tensed membrane, showed very clearly the effect of pure tone loudness increases on the travelling wave response of the cochlea at that frequency. Three principal effects of increased intensity, which all point very definitely to "hardening spring" membrane non-linearities, are:-

- (i) the point of maximum partition amplitude shifted towards the apical end
- (ii) the amplitude envelope became more "spread out" along the partition
- (iii) the sensitivity of the partition response, as measured by the ratio of partition amplitude to stapes amplitude, decreased.

As a result of this physical cochlear modelling research programme, it is considered worth designing further experiments and new models. Inclusion of a membranous labyrinth, or scala media, bounded by a flaccid membrane and an elastic membrane, should allow good matching of all dimensionless parameters in cochlear model design, and the influences of both the scala vestibuli sectional constriction, and the spiral, whorled form of the two scalae in the human cochlea could well be examined with new models. Model responses to acoustic transients and complex signals should also be investigated.

For the present, cochlear model results imply that mathematical model design should be based upon such the same values for cochlear partition mass and elasticity, perilymph density and viscosity, and scalae sectional areas and shapes as were used for the design of physical model properties.

VII REFERENCES

1. Zur Physiologie des Labyrinths. - Part 7 -
Die Erzeugung von Schallbildern in der Camera Acustica
J. R. Ewald
Pflug. Arch. ges. Physiol. vol. 93, 1903, pp. 485 - 500
- Also:
Bemerkungen zur Schallbildertheorie
Zentralbl. Physiol. vol. 28, 1914, p. 756
2. A note on the resonating system in the cochlea with demonstration of
a model illustrating the action of a hitherto neglected factor.
G. Wilkinson
Jnl. Physiol. 56, 1922, ii - iv.
3. The Mechanism of the Cochlea
G. Wilkinson and A.A. Gray
Macmillan and Co. Ltd., London, 1924.
4. Experiments in Hearing
G. von Békésy
McGraw Hill, New York, 1960.
5. Fluid Motion in Cochlear Models
J. Tonndorf
Jnl. Acoust. Socy. Am. 29, 1957, pp. 558 - 568.
6. Dimensional Analysis of Cochlear Models
J. Tonndorf
Jnl. Acoust. Socy. Am. 32, 1960, pp. 493 - 497.
7. Time/Frequency Analysis along the Partition of Cochlear Models
J. Tonndorf
Jnl. Acoust. Socy. Am. 34, 8, Sept. 1962, pp. 1337 - 1350.

8. **The Physics of the Ear.**
T. S. Littler
Pergamon. London. 1965.
9. **Observations through Cochlear Fenestra**
H. B. Perlman
Laryngoscope. 60, 1950, p. 77.
10. **Akustische Messungen an einem mechanischen Modell des Innenohres**
H. G. Diestel
Acustica. 4, 1954, p. 421.
11. **The Vestibular and Cochlear Aqueducts**
B. J. Anson et al.
3rd Sympos. on The Role of the Vestibular Organs in Space Exploration
N.A.S.A. SP - 152, 1967, pp. 125 - 196.
12. **An Explanation of the Travelling Wave Theory of Hearing**
R. Guelke
Med. & Biol. Eng., (Pergamon), 4, 1966, pp. 349 - 356.
13. **Theory of Hearing**
E. G. Wever
Wiley, New York, 1949.
14. **On the Dynamics of the Cochlea**
H. Fletcher
Jnl. Acoust. Socy. AM. 23, 6, Nov. 1951, pp. 637 - 645.
15. **A Dynamical Theory of the Cochlea**
L. C. Peterson and B. P. Bogert
Jnl. Acoust. Socy. Am. 22, 3, May 1950, pp. 369 - 381.
16. **Theorie Der Schneckenmechanik**
J. Zwislocki
Acta Oto-Laryng. Suppl. LXXII 1948.

17. **Tables of Physical and Chemical Constants**
 G. W. C. Kaye and T. H. Laby
 Longmans. London. 13th Edition, 1966.
18. **The Analytical Mechanism of the Internal Ear**
 T. Wrightson and A. Keith
 Macmillan. London. 1918.
19. **Physical Properties of the Labyrinthine Fluids and Quantification
 of the Phenomenon of Caloric Stimulation**
 R. W. Steer Jr. et al
 N.A.S.A. SP - 152, 1967, pp. 409 - 420.

MATHEMATICAL MODEL OF THE COCHLEA

Chapter 6

Contents

	Symbols	Page 1
	Assumptions	Page 3
I.	Equations of Fluid Motion	Page 5
II.	Fluid Boundary Conditions	Page 10
III.	Non Linear Partition Dynamics	Page 11
	Inertia	Page 11
	Damping	Page 12
	Stiffness	Page 12
	Equation of Partition Motion	Page 12
	Solution of Cubic Equation	Page 15
IV.	Numerical Solution of Differential Equations	Page 17
V.	Computer Programming	Page 19
VI.	Discussion of Results of Mathematical Model Computations	Page 22
VII.	References	Page 29

Appendix

I.	Rayleigh Motion of a Viscous, Oscillating Fluid	Page 30
----	----------------------------------------------------	---------

MATHEMATICAL MODELSymbols

t	time, secs.	
ω	circular frequency of excitation,	radians/sec.
f	cyclic frequency of excitation,	Hz
$A_1(x)$	cross sectional area of scala vestibuli at any section distant x cm from basal end	cm^2
$A_2(x)$	cross sectional area of scala tympani at any section distant x cm from basal end	cm^2
$b(x)$	width of basilar membrane (and of the single membrane whose stiffness, mass and damping represents that of the scala media) at any section distant x cm from basal end	cm
$m(x)$	effective mass per unit area of partition at section x	gm/cm^2
A_s	area of stapes footplate	cm^2
A_r	area of round window	cm^2
$P_1(x, t)$	instantaneous fluid pressure at section x and time t in scala vestibuli	dynes/cm^2
$P_2(x, t)$	instantaneous fluid pressure at section x and time t in scala tympani	dynes/cm^2
$D_1(x, t)$	fluid displacement in x direction at section x , time t , in scala vestibuli	cm/sec.
$D_2(x, t)$	fluid displacement in x direction at section x , time t , in scala tympani	cm/sec.
$P_e(x, t)$	instantaneous fluid pressure difference across scala media at section x , time t	dynes/cm^2
$D_e(x, t)$	instantaneous maximum displacement of the partition effective membrane from its mean position in the x direction at section x , time t .	cm/sec.

E_z	basilar membrane shape displacement factor, linking D_z to volumetric displacements	
ρ	density of perilymph	gm/cm ³
μ	dynamic viscosity of perilymph	c.g.s. poise
$D_s(t)$	instantaneous displacement of stapes footplate from its mean position at time t.	cm.
$H(x,s)$	Laplace s domain system transfer function	
a	speed of sound in perilymph	cm/sec.
j	$\sqrt{-1}$	
k	constant $k = 2\pi\rho\mu\omega$	
K1 to K9	constants	
$C(x)$	viscous damping coefficient of element of partition per unit surface area at section x	dynes sec/cm ³
$C_c(x)$	linear critical damping coefficient of element of partition per surface area at section x.	
$E(x)$	modulus of linear elasticity of partition effective membrane at section x.	dynes/cm ²
$t(x)$	effective thickness of basilar membrane and of partition effective membrane at section x.	cm.
$\alpha(x)$	a partition linear elasticity coefficient $\alpha = \frac{16 G(x)}{9m(x)}$	
$\beta(x)$	a partition non-linear elasticity coefficient $\beta = \frac{16 \psi(x)}{9m(x)}$	
$F(x)$	a partition excitation force coefficient $F = \frac{16 P_z(x) }{9m(x)}$	
G,H	components of F	
ϕ	angle by which partition response lags behind driving force F	radian
$\omega_3(x)$	a variable representing $\omega^2 - \alpha(x)$	
$G(x)$	partition linear pressure stiffness	dynes/cm ³
$\psi(x)$	partition non-linear pressure stiffness	dynes/cm ⁵

$c(x)$	a partition damping coefficient $c(x) = \frac{C(x)}{m(x)}$	
a	approximate partition response amplitude	cm.
A	square of a	-
y	function of A in equns. (32) and (35) or variable in illustrative equation (36) for numerical integration.	-
p, q	coefficients of a reference cubic equation, $y^3 + py + q = 0$	-
D	discriminant of the reference cubic equation	-
θ	angle involved in solving reference cubic equation	-
RP_1	real part of P_1	
IP_1	imaginary part of P_1	
θ_z	phase angle of P_z	radians
	phase of D_z relative to P_z	radians
ϕ	phase angle of D_z	radians
$P_s(t)$	instantaneous mean pressure of stapes footplate	dynes/cm ²
h	numerical solution interval length	cm.
f_1	numerical integration factors (equn. (39))	

Assumptions

Before writing the various equations for the cochlear mathematical model, the following assumptions are made.

1. planar compression and rarefaction waves exist in both scalae.
2. wave lengths in scalae are assumed long with respect to scala depths, i.e., shallow water waves are assumed to exist, and vertical fluid particle velocities are ignored.
3. the scala media may be regarded as a single partition geometrically identical to the basilar membrane, and as a large number of uncoupled, separate single degree of freedom elements.
4. scale bony walls are rigid, and fluids are Newtonian.
5. except in cases of intense excitation, fluid particle motion is sinusoidal when the cochlea is excited by a pure tone input.

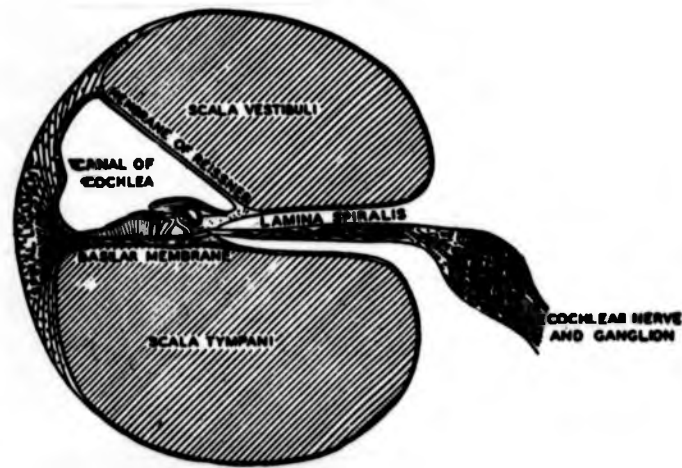


Figure 1a. Approximate sectional arrangement of cochlea, showing the cochlea canal, or scala media, which is represented in cochlear models as a single membrane partition

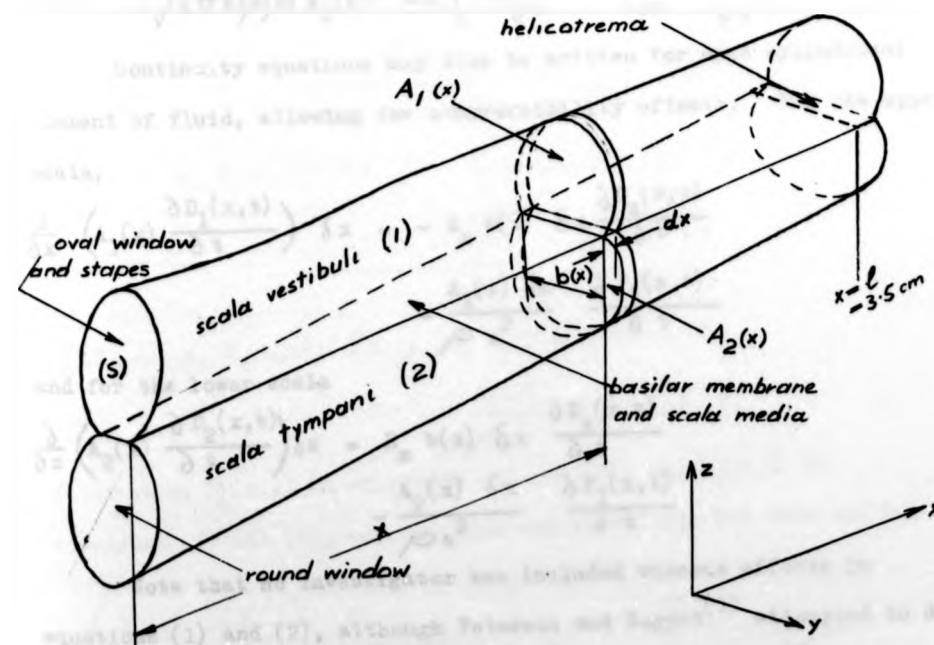
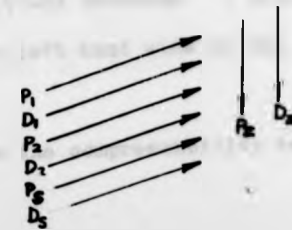


Figure 1 Idealized arrangement of the cochlea for mathematical model



I. EQUATIONS OF FLUID MOTION

Equations for forces acting on small cylindrical elements of fluid of length δx in each scala may be written (See Fig.1). For the scala vestibuli, three force terms are included; pressure, inertia and viscous forces (see appendix I to this chapter):

$$-A_1(x) \frac{\partial P_1(x,t)}{\partial x} \delta x - \rho A_1(x) \delta x \frac{\partial^2 D_1(x,t)}{\partial t^2} + \sqrt{2\pi\omega\rho\mu} A_1(x) \delta x \left(\frac{\partial D_1(x,t)}{\partial t} + \frac{1}{\omega} \frac{\partial^2 D_1(x,t)}{\partial t^2} \right) \quad (1)$$

and for the scala tympani

$$-A_2(x) \frac{\partial P_2(x,t)}{\partial x} \delta x - \rho A_2(x) \delta x \frac{\partial^2 D_2(x,t)}{\partial t^2} + \sqrt{2\pi\omega\rho\mu} A_2(x) \delta x \left(\frac{\partial D_2(x,t)}{\partial t} + \frac{1}{\omega} \frac{\partial^2 D_2(x,t)}{\partial t^2} \right) \quad (2)$$

Continuity equations may also be written for each cylindrical element of fluid, allowing for compressibility effects. For the upper scala,

$$\frac{\partial}{\partial x} \left(A_1(x) \frac{\partial D_1(x,t)}{\partial t} \right) \delta x - E_z b(x) \delta x \frac{\partial D_z(x,t)}{\partial t} - \frac{A_1(x) \delta x}{\rho a^2} \frac{\partial P_1(x,t)}{\partial t} \quad (3)$$

and for the lower scala

$$\frac{\partial}{\partial x} \left(A_2(x) \frac{\partial D_2(x,t)}{\partial t} \right) \delta x - E_z b(x) \delta x \frac{\partial D_z(x,t)}{\partial t} - \frac{A_2(x) \delta x}{\rho a^2} \frac{\partial P_2(x,t)}{\partial t} \quad (4)$$

Note that no investigator has included viscous effects in equations (1) and (2), although Peterson and Bogert⁽¹⁾ attempted to do so. Several investigators, including Klatt and Peterson⁽²⁾, wrote equations (1) and (2) erroneously, with the left hand side in the form

$$- \frac{\partial}{\partial x} (A P) \delta x$$

and only Fletcher⁽³⁾ and Bogert⁽¹⁾ included the compressibility term

in equations (3) and (4). According to his definition for D_z , Klatt^(2,4) also has a sign error in these latter two equations.

Assuming that at least in all hydrodynamic action the cochlear system is approximately linear, which assumption is certainly justifiable at low intensities, a system transfer function may be defined in Laplace transform notation:-

$$H(x,s) = \frac{D_z(x,s)}{D_z(s)}$$

and Laplace transform notation is used in the following working.

Equations (1) to (4) in the s domain, when initial conditions may be neglected, become:-

$$-\frac{\partial P_1(x,s)}{\partial x} \delta x = D_1(x,s) \left[\rho s^2 + (s + \frac{s}{\omega}) \sqrt{\frac{2\pi\omega\rho\mu}{A_1(x)}} \right] \delta x, \quad (5)$$

$$-\frac{\partial P_2(x,s)}{\partial x} \delta x = D_2(x,s) \left[\rho s^2 + (s + \frac{s}{\omega}) \sqrt{\frac{2\pi\omega\rho\mu}{A_2(x)}} \right] \delta x, \quad (6)$$

$$\begin{aligned} \frac{\partial}{\partial x} (A_1(x) \cdot D_1(x,s)) \delta x &= -E_z b(x) \cdot D_z(x,s) \delta x \\ &\quad - \frac{A_1(x)}{\rho a^2} \cdot P_1(x,s) \delta x, \end{aligned} \quad (7)$$

and

$$\begin{aligned} \frac{\partial}{\partial x} (A_2(x) \cdot D_2(x,s)) \delta x &= E_z b(x) \cdot D_z(x,s) \delta x \\ &\quad - \frac{A_2(x)}{\rho a^2} \cdot P_1(x,s) \delta x \end{aligned} \quad (8)$$

Eliminating $D_1(x,s)$ in equations (5) and (7), and $D_2(x,s)$ in equations (6) and (8), one equation may be written for each scala:-

$$\begin{aligned} \frac{\partial}{\partial x} \left(\frac{A_1(x) \frac{\partial P_1(x,s)}{\partial x} \delta x}{\left(\rho s^2 + (s + \frac{s}{\omega}) \sqrt{\frac{2\pi\omega\rho\mu}{A_1(x)}} \right) \delta x} \right) \delta x &= \frac{A_1(x)}{\rho a^2} P_1(x,s) \delta x \\ &= E_z b(x) D_z(x,s) \delta x \end{aligned} \quad (9)$$

$$\frac{\partial}{\partial x} \left(\frac{A_2(x) \frac{\partial P_2(x,s)}{\partial x} \delta x}{\left(\rho s^2 + \left(s + \frac{s^2}{\omega} \right) \sqrt{\frac{2\pi \omega \rho \mu}{A_2(x)}} \right) \delta x} \right) \delta x - \frac{A_2(x)}{\rho a^2} P_2(x,s) \delta x$$

$$= -E_z b(x) D_z(x,s) \delta x \quad (10)$$

It is not convenient to combine equations (9) and (10) in the manner done by Peterson and Bogert with simpler equations in which $A_1(x) = A_2(x)$, to give P^+ and P^- pressure variables describing longitudinal and transverse pressure propagation modes, where

$$P^+(x,s) = P_1(x,s) + P_2(x,s)$$

$$\text{and } P^-(x,s) = P_1(x,s) - P_2(x,s)$$

The few investigations which bear any comparison with the above approach up to this point have assumed identical scalae areas, and have usually attempted solutions for their very much simpler equations for one scale only. Klatt and Peterson assumed that $D_1(x,s) = -D_2(x,s)$ and that $P_1(x,s) = P_2(x,s)$ thereby eliminating P_2 and D_2 variables, and making $P_z(x,s)$ zero. It is not clear how such an approach can possibly be substantiated.

Equations (9) and (10) may now be rationalized, inserting $s = j\omega$ in order to limit considerations of the variables P_1 , P_2 and D_z to the steady state case of pure tone excitation at frequency ω . Note that a prime denotes differentiation with respect to x , for example,

$$\frac{dP}{dx} = P' \quad \text{and} \quad \frac{d^2P}{dx^2} = P''$$

and also that each of the variables P'' , P' , P and D_z is considered to be complex in time.

Hence if $k = 2\pi\omega\rho\mu$, equation (9) becomes

$$\left(\frac{A_1 P_1'}{\rho\omega^2 + \sqrt{\frac{k}{A_1}} \omega(1-j)} \right)' = -E_z b D_z - \frac{A_1 P_1}{\rho a^2}$$

$$\therefore \frac{A_1 P_1'' + P_1' A_1'}{\left(\rho\omega^2 + \omega\sqrt{\frac{k}{A_1}} \right) - j\omega\sqrt{\frac{k}{A_1}}} + \frac{\omega\sqrt{k}(1-j) A_1' P_1'}{2\sqrt{A_1} \left[\left(\rho\omega^2 + \omega\sqrt{\frac{k}{A_1}} \right) - j\omega\sqrt{\frac{k}{A_1}} \right]^2} =$$

$$= -E_z b D_z - \frac{A_1 P_1}{\rho a^2} \quad (11)$$

Let $K_1 = \rho\omega + \sqrt{\frac{k}{A_1}}$, $K_2 = \sqrt{\frac{k}{A_1}}$, and $K_3 = K_1^2 + K_2^2$

The left hand side of equation 11 then simplifies to

$$\begin{aligned} & \frac{(A_1 P_1'' + P_1' A_1')(K_1 + j K_2)}{\omega K_3} + \frac{A_1' P_1' K_2 (K_1^2 - K_2^2 + 2K_1 K_2)}{2 \omega K_3^2} \\ & \quad - \frac{j(K_1^2 - K_2^2 - 2K_1 K_2) K_2 A_1' P_1'}{2 \omega K_3^2} \\ & = \frac{A_1 (K_1 + j K_2)}{\omega K_3} \left[P_1'' + \frac{P_1' A_1'}{A_1} + \frac{P_1' A_1' K_2}{2 A_1 K_3^2} \left((K_1^2 - K_2^2 + 2K_1 K_2) \right. \right. \\ & \quad \left. \left. - j(K_1^2 - K_2^2 - 2K_1 K_2) \right) (K_1 - j K_2) \right] \\ & = \frac{A_1}{\omega (K_1 - j K_2)} \left[P_1'' + \frac{P_1' A_1'}{A_1} + \frac{P_1' A_1' K_2}{2 A_1 K_3} \left((K_1 + K_2) - j(K_1 - K_2) \right) \right] \\ & = \frac{A_1}{\omega (K_1 - j K_2)} \left[P_1'' + \frac{P_1' A_1'}{2 A_1 K_3} \left((2K_1^2 + K_1 K_2 + 3K_2^2) - j(K_1 K_2 - K_2^2) \right) \right] \end{aligned}$$

If variables P_1'' , P_1' , P_1 and D_z are now separated into positive real (in phase) and positive imaginary (in quadrature) components, for example, $P_1 = R P_1 + j I P_1$, then L.H.S. of equation (11) becomes

$$\frac{A_1}{\omega (K_1 - j K_2)} \left[R P_1'' + j I P_1'' + \frac{A_1'}{2 A_1 K_3} \left\{ R P_1' \left(3K_2^2 + 3K_1 K_2 + 2K_1 \rho\omega \right) \right. \right. \\ \left. \left. + I P_1' \cdot K_2 \rho\omega + j \left(I P_1' \left(3K_2^2 + 3K_1 K_2 + 2K_1 \rho\omega \right) - R P_1' \cdot K_2 \rho\omega \right) \right\} \right]$$

Additional "constants" K_4 to K_9 are now defined in order to simplify this expression and also equation (11). As these values of k and K_1 to K_9 are necessarily involved in the subsequent computer programmes, they are all listed together at this point so as to avoid future additional listings or definitions.

The L.H.S. of equation (11) thus becomes

$$\frac{A_1}{\omega (K_1 - j K_2)} \left[R P_1'' + j I P_1'' + R P_1' \cdot K_4 - I P_1' \cdot K_5 + j (I P_1' \cdot K_4 + R P_1' \cdot K_5) \right]$$

where $k = 2\pi\omega\rho\mu$

$$K1 = \rho\omega + \sqrt{\frac{k}{A}}$$

$$K2 = \sqrt{\frac{k}{A}}$$

$$K3 = K1^2 + K2^2$$

$$K4 = (3.K2^2 + 3K1.K2 + 2.K1.\rho.\omega) \frac{A'}{2A.K3}$$

$$K5 = -K2.\rho.\omega \frac{A'}{2A.K3}$$

$$K6 = \frac{\omega}{\rho a^2} K1$$

$$K7 = \frac{\omega}{\rho a^2} K2$$

$$K8 = \frac{E_b \omega}{A} K1$$

$$K9 = \frac{E_b \omega}{A} K2$$

Thus equation (11), for the scala vestibuli, becomes

$$\begin{aligned} R P_1'' + j I P_1'' = & - R P_1' K4 + I P_1' K5 + j(-I P_1' K4 - R P_1' K5) \\ & - R P_1' K6 - I P_1' K7 + j(-I P_1' K6 + R P_1' K7) \\ & - R D_z K8 - I D_z K9 + j(-I D_z K8 + R D_z K9) \end{aligned} \quad (12)$$

As there must exist equality even in a second order differential equation both between real components and between imaginary components, equation (12) for the scala vestibuli may be written as two separate equations (13) and (14). Hence, for scala vestibuli, using A_1 and A_1' values in the K terms above, equations (9), (11) and (12) give

$$R P_1'' = - R P_1' K4 + I P_1' K5 - R P_1' K6 - I P_1' K7 - R D_z K8 - I D_z K9 \quad (13)$$

and

$$I P_1'' = - I P_1' K4 - R P_1' K5 - I P_1' K6 + R P_1' K7 - I D_z K8 + R D_z K9 \quad (14)$$

Similarly, for the scala tympani, using A_2 and A_2' values in the K terms above, equation (10) gives

$$R P_2'' = - R P_2' K4 + I P_2' K5 - R P_2' K6 - I P_2' K7 + R D_z K8 + I D_z K9 \quad (15)$$

$$I P_2'' = - I P_2' K4 - R P_2' K5 - I P_2' K6 + R P_2' K7 + I D_z K8 - R D_z K9 \quad (16)$$

Note that equations (13), (14), (15) and (16) comprise four simultaneous second order differential equations.

II. FLUID BOUNDARY CONDITIONS

At the basal end of the scala vestibuli, i.e., at the stapes, it is assumed that

$$D_s(t) A_s = D_1(o,t) A_1(o) \quad (17)$$

and that

$$P_1(o,t) = P_s \quad (18)$$

and also, from equation (1), that

$$P_1'(o,t) = \rho \omega^2 D_1(o,t) \quad (19)$$

At the round window, the following approximate continuity relationship for the whole cochlea, which does not take account of perilymph compressibility, is assumed:-

$$D_s(t) A_s = D_2(o,t) A_2(o) \quad (20)$$

$$\text{i.e. } D_2(o,t) = \frac{D_1(o,t) A_1(o)}{A_2(o)}$$

From equation (2), it is also assumed that

$$P_2'(o,t) = \rho \omega^2 D_2(o,t) \quad (21)$$

The relationship between round window displacement and pressure is not known. It is probably non-linear, but the acoustic impedance of the round window membrane alone, which separates the air of the tympanum from the cochlear fluids, must be very small compared with that of the whole cochlea. Although the assumption is not critical, assume

$$P_2(o,t) = 0 \quad (22)$$

The helicotrema may be modelled as a distal end condition where the following relationships apply:-

$$D_1(3.5,t) A_1(3.5) = - D_2(3.5,t) A_2(3.5) \quad (23)$$

and, neglecting fluid frictional pressure losses through the capillary-bore helicotrema opening in cases where $D_1(3.5,t)$ is not zero,

$$P_1(3.5,t) = P_2(3.5,t) \quad (24)$$

$$\left. \begin{aligned}
 \text{and } P_1'(3.5, t) &\approx \rho \omega^2 D_1(3.5, t) \\
 \text{and } P_2'(3.5, t) &\approx \rho \omega^2 D_2(3.5, t) \\
 \text{i.e. } P_1'(3.5, t) &= -P_2'(3.5, t) \frac{A_2(3.5)}{A_1(3.5)}
 \end{aligned} \right\} \quad (25)$$

It becomes apparent that it is difficult to apply basal end boundary conditions simultaneously with apical end conditions. In the numerical methods of solution which follow, these boundary conditions are viewed rather as initial value conditions, and only by a fully iterative method can conditions at both ends be simultaneously satisfied, principally because neither sets of end conditions are complete. For example, in equations (17) and (18), the relationship in both phase and amplitude between $P_1(o, t)$ and $D_1(o, t)$, which would define the input impedance of the entire cochlea (and largely solve the problem of dynamical response) is not known, although chapter 2 offers some approximate (and unreliable) Bekesy experimental data by which to estimate the order of oval window input impedance at various frequencies.

The most powerful initial value conditions are probably those pertaining to the helicotrema, particularly the cochlear model experimental conditions also noted by Bekesy⁽²⁾ that for all but lowest frequencies $D_1(3.5, t)$, $D_2(3.5, t)$ and $D_z(3.5, t)$ are all zero.

III. NON LINEAR PARTITION DYNAMICS

Inertia

For a membranous partition of width b , deflecting in sectional view according to the relationship suggested in chapter 3, i.e.,

$$s = y^3 - b y^2$$

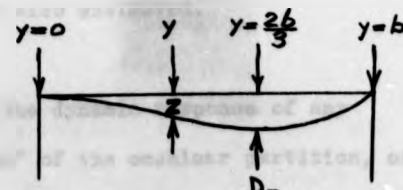


FIGURE 2

(see adjacent figure 2)

it is clear that the maximum deflection at any section, D_z , occurs when the distance $y = \frac{2}{3}b$, giving $D_z = \frac{4b^3}{27}$. From this relationship it may also be shown that the total inertia force on a section of full width b and length δx of such a membrane, having an effective mass per unit surface area, m , at any particular section, is:-

$$\text{inertia force} = \frac{9}{16} m b \delta x \frac{d^2 D_z}{dt^2}.$$

that is, $9/16$ of the area and mass of that element of membrane of length δx and occupying the full width of the intact membrane may be considered as accelerating with the point on the membrane subject to the maximum amplitude and acceleration of that section.

Damping

As each small element of area of the membrane is associated with the disturbance of a particular volume of viscous liquid, membranes and cells etc. in the scala media, and the motion of a large area of membrane must induce proportionately larger viscous damping forces than the motion of a smaller area at the same section, a viscous damping coefficient C per unit area is defined. Consequently the total damping force on a "slice" of the partition may also be considered as acting upon $9/16$ of the area of the non-uniform velocity membrane when the force is calculated on the basis of the maximum velocity of the partition at that section.

$$\text{That is, viscous force} = \frac{9}{16} C b \delta x \frac{dD_z}{dt}$$

Stiffness

The relationship, partition deforming pressure = $\bar{\sigma} D_z + \Psi D_z^3$ was derived in chapter 4, where the linear and non-linear pressure stiffness, $\bar{\sigma}$ and Ψ respectively, were also estimated.

Equation of Partition Motion

The general equation describing the dynamic response of any (independent from its neighbours) "slice" of the cochlear partition, of small length δx , at any section distant z cm. from the stapes where the

various "constants", m, b, C, ϵ, ψ , and $P_z(t) = P_1(t) - P_2(t)$ are known

$$\text{is } \frac{9}{16} m b \delta x \ddot{D}_z + \frac{9}{16} C b \delta x \dot{D}_z + \epsilon b \delta x D_z + \psi b \delta x D_z^3 \\ = P_z(t) b \delta x \quad (26)$$

If we now let $c = \frac{C}{m}$, $\alpha = \frac{16}{9} \frac{\epsilon}{m}$

$$\beta = \frac{16}{9} \frac{\psi}{m} \text{ and } F = \frac{16}{9m} |P_z|$$

then if ω is the circular frequency of (approximately) sinusoidal motion and excitation of the element of membrane, and ϕ is the angle by which the response $D_z(t)$ lags behind the exciting pressure differential $P_z(t)$,

$$\ddot{D}_z + c \dot{D}_z + \alpha D_z + \beta D_z^3 = F \cos(\omega t + \phi) \\ = A \cos \omega t - B \sin \omega t \quad (27)$$

where $F^2 = A^2 + B^2$, $\cos \phi = \frac{A}{F}$ and $\sin \phi = \frac{B}{F}$

After much searching for, and many attempts to use other methods it was decided that in view of the requirement of the digital computer numerical solution for equations (13) to (18) for rapid access to solutions to equation (27), the approximate method of Duffing was the most satisfactory means by which to solve the above second order cubic differential equation. A number of interesting order calculations and conditional tests, including the establishment of various relationships between the variables, including a non-linear "critical" damping constant as a function of ω, F, α and β , were performed on Duffing's equation. However, these calculations were not found to have any relevance to the problem in hand except for very large amplitudes, and may be published at another time.

As a first approximation, take

$$D_{z1} = a \cos \omega t,$$

giving

$$\left(\frac{3}{4} a^3 \beta - a \omega^2 + \alpha a\right) \cos \omega t - c a \omega \sin \omega t + \frac{a^3 \beta}{4} \cos 3\omega t \\ = G \cos \omega t - H \sin \omega t \quad (28)$$

Therefore, approximately,

$$H = c a \omega$$

$$\text{and } G = \frac{3}{4} a^3 \beta - a \omega^2 + \alpha a$$

$$\text{and } F^2 = \left(\frac{3}{4} a^3 \beta - a \omega^2 + \alpha a \right)^2 + c^2 a^2 \omega^2 \quad (29)$$

$$\text{and } \phi = \sin^{-1} \left(\frac{c a \omega}{F} \right) \quad (30)$$

$$= \cos^{-1} \left(\frac{\frac{3}{4} a^3 \beta - a \omega^2 + \alpha a}{F} \right)$$

When the amplitude a is small, the $\cos 3 \omega t$ term in equation (28) may be ignored. The value of D_{z_2} arising for use as a second approximation is apparently

$$D_{z_2} = a \cos \omega t + \frac{a^3 \beta}{36 \omega^2} \cos 3 \omega t$$

and this and other approximations finally yield a wave form approaching that of a truncated sine wave or trapezoid for higher intensity excitations.

Considering the first approximation to element amplitude, a , to be perfectly adequate for most sound intensity levels, it remains necessary to solve equation 29, which contains a to the power 6. Expanded,

equation 29 becomes

$$\frac{9}{16} a^6 \beta^2 + a^2 (\alpha - \omega^2)^2 + \frac{3}{2} a^4 \beta (\alpha - \omega^2) + c^2 \omega^2 a^2 = F^2$$

Substituting $A = a^2$, this equation becomes a cubic in A :-

$$A^3 - \frac{8}{3} \frac{(\omega^2 - \alpha)}{\beta} A^2 + \frac{16}{9} \left[\frac{\omega^2 c^2 + (\omega^2 - \alpha)^2}{\beta^2} \right] A - \frac{16 F^2}{9 \beta^2} = 0 \quad (31)$$

The A^2 term is removed by use of the substitution

$$A = y + \frac{8}{9} \frac{(\omega^2 - \alpha)}{\beta} \quad (32)$$

giving the rationalized cubic equation (32)

$$y^3 - \frac{16}{27 \beta^2} \left[(\omega^2 - \alpha)^2 - 3 \omega^2 c^2 \right] y + \frac{128}{9^3 \beta^3} \left[(\omega^2 - \alpha)^3 + 9 \omega^2 c^2 (\omega^2 - \alpha) \right] - \frac{16 F^2}{9 \beta^2} = 0 \quad (33)$$

Applying Descartes rule of signs to equations (29), (31) and (32), and remembering that for real solutions of a , A must be positive, it is clear that there may be either three or one real positive solutions for A .

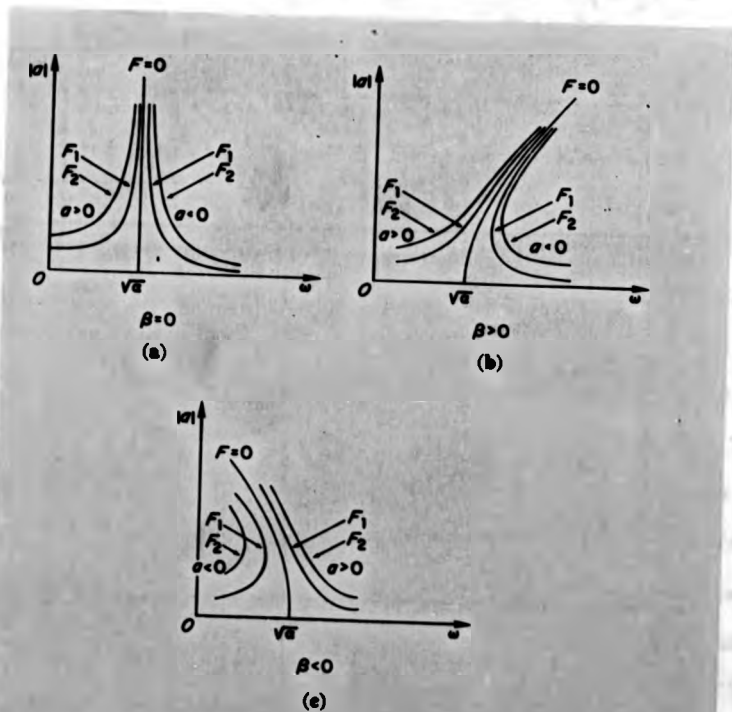


Figure 6-3 Three families of response curves for equation 6-34 (page 6-15).
 (a) refers to the linear case when $\beta = 0$, when $F = 0$, F_1 and F_2 , where $F_1 < F_2$.
 (b) and (c) refer to non-linear systems (without damping). (b) refers to a hard spring where $\beta > 0$ and (c) to a soft spring where $\beta < 0$.

The sign taken by \underline{a} for each the derivation of equation () a simple cubic in \underline{a} :-

$$\frac{3}{4} \underline{a}^3 - (\omega^2 - \alpha) \underline{a}$$

Figure 3 very convenient equation (34) for both $\beta =$ offers only one real root, and $\omega > \sqrt{\alpha}$, the value of the alternative two roots a unique root of \underline{a} is the one approaches zero as ω incre

When damping is incl that it may be concluded th off near to the curve $F = 0$ if damping is not large, a jump from a response of hi change of phase, as frequ $\sqrt{\alpha}$. Thus in the damped always positive provided t to estimate phases.

Solution of Cubic Equation

Equation (33) may b tested conditional approac Compare equation (33) with

$$y^3 + py + q = 0.$$

The discriminant, D , of th

$$D = \left(\frac{p}{3}\right)^3 + \left(\frac{q}{2}\right)^2$$

Hence for equation 33, it

The sign taken by \underline{a} for each of these is made clear by consideration of the derivation of equation (29) when no damping is present, which becomes a simple cubic in \underline{a} :-

$$\frac{3}{4} a^3 \beta - (\omega^2 - \alpha) a = F \quad (34)$$

Figure 3 very conveniently shows the graphical solution of equation (34) for both $\beta = 0$ and $\beta > 0$. Clearly, when the equation offers only one real root, \underline{a} is positive, and when all three roots are real, and $\omega > \sqrt{\alpha}$, the value of \underline{a} having the greatest modulus is positive, and the alternative two roots are negative. Then the (negative) mechanically unique root of \underline{a} is the one having the smallest modulus, and which approaches zero as ω increases.

When damping is included figure 3 remains appropriate, except that it may be concluded that the former response curves are rounded off near to the curve $F = 0$ instead of being asymptotic to it. Also, if damping is not large, at some frequency $\omega > \sqrt{\alpha}$, the system must jump from a response of high amplitude \underline{a} to minimum amplitude \underline{a} , with a change of phase, as frequencies are increased from zero through and beyond $\sqrt{\alpha}$. Thus in the damped case of equation (29) \underline{a} may be considered always positive provided that equations (30) are used carefully in order to estimate phases.

Solution of Cubic Equation Approximation

Equation (33) may be solved for all cases by the following well-tested conditional approach:

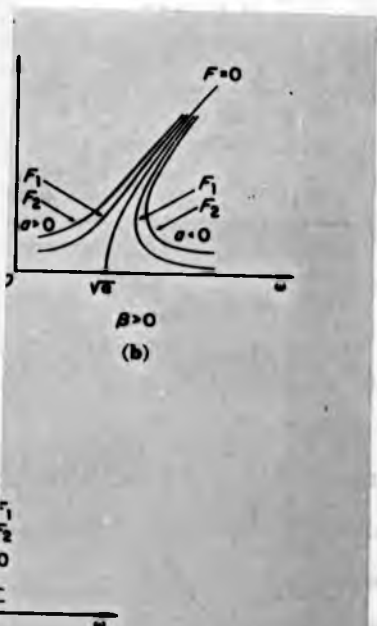
Compare equation (33) with the identical cubic equation

$$y^3 + py + q = 0.$$

The discriminant, D , of this equation is

$$D = \left(\frac{p}{3}\right)^3 + \left(\frac{q}{2}\right)^2$$

Hence for equation 33, its discriminant is



miles of response curves
tion 6-34 (page 6-15).
a linear case when $\beta = 0$,
and F_2 , where $F_1 < F_2$.
r to non-linear systems
(b) refers to a hard
0 and (c) to a soft
0.

$$D = -\left\{ \frac{16}{81\beta^2} \left[(\omega^2 - \alpha)^2 - 3\omega^2\alpha^2 \right] \right\}^3 + \left\{ \frac{64}{9^3\beta^3} \left[(\omega^2 - \alpha)^3 + 9\omega^2\alpha^2(\omega^2 - \alpha) \right] - \frac{8\beta^2}{9\beta^2} \right\}^2$$

Case 1 $D = 0$; 3 real roots, 2 being equal

$$y = -2 \left(\frac{\alpha}{2}\right)^{\frac{1}{3}}, \left(\frac{\alpha}{2}\right)^{\frac{1}{3}}, \left(\frac{\alpha}{2}\right)^{\frac{1}{3}}$$

Case 2 $D < 0$; 3 real and distinct roots

$$y = 2 \left(\frac{-p}{3}\right)^{\frac{1}{3}} \cos\left(\frac{\theta}{3}\right), 2 \left(\frac{-p}{3}\right)^{\frac{1}{3}} \cos\left(120^\circ \pm \frac{\theta}{3}\right)$$

$$\text{where } \cos \theta = \left(\frac{-q}{2}\right) \left(\frac{-3}{p}\right)^{\frac{1}{2}}$$

Case 3 $D > 0$; 1 real root and 2 conjugate imaginary roots

(a) $p > 0$

$$y = 2 \left(\frac{p}{3}\right)^{\frac{1}{3}} \sinh\left(\frac{\theta}{3}\right), \left(\frac{p}{3}\right)^{\frac{1}{3}} \left[-\sinh\left(\frac{\theta}{3}\right) \pm j\sqrt{3} \cosh\left(\frac{\theta}{3}\right) \right]$$

$$\text{where } \sinh \theta = \left(\frac{-q}{2}\right) \left(\frac{3}{p}\right)^{\frac{1}{2}}$$

(b) $p < 0, q > 0$

$$y = -2 \left(\frac{-p}{3}\right)^{\frac{1}{3}} \cosh\left(\frac{\theta}{3}\right), \left(\frac{-p}{3}\right)^{\frac{1}{3}} \left[\cosh\left(\frac{\theta}{3}\right) \pm j\sqrt{3} \sinh\left(\frac{\theta}{3}\right) \right]$$

$$\text{where } \cosh \theta = \left(\frac{q}{2}\right) \left(\frac{-3}{p}\right)^{\frac{1}{2}}$$

(c) $p < 0, q < 0$

$$y = 2 \left(\frac{-p}{3}\right)^{\frac{1}{3}} \cosh\left(\frac{\theta}{3}\right), \left(\frac{-p}{3}\right)^{\frac{1}{3}} \left[-\cosh\left(\frac{\theta}{3}\right) \pm j\sqrt{3} \sinh\left(\frac{\theta}{3}\right) \right]$$

$$\text{where } \cosh \theta = \left(\frac{-q}{2}\right) \left(\frac{-3}{p}\right)^{\frac{1}{2}}$$

All cases above yielding real roots were programmed for the computations which follow, although it was later realized that for the estimated range of values for β , the most likely values for partition damping were too large to permit the case for $D \leq 0$.

Having calculated the root y , amplitude a was determined from equation (32), giving

$$a = \left[y + \frac{8}{9} \left(\frac{\omega^2 - \alpha}{\beta} \right) \right]^{\frac{1}{3}} \quad (35)$$

$$\text{As } P_1 = RP_1 + j IP_1 \text{ and } P_2 = RP_2 + j IP_2$$

$$\therefore P_z = RP_z + j IP_z \\ = (RP_1 - RP_2) + j (IP_1 - IP_2)$$

\(\therefore\) Relative to some datum phase angle, the phase angle of P_z ,

$$\theta_z = \tan^{-1} \frac{I P_z}{R P_z}$$

But γ = angle by which membrane response at any section lags behind the driving force P_z at that section.

\(\therefore\) $\phi = \gamma + \theta_z$ = membrane response phase angle at any section relative to the datum phase angle, i.e.,

$$D_z = |D_z| e^{j(\phi + \omega t)}$$

Note that θ_z is the phase angle of P_z at any section relative to some initially defined phase, which, when working from the stapes end and using conditions of P_1, P_2, P_1', P_2' etc. local to $x = 0$ as initial values, may be zero phase angle for the stapes driving pressure P_s or may be zero phase angle for stapes displacement D_s , or a zero reference phase angle need not be defined for either of these cases provided that phase relationships between P_s and D_s are considered sensibly.

The same situation applies when numerical computations commence from the apical end, where for example, fluid displacements $D_1(3.5, t)$ or $D_2(3.5, t)$ (and therefore $P_1'(3.5, t)$ or $P_2'(3.5, t)$) may be given zero or some other reference phase angle, relative to which the phase variations of all variables at all sections may be calculated.

IV. NUMERICAL SOLUTION OF DIFFERENTIAL EQUATIONS

The most widely used, accurate interpolative approach for numerical solution of first-order differential equations is the Runge-Kutta method, which uses terms up to the fourth derivative. The same method may be used for a second-order differential equation, when the equation is split up into two first-order equations. Or, instead of using the Runge-Kutta method for second-order equations, a more direct approach by Nystrom, given

in Grove⁽⁵⁾, may be used. The equation in x and y of the form

$$y'' = f(x, y, y')$$

is appropriate for the Nystrom method, and values of x, y and y' at an initial point must be known.

$$\text{Consider } y'' = f(x, y, y') \quad (36)$$

$$\text{Then } y_{m+1} = y_m + hy'_m + \frac{h^2(f_1 + f_2 + f_3)}{6} \quad (37)$$

$$\text{and } y'_{m+1} = y'_m + \frac{h(f_1 + 2f_2 + 2f_3 + f_4)}{16} \quad (38)$$

$$\begin{aligned} \text{where } f_1 &= f(x_m, y_m, y'_m) \\ f_2 &= f\left(x_m + \frac{h}{2}, y_m + \frac{hy'_m}{2} + \frac{h^2 f_1}{8}, y'_m + \frac{h f_1}{3}\right) \\ f_3 &= f\left(x_m + \frac{h}{2}, y_m + \frac{hy'_m}{2} + \frac{h^2 f_1}{8}, y'_m + \frac{h f_2}{2}\right) \\ f_4 &= f\left(x_m + h, y_m + hy'_m + \frac{h^2 f_3}{2}, y'_m + hf_3\right) \end{aligned} \quad (39)$$

Starting with initial values x_m, y_m, y'_m and an interval length h (which may be changed after any interval in the calculation) the values f_1, f_2, f_3 and f_4 are calculated in turn, and values for y_{m+1} and y'_{m+1} for the beginning of the following interval are calculated. The shorter the interval length the higher the accuracy, but a reasonable value for h can easily be discovered to provide adequate accuracy particularly when h can be readily changed in different regions. It was originally intended to use the automatic error analysing and interval changing technique of Merson, given by Lance⁽⁶⁾, but for simultaneous second order differential equations the slowness of the method outweighs the advantages.

Note that in the case of the simultaneous second order differential equations (13) and (14) in P_1, P_1', P_1'' and x , and (15) and (16) in P_2, P_2', P_2'' and x where y in equation (36) is replaced by P_1 or P_2 , the above Nystrom method, summarized by equations (37), (38), and (39), is not straightforward. Simultaneous values of P_1 and P_2 must be applied via equations (29) to (33) to provide a value for D_g , and the variable

D_z must be considered as part of the x function in equation (36), and must constitute the value of D_z (or x) appropriate to the values of P and P' (or y and y') already forming initial values in equations (39). Note that had the Nystrom method not been used, the Runge-Kutta method would have necessitated the solving of eight simultaneous first order differential equations.

V. COMPUTER PROGRAMMING

Being written in basic A.S.A. Fortran, the mathematical cochlear model computer programmes (as included in the rear pocket of the thesis) are fairly readily comprehensible and do not require a phrase by phrase explanation.

For the sake of clarity the following list defines the variables used in computer programming.

<u>Programme Identifier</u>	<u>Section</u>	<u>Variable</u>
F	MP	Frequency H_z
C	"	speed sound a
EB	"	factor E_z
U	"	viscosity μ
RHO	"	density ρ
K	"	No. of intervals
H	"	Length of intervals, h
B	"	width of basilar membrane b
ET	"	dynes/cm. E_t
W	"	radians/sec. ω
T2	"	τ
PIR etc.	"	$RP_1(x,s)$
PIU etc.	"	$IP_1(x,s)$
PI2R etc.	"	$RP_2'(x,s)$
PI2U etc.	"	$IP_2'(x,s)$
X	"	x

<u>Programme Identifier</u>	<u>Section</u>	<u>Variable</u>
IR	MP	$R D_z(x, s)$
DU	"	$I D_z(x, s)$
PHI etc.	"	ϕ
FIR etc.	"	$R f_1$
FIU etc.	"	$I f_1$
F2R4 etc.	"	$R f_4$
F2U4 etc.	"	$I f_4$
PIR	"	$R P_z(x, s)$
PDU	"	$I P_z(x, s)$
A1	Sub.1	$A_1(x)$
AI1	"	$A_1'(x)$
S	Sub.2	$m(x)$
Q	"	$o(x)$
Z	"	$\beta(x)$
A	"	$\alpha(x)$
F	"	F
AMP	"	$ D_z $
A - A1 or A2	Sub.3	$A_1(x)$ or $A_2(x)$
C1 to C9	Subs. 3 & 1	K1 to K9
C10	Sub.3	k

MP refers to main programme, in which important constants and physical properties are allocated to identifiers, initial conditions are set for the Nystrom numerical integration along the cochlea, intervals selected and the actual interpolative solution of hydro-dynamic differential equations is achieved. In other subsequent phrases and lines, calculated values are normalised and the print-out format of data specified.

Sub.1 refers to the first subroutine, labelled CALC, in which the f_1 values for equations (37) to (39) are directly calculated from the four simultaneous second order differential equations (13) to (16).

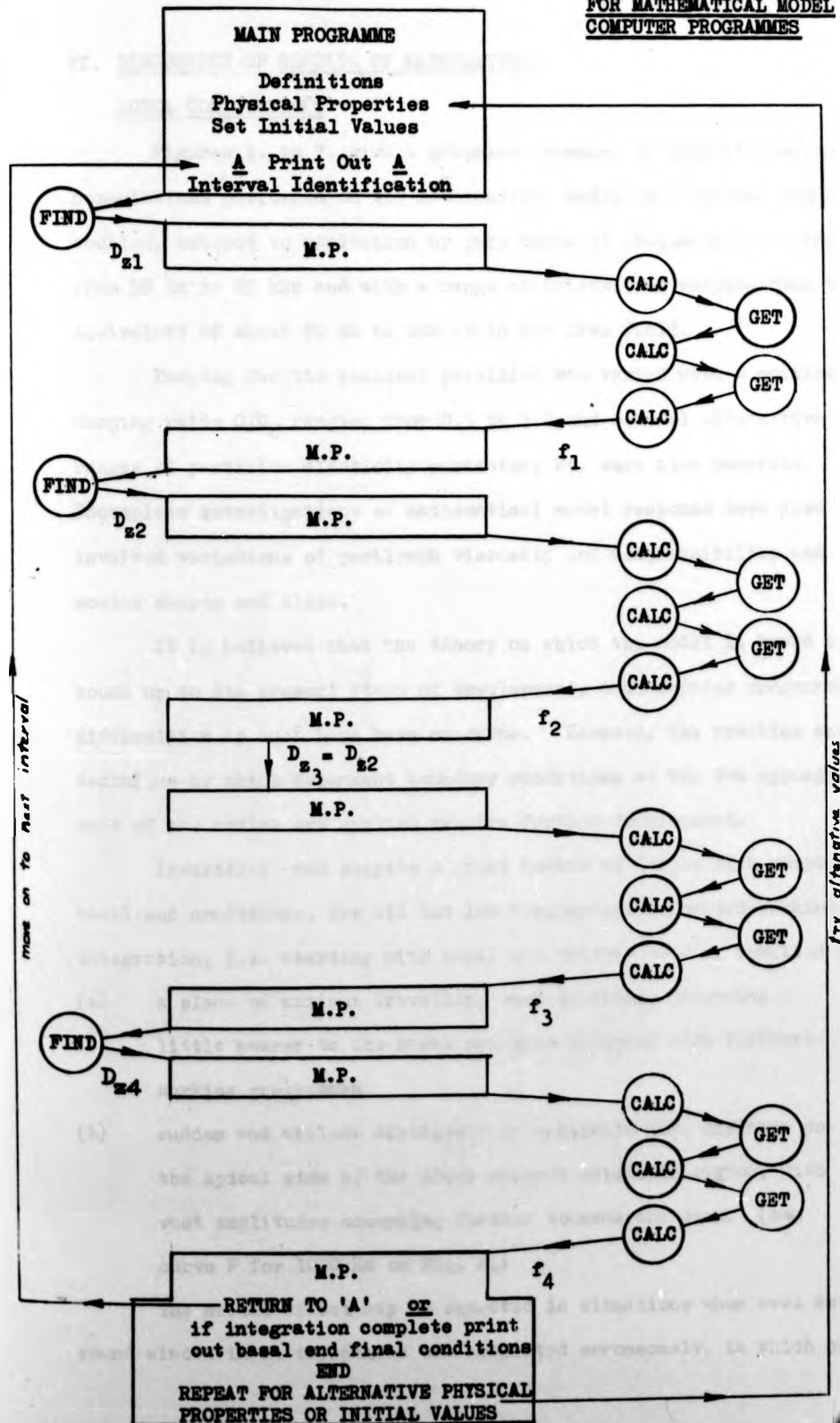
Sub.3 labelled "SUBROUTINE GET" refers to the third subroutine, which calculates the "constants" K1 to K9 used in SUBROUTINE CALC.

Sub.2. in which most of the early programming errors were located, is labelled SUBROUTINE FIND and in this subroutine the complete formation of and solution to the non linear, cubic, second-order differential equation for partition dynamic response and its cubic equation simplification using Duffing's solution is carried out. A modified flow chart describes the functioning of the computer programme.

It will be appreciated that the development of this type of solution to cochlear dynamics, and the trials of a large number of combinations of physical parameters and initial value conditions necessitated many variations in computer programmes.

Programmes can generally be divided into two types; those taking initial conditions at the stapes, in which case several alternatives for input impedance details must be included, and those working from the helicotrema towards the basal end, in which case the signs of $A'_1(x)$ and $A'_2(x)$ must be reversed. The illustration programme included in the rear pocket is of the latter type, and this approach, although not necessarily yielding required pressure-displacement relationships at the stapes end, was found to be considerably more stable than the "forward-working" programme approach. The "backward-working" type of numerical integration programme also differed from the alternative stapes-commencing type of solution by being largely insensitive to ill-conditioned initial values.

**MODIFIED FLOW CHART
FOR MATHEMATICAL MODEL
COMPUTER PROGRAMMES**



VI. DISCUSSION OF RESULTS OF MATHEMATICAL

MODEL COMPUTATIONS

Figures 4. to 7. give a graphical summary of typical results of computations performed on the mathematical model of a typical human cochlea, subject to excitation by pure tones of frequencies ranging from 50 Hz to 20 kHz and with a range of intensities varying from the equivalent of about 40 db to 140 db in the free field.

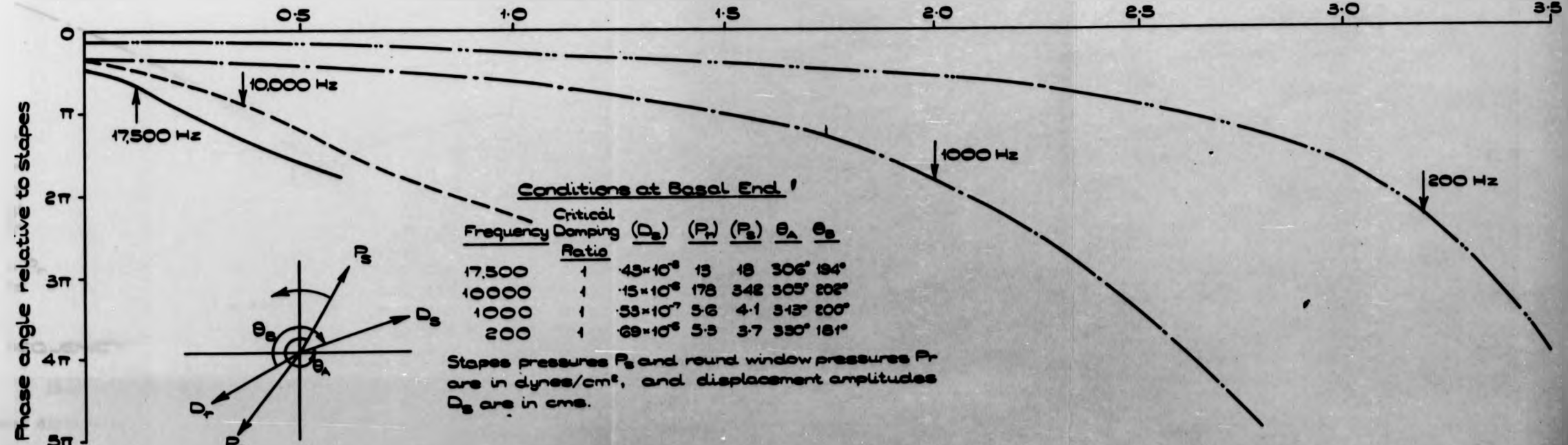
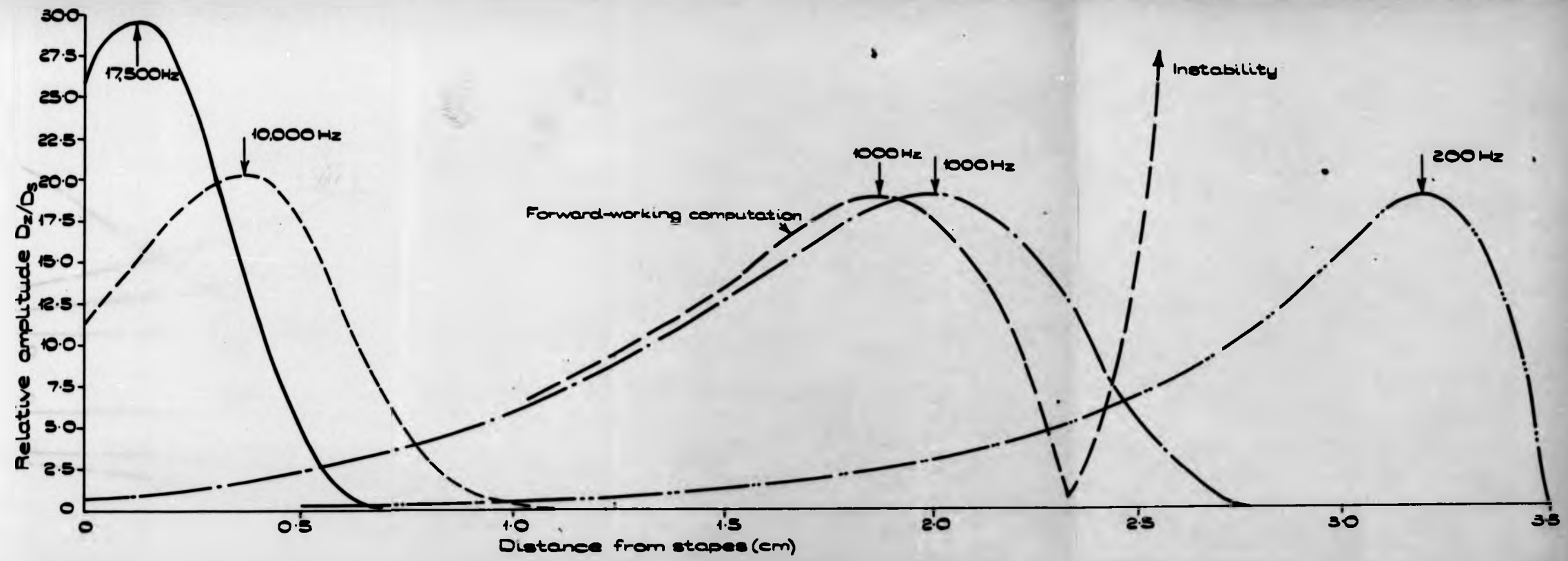
Damping for the cochlear partition was varied with a critical damping ratio C/C_0 ranging from 0.5 to 3.0 and several alternative ranges of partition elasticity parameter, E_t , were also inserted. Incomplete investigations of mathematical model response have also involved variations of perilymph viscosity and compressibility and scalae shapes and sizes.

It is believed that the theory on which the model is based is sound up to its present stage of development, and computer programming difficulties as such have been overcome. However, the practice and technique by which dependent boundary conditions at the two opposite ends of the scalae are applied require further development.

Invariably, and despite a great number of trials with varying basal end conditions, for all but low frequencies a forward-working integration, i.e. starting with basal end initial values, resulted in

- (a) a place of maximum travelling wave amplitude occurring a little nearer to the basal end than happened with backward-working programmes.
- (b) sudden and violent divergence of amplitude some distance on the apical side of the above maximum amplitude region, with vast amplitudes occurring further towards the apex. (see curve F for 1000 Hz on Fig. 4.)

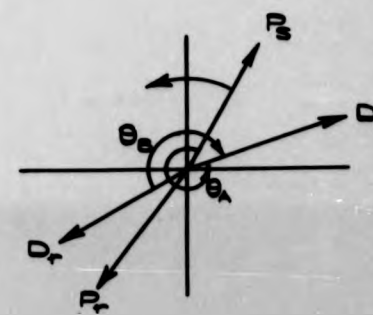
The second effect may be expected in situations when oval and round window in-ut impedances are estimated erroneously, in which case



Conditions at Basal End

Frequency	Critical Damping Ratio	(P_r)	(P_s)	θ_A	θ_B
17,500	1	45×10^6	13	18	$306^\circ 194'$
10,000	1	15×10^6	178	342	$305^\circ 202'$
1,000	1	53×10^7	5.6	4.1	$313^\circ 200'$
200	1	69×10^6	5.3	3.7	$350^\circ 181'$

Stapes pressures P_s and round window pressures P_r are in dynes/cm², and displacement amplitudes D_s are in cms.



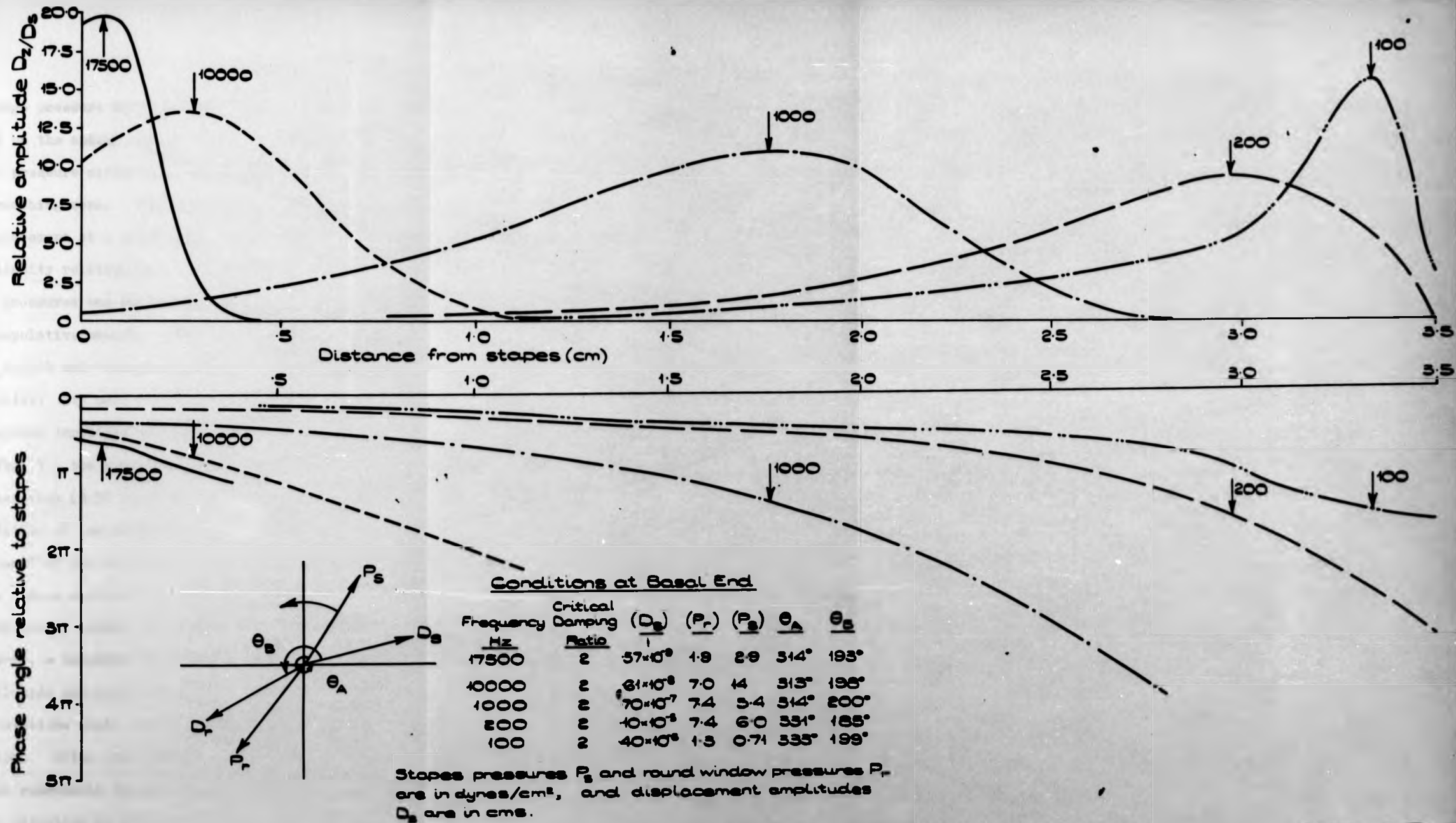
MATHEMATICAL MODEL RESPONSE AS A FUNCTION OF FREQUENCY.

Figure 4

Relative amplitude D_z/D_s

Phase angle relative to stapes

These dif
so sets o
Phase Rel
P1



MATHEMATICAL MODEL RESPONSE AS A FUNCTION OF FREQUENCY.

Figure 5

There has not been time either to investigate these difficulties, but a great deal has been learned from the 100 or so sets of useful mathematical model response data.

Phase Relationships

Figs. 4 and 5 permit a comparison of the relationship between the stapes and distance along the cochlea

a large pressure difference may remain between the two scalae at an area on the apical side of the appropriate amplitude envelope where both pressure differences and absolute scalae pressures should be approaching zero. Such a situation generates an appreciable partition displacement at a phase angle likely to disturb equilibrium in the continuity relationship, resulting in additional fluid displacements and pressures and sudden instability in the Nystrom-Runge Kutta interpolative method. This situation does not arise when working from the apical end towards the stapes. However, despite excellent stability with such backwards-working computations, it is probable that resulting amplitude envelopes are not always accurate. For example, in Fig. 7., the backwards-computations took initial values not at the helicotrema (3.50 cms.) but at 3.35 cms., in order to simulate a condition of low intensity of excitation (and consequently diminished "spread" of the amplitude envelope) at 200 Hz. Resulting envelopes were indeed sharper than those shown in the result (Fig. 6.) for a considerably louder 200 Hz tone for the same damping conditions. However, a secondary bulge has appeared which distorts the expected basal-side envelope curvature. In addition, backwards-working computations quite naturally present a real pressure at the round window. Often this exceeds the amplitude of the oval window pressure, which represents the driving pressure applied by the stapes footplate. This situation is not inadmissible mathematically, but neither is it representative of the physical situation.

There has not been time either to investigate fully or to correct these difficulties, but a great deal has been learned from the 100 or so sets of useful mathematical model response data.

Phase Relationships

Figs. 4 and 5 permit a comparison of the relationship between membrane phase lag relative to the stapes and distance along the cochlea

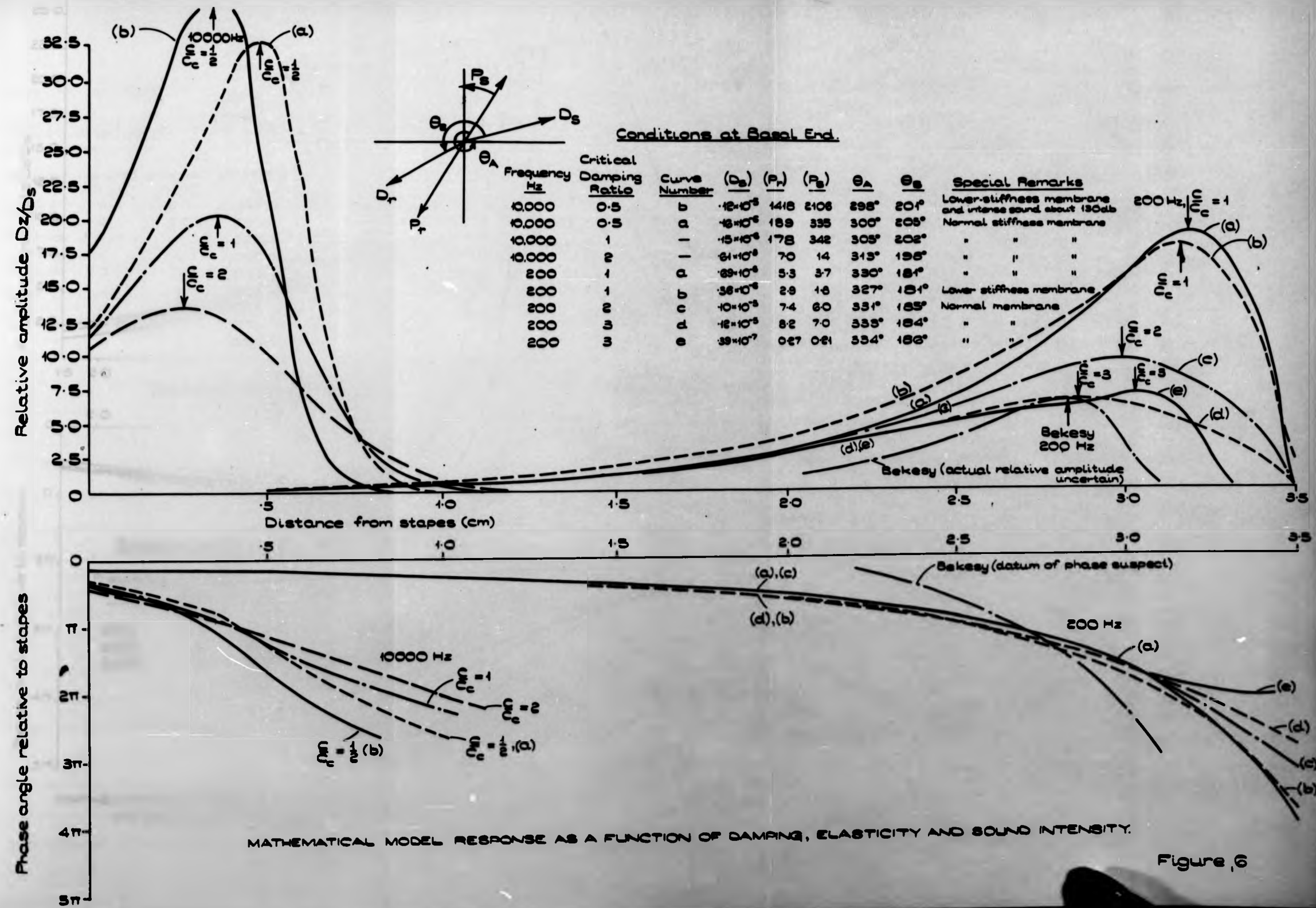
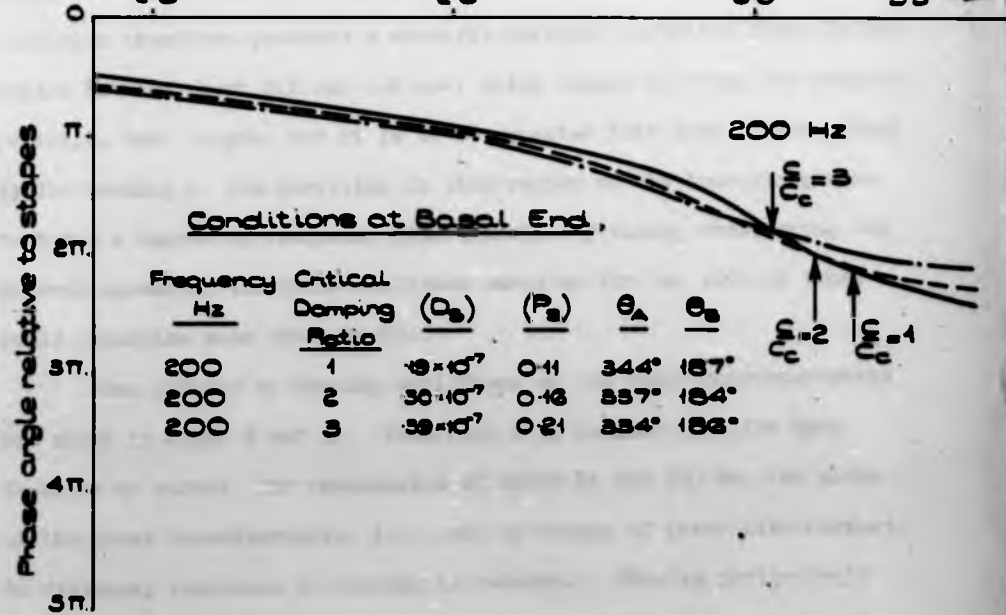
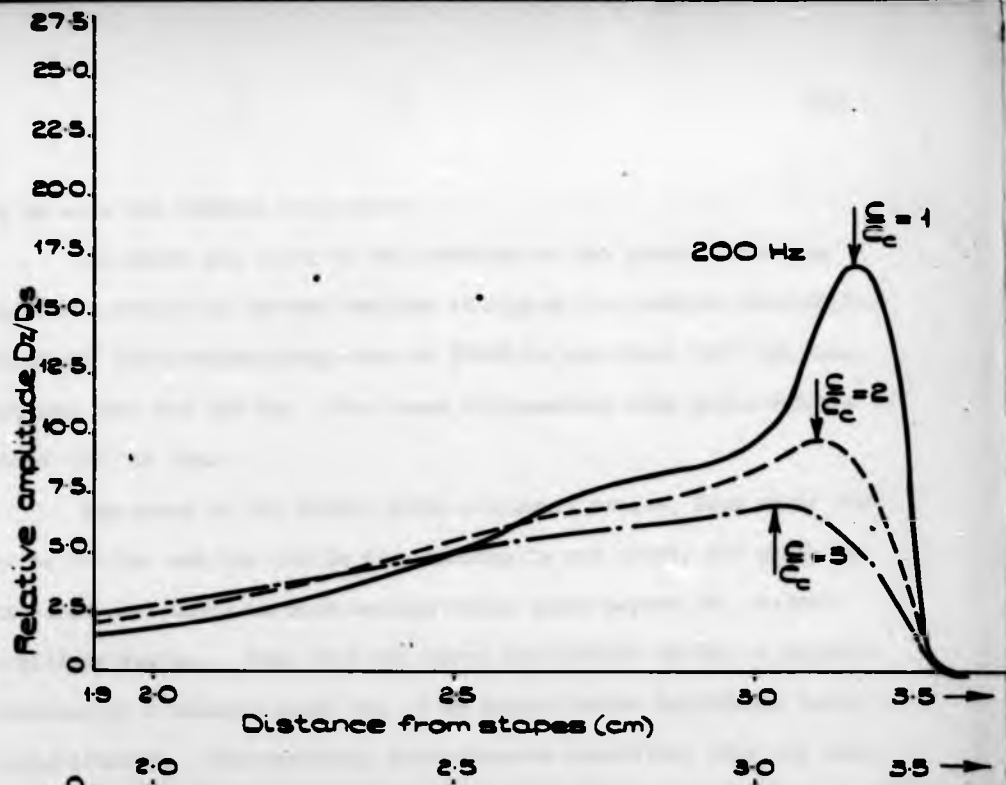


Figure 6



MATHEMATICAL MODEL RESPONSE TO QUIET SOUNDS (200 HZ AT 40 db) AS A FUNCTION OF DAMPING.

Figure 7

to be made for various frequencies.

The phase lag angle of the membrane at the place of maximum amplitude evidently becomes smaller at higher frequencies, approaching about 45° for a stimulating tone of 20000 Hz and about 360° for tones between 1000 and 200 Hz. For lower frequencies, this angle reduces to about 180° or less.

For tones in the middle audio-frequency ranges, from about 2000 Hz to 500 Hz, and for 200 Hz when damping is not great, the phase vs distance plot shows an increasingly steep slope beyond the maximum amplitude region. Note that the curve for 1000 Hz in Fig. 4 rapidly descends to a maximum phase lag of $2\frac{1}{2}$ cycles before amplitudes become insignificant. The resulting instantaneous travelling wave for this condition therefore presents a strongly deformed partition shape in the region between about 2.2 and 2.6 cms. which always contains one complete partition wave length, and it is to be expected that such intense local cyclic bending of the partition in this region of the travelling wave restores a degree of frequency discriminability which, considering the general spread of the whole amplitude envelope for the 1000 Hz tone, would otherwise seem unattainable.

Some effects of damping variations on the phase characteristics are shown in Figs. 6 and 7. From Fig. 6 it is seen that for both families of curves, for frequencies of 10000 Hz and 200 Hz, the slope of the phase characteristic, i.e. rate of change of phase with respect to distance, increases as damping is reduced. This is particularly illustrated in Fig. 6, but is less noticeable in Fig. 7, where sound excitation intensities are smaller.

Thus it appears, from considerations of hair cell and organ of Corti cilia shearing actions, that reduced scala media viscous damping properties, which result in increased rate of change of phase characteristics and increased phase lag angles, improve the potential

of the organ to discriminate frequency. Comparison of Figs. 6 and 7 for the 200 Hz case also permits a second important conclusion to be drawn that associated with "spread" of the amplitude envelope upon exposure of the cochlea to higher intensity tones there is also a compensating "improvement" of the phase vs distance characteristic, at least for lower frequency tones.

Intensity and Amplitude Relationships

The first and most obvious observation that may be made concerning the shape of partition amplitude envelopes is that the place of maximum amplitude becomes more sharply defined as damping is decreased and as sound excitation intensity is also reduced.

Within the limited range of intensity variations for which pure tones of any one frequency have as yet been tested upon the theoretical model, little dependence of relative amplitude of the partition at the place of maximum amplitude upon intensity has been noted. Further computations are expected to reveal a non-linear maximum relative amplitude vs sound intensity characteristic, particularly as sounds in excess of about 110 db are admitted to the model.

Except for very high audio-frequency sounds, critical damping ratios of one half, unity, two and three resulted in maximum partition to stapes amplitude ratios of about 32, 20, 12 and 7 respectively. Inspection of the results included in Figs 4 to 7 and of the remaining computer results invariably shows that while relative amplitudes do display a gentle increase as sound frequencies are increased from 200 Hz towards 8000 to 10000 Hz, above this frequency the relative amplitude envelope rises rapidly. The maximum relative amplitude for sounds of 17500 Hz rises to a value of 50 for a critical damping ratio of 0.5, and to 30 and 20 for damping ratios of 1.0 and 2.0 respectively.

These values seem to be greatly in excess of the very approximate values of partition relative amplitude somewhat tentatively implied by

von Békésy⁽⁷⁾, but well within the range suggested by Boyle & Johnstone⁽⁹⁾, from their experiments conducted on cochlear partition amplitudes in the region of the stapes. Two relative amplitude values have been named by these latter authors, albeit with no great confidence, namely 25 and 50.

It is very difficult to deduce any comparative data concerning elasticity, damping, phase, or relative amplitude from the quantitative partition response data of von Békésy. His data for 200 Hz is considered to be the most reliable of his (low frequency only) response results, and it is only as regards the amplitude envelope shape and place, and the shape and slope of the phase plot that this result constitutes genuine experimental data. Other data by Békésy (see chapter 2, section IIIa(2)) implies a maximum relative amplitude value of 2 for 200 Hz cochlear stimulation, but this value is considered to be several times too small and the amplitude envelope for this result is included in Fig. 6 with a maximum relative amplitude set arbitrarily at 7.5. Note also that it is known that human cochleas tested and examined by Békésy were subject to relatively intense pure-tone excitations.

The shape of the envelope for this Békésy experimental result for 200 Hz compares, in Fig. 6, best with the curve (e), for critical damping ratio of 3 for a relatively low intensity sound. The place of this amplitude maximum also suggests high damping coefficients, if it is assumed that the theoretical model partition elasticity and stiffness relationships are correct. On the other hand, the Békésy phase plot has a shape and slope appropriate only to intense excitation of a lightly damped partition. This latter evidence, whose implications concerning mathematical model physical properties conflicts with former deductions made about damping from considerations of the amplitude envelope shape, seems powerful enough to allow the conclusions that:

- (a) the apical end of the cochlea is not very heavily damped, and is probably subject to a critical damping coefficient of between 0.5 and 1.0.

von Békésy⁽⁷⁾, but well within the range suggested by Boyle & Johnstone⁽⁹⁾, from their experiments conducted on cochlear partition amplitudes in the region of the stapes. Two relative amplitude values have been named by these latter authors, albeit with no great confidence, namely 25 and 50.

It is very difficult to deduce any comparative data concerning elasticity, damping, phase, or relative amplitude from the quantitative partition response data of von Békésy. His data for 200 Hz is considered to be the most reliable of his (low frequency only) response results, and it is only as regards the amplitude envelope shape and place, and the shape and slope of the phase plot that this result constitutes genuine experimental data. Other data by Békésy (see chapter 2, section IIIa(2)) implies a maximum relative amplitude value of 2 for 200 Hz cochlear stimulation, but this value is considered to be several times too small and the amplitude envelope for this result is included in Fig. 6 with a maximum relative amplitude set arbitrarily at 7.5. Note also that it is known that human cochleas tested and examined by Békésy were subject to relatively intense pure-tone excitations.

The shape of the envelope for this Békésy experimental result for 200 Hz compares, in Fig. 6, best with the curve (e), for critical damping ratio of 3 for a relatively low intensity sound. The place of this amplitude maximum also suggests high damping coefficients, if it is assumed that the theoretical model partition elasticity and stiffness relationships are correct. On the other hand, the Békésy phase plot has a shape and slope appropriate only to intense excitation of a lightly damped partition. This latter evidence, whose implications concerning mathematical model physical properties conflicts with former deductions made about damping from considerations of the amplitude envelope shape, seems powerful enough to allow the conclusions that:

- (a) the apical end of the cochlea is not very heavily damped, and is probably subject to a critical damping coefficient of between 0.5 and 1.0.

- (b) mathematical model partition stiffness at the section about 3.0 cm. from the stapes is higher than that obtaining in the cochlea (a conclusion also borne out by the proximity of the response envelope for the 100 Hz tone (Fig. 5) to the helicotrema, in a place more appropriate to the 50 Hz tone).
- (c) mathematical model partition stiffness gradient towards the apical end is smaller than that obtaining in the cochlea (a conclusion also supported by a comparison of the place vs frequency relationship obtained by Bekesy for low frequency tones)(see chapter 2. Figs. 2-2, 2-3 and 2-6).

From the high frequency results of Figs. 4, 5 and 6, it is reasonable to conclude that at the basal end of the cochlea the critical damping coefficient also lies between about 0.5 and 1.0; that is, this damping coefficient is approximately constant throughout the cochlea. Being based upon a viscous damping coefficient per unit area of the basilar membrane surface, and applying to the whole scala media whose internal geometry does not vary greatly from the basal to the apical end, it would be assumed to a first approximation that the degree of damping is indeed uniform. The slight amount of medical and experimental evidence available also suggests that intact amplitude envelopes for partition response to frequencies up to about 25 kHz should be evident at the basal end, and therefore it is suggested that the stiffness of the mathematical model partition is not large enough at the stapes end.

Note that in Fig. 6 curve b for 10 kHz and curve b for 200 Hz are both computed for the trial case of a lower partition elasticity, when, instead of the relationship

$$E_t = 160000 - 40000 \times \text{dynes/cm.}$$

the following relationship was employed:-

$$E_t = 100000 - 20000 \times \text{dynes/cm.}$$

The effect of the latter relationship on the place of the 10 kHz amplitude

envelope was to move the whole curve only 1 millimeter basal-wards despite the 37% decrease in elasticity and stiffness of the partition in this region. At the same time the maximum amplitude of the partition was increased and the phase plot significantly steepened.

The effect of the new elasticity relationship on the 200 Hz response curves (for C/C_0 of unity) was also examined. Note that the value of Δt occurring at the place of maximum amplitude was practically the same (35000 dynes/cm.) as in the former case, so that any effect on responses in this region was to be primarily a function of local stiffness gradient rather than the local absolute value of stiffness. The decrease in gradient is some 33% which does not appear to have much effect at the maximum amplitude region but it has resulted in a generally broader, less sharply defined envelope.

Figures 4 to 7 also contain a tabulation of basal end oval and round window conditions for each test. The angle θ_B , giving the lag of round window motions behind oval window movements, is never exactly 180° , as would be expected with incompressible fluid, but for most frequencies is about 20° more than π radians. Note that for lower frequencies (about 200 Hz) the angle θ_B approaches closely to 180° , while for a frequency of 17500 Hz, when the distance from the round and oval windows to the place of maximum partition amplitude is only about a millimeter, the angle θ_B remains as high as 193° . The angle between the vectors (in time) representing P_s and P_r , the stapes and round window oscillating pressures, was always close to π radians.

Another effect which is apparently confusing from consideration of single-degree-of-freedom vibrating systems, but which may be reconciled with the mechanics of travelling wave-producing systems, is summarized by the values calculated for the angle θ_A , which gives the lag of the forward motion amplitude of the stapes and oval window, D_s , behind the stapes driving force P_s . This angle varies from about -60° (300° to 315°)

at highest frequencies to -20° (330° to 340°) at low frequencies.

Further decisions and discussions concerning the mathematical model and its results are to be found in the concluding chapter.

VII. REFERENCES

1. **A Dynamical Theory of the Cochlea**
L.C.Peterson and B.P.Bogert
Jnl.Accoust.Socy.Am. Vol 22. May 1950. No. 3. pp 369-381
 2. **Re-examination of a Model of the Cochlea**
D.H.Klatt and G.E.Peterson
Jnl.Accoust.Socy.Am. Vol.40. Jan 1966. No.1. pp 54-61
 3. **On The Dynamics of the Cochlea**
H.Fletcher
Jnl.Accoust.Socy.Am. Vol 23. 1951. No.6. pp 637-645
 4. **Theories of Aural Physiology**
D.Klatt
Univ.Mich.Commun.Sci.Lab.Rept. No.13. Nov.1964
 5. **Brief Numerical Methods**
W.E.Grove
Prentice-Hall Inc. N.J. 1966
 6. **Numerical Methods for High Speed Computers**
G.N.Lance
Iliffe and Sons Ltd. London 1960
 7. **Experiments in Hearing**
G.von Békésy
McGraw-Hill. N.Y. 1960
 8. **The Theory of Sound Vol.II**
Lord Rayleigh
Macmillan. London 1940
 9. **Basilar Membrane Vibration Measured with the Mossbauer Technique**
A.J.F.Boyle and B.M.Johnstone
Science Vol 158. Oct. 1967. pp 389-390
-

APPENDIX I RAYLEIGH MOTION OF A VISCOUS, OSCILLATING FLUID

The terms used to allow for viscous effects in liquids moving or oscillating with respect to a solid boundary, or vice versa, in the force or rate of change of momentum equations, are derived below. This derivation is based upon (and expands upon) the treatise by Rayleigh⁽⁸⁾.

Consider a general viscous fluid field in an x, y, z , space in which a solid, infinite plane yz executes simple harmonic vibrations in the y direction parallel to itself. Let the fluid velocity at any point (x, y, z) be $\bar{w} = \bar{i} u + \bar{j} v + \bar{k} w$, and assume that u and w components of velocity are zero, giving velocity variations $\bar{w} = \bar{j} v$ which are functions of x only.

From first principles, if $\rho X dV$, $\rho Y dV$ and $\rho Z dV$ are impressed forces acting on an element of mass ρdV , and X is an acceleration function or body force per unit mass in the x direction, then, neglecting all shearing or viscous effects, the equation of equilibrium is

$$dp = \rho (X dx + Y dy + Z dz)$$

where dp is a variation in pressure corresponding to changes dx , dy and dz in the co-ordinates x , y and z of the point at which pressure is estimated.

Using D'Alembert's principle, equations of motion may be written replacing X by $X - \frac{Du}{Dt}$, where $\frac{Du}{Dt}$ is the Lagrangian, substantive acceleration of the fluid particle considered:-

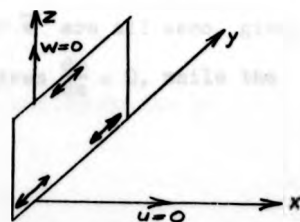
$$\frac{Du}{Dt} = \frac{du}{dt} + u \frac{du}{dx} + v \frac{du}{dy} + w \frac{du}{dz}$$

$$\frac{Dv}{Dt} = \frac{dv}{dt} + u \frac{dv}{dx} + v \frac{dv}{dy} + w \frac{dv}{dz} \text{ etc.}$$

Hence, with no friction or viscous effects,

$$\frac{dp}{dx} = \rho \left(X - \frac{Du}{Dt} \right)$$

$$\frac{dp}{dy} = \rho \left(Y - \frac{Dv}{Dt} \right) \text{ etc.}$$



When frictional force terms are added, and the three complete Navier-Stokes equations are combined into one vectorial equation, we have

$$\rho \frac{D\bar{w}}{Dt} = \rho \bar{F} - \text{grad } p + \mu (\nabla^2 \bar{w} + \frac{1}{3} \text{grad div } \bar{w})$$

where $\bar{F} = \bar{i} X + \bar{j} Y + \bar{k} Z$

For the x direction only, the Navier equation gives

$$\rho \left(\frac{Du}{Dt} - X \right) + \frac{dp}{dx} - \mu \nabla^2 u - \frac{1}{3} \mu \frac{d}{dx} \left(\frac{du}{dx} + \frac{dv}{dy} + \frac{dw}{dz} \right) = 0$$

and for the y direction,

$$\rho \left(\frac{Dv}{Dt} - Y \right) + \frac{dp}{dy} - \mu \nabla^2 v - \frac{1}{3} \mu \frac{d}{dy} \left(\frac{du}{dx} + \frac{dv}{dy} + \frac{dw}{dz} \right) = 0$$

and similarly for the z direction.

If body forces are not considered and $\bar{F} = 0$, then the first of these three equations, for which $\frac{Du}{Dt}$, X , $\nabla^2 u$ and $\text{div } \bar{w}$ are all zero, gives $\frac{dp}{dx} = 0$. The third equation for the z direction gives $\frac{dp}{dz} = 0$, while the second, for which $\frac{Dv}{Dt}$ is zero by definition, gives

$$\rho \frac{Dv}{Dt} - \mu \nabla^2 v = 0$$

which in turn may be simplified to give the basic relationship describing Rayleigh motion in viscous liquids:-

$$\frac{\partial v}{\partial t} = \frac{\mu}{\rho} \frac{\partial^2 v}{\partial x^2}$$

Case 1 Consider the case where $v(x,t)$ is complex. Try $v(x,t) = V(x) T(t)$ where $v(x,t)$, $V(x)$ and $T(t)$ all have both real and imaginary parts, and try

$$T(t) = e^{i\omega t} \quad \text{where } i = j = \sqrt{-1}$$

$$\text{Then } \frac{\partial v}{\partial t} = V(x) i\omega e^{i\omega t} = i\omega v$$

$$\text{and } \therefore \frac{\partial^2 v}{\partial x^2} = \frac{i\omega\rho}{\mu} v$$

for which a general solution $V(x)$, which must have real and imaginary parts is

$$V(x) = A e^{-mx} + B e^{mx}$$

$$\text{where } m^2 = \frac{i\omega\rho}{\mu} \text{ and hence } m = \sqrt{\frac{i\omega\rho}{2\mu}} (1 + i)$$

Now if $V(x) \rightarrow 0$ as $+x \rightarrow +\infty$, then $B = 0$

$$\therefore v(x,t) = A e^{(-\sqrt{\frac{i\omega\rho}{2\mu}})x} e^{-i(\sqrt{\frac{i\omega\rho}{2\mu}})x} e^{i\omega t}$$

$$= A e^{-\left(\frac{\omega \rho}{2\mu}\right)x} \left[\cos(\omega t - \sqrt{\frac{\omega \rho}{2\mu}} x) + i \sin(\omega t - \sqrt{\frac{\omega \rho}{2\mu}} x) \right]$$

$$\therefore \frac{\partial v(x,t)}{\partial x} = A \left(-\sqrt{\frac{\omega \rho}{2\mu}} \right) e^{-\left(\frac{\omega \rho}{2\mu}\right)x} e^{i\omega t} e^{-\left(\frac{\omega \rho}{2\mu}\right)x} (1+i)$$

$$\text{and } \frac{\partial v(x,t)}{\partial t} = A e^{-\sqrt{\frac{\omega \rho}{2\mu}} x} e^{i(\omega t - \left(\frac{\omega \rho}{2\mu}\right)x)} i \omega$$

Therefore, on the yz boundary,

$$v(0,t) = A (\cos \omega t + i \sin \omega t)$$

$$\text{and } \frac{\partial v(0,t)}{\partial x} = A \left(-\sqrt{\frac{\omega \rho}{2\mu}} \right) (\cos \omega t + i \sin \omega t) (1+i)$$

$$= v(0,t) (1+i) \left(-\sqrt{\frac{\omega \rho}{2\mu}} \right)$$

$$\text{and } \frac{\partial v(0,t)}{\partial t} = A i \omega (\cos \omega t + i \sin \omega t)$$

$$= v(0,t) i \omega$$

$$\text{Hence } \frac{\partial v(0,t)}{\partial x} = \left(-\sqrt{\frac{\omega \rho}{2\mu}} \right) (v(0,t) + \frac{1}{\omega} \frac{\partial v(0,t)}{\partial t})$$

Therefore, tangential force per unit of area acting on the yz plane due to relative fluid oscillations is

$$\tau = \mu \frac{\partial v(0,t)}{\partial x}$$

$$\therefore \tau = -\sqrt{\frac{1}{2} \omega \rho \mu} \left(v(0,t) + \frac{1}{\omega} \frac{\partial v(0,t)}{\partial t} \right)$$

Case 2 when $v(x,t)$ is real, with no complex component put

$$v'(x,t) = v(x,t) + i v''(x,t) \quad \text{and}$$

$v'(x,t) = V(x), T(t)$. Here $v'(x,t)$, $V(x)$ and $T(t)$ are all complex and $v(x,t) = \text{Real part of } v'(x,t)$. Then as previously.

Note that in either case, the expression for τ has a more general form:

tangential force on layer of liquid at any section x is

$$\mu \frac{\partial v(x,t)}{\partial x} = -\sqrt{\frac{1}{2} \omega \rho \mu} \left(v(x,t) + \frac{1}{\omega} \frac{\partial v(x,t)}{\partial t} \right)$$

Note that for all x , the viscous tangential force reveals a viscous force component which is proportional to v and a virtual inertia component, proportional to acceleration.

Now consider a rigid-walled tube of constant area of section A , inside perimeter S , in which the square fluid velocity profile across sections X and $X + \delta X$ is V . Then the viscous force at the walls of the small

section of length δX , when, for a near circular tube, $S = 2\sqrt{A\pi}$,
is given by

$$\text{viscous force opposing motion} = -\sqrt{2\pi\omega\rho\mu A} \delta X \left(V + \frac{1}{\omega} \frac{\partial V}{\partial t} \right)$$

This expression was used in the fluid-force-momentum equations
(1) and (2) of Section I of this chapter.

CONCLUSIONS

Chapter 7

Contents

I. Physical Models	Page 1
II. Mathematical Model	Page 3
III. Physical Properties of the Cochlea	Page 7
IV. Research on Hearing	Page 9

I. PHYSICAL MODELS

The methods of design, manufacture and testing of physical models are considered most satisfactory and the degree of experimental accuracy with which quantitative model response data has been extracted from these models has not been achieved in any other investigation known to the writer.

Results of both mathematical and physical model tests indicate that a wider-band frequency response should be sought in future physical model component designs and experiments and that a larger amplitude response should be expected of physical models, particularly at the highest frequencies in the (scaled) audio-frequency range.

The problems of modelling the mass of the scala media in physical models, when a single rubber membrane is supposed to represent the cochlear partition in all respects, will be largely overcome in future models which will include a triangular, fluid-filled model cochlear duct, bounded by two membranes. Such an arrangement will also allow natural damping conditions, dependent on endolymph viscosity, to be simulated with some accuracy.

The physical modelling programme has also been somewhat restricted by the relatively narrow range of membrane elasticity variations which may be applied when using rubber sheeting supplies for partition membranes. Other materials or other latex preparations will be sought from which a wider range of membrane elasticities may be obtained. A correctly designed, double-membrane, triangular scala media will doubtless also assist in preparing model partitions with a wider range of stiffnesses obtaining from the basal to the apical ends of cochlear models. It may also prove necessary to pre-tension the basal end of membranes in order to provide adequate stiffness values.

Having established a wider frequency range for model partition response, as regards both phase and amplitude effects it is suggested that new physical model experiments should be designed:

- (a) to allow close inspection of the effects of sound intensity changes on travelling wave response, that is, to correlate rate of change of phase with distance increases following a sound intensity increase with corresponding decrease of rate of change of amplitude with distance.
- (b) to prepare quantitative data on complex travelling wave response to non-pure-tone excitation, including both complex signals and transients.

There seems to be little point in pursuing further an experimental programme to investigate cochlear scala geometric and size effects. Although uncontrolled variations of model membrane thickness and of the machined width of the membrane slot in the perspex models tended to obscure some results, the conclusions of the extensive model test programme with regard to effects of scalae shape and area variations, and size, are well supported, and are illustrated and discussed at length in chapter 5. Basically, a slightly smaller form of model C1, which contained typical human cochlear scalae sectional area variations, was found to provide an optimum place and amplitude response to the widest range of frequencies. Models containing scalae bores substantially larger than those of model C1 performed very poorly by comparison while smaller diameter scalae models displayed very satisfactory frequency response place effects, but, as sound intensities were increased, their partition amplitudes were sometimes inhibited.

One further model is at present under construction, based on the shape and dimensions of model C7 (Fig. 5 - 6), but with slightly reduced scala areas and with a membrane slot width of exactly that specified by the design drawing. As wide a range of membrane elasticities as possible will be tested in this model, which is similar to but simpler than model C1, in order to confirm the conclusions concerning the potential response of model C1 in comparison with that of other designs of model.

One further advanced model, designed and manufactured to simulate the coiled whorls of the human cochlea, is ideally required in order to test the assumption that both mathematical and physical models may be simplified to represent a geometrically linear, parallel-ducted cochlea. It is generally implied by previous cochlear model investigators that such a model is not worth the effort. However, as such a course presents the only method by which the "straightening-out" simplification can be substantiated, the possibilities of a coiled model are being examined. Such a model would be of immense assistance in an experimental study of hearing by (skull-conducted) bone conduction. Existing models indicated that a relatively good partition travelling wave response could be elicited when, in the absence of a normal stapes sound input, the entire model was vibrated in the longitudinal direction over a wide range of frequencies. The practical implications of this effect, involving inertial loading of fluid particles, can only be assessed when the detailed shape and geometry of the cochlea is simulated.

II. MATHEMATICAL MODEL

Concerning the instability of the Nystrom-Runge-Kutta numerical method of integrating the four simultaneous second order differential equations, all linked by a second order non-linear equation, it may be necessary to re-arrange these equations or to avoid the separation of time-complex variables into in-phase and quadrature components. However it is likely that the problem of divergence of solutions accompanying a forward-working integration, that is, one when initial value conditions are applied at the basal end, will be overcome by a progressively-correcting or relaxation numerical approach. For example, an initial integration commencing at the helicotrema yields (as has been illustrated) a set of variables for pressure, first space derivative of pressure, and fluid displacement, with amplitudes and phases of each, at the oval and round windows. These values may then be amended, setting, for example, round

window pressure amplitudes to zero, and used as initial values in a forward working integration. If this second process remains unstable then new helicotrema-end initial values must be tried in the original, backwards-working integration in order to yield physically acceptable conditions at the round window, or alternatively, amendments to the equations must be considered.

If divergence can be avoided in the second integration, then the trends of initial value changes at either end can be noted and the basal end conditions successively amended to suit the particular problem. Finally, identical travelling waves will result from integrations working in either direction.

This process need not be extravagant regarding computer machine time, as the number of integration intervals can be considerably reduced in the earlier summations. The main difficulty to be overcome in choosing initial values for a forwards-working integration has always concerned the input impedance of the cochlea at the oval window. Fortunately, a backwards-working integration run, regardless of its own apical end initial values, provides what must be considered as fairly accurate data describing the complex impedance of the oval window.

The ratio of P_g to D_g , being stapes pressure amplitude to amplitude of stapes displacement for a number of sound frequencies and partition critical damping coefficients, as derived from mathematical model results, is compared in table 1 with round and oval window impedance data given by von Békésy (see Chapter 2 Fig. 2-1). The Békésy data is converted to the above form by use of a figure of 0.03 cm^2 for the mean area of the oval window and by use of Békésy's own eardrum-to-stapes-footplate middle ear pressure transformation data. This latter data is based on the statics of eardrum and stapedia footplate area differences and is not considered either reliable or necessarily appropriate to the dynamic case of middle-ear response. It will be noted that impedance

ratios P_s/D_s , as compared in Fig. 1, do not agree well, although the trend obtained in the mathematical model, of much increased impedance at high frequency would appear to be supported by the trend of the truncated Bekesy data.

TABLE 1 Oval Window input impedance P_s/D_s

Mathematical Model			Bekesy Data	
Frequency Hz	Critical Damping Ratio	$\frac{P_s}{D_s}$	P_{cardrum}	$\frac{P_s}{D_s}$
17,500	0.5	$.37 \times 10^{10}$	-	-
	1.0	$.41 \times 10^{10}$		
	2.0	$.50 \times 10^{10}$		
10,000	0.5	$.21 \times 10^{10}$	-	-
	1.0	$.22 \times 10^{10}$		
	2.0	$.24 \times 10^{10}$		
1,000	1.0	$.77 \times 10^8$	1.0×10^8	1.7×10^9
	2.0	$.78 \times 10^8$		
200	1.0	$.58 \times 10^7$	4.2×10^7	5.0×10^8
	2.0	$.55 \times 10^7$		
200 (Linear Stiffness only)	1.0	$.22 \times 10^7$		
	2.0	$.23 \times 10^7$		
200 (Non-Linear stiffness but lower range of Et)	1.0	$.50 \times 10^7$		
	2.0	$.55 \times 10^7$		
100	2.0	$.18 \times 10^7$	4.2×10^7	4.2×10^8

A feature of the mathematical model requiring further development is the present treatment of each element of length of the cochlear partition as an independent, single-degree-of-freedom dynamic system, rather than consideration of the whole tapering partition membrane as a distributed parameter system. The errors in the assumption have not as yet been

assessed. Clearly, in areas of the partition where the rates of change of phase of the partition with respect to distance are large, and the membrane undergoes appreciable travelling-wave deformation, the restraints applied to one element of membrane by adjoining elements may, depending upon the (unknown) longitudinal elastic and stiffness properties of the membrane at that section, be significant enough to change deflected shapes and reduce local amplitudes of deformation. Phase relationships local to the restrained area may also be influenced. The design of a mathematical solution for a complete, tapering membrane system with large numbers of degrees of freedom and tapering properties of mass, stiffness and damping is a formidable task, but by treating the single effective membrane which represents the partition as a rectangular membrane in certain restricted regions under consideration, a solution may be possible. Assumptions concerning the (linear) stiffness coefficients involved in restraining longitudinal deformations of the centre of the membrane would have to be made, and at the least, the order of the longitudinal restraining forces could be compared with the order of the transverse linear and non-linear restoring forces. Although the dynamics of a damped, two dimensional, uniform rectangular membrane of linear stiffness, subject to forced vibrations, has been solved by the writer, further attention must be given to this problem.

An approximation is also involved in neglecting the inertia forces associated with transverse motions of areas of fluid near to the oscillating cochlear partition in the scalae. As partition amplitudes may exceed stapelial amplitudes by 20 or 30 times, the assumption that transverse motions of the perilymph in the scalae are insignificant compared to longitudinal motions of elements of fluid must be checked. This matter has been debated previously (Chapter 2 section IV), and other cochlear theorists have agreed that the approximation included herein is justified. However, further calculations may indicate that a portion of the mass of

the fluid in each element of scala should be added to the oscillating mass of the partition.

It is hoped that the importance or otherwise of this effect, and also of the previous effect of longitudinal membrane restraints, may be assessed by comparing the response of a physical model with the theoretical response of the same model.

III. PHYSICAL PROPERTIES OF THE COCHLEA

The calculation of effective mass of the scala media in Chapter 3 is considered reasonable, and the use of the figure of 0.02 g/cm^2 for the approximately constant mass per unit area of the scala media is recommended. In the event that cochlear duct shape geometric variations other than those employed are considered more typical of the human cochlea, then the theory and computational methods which are developed in chapter 3 are sufficiently adaptable to rapidly provide new effective mass variations.

Formulae and equations are developed in Chapter 4 for stiffness of the cochlear partition as a function of the elasticity and thickness of a single effective membrane identical with the basilar membrane but representing the whole partition. The range of values calculated for this elasticity parameter, E_t , which is the product of the linear modulus of elasticity of the membrane in dynes/cm² and the effective thickness of the membrane in cms. is

$$E_t = (160\ 000 - 40\ 000 X) \text{ dynes/cm}$$

where X cms. is the distance of the section considered from the oval window.

In the light of physical and particularly mathematical model tests, it is suggested that this range of values for E_t , representing a variation in elasticity parameter E_t of eight times from base to apex of the cochlea, is not sufficient, and that a variation of as much as sixty times may be required to match von Békésy's experimental data

on the place of low frequency travelling waves as well as the otherwise known human cochlear frequency response; for example

$$Et = (320\ 000 - 90\ 000 X) \text{ dynes/cm}$$

An exponential form for this relationship may also be discovered to be more suitable.

It must be borne in mind that the unique experimental evidence on which this suggested increase in elasticity gradient is mainly based is submitted by von Békésy, who is likewise responsible for the static stiffness data on which was necessarily based the original calculations for partition elasticity. Rather than to cast serious doubt on the accuracy of Békésy's cochlear dynamic response data, it is stressed (in chapter 4) that the static stiffness data is extremely dubious and contradictory and its mis-use by both Békésy and other theorists indicates frequent lack of comprehension of the mechanics involved. The most incredible aspect of this situation is the number of totally different and unrelated ranges of partition linear stiffness that past cochlear theorists have allegedly estimated from Békésy's data.

More urgently even than an experimental confirmation of the nature of high frequency travelling waves occurring in the basal extreme of the cochlear partition, new experimental data on the sub-microscopic nature, variations in structure, and the resistances to static deformations of the human basilar membrane and cochlear scala membranes is required.

It is estimated that although the degree of viscous damping naturally inherent in a fluid-filled, membranous partition such as the scala media is appreciable, and vital to the required nature of the partition dynamic response, a critical viscous damping coefficient of unity is not exceeded. Note that such a damping coefficient is considered relative to the linear component of partition stiffness only, and for large amplitudes of partition vibration (for example, above

0.001 cm.) when non linear stiffness effects must be very significant, the concept of critical damping is misleading and inadequate.

It is possible that, after the manner of the scala media fluid field analysis of chapter 3, simplified Navier-Stokes equations involving the viscosity of endolymph could be manipulated to enable a fair estimation of the velocity-dependent forces required to act upon a moving basilar membrane in order to overcome the resultant viscous forces within the scala media fluid. However, as the damping properties of internal scala media structures and membranes, particularly the tectorium, cannot be included in a calculation of viscous damping properties, it is preferable to derive this information experimentally. Bekesy devoted considerable time to discussions of partition damping conditions but without new experimental data any re-analysis of his appropriate pages would be an irrelevance.

IV. RESEARCH ON HEARING

Thus the present-day knowledge of the action of the cochlea may be gauged.

Mathematical models, whose assumptions are justifiable, which are capable of providing instantaneous arrays of superficially distributed hair cell electrical polarisations resulting from cochlear partition mechanical disturbances, will doubtless disclose many more details concerning partition and basilar membrane dynamic response which are relevant to the discrimination of frequency and sensitivity to intensity in the process of hearing. However, as it has been argued in other places in this document, models as complete as this are not worth developing until the dynamical theories, and the relevant physical properties of the systems concerned, of both the middle and the inner ear are thoroughly refined, lest critical, latent features of the response of the peripheral hearing system be overlooked.

In all branches of research into mammalian hearing there appears to be an enormous amount of effort directed towards the comprehension

of nervous system action potentials at various neural levels, of electroencephalographic records, and even more fundamentally, of various subjective hearing phenomena, all of which effects must be due to the combined responses of both peripheral and central hearing systems. From this point of view alone, in the broadest sense, it would appear to be logical to attempt to separate these two systems, and to focus some attention on the response of their interface, namely, the hair cell bodies innervated in the organ of Corti by the nerves of the spiral ganglion.

While medical practice involving the inner ear largely remains within the realms of biochemistry, a medical appreciation of the mechanical aspects of the cochlea will eventually prove desirable. In addition to the study of bone-conducted hearing already mentioned, such cochlea fringe details as optimum stapes-prosthesis loci of motion and frequency responses and oval window ligament and round window membrane compliances are already assuming some surgical interest. The frequencies of sounds produced by surgeons' middle-ear bone burrs, for example, and the vibration intensities of these drills at various tympanum and mastoid emplacements are also considered conditions pertinent to the incidence of permanent cochlear damage during middle ear surgery, and this problem, although involving more research, clearly involves cochlear dynamics.

Similarly, modern surgical techniques by which defective ossicles are replaced demand more rather than less appreciation of the exact dynamical role of the middle ear, certain changes in whose natural response may or may not result in substantial and presumably undesirable changes in the subsequent response of the cochlea.

It is therefore to be hoped that engineering research of the whole hearing mechanism, and particularly the cochlea, will advance.

Attention is drawn to the fact that the copyright of this thesis rests with its author.

This copy of the thesis has been supplied on condition that anyone who consults it is understood to recognise that its copyright rests with its author and that no quotation from the thesis and no information derived from it may be published without the author's prior written consent.

II

C NATURAL COCHLEA JKG BACK NL 12 28/6/69
C FREQUENCY 1000 CPS, 999 INTERVALS, ALF, FM, ZNLF, F, M
C DAMP=1
C SUBROUTINES IMPROVED
C ET=160000-400000X, IZ=10-2, 50*X
C DAMP SHOULD BE A FUNCTION OF ALF
C USES THETA=GAUSS

COMMON RHO, M, C, EB, U, DAMP, ZNLF, ALF, FM
A100=1.000
F=1000.0
C=145000.0
EB=9.0/16.0
U=0.0197
RHO=1.03
K=500
A=FLOAT(K)
M=2.0/3.1415927
M=3.5/19
M=1

DO 11 J=1, 100, 99
PIR=0.0
PIU=0.0
P2R=PIR
P2U=PIU
PI1R=0.01*FLOAT(J)
PI2R=PI1R
PI1U=PI1R
PI2U=PI2R
DAMP=FLOAT(M)
ZNLF=1.00
ALF=1.000
FM=1.00

WRITE(2, 21)F
WRITE(2, 22)A9
WRITE(2, 26)DAMP, ZNLF, ALF, FM
WRITE(2, 27)

DO 11 I=90, 900

X=3.5-0.5*I=HE*FLOAT(I-1)
CALL FIND(DR, DU, PIR, PIU, P2R, P2U, X)

DSORT(DR+DU+DU)

PHI=ATAN2(DU, DR)

PHI=30.0*PHI/3.14159

WRITE(2, 28)X, D, PHI

CALL CALC(PIR, PIU, P2R, P2U, PI1R, PI1U, P12R, P12U, P1R, P1U, P2R, P2U,

1DR, DU, X)

X2=X+XZ, 0

PIR2=PIR+HE*PIR/2, 0, HE*PIR/8, 0

PIR2=PIR+HE*PIR/3, 0

PIU2=PIU+HE*PIU/2, 0, HE*PIU/8, 0

PIU2=PIU+HE*PIU/3, 0

P2R2=P2R+HE*P2R/2, 0, HE*P2R/8, 0

P2R2=P2R+HE*P2R/3, 0

P2U2=P2U+HE*P2U/2, 0, HE*P2U/8, 0

P2U2=P2U+HE*P2U/3, 0

CALL FIND(DR2, DU2, P1R2, P1U2, P2R2, P2U2, X2)

CALL CALC(PIR2, PIU2, P2R2, P2U2, P1R2, P1U2, P12R2, P12U2, P1R2, P1U2,

1P2R2, P2U2, DR2, DU2, X2)

PIR3=PIR+HE*PIR/2, 0

PIU3=PIU+HE*PIU/2, 0

PI2R3=PI2R+HE*PI2R/2, 0

PI2U3=PI2U+HE*PI2U/2, 0

CALL CALC(PIR3, PIU3, P2R3, P2U3, P1R3, P1U3, P12R3, P12U3, P1R3, P1U3,

1P2R3, P2U3, DR3, DU3, X3)

X4=X+XZ, 0

PIR4=PIR+HE*PIR+HE*PIR/2, 0

PIR4=PIR+HE*PIR3

PIU4=PIU+HE*PIU+HE*PIU/2, 0

PIU4=PIU+HE*PIU3

P2R4=P2R+HE*P2R+HE*P2R/2, 0

P2R4=P2R+HE*P2R3

P2U4=P2U+HE*P2U+HE*P2U/2, 0

P2U4=P2U+HE*P2U3

CALL FIND(DR4, DU4, P1R4, P1U4, P2R4, P2U4, X4)

CALL CALC(PIR4, PIU4, P2R4, P2U4, P1R4, P1U4, P12R4, P12U4, P1R4, P1U4,

1P2R4, P2U4, DR4, DU4, X4)

PIR5=PIR+HE*PIR+HE*PIR+HE*PIR/2, 0

PIR5=PIR+HE*PIR4+HE*PIR/2, 0

P2R5=P2R+HE*P2R+HE*P2R+HE*P2R/2, 0

P2R5=P2R+HE*P2R4+HE*P2R/2, 0

PIU5=PIU+HE*PIU+HE*PIU+HE*PIU/2, 0

PIU5=PIU+HE*PIU4+HE*PIU/2, 0

P2U5=P2U+HE*P2U+HE*P2U+HE*P2U/2, 0

P2U5=P2U+HE*P2U4+HE*P2U/2, 0

IF (I, NE, K) GO TO 11

PI=DSORT(PIR+PIU+PIU+PIU)

ETA=ATAN2(PIU, PIR)*180.0/3.1415927

PI=DSORT(P2R+P2U+P2U+P2U)

ETA2=ATAN2(P2U, P2R)*180.0/3.1415927

PI=DSORT(PI1R+PI1R+PI1R+PI1R)

ZETA=ATAN2(PI1U, PI1R)*180.0/3.1415927

PI=DSORT(PI2R+PI2R+PI2R+PI2R)

ZETA2=ATAN2(PI2U, PI2R)*180.0/3.1415927

DO 12 I=1, (RHO+HE)

PDR=PIR-P2R

PDU=PIU-P2U

PI=DSORT(PDR+PDR+PDR+PDR)

ETA=ATAN2(PDU, PDR)*180.0/3.1415927

ZETA=ZETA2-ZETA1

IF (ZETA, LT, 180.0) ZETA=360.0-ZETA

AP1=PI/100

AP1=1360.0*(ZETA1-ZETA)

WRITE(2, 1)PI, ETA1, P2, ETA2, PD, ETA

WRITE(2, 2)D01, ZETA1, D02, ZETA2, ZETA

WRITE(2, 3)AP1, AP101

WRITE(2, 3)1

WRITE(2, 3)PIR

WRITE(2, 3)PIU

WRITE(2, 3)P2R

WRITE(2, 3)P2U

WRITE(2, 3)PI1R

WRITE(2, 3)PI1U

WRITE(2, 3)PI2R

PI=HE*PIU3

PI=HE*PI2R+HE*PI2R/2, 0


```

A123,14159*DI*DI11/2,0
A11-A11
A23,14159*02*02/4,0
A123,14159*02*02/2,0
A12-A12
C10=SORT(2,0,3,14159*RH00U)
CALL GET(C4,C5,C6,C7,C8,C9,B,A1,A11,C10)
FIR=PIR+C4+PIU+C5+PIR+C6+PIU+C7+DR+C8+DU+C9
F1U=PIR+C5+PIU+C6+PIR+C7+PIU+C8+DR+C9+DU+C8
CALL GET(C4,C5,C6,C7,C8,C9,B,A2,A12,C10)
F2R=PIR+C4+PIU+C5+PIR+C6+PIU+C7+DR+C8+DU+C9
F2U=PIR+C5+PIU+C6+PIR+C7+PIU+C8+DR+C9+DU+C8
RETURN
END
SUBROUTINE FIND(DR,DU,PIR,P1U,P2R,P2U,X)
COMMON MHO,M,C,E,B,U,DAMP,ZMLF,ALP,FM
IF (X.GT.0,750) GO TO 1
S0,0150*0,0007*X
GO TO 3
1 IF (X.GT.2,670) GO TO 2
S0,020
GO TO 3
2 S0,020*0,013333*(X-2,670)
3 SPM*5
E716000,0-40000,0*X
B0,0122*0,0110*X
B4B*4
T210,0-2,56*X
QBAMP=SORI(ET*2*S0,0/(B4*16,0*10,0*09))/(10*9,0/10,0)

```

```

Z=ZNF*16,0*100,0*ET/(9,0*5*04)
A=ALF*16,0*ET*2/(9,0*5*0*10,0*05)
PDR=PIR-P2R
PDU=PIU-P2U
F116,0=SORT(PDR*PDR*PDU)/(9,0*5)
Z2Z*Z
H2H*H
Q2*0*0
H3H2-A
PA16,0*15,0*H2*02=H3M3)/(27,0*22)
QA16,0*(8,0*H3*03+2,0*H2*02*H3-01,0*F*F*Z)/(729,0*Z*Z)
D4,0*(PA*10,0*0*0*0*27,0*1*Q*10,0*0*0*0*2)
IF (D) 4,5,5
4 D=SORT(1-4,0*PA/3,0)
DAD*1,0
D3*3,0*0A/(PA*04)
D5*1,0/D3=SORT(1,0-03*03)
D6=ATAN(D5)
IF (D3,1,0,0) D6*3,14159*06
D8*06/3,0
D7=COS(D6)
D8=COS(2,0*3,14159/3,0*06)
D9=COS(2,0*3,14159/3,0*06)
D10*0,0*H3/12*0,07
D7/D4*07*010
IF (D7,1,0,0) D7*10,0
D8*04*08*010
IF (D8,1,0,0) D8*14,0
D9*04*09*010
IF (D9,1,0,0) D9*19,0
TRY*07
IF (D6,1,0,0) TRY*06
IF (D9,1,0,0) TRY*09
AMP=SORT(TRY)
UU TO 0
3 IF (PA) 7,7,0
D4=SORT(1-5,0*PA/3,0)
DAD*2,0
D3*3,0*0A/(PA*04)
IF (D4,1,0,0) D3*03
D32=SORT(D3*03*1,0)
D33=ALG(D3*03*032)
D34=D33/3,0
D35*0,0*(EXP(D34)*EXP(-D34))
Y0*035
AMP=SORT(Y*0,0*H3/(2*0,0))
GO TO 6
5 D=SORT(1-0*PA/3,0)
DAD*4,0
D3*3,0*0A/(PA*04)
D32=SORT(D3*03*1,0)
D33=ALG(D3*03*032)
D34=D33/3,0
D35*0,0*(EXP(D34)*EXP(-D34))
Y0*035
AMP=SORT(Y*0,0*H3/(2*0,0))
GO TO 6
6 ANT*AMP

```

```

D9*00H
D10*0,75*AMP*AMP*Z*H2*A
GAM=ATAN(D9/D10)
IF (GAMA,1,0,0) GAMA*3,14159*0A*H
THEY=ATAN2(PDU,PDR)
PHI=THEY*GAMA
DREAL=COS(PHI)
DUSANT=SIN(PHI)
RETURN
END
SUBROUTINE GET(C4,C5,C6,C7,C8,C9,B,A1,A11,C10)
COMMON MHO,M,C,E,B
RA=SORT(A)
C2=C10/RA
C1=C0*RH0+C2
C3=AI/(2,0*A*(C1*C1+C2*C2))
C4=C3*(3,0*C2*C2*3,0*C1*C2+2,0*RH0*H*C1)
C5=C3*RH0*H*C2
C6=H*C1/(RH0*C4)
C7=H*C2/(RH0*C4)
C8=EB*H*H*C1/A
C9=EB*H*H*C2/A
RETURN
END

```

C COCKLEA DETAILED CASE SOURCE 2 JKC 9/777 ELLIOT CMPLX ROUTINES

DIMENSION X(40),V(40),XL(40),XM(40),XNB(40)

REAL M,N,L
COMPLEX Z,J,K, TRANSZ,MOVEZ
COMMON AB,GZ,FZ,A7,N

```
1781  
DO 11 16=0,35,5  
XL(17)=16  
XSXL(17)  
XM(1)=1125  
XM(2)=1071  
XM(3)=1000  
XM(4)=918  
XM(5)=857  
XM(6)=837  
XM(7)=900  
XM(8)=1000  
N=(A10*XM(17))/1000.0  
S=SIN(82)  
C=COS(82)  
XNB(17)=290  
XNB(27)=235  
XNB(37)=190  
XNB(47)=160  
XNB(57)=140  
XNB(67)=135  
XNB(77)=150  
XNB(87)=165  
F1=0.192*0.0116*XS  
ML=(F1*A10*XNB(17))/100.0  
AL=3.14159*(65.0-XS)/180.0  
S=SIN(AL)  
C=COS(AL)  
M=SA/CA  
H1=ML*SA*SN/(SIN(3.14159*AL*82))  
AR=H1*DL/2.0  
F=F1/H1  
Q=(0.355-0.01*XS)*F  
X=CH/SN  
L=L/M*X  
A7=SN*SN  
E=1/A7  
GZ=A7*Q*SN  
FZ=A7*(F-Q)*SN  
AB=FZ  
FZ=AB*GZ  
AB=1000/(3.1416*SORT(1+M*H1))  
U=Q  
V=Q  
L=1  
DO 10 13=125,9875,250  
P=15*A10/10000.0  
IF (XB) 4,5,5  
4 X=AP/M
```

2

```
X(1)=XE*XB  
X=X(1)  
A21=(M*CN*SN)/SN  
Q=1-M*X  
CALL CALC(TT,SS,XA,0)  
V(1)=AB*(M*TT*SS)  
IF (XA) 10,14,14  
10 G=XA/XB  
YY=Q1  
GO TO 13  
5 X(1)=L*P  
X=X(1)  
X=XA-XB  
A21=1.000  
IF (XC) 6,7,7  
6 V(1)=Q  
Q=XA/XB  
GO TO 8  
7 Q=1-M*X  
CALL CALC(TT,SS,XA,0)  
V(1)=AB*(M*TT*SS)  
8 IF (Q=0.0125) 10,14,14  
14 YY=0.0125  
15 CALL CALC(TT,SS,XA,YY)  
U=SS*Q*2.0  
M=TT*Q*2.0  
YY=YY*0.0250  
IF (Q,DE,YY) GO TO 15  
10 I=101  
R=(U*H1)*2.0*E1**4/1979137  
U=Q  
N1=Q*F  
R2=R1*(N1,N,UI,M1)  
R3=R1*(UI,N,UI,M1)  
R=R/(R2+R3)  
R=R/A21  
P1=90/N  
P2=180*ATAN(M)/3.14159  
P3=1.05*R*AR/100  
P4=10*R3/F  
WRITE(2,47)XS  
WRITE(2,48)P1  
WRITE(2,49)P2  
WRITE(2,46)M1  
WRITE(2,50)G  
WRITE(2,51)F  
WRITE(2,52)(X(1),131,40)  
WRITE(2,53)(V(1),131,40)  
WRITE(2,54)R  
WRITE(2,55)P3
```

Q=1-M*X
CALL CALC(TT,SS,XA,0)
V(1)=AB*(M*TT*SS)

```

001-NOX
CALL CALC(TT,SS,XA,0)
V(I)=AB*(M*TT+SS)
IF (XA) 16,14,14
16 01XA/XB
YY=01
GO TO 17
5 X(I)=L*P
XA*(I)
XCXA-XB
A21=1.000
IF (XC) 6,7,7
6 V(I)=0
0XA/XB
GO TO 8
7 001-M*XC
CALL CALC(TT,SS,XA,0)
V(I)=AB*(M*TT+SS)
8 IF (0=0,0123) 10,14,14
14 YY=0.0125
15 CALL CALC(TT,SS,XA,YY)
UNSS=2*U
WTT=2*W
YY=YY*0.0250
IF (0.05,YY) GO TO 15
10 1=1
R=(U+H)*2*F*E1=4/19791,37
J1=6
N1=6*F
R2=R1*(N1,N,U1,M1)
R3=R1*(U1,N,U1,M1)
R4=R/(R2+R3)
R5=R/AZ1
P1=90/N
P2=180*ATAN(M/3,14159
P3=1.090*AR/100
P4=10*P3/F
WRITE(2,47)XS
WRITE(2,48)P1
WRITE(2,49)P2
WRITE(2,46)M1
WRITE(2,50)G
WRITE(2,51)F
WRITE(2,52)X(I),1=1,40)
WRITE(2,53)(V(I),1=1,40)
WRITE(2,54)R
WRITE(2,55)P3
WRITE(2,56)P4
17=17*1
11 CONTINUE
11 STOP
47 FORMAT(19H1SECTION XS IN MMS,F4,1)
48 FORMAT(11HSMALL ANGLE,F6,2)
49 FORMAT(16HREISSNERS ANGLE,F4,1)
46 FORMAT(137HREQUIRED SPACE MULTIPLICATION FACTOR,F5,3)
50 FORMAT(3HX1=,F9,3)
51 FORMAT(3HP=,F6,3)

52 FORMAT(8H X=,10(2X,F7,9)/1M ,10(2X,F7,9)/1M ,10(2X,F7,9)
1/1M ,10(2X,F7,9)
53 FORMAT(8H 10000V=,10(F9,3)/1M ,10(F9,3)/1M ,10(F9,3)/
54 FORMAT(2HRE,=E19,8/)
55 FORMAT(15HREFFECTIVE MASS OF BAS,MEMB, GMS/CM OF LENGTH,E19,8/)
56 FORMAT(15HREFFECTIVE MASS OF BAS,MEMB, GMS/CM2 OF AREA ,E19,8)
END
SUBROUTINE CALC(TT,SS,XA,YY)
REAL N
COMPLEX Z,J,K,TRANSZ,MOVEZ
COMMON AB,GZ,PZ,A7,N
K=CMPLX(XA,YY)
Z=TRANSZ(K,A7,N)
X=REAL(Z)
Y=AIMAG(Z)
A7=AB+XX
B7=AB-XX
C=Z+XX
D=XX-GZ
Y8=YY
C1=C2=A-PZ
B1=B2=B-PZ
P2=2*FZ
Z=Z+C*YS
D5=8*D*YS
A3=ATAN(A/Y)=ATAN(C/Y)
B1=ATAN(B/Y)=ATAN(D/Y)
Z1=ALOG((YS+A*Y)/(YS+C*Y))
Z2=ALOG((YS+B*Y)/(YS+D*Y))
SAY=FZ+C2*A1-D2*B1=0.5*Y*(C1*Z1+D1*Z2)
T=0.5*XX*(C1*A1-D1*B1)*0.5*(C2*Z1+D2*Z2)
A=EN=1.000=1.000
JUN=MOVEZ(K,A7,A20)
B1=REAL(J1)+AIMAG(J1)
T1=0.5*REAL(J2)+0.5*AIMAG(J2)
RETURN
END
COMPLEX FUNCTION TRANSZ(K,A7,N)
REAL N
COMPLEX K
TRANSZ=A7*(CEXP(N*LOG(K)))
RETURN
END
COMPLEX FUNCTION MOVEZ(K,A7,A20)
COMPLEX K
MOVEZ=A7*(CEXP(A20*LOG(K)))
RETURN
END
FUNCTION R3(X,N,U3,M1)
REAL N
UN=U1*EN
M=N*J*EN
E2=UN*W
E3=UN*W
E4=1/(4*N+1)
E5=2*E2/(3*EN+1)
E6=(2*E3+E2*E2)/(2*N+1)
E7=2*E3*E2/(N+1)
E8=E3*E3
R3=E4*X*(4*N+1)-E5*X*(3*N+1)+E6*X*(2*N+1)+E7*X*(N+1)+E8*X
RETURN
END

```

6

Attention is drawn to the fact that the copyright of this thesis rests with its author.

This copy of the thesis has been supplied on condition that anyone who consults it is understood to recognise that its copyright rests with its author and that no quotation from the thesis and no information derived from it may be published without the author's prior written consent.

II

D31784'80

END